UNIVERSITY of OULU

RES TERRAE

Publications of the Department of Geosciences University of Oulu
Oulun yliopiston geotieteiden laitoksen julkaisuja

Ser. A, No. 28
2009

Teemu Öhman

The structural control of polygonal impact craters

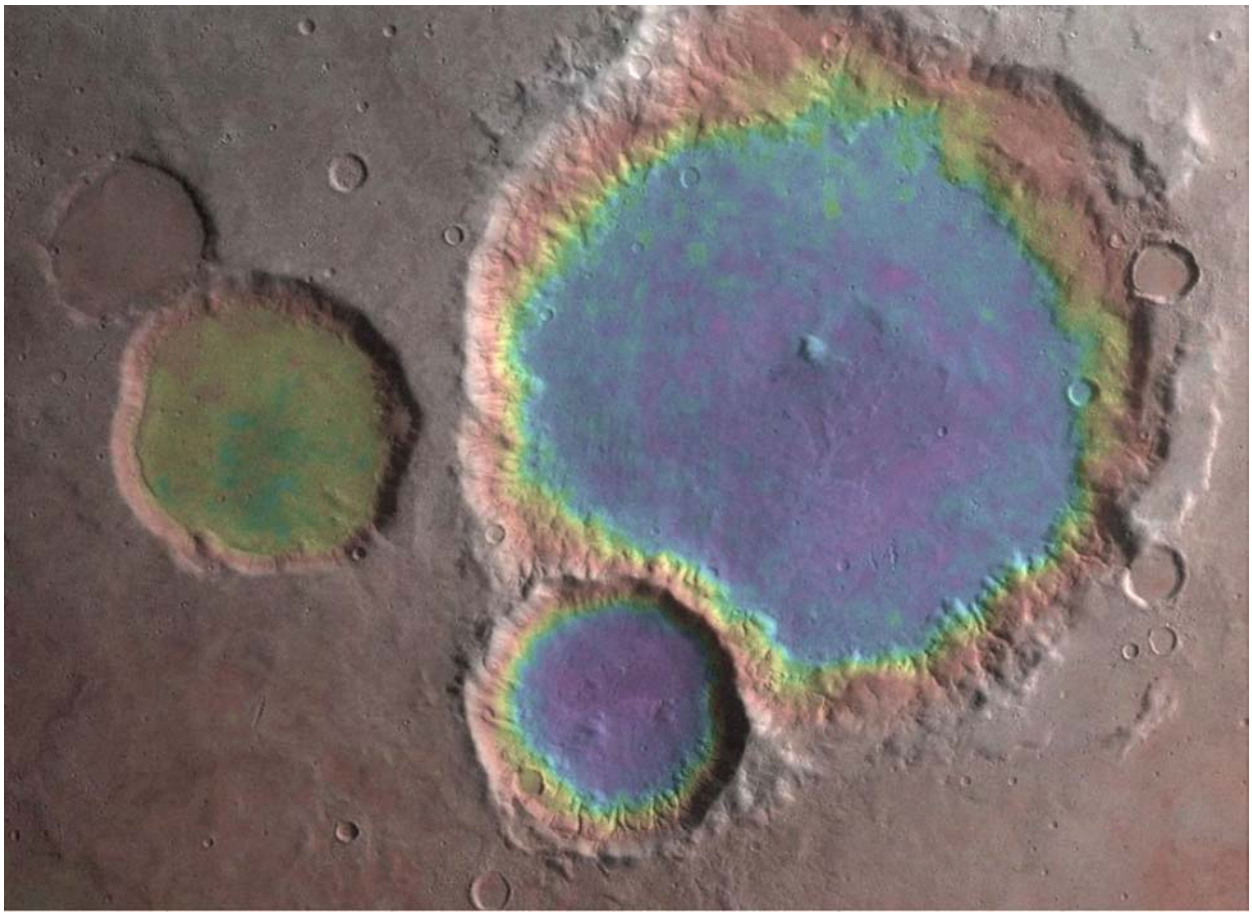

The Structural Control of Polygonal Impact Craters

TEEMU ÖHMAN

Academic dissertation to be presented, with the assent of the Faculty of Science of the University of Oulu, for public defence in Auditorium GO101, Linnanmaa, on October 3rd, 2009, at 12 o'clock noon

OULUN YLIOPISTO, OULU 2009

Teemu Öhman

The structural control of polygonal impact craters

Res Terrae, Ser. A, No. 28, OULU, 2009

RES TERRAE - Publications of the Department of Geosciences, University of Oulu, Oulun yliopiston geotieteiden laitoksen julkaisuja

Ser. A, Contributions	**ISSN 0358-2477**
Ser. B, Raportteja - Reports	**ISSN 0358-2485**
Ser. C, Opetusjulkaisuja - Teaching material	**ISSN 0358-2493**

Julkaisu ja levitys - Published and distributed by:

Oulun yliopisto, geologian osasto - University of Oulu, Department of Geosciences, P.O. Box 3000, FI-90014 University of Oulu, Finland

Telephone:	**08-5531430, International tel: +358-8-5531430**
Telefax:	**08-5531484, International fax: +358-8-5531484**
E-mail:	**pekka.tuisku@oulu.fi**
www:	**http://cc.oulu.fi/~resterr/**

“We put the work in,
we put the time in.
What did we get back?
Virtually nothing.

We put the effort in,
our whole lives in.
And in the end we’re
second class citizens.”

– TV *SM!TH*

Rakenteellisesti kontrolloidut törmäyskraatterit

TEEMU ÖHMAN

Geotieteiden laitos, ja Fysikaalisten tieteiden laitos, PL 3000, 90014 Oulun yliopisto

Tiivistelmä

Kuussa on ainakin 1800-luvun lopulta lähtien tiedetty olevan runsaasti kraattereita, jotka muodoltaan poikkeavat tavallisimmista pyöreistä kraattereista. Yleisimmin tällaiset törmäyskraatterit muistuttavat osittaisia säännöllisiä monikulmioita, useimmiten kuusikulmioita. Etenkin 1960–1970-luvuilla niitä tutkittiin melko paljon, mutta sittemmin niiden merkitys ja jopa olemassaolo on suurelta osin unohdettu. Tässä väitöskirjatyössä tutkittiin näiden monikulmaisten törmäyskraatterien esiintymistä, syntyprosessia ja merkitystä maankaltaisten taivaankappaleiden geotektonisen kehityksen selvittämisessä, sekä luotiin melko kattava katsaus aiempiin tutkimuksiin aiheesta 1900-luvun alkuvuosikymmeniltä alkaen.

Päätutkimuskohteena oli Marsin eteläinen kraatteroitunut ylänköalue Hellaksen ja etenkin Argyren törmäysaltaiden ympärillä. Tutkimus tehtiin etenkin Viking MDIM 2.0-, mutta osin myös THEMIS- ja MOC-WA-kuva-aineistoja analysoimalla. Lisäksi tutkittiin koko Venuksen läpimitaltaan yli 12 km olevien törmäyskraatterien populaatio Magellan-luotaimen SAR-tutkakuva-aineistolla, sekä osa Kuun lähipuolen eteläisiä ylänköjä Consolidated Lunar Atlas -valokuvien perusteella.

Väitöskirjatyön perusteella on selvää, että monikulmaisia törmäyskraattereita esiintyy kaikenlaisilla Aurinkokunnan kiinteäkuorisilla kappaleilla, joiden pinnalla on törmäyskraattereita. Marsissa, Venuksessa ja Kuussa ne muodostavat yleensä noin 15%–20% törmäyskraatteripopulaatiosta. Ne muodostuvat heti kraatterin syntyessä, eikä myöhempi eroosio vaikuta merkittävällä tavalla niiden monikulmaisuuteen. Niiden suorien sivujen suunnat heijastelevat kohdemateriaalissa törmäyshetkellä vallinneita heikkoussuuntia, joten niitä voidaan käyttää paleotektoniseen tutkimukseen. Marsin ylängöillä tällaisia suuntia ovat etenkin vanhojen törmäysaltaiden synnyttämät konsentriset ja radiaaliset rakoilusysteemit. Marsin tektoniikan tutkimuksessa yleisesti käytetyt hautavajoamat ja ryppyharjanteet sen sijaan ovat tutkimusalueella vaikuttaneiden myöhempien tapahtumien, etenkin Tharsiksen vulkaanisen kompleksin kontrolloimia. Venuksen pinnalla tilanne on samankaltainen, sillä kraatterien suorat sivut poikkeavat tasankojen ryppyharjanteiden suunnista, mutta vastaavat erittäin hyvin mm. vanhan tesseran ja nuorten siirrosvyöhykkeiden rakenteiden suuntia.

Monikulmaisten törmäyskraattereiden kokojakauma poikkeaa selvästi muiden kraattereiden kokojakaumasta. Marsin, Venuksen ja Kuun kraatterit muodostuvat monikulmaisiksi useimmiten siinä tapauksessa, että niiden läpimitta on noin 1–5× maljakraattereiden ja kompleksikraattereiden välinen vaihettumisläpimitta. Tutkimus antaa myös viitteitä siitä, että kaikkein suotuisin syntyläpimitta kasvaa painovoiman kasvaessa.

Monikulmaisten törmäyskraattereiden syntymekanismit ovat edelleen osittain tuntemattomia. Kraatteroitumisprosessin kaivautumisvaiheessa tapahtuva heikkouspintojen suuntainen laajeneminen ei liene vallitseva mekanismi maljakraattereiden tapauksessa. Muokkautumisvaiheessa tapahtuva kompleksikraatterien reunojen romahtaminen pitkin heikkouspintoja sen sijaan on todennäköisesti yleinen syntymekanismi. Näiden aiemmin esitettyjen syntymallien ohella väitöskirjatyössä esitetään uutta, kolmatta syntymallia, joka selittää niin maljakraatterien kuin pienten kompleksikraatterien heikkouspintojen suuntaiset reunat. Malli perustuu kaivautumisvaiheessa tapahtuviin kraatterin reunan ylityöntöihin, jotka tapahtuvat pitkin kohteen vallitsevia rakosuuntia tai muita vastaavia heikkouspintoja.

Työssä saadut tulokset osoittavat, että monikulmaiset törmäyskraatterit ovat rakenteellisesti kontrolloituja, minkä ansiosta niitä voidaan käyttää alueellisiin paleotektonisiin tutkimuksiin. Ne tarjoavat mahdollisuuden tutkia vanhempia prosesseja kuin muut planeettageologisessa tutkimuksessa nykyisin yleisesti käytetyt tektoniset rakenteet. Lisäksi on ilmeistä, että törmäyskraattereiden syntyprosessissa on vielä lukuisia heikosti tunnettuja ilmiöitä, joiden selvittämisessä rakennegeologinen tutkimus niin Maapallon kuin muidenkin taivaankappaleiden kraattereiden osalta on avainasemassa.

The Structural Control of Polygonal Impact Craters

TEEMU ÖHMAN

Department of Geosciences, and Department of Physical Sciences, University of Oulu, P.O. Box 3000, FI-90014 University of Oulu, Finland

Abstract

Polygonal impact craters (PICs) have been known at least since the late 1800s, and they were studied to some extent in the 1960s and 1970s. Since then they have been largely neglected. In addition to giving an account on the history of PIC studies, this thesis focuses on the occurrence, formation, and significance of PICs. The study areas encompass parts of the southern highlands of Mars particularly around the Argyre impact basin, the entire surface of Venus, and a part of the near-side highlands of the Moon.

It is evident that the PICs are structurally controlled, and occur throughout the Solar System on all types of bodies with rigid, cratered crusts. On Mars, Venus, and the Moon they make up ~15%–20% of the impact crater population. The polygonal plan view is established when the crater forms, and subsequent crater degradation does not have a significant effect on it. The orientations of the straight segments of the PIC rims generally reflect old planes of weakness in the crust. In the case of Mars, such planes are typically formed by the radial and concentric fracture patterns surrounding the impact basins. Later tectonic events like the development of the Tharsis bulge control the wrinkle ridges and the graben, but do not affect the crater polygonality. Similarly, in the case of Venus, PIC rim strikes match e.g. the orientations in tessera and rifts, but not the ridges. Thus, in paleotectonic mapping PICs can reveal tectonic processes not readily observed otherwise.

The size distributions of PICs and non-polygonal craters are markedly different: PICs "favour" small to mid-sized complex craters. Previous models of PIC formation do not fully explain all the observations, and therefore a third model is introduced. This model is applicable both to simple and small complex craters, and involves thrusting along joint sets or other similar dominating sets of pre-existing planes of weakness in the target.

Key words: Impact cratering, structural control, Mars, Venus, Moon, impact basins.

CONTENTS:

Abstract...3

A list of the most essential abbreviations, acronyms and symbols used in this work...8

A statement on the authorship of the thesis and the included papers... 10

Acknowledgements... 13

1 Introduction and the purpose of the study ... 15

1.1 Background and goals ... 15

1.2 The structure of the thesis ... 17

2 Impact cratering phenomenology ... 20

2.1 Basic impact processes ... 20

2.1.1 Simple and complex craters ... 20

2.1.2 Impact basins ... 26

2.2 Craters, basins and fractures ... 31

2.3 Factors governing the crater shape ... 34

2.3.1 Impact angle ... 34

2.3.2 Clustered impacts ... 36

2.3.3 Projectile velocity and shape ... 37

2.3.4 Target effects: topographic variations and layering ... 38

3 The environment of lunar, Venusian and Martian impact cratering ... 40

3.1 The Moon ... 40

3.2 Venus ... 42

3.3 Mars ... 44

4 Geologic background of Hellas and Argyre regions ... 48

4.1 General characteristics ... 48

4.2 The geologic units ... 49

4.3 The impact basins ... 50

4.4 Tectonics ... 52

4.5 Volcanic, glacial, lacustrine, fluvial and eolian features ... 57

5 An outline of impact crater morphologies characteristic to the Moon, Mars and Venus . 60

5.1 Short observational history ... 60

5.2 General morphology ... 61

5.2.1 The Moon ... 63

5.2.2 Mars ... 65

5.2.3 Venus ... 66

5.3 Untypical central structures ... 69

5.4 Ejecta blankets and other exterior phenomena ... 71

5.4.1 Lunar ejecta, secondary craters and rays ... 71

5.4.2 Martian ejecta blankets ... 74

5.4.3 Ejecta and atmospheric impact phenomena on Venus ... 77

5.5 Various Martian and Venusian impact oddities ... 79
5.5.1 Stealth craters and basins ... 79
5.5.2 Peripheral peak rings ... 80
5.5.3 Clustered impacts and crater fields ... 81
5.6 Polygonal impact craters vs. "ordinary" impact crater morphologies ... 82
6 The structural control of impact craters ... 83
6.1 Previous studies on planetary polygonal impact craters ... 83
6.1.1 Lunar PICs ... 83
6.1.2 Martian PICs ... 94
6.1.3 PICs on Mercury ... 96
6.1.4 Venusian PICs ... 98
6.1.5 PICs on other heavenly bodies ... 99
6.2 Studies of terrestrial polygonal and structurally controlled craters ... 100
6.2.1 Simple craters ... 100
6.2.2 Complex craters ... 102
6.3 Impact and explosion experiments concerning polygonal craters ... 107
6.4 Modern models of PIC formation mechanisms ... 108
6.4.1 Simple PICs and crater excavation ... 108
6.4.2 Complex PICs and the crater modification stage ... 110
7 Data and methods ... 113
7.1 Image datasets ... 113
7.1.1 Martian data ... 113
7.1.2 Venusian data ... 114
7.1.3 Lunar data ... 115
7.2 Definitions and classifications ... 116
7.3 Measuring methods ... 118
7.4 Data presentation and statistical methods ... 121
8 Results ... 124
8.1 Distribution and abundance of PICs ... 124
8.2 General morphology and polygonality ... 127
8.3 Degradational stages ... 129
8.4 Diameter ... 133
8.5 Simple and complex PIC rim strike orientations and other tectonic structures ... 134
8.6 The effect of illumination geometry ... 141
9 Discussion ... 146
9.1 The universality of polygonal impact craters ... 146
9.2 The illumination geometry and its effects ... 147
9.3 The number of straight rim segments and their mutual angles ... 149
9.4 The importance of target fracturing ... 150
9.5 Basin-induced fracturing and PICs ... 151
9.6 PICs and other tectonic indicators ... 152
9.7 Crater degradation as the origin of polygonal craters? ... 157

9.8 Crater modification stage and polygonal impact craters 159
9.9 An accompanying PIC formation mechanism? 161
9.10 Size distribution 165
9.10.1 PICs and Venusian plains 169
9.11 PICs and target material classification 171
9.12 Further possibilities for future studies regarding polygonal impact craters 172
10 Summary and conclusions 175
11 References 178

Appendices 223

APPENDICES:

Appendix 1:
Data of successful missions to the Moon (3 pp.)

Appendix 2:
Data of successful missions to Mars (1 p.)

Appendix 3:
Data of successful missions to Venus (1 p.)

Appendix 4a:
Data of polygonal impact craters in the Argyre region of Mars (8 pp.)

Appendix 4b:
Polygonal impact crater rim strike measurements in the northeastern Argyre region of Mars using MOC-WA imagery (1 p.)

Appendix 5a:
Data of polygonal impact craters on Venus (4 pp.)

Appendix 5b:
Matches between polygonal impact crater rim and tectonic structure orientations on Venus (4 pp.)

Appendix 6:
Data of polygonal impact craters in the TINN area of the Moon (2 pp.)

ORIGINAL PAPERS (not included in this electronic version of the thesis):

Paper I:

Öhman, T., Aittola, M., Kostama, V.-P. & Raitala, J., 2005. The preliminary analysis of polygonal impact craters within greater Hellas region, Mars. In: Koeberl, C. & Henkel, H. (Eds.), Impact Tectonics, pp. 131–160. Berlin Heidelberg, Springer-Verlag.

Paper II:

Öhman, T., Aittola, M., Kostama, V.-P., Hyvärinen, M. & Raitala, J., 2006. Polygonal impact craters in Argyre Region, Mars: evidence for influence of target structure on the final crater morphology. Meteoritics & Planetary Science 41 (8), 1163–1173.

Paper III:

Öhman, T., Aittola, M., Kostama, V.-P., Raitala, J. & Korteniemi, J., 2008. Polygonal impact craters in Argyre Region, Mars: implications for geology and cratering mechanics. Meteoritics & Planetary Science 43 (10), 1605–1628.

Paper IV:

Aittola, M., Öhman, T., Leitner, J. J. & Raitala, J., 2007. The characteristics of polygonal impact craters on Venus. Earth, Moon and Planets 101, 41–53.

Paper V:

Aittola, M., Öhman, T., Leitner, J. J., Kostama, V.-P. & Raitala, J., 2009. The structural control of Venusian polygonal impact craters. Icarus, doi:10.1016/j.icarus.2009.08.004. In press. 32 pp.

Paper VI:

Öhman, T., Aittola, M., Korteniemi, J., Kostama, V.-P. & Raitala, J., 2009. Polygonal impact craters in the Solar System: observations and implications. In: Gibson, R. L. & Reimold, W. U. (Eds.): Large Meteorite Impacts and Planetary Evolution IV. Geological Society of America Special Paper. Geological Society of America. In press. 41 pp.

A LIST OF THE MOST ESSENTIAL ABBREVIATIONS, ACRONYMS AND SYMBOLS USED IN THIS WORK

AU: Astronomical Unit (mean distance between the Earth and the Sun, about 149 600 000 km)

CLA: Consolidated Lunar Atlas

C1-MIDR: Once Compressed Mosaicked Image Data Record, produced from Magellan data

CTX: Context camera (onboard the Mars Reconnaissance Orbiter spacecraft)

***D*:** rim-crest (rim-to-rim) diameter of an impact crater[1]

***d*:** apparent depth (from the rim crest to the floor of the apparent crater) of an impact crater

d_e**:** depth of excavation of an impact crater

$\mathbf{D_{crit}}$**:** critical value in Kolmogorov–Smirnov test, against which the D-value is compared

D_t**:** diameter of the transient cavity

d_t**:** depth of the transient cavity

D_{tr}**:** Diameter of the transition from simple to complex crater morphology

DEM: Digital Elevation Model

DTM: Digital Terrain Model

D-value: the largest difference between two variables in Kolmogorov–Smirnov two-sample test

E_k**:** Kinetic energy (of the impacting projectile)

ESA: European Space Agency

FMIDR: Full-resolution Mosaicked Image Data Record, produced from the Magellan data

***g*:** gravitational acceleration [m/s^2]

HiRISE: High Resolution Imaging Science Experiment (onboard the Mars Reconnaissance Orbiter spacecraft)

HRSC: High Resolution Stereo Camera (onboard the Mars Express spacecraft)

K–S test: Kolmogorov–Smirnov test

LAC: Lunar Aeronautical Chart

LIDAR: LIght Detection And Ranging (essentially a laser radar)

***m*:** mass (of the impacting projectile)

MESSENGER: NASA's MErcury Surface, Space ENvironment, GEochemistry and Ranging spacecraft

MEX: ESA's Mars Express spacecraft

MDIM: Mars Mosaicked Digital Image Model (based on Viking imagery)

MGS: NASA's Mars Global Surveyor spacecraft

MOC-WA: Mars Observer Camera – Wide Angle (onboard the Mars Global Surveyor spacecraft)

MOC-NA: Mars Observer Camera – Narrow Angle (onboard the Mars Global Surveyor spacecraft)

MOLA: Mars Observer Laser Altimeter (onboard the Mars Global Surveyor spacecraft)

MRO: NASA's Mars Reconnaissance Orbiter spacecraft

***n*:** The number of measurements

NASA: National Aeronautics and Space Agency

NEA: Near Earth Asteroid

NEAR–Shoemaker: NASA's Near Earth Asteroid Rendezvous spacecraft (renamed after launch)

NEO: Near Earth Object

***p*:** Probability of an event happening ($p+q=1$)

PIC: Polygonal Impact Crater

PIGWAD: Planetary Interactive G.I.S.-on-the-Web Analyzable Database (USGS Planetary GIS Web Server)

PPR: Peripheral Peak Ring

***q*:** Probability of an event not happening ($p+q=1$)

SAR: Synthetic Aperture Radar (in this thesis referring to the radar onboard NASA's Magellan spacecraft)

THEMIS: THermal Emission Imaging System (onboard the Mars Odyssey spacecraft)

TINN: A study area on the southern near-side highlands of the Moon in the vicinity of Tranquillitatis, Insularum, Nubium, and Nectaris impact basins

USGS: United States Geological Survey

***v*:** velocity (of the impacting projectile)

v_{esc}**:** escape velocity

θ**:** impact angle (measured from the horizontal)

σ_1**,** σ_2**,** σ_3**:** maximum, intermediate and minimum principal stress axes, respectively

χ^2**:** chi-squared test

[1] However, the major problematics associated with the term "diameter" outlined by Turtle et al. (2005) should be noted here.

A STATEMENT ON THE AUTHORSHIP OF THE THESIS AND THE INCLUDED PAPERS

The foundations for this Ph.D. project about polygonal impact craters (PICs) were laid during the discussions between myself and then Lic.Phil., now Ph.D. Marko Aittola in the fall of 2001, while doing preliminary target selection for the HRSC camera, currently onboard the ESA's Mars Express spacecraft. This thesis consists of six original papers, referred to as Papers I–VI, and an introductory and summary section. The included Papers are:

Paper I:

Öhman, T., Aittola, M., Kostama, V.-P. & Raitala, J., 2005. The preliminary analysis of polygonal impact craters within greater Hellas region, Mars. In: Koeberl, C. & Henkel, H. (Eds.), Impact Tectonics, pp. 131–160. Berlin Heidelberg, Springer-Verlag.

Paper II:

Öhman, T., Aittola, M., Kostama, V.-P., Hyvärinen, M. & Raitala, J., 2006. Polygonal impact craters in Argyre Region, Mars: evidence for influence of target structure on the final crater morphology. Meteoritics & Planetary Science 41 (8), 1163–1173.

Paper III:

Öhman, T., Aittola, M., Kostama, V.-P., Raitala, J. & Korteniemi, J., 2008. Polygonal impact craters in Argyre Region, Mars: implications for geology and cratering mechanics. Meteoritics & Planetary Science 43 (10), 1605–1628.

Paper IV:

Aittola, M., Öhman, T., Leitner, J. J. & Raitala, J., 2007. The characteristics of polygonal impact craters on Venus. Earth, Moon and Planets 101, 41–53.

Paper V:

Aittola, M., Öhman, T., Leitner, J. J., Kostama, V.-P. & Raitala, J., 2009. The structural control of Venusian polygonal impact craters. Icarus, doi:10.1016/j.icarus.2009.08.004. In press. 32 pp.

Paper VI:

Öhman, T., Aittola, M., Korteniemi, J., Kostama, V.-P. & Raitala, J., 2009. Polygonal impact craters in the Solar System: observations and implications. In: Gibson, R. L. & Reimold, W. U. (Eds.): Large Meteorite Impacts and Planetary Evolution IV. Geological Society of America Special Paper. Geological Society of America. In press. 41 pp.

All the text in Papers I and II was written by me, except for the paragraph on the geologic outlines of Hellas region, for which the original draft, subsequently significantly edited by me, was written by then Lic.Phil., now Ph.D. Veli-Petri Kostama. All the PIC rim strike measurements used in all the Papers were made by me, except for the craters located in Malea Planum in Paper I (measurements by V.-P. Kostama). In Paper I, myself, M. Aittola and V.-P. Kostama all mapped polygonal craters in about two thirds of the study area. In Paper II, Mr. Matias Hyvärinen made the original mapping of polygonal craters, upon which I based the final selection of craters. Mr. Hyvärinen also made the classification of degradational stages in Paper II, roughly half of which I later corroborated.

The projection conversion of MOC-WA mosaic in Paper II was done by Lic.Phil. Terhi Törmänen. In Paper I, M. Aittola made Figs. 1 (and the Hellas part of Fig. 21 in the summary and introduction part of the thesis), 2 and 13 (reproduced here as Fig. 31), and V.-P. Kostama made the final plots of the rose diagrams (Figs. 7–12), and made also the Viking–THEMIS comparison images (Figs. 5 and 6). All figures in Paper II were made by me, except for Fig. 1 (made by M.Sc. Jarmo Korteniemi and myself as acknowledged).

The statistical analyses in Papers II and III were made by me, except for the χ^2 verification, which was carried out by M. Aittola. In Paper III, I made all the measurements and classifications, and wrote all the text except some of the paragraphs about tectonic background (mostly reproduced here in the summary and introduction part of the thesis), where input by Dr. James Dohm was important. In Paper III, J. Korteniemi made Fig. 2 (with slight editing by me), and Fig. 11 (reproduced here as Fig. 39) was made by J. Korteniemi and myself.

Paper IV was mainly written by M. Aittola. My contribution included the selection of PICs (in collaboration with, and based on a preliminary selection of potential candidates done by M. Aittola), input on the theme, structure, and conclusions of the paper, writing some of the paragraphs, and plenty of editorial comments. In Paper V the measurements of PIC rim strikes were carried out by me. My written contribution in Paper V was also substantially larger than in Paper IV, as most of the introduction, data and methods, and conclusions, as well as the sections dealing with the depths of excavation, non-correlations between PICs and tectonics, and the aspects of correlation between Venusian data and other bodies were written by me. The end result is an equal input between M. Aittola and myself.

Figures in Paper IV are by M. Aittola, and three figures from Paper IV were edited considerably by me and included here in the summary and introduction part of this thesis as Fig. 27. The geologic

mapping figure 3 by M. Aittola (with some editing by me) from Paper V is reproduced here as Fig. 34. Other figures in Paper V are done by me.

In Paper VI, the preliminary selection of lunar PICs, as well as the pre-processing of the CLA image dataset used in that part of the study was done by Mr. Mika Kallo. The text of Paper VI, as well as the figures (except Fig. 2, which is an edited version of Fig. 11 in Paper III) were made by me. The data of missions to Venus presented in Appendix 3 were originally compiled by M. Aittola, and subsequently significantly modified and updated by me.

My Licentiate thesis (Öhman, 2007a) included Papers I and II of this Ph.D. thesis, and some preliminary data from Paper III. The data presented in this Ph.D. thesis and Paper III should be regarded as clearly superseding the preliminary views and conclusions of my Licentiate thesis. Some of the sections in the introductory and summary part of this Ph.D. thesis are edited versions of the text that originally appeared in my Licentiate thesis.

I gratefully acknowledge the input, comments and ideas of all the co-authors of Papers I–VI, as well as the other contributing colleagues. This statement has been agreed upon by all the co-authors of the included Papers.

ACKNOWLEDGEMENTS

The use of Viking imagery and Mars Orbiter Laser Altimeter data obtained from NASA's Planetary Data System, the Mars Orbiter Camera and Context Camera images processed by Malin Space Science Systems, the High Resolution Imaging Science Experiment image by the Lunar and Planetary Laboratory in the University of Arizona, and the High Resolution Stereo Camera image and the preliminary HRSC DTM data by the German Aerospace Center (DLR, Deutsches Zentrum für Luft- und Raumfahrt), as well as the efforts of the respective science teams is acknowledged. This research has also made substantial use of the data provided by the Nordic Regional Planetary Image Facility in the University of Oulu, and NASA's Astrophysics Data System Bibliographic Services.

Academy of Finland; Barringer Crater Company; Division of Atmospheric Sciences and Geophysics of the University of Helsinki; ESF-IMPACT programme (Prof. Christian Koeberl); Faculty of Science of the University of Oulu; Finnish Graduate School in Geology; Jenny and Antti Wihuri Foundation; Kalle, Yrjö and Vilho Väisälä Foundation of the Finnish Academy of Science and Letters; Lapland, and North Ostrobothnia Regional Funds of the Finnish Cultural Foundation; Magnus Ehrnrooth Foundation, and the Sohlberg Delegation of the Finnish Society of Sciences and Letters; NorFA, and NordForsk Network on Impact Research (Prof. Henning Dypvik); Oskar Öflunds Stiftelse, Pallasite Press (Brian Mason travel award); Seppo Säynäjäkangas Science Foundation; the Social Insurance Institution of Finland (Kela), and the Space Institute of the University of Oulu are thanked for partial financial support to various different aspects of my impact cratering studies over the years, thus making this Ph.D. thesis possible.

The staff and the students of the Planetology Group of the University of Oulu since 1995 and in particular during 2001–2009 are thanked for creating the fun and inspiring atmosphere, and for the necessary on-the-job exercise that still vitalises both the body and the soul. Dr. Marko Aittola and Dr. Petri Kostama are particularly thanked for warmly welcoming an "outsider" into the group. Thanks also to the people in the Division of Geophysics of the University of Oulu for the hospitality and general friendliness during the years I physically spent there. The Department of Geosciences of the University of Oulu is thanked for the permission to use the photocopier. M.Sc. Hanna Lahtela, Ph.D. Paula Lindgren, M.Sc. Karla Tiensuu, and Ph.D. Evelin Verš are warmly thanked for providing references that otherwise would have been quite hard and expensive to obtain. Ph.D. Ann Bäckström is thanked for her valuable comments on some issues about fracturing, particularly in the case of Paper III. Thanks go also to the reviewers and associate editors for their major contributions to improve the form and content of the included Papers and, hence, this Ph.D. thesis.

My supervisor, docent Jouko Raitala is thanked for the continuous support and encouragement, as well as his laid-back attitude towards supervision ever since my M.Sc. thesis. My other supervisor – also since my undergraduate studies – docent Pekka Tuisku is also thanked for the liberal geoscientific supervision and his broadmindedness regarding what counts as "geosciences", as well as for the permission to publish the thesis in the Res Terrae series.

The official reviewers of this thesis, professor Alexander Basilevsky and Dr. Boris Ivanov, are warmly thanked for their constructive comments, which substantially improved the content and structure of the thesis.

M.Sc. Marko Holma, the other half of the notorious Hölman brothers, deserves my gratitude for reading and commenting on parts of an early version of the introduction and summary, for innumerable discussions over the past 14 years (occasionally related to geosciences), and for that illuminous and innovative moment when he came up with the acronym "PIC". Particularly he is thanked for still making extremely bad jokes, although selling the remains of his soul to the brutal world of exploration geology radically diminished their number.

My colleagues, particularly the ones in ESIR, are also thanked for friendship, fruitful co-work and invigorating conversations. My wholehearted gratitude is directed to my family for the general support throughout my life, and making my existence possible in the first place.

Special thanks to T.V. Smith for still keeping up the good fight, and being a perfect gentleman while doing it.

1 INTRODUCTION AND THE PURPOSE OF THE STUDY

1.1 Background and goals

"When an irresistible force meets an immovable object", an impact crater is formed (Baldwin, 1963). This is "the most fundamental of all processes that have taken place on the terrestrial planets" (Shoemaker, 1977). That basic fact that should be kept in mind in almost all geologic studies, although later processes, such as tectonics, volcanism, fluvial and eolian erosion and sedimentation have substantially obliterated the record of impacting bodies – the impact craters – on different planets, and especially on the Earth.

The number, distribution, and state of preservation of impact craters reflect the geologic history of the planet, and their morphology can reveal physical properties of the target material, as well as the mechanics of the cratering process (Wood & Andersson, 1978). With this Ph.D. study I am attempting to obtain a better understanding of this fundamental process and its consequences. The goals of this Ph.D. thesis include: 1) to increase our knowledge of Martian and Venusian (and partly also lunar) geology, in particular some of their tectonic aspects, and especially 2) to gain a deeper insight of the impact cratering process itself, particularly the interaction between crater formation and target structures. I have been aiming to these goals mainly by studying polygonal impact craters (PICs) in the regions dominated by the humungous impact basins of Hellas and Argyre, partially also Isidis, in the southern hemisphere of Mars. Other branches of PIC studies in this thesis reach the entire globe of Venus, and to a lesser extent also lunar near-side highland area characterised by the outer parts of Tranquillitatis, Insularum, Nubium, and particularly Nectaris impact basins (Wilhelms, 1987; Spudis, 1993). Thus, in this thesis, PICs are studied from two perspectives: as a poorly understood natural phenomenon, and as a tool aiding in understanding the geologic evolution of the celestial bodies in question. These two perspectives, to some extent, can be regarded as theory and its application.

Despite the importance of impact cratering, the study of impact craters and the cratering process(es) is a young branch of science. The significance of impacts has become more renowned only since the Cold War space race, especially in the aftermath of the highly successful Apollo programme in the late 1960s and early 1970s. This is regardless of the facts that lunar craters drew the attention of the first observer using a telescope for astronomical studies, Galileo Galilei, already in the autumn of 1609, and that for example one of the last great truly multi-disciplinary scientists, Alfred Wegener, explained their origin basically correctly in the early 1920s. (e.g. Wegener, 1975; Hoyt, 1987; Mark, 1987; Greene, 1998; Schultz, 1998; Galilei, 1999; Koeberl, 2001).

In the early 1980s impact geology was for a while almost in the forefront of geosciences due to the connection established between the demise of the dinosaurs and impacts (Alvarez et al., 1980; Smit & Hertogen, 1980; French, 1990; Glen, 1994; for an amusing personal account, see Alvarez, 1997). Impacts have also gained wide publicity for example during the spectacular fiery plunge of the comet Shoemaker–Levy 9 into Jupiter's atmosphere in the summer of 1994 (e.g. Orton et al., 1995), and during NASA's Deep Impact mission, which blasted a crater in the comet P/Tempel-1 in July 2005 (e.g. A'Hearn et al., 2005). Yet, despite some claims to the contrary (e.g. Reimold, 2003; French, 2004), the study of impact processes and the resulting craters can still be regarded as being very much on the sidelines of geo- and physical sciences.

The major gaps that still exist in our knowledge of impact cratering are not only due to lack of effort. The process itself presents huge obstacles to a keen mind. The pressures, temperatures and strain rates encountered in impact process are all magnitudes higher than in "ordinary" geologic phenomena (e.g. Melosh, 1989). Thus, laboratory experiments are often very difficult and quite expensive, and due to obvious necessity they have to be scaled down from the natural phenomena under scrutiny. This of course hampers their reliability. Because of the very active geologic and biologic processes on our living planet, detailed field studies of large, fresh impact craters that would be the most important ones for understanding the impact phenomenon itself, are almost impossible.

This is where the planetary perspective lends its helping hand. Resurfacing processes are substantially slower on other terrestrial planets, even on planets like Venus and Mars that have been geologically quite active recently, or still are. Therefore, the relatively pristine characteristics of impact craters of various sizes formed in different types of target material can be studied despite their almost total absence from the surface of the Earth. The downside of planetary impact studies is, however, that with the exception of some lunar impact basins (e.g. Spudis, 1993), a few very small craters on the Moon and Mars, and small blocks ejected from unknown impact sites as meteorites (e.g. McSween, 1999), no *in situ* studies of impact craters by manned or robotic missions on the surfaces of other worlds have so far been achievable. This fundamental drawback emphasises the need to have a diverse set of instruments onboard the orbiting spacecraft in order to obtain as multi-faceted view of the craters and cratering process as reasonably possible. Having said this, it ought to be kept in mind that the ground-truth data regarding impact cratering should always, as far as it is feasible, come from detailed field and laboratory studies of terrestrial impact structures, aided by sophisticated computer modelling. The most beneficial approach has of course so far been the combination of these two viewpoints, planetary and terrestrial. Applying this combination to the

study of structurally controlled polygonal impact craters is also the approach chosen for this Ph.D. thesis.

The formation, significance and utilisation of polygonal impact craters have to my knowledge not been the focus of a concise scientific study before. Literature on the subject is if not really copious but at least existing, but in the bulk of this literature the substance is fairly meagre with respect to PICs. Only a handful of previous studies have actually focused on PIC problematics. One problem has also been that previous studies have generally lacked a definition of a polygonal crater, and that no comparative studies – essential if one wishes to investigate the general PIC formation processes – have been made. This Ph.D. study aims for a small part to remedy this unfortunate shortcoming. Instead of focusing on craters on one heavenly body, three vastly different cratering environments – Mars, Venus, and the Moon, complimented by examples from earlier case studies from terrestrial impact structures – have been chosen in order to find out if there are any "universal" processes at work in the formation of PICs. With a fairly thorough review of earlier works, the use of consistent definitions and classifications, and studies concerning planetary bodies with highly divergent histories, it is hoped that a coherent image of fascinating geologic phenomena emerges. What at least becomes clear is that impact craters are not merely circular holes in the ground, but highly complex geologic structures that can also aid in the interpretation of the geologic history of the surrounding regions.

1.2 The structure of the thesis

This introductory part of the thesis is not aimed as a mere summary of Papers I–VI. Rather, I have taken the liberty of using the possibility to discuss various different topics relevant to the main themes of the thesis in a somewhat more thorough manner. This approach also enables readers not familiar with some specifics of impact cratering or the peculiarities of Martian and Venusian impact craters to hopefully understand what the craters studied in this Ph.D. thesis are like, how they differ from each other, and particularly, how and why various different characteristics of craters were used in this work. Paper VI is more of a summary of the work included in this thesis than the actual summary and introduction part of the thesis.

In Chapter 2, in addition to providing the very basics of general impact crater formation, slightly more emphasis is given to elucidate what aspects of impact cratering govern the morphology of the end result of the process, and whether or not these can lead to craters reminiscent of PICs. After a brief introduction to the Martian, Venusian, and lunar cratering environments (Chapter 3) that greatly influence the crater morphologies on these bodies, Chapter 4 provides a somewhat elaborate

geotectonic background of the Argyre study area on Mars. To a lesser extent, also some background on the geology of the greater Hellas region is included, regardless of the fact that notably less geologic analysis has been done about the polygonal craters in the Hellas region. However, as the study areas are practically continuous, and similar features of e.g. the PIC distribution in different geologic units and PIC rim orientations can be seen in both areas, the inclusion of the geologic context of the Hellas region is a necessity for understanding the PIC data. This Chapter provides the necessary background information for understanding the "application" part of this thesis regarding Mars. As the Venusian part of this thesis deals with the whole planet, a similar introduction of Venusian geology is not given, but merely the broad outlines are described in Chapter 3. Because the lunar PIC data presented in Paper VI have so far been studied only tentatively, i.e. with respect to their implications for PICs and not for the lunar geology, introduction to the geology of the TINN study area (near Tranquillitatis, Insularum, Nubium and Nectaris impact basins) on the Moon is not included in this thesis. Some general remarks, however, are included in Chapter 3.

Chapter 5 describes the major types of morphological variation of impact craters on the surfaces of the Moon, Mars and Venus. Its purpose is to emphasise the differences of these bodies from the impact cratering point of view, and it also gives further reasoning for the selection and use of some of the various morphologic criteria and variables that were used when polygonal craters were compared to the non-polygonal ones (particularly in Papers III, IV, and VI). Therefore, the contents of Chapters 2 and 5 are most likely quite familiar to readers acquainted with impact cratering and crater morphology.

Chapter 6, entitled "The structural control of impact craters", includes in some respects a fairly detailed account on previous studies regarding polygonal impact craters. Nevertheless, no effort has been made to acquire *all* the historic references to polygonal craters, not even all of the ones that are known to me. As such, Chapter 6 is not aiming to be a work on the history of impact cratering science. However, as polygonal craters form a fascinating sidetrack of the evolution of impact crater research, and touch some key questions of cratering that were heatedly debated in the past – mainly the issue of the volcanic or impact origin of (lunar) craters – and as such a compilation to my knowledge has not been published before and cannot be included in any typical research paper, it seems justified to me to include it in this thesis, even though it may be perceived as somewhat excessive compared to other sections of the thesis. A shorter review on the historical part of the study is provided in Paper VI.

Chapters 7 and 8 are fairly straightforward descriptions of the methods and results, respectively. Methods, however, are described in a bit more detail than in the accompanying Papers. Chapter 9,

on the other hand, is a fairly broad discussion on the various implications of the results, both the "theory" and "application" parts. Again, the opportunity of considering, and sometimes speculating on, the different aspects of the PIC formation and their geologic significance in a more in-depth way is taken. The summary and conclusions (Chapter 10) have been intended as a concise view to the most significant aspects of this Ph.D. thesis.

2 IMPACT CRATERING PHENOMENOLOGY

The formation of impact craters is an extremely complex series of processes, many of them currently poorly understood. It is not the purpose of this Ph.D. thesis to provide an exhaustive background on impact cratering. Thus, merely a crude outline of the main stages and processes of impact cratering are given here. For a substantially more detailed account on various aspects of impact cratering the interested reader is referred to, for instance, the excellent works by French (1998) and especially Melosh (1989), and to the numerous classic papers compiled in French and Short (1968) and Roddy et al. (1977). As, for example, shock metamorphism (e.g. Chao, 1968; French, 1968, 1998; Stöffler, 1972, 1974; Stöffler & Langenhorst, 1994; Grieve et al., 1996; Langenhorst & Deutsch, 1998) and atmospheric effects of impacts (e.g. Pierazzo et al., 1998) are for the most part unrelated to the topic of this thesis, they are not dealt with here except for a very few general comments. In addition, secondary cratering will only be briefly dealt with regarding crater morphology and its implications for this study, whereas its critical effect on dating planetary surfaces will not be discussed (e.g. Hartmann & Barlow, 2006, and references therein).

The still largely unknown mechanism(s) of multi-ring impact basin formation and subsequent modification (e.g. papers in Schultz & Merrill, 1981; Spudis, 1993) have major significance for the crustal evolution of terrestrial planets, so in some respects a bit more detailed outlook is given on that subject. As the main focus of this thesis is crater morphology and its implications, more comprehensive, yet still cursory accounts are given on the various “unusual” crater morphologies and structures.

2.1 Basic impact processes

2.1.1 Simple and complex craters

Impact crater formation is traditionally divided into three distinct stages (Gault et al., 1968). In nature, however, it is impossible to have such sharply defined boundaries between the different stages because these stages overlap forming a continuum, and several complex processes are acting simultaneously. However, for better comprehensibility of the impact craters’ formation mechanism, the division into 1) contact and compression, 2) excavation, and 3) modification stages has proven useful (Fig. 1).

In the contact and compression stage, the projectile having a cosmic velocity hits the target material, emanating a compressional supersonic shock wave into both the target material and the projectile itself (Fig. 1a). This first phase of the cratering process is also the fastest, and it ends

when the shock wave has reached the free trailing surface of the projectile. During this time the projectile has penetrated into the target to a depth roughly comparable to its diameter. (Gault et al., 1968; Melosh, 1989; French, 1998)

When the shock wave reaches any free, unconfined surface, in this case the rear surface of the projectile, a tensile rarefaction wave (also known as the release wave or the decompression wave) is formed. This marks the beginning of the excavation stage. The rarefaction wave is actually moving faster than the shock wave, because of the higher density of the shock-compressed material.[2] Further rarefaction waves form from e.g. the ground surface, and as they interact together, they form a complex rarefaction field decompressing the shocked target and projectile material. This rapid decompression of highly shocked material causes the vaporisation, melting and brecciation of the target, and also leads to the formation of the excavation flow directed upward and outward (Fig. 1c), which is actually responsible for opening the crater. (e.g. Gault et al., 1968; Grieve, 1987; Melosh, 1989; French, 1998)

Compared to "ordinary" geologic environments, the conditions during these early stages of impact cratering are extreme: pressure can be several hundred GPa's, temperature can reach 10 000ºC, and strain rates are typically over ten decades higher than normally encountered in geology, being up to 10^6/s. (e.g. Gault et al., 1968; Grieve, 1987; Melosh, 1989; French, 1998)

The crater that is formed at this point – the so called transient cavity or transient crater, or the primary crater[3] – is very different from the final crater (e.g. Shoemaker, 1960; Dence, 1968; Melosh, 1989). This bowl-shaped transient crater has a depth/diameter (*d/D*) ratio of about 1/4–1/3, apparently regardless of the size of the crater.[4] The increase of the crater's depth ceases before the increase of the diameter, hence the non-spherical shape of the cavity. When the transient cavity has also reached its final diameter, the excavation stage turns into the modification stage (Fig. 1d). Up to this point, the crater development has according to most researchers been independent of the size, i.e. all craters from the smallest simple craters to impact basins go through essentially similar contact and compression, and excavation stages. (e.g. Dence et al., 1977; Melosh, 1989)

---

[2] The supersonic nature of the shock and rarefaction waves is one of the crucial points in understanding the basics of cratering mechanics: the speeds of the waves are higher than the seismic (i.e. acoustic) velocities of the target material(s), which is often emphasised with the term *hypervelocity* impact cratering.

[3] "Transient crater" and "transient cavity" are used synonymously in this thesis unless otherwise stated, regardless of the fact that sometimes a difference is made with "transient cavity" referring to the expanding structure, and "transient crater" describing the non-existing largest extent of the transient cavity (see e.g. Croft, 1981a; and Turtle et al., 2005). This obsolete meaning of the term "primary crater" is not to be mixed with the actively used meaning, i.e. a crater formed by a direct impact from space, not by a secondary impact.

[4] It is worth noting that there has been some fairly recent debate about the reality of the "deep transient cavity" model. See, for example Osinski and Spray (2003), and Sharpton and Dressler (2003). See also the speculations by Schultz and Gault (1986) about the shallowness of large craters due to the modification of cratering flow field.

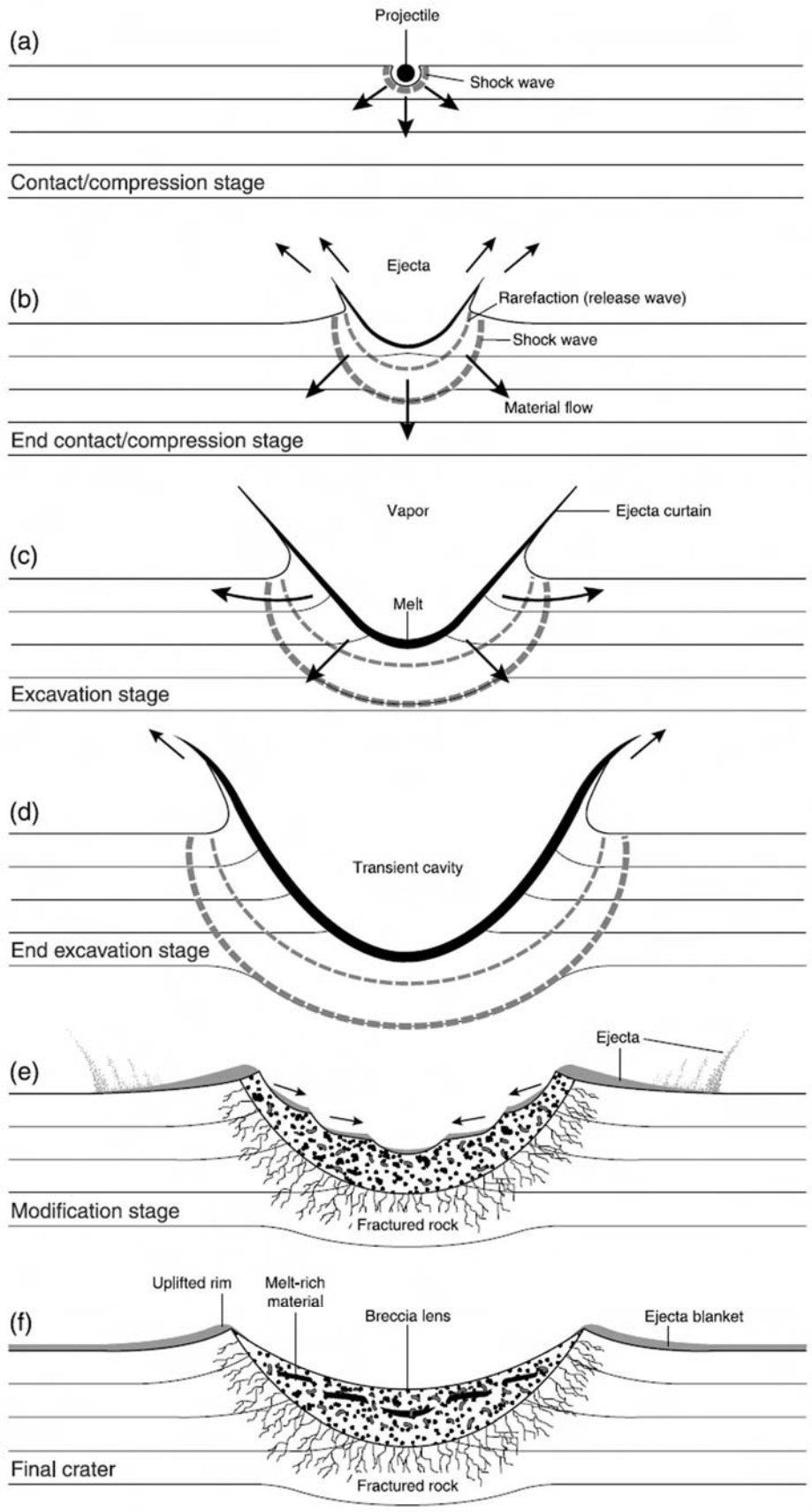

Figure 1. The formation of simple impact craters. (French, 1998)

There are two really important aspects of the modification stage of complex craters. One is the formation of central uplift, which actually began already in the late phases of the excavation stage (Fig. 2b). Second is the collapse of the transient cavity rim that grew far too high and steep in the excavation stage to be gravitationally stable (Fig. 2c$_1$). In smaller, so called simple craters (Dence, 1964; Fig. 3a) neither of the processes is particularly effective. By definition there is no central uplift in simple craters, and also the collapse of the crater rim is rather modest. Mainly the collapse of simple craters is characterised by the sliding of impact melt and breccia that were lining the inner walls of the transient cavity to the bottom of the crater (Fig. 1e). There they form a breccia lens with interspersed smaller pods of impact melt. This results in bowl-shaped simple craters with a typical *d/D* ratio of about 1/5. The transition diameter (D_{tr}) from simple to complex impact craters is mainly dependent on gravity (it is proportional to 1/*g*). Therefore, on any particular celestial body the simple-to-complex transition takes place on a roughly constant diameter, although variations in the target properties can cause some notable changes in different parts of the planet (see Chapter 4.2). (e.g. Dence, 1968; Pike, 1980a, b, 1988; Grieve, 1987; Melosh, 1989)

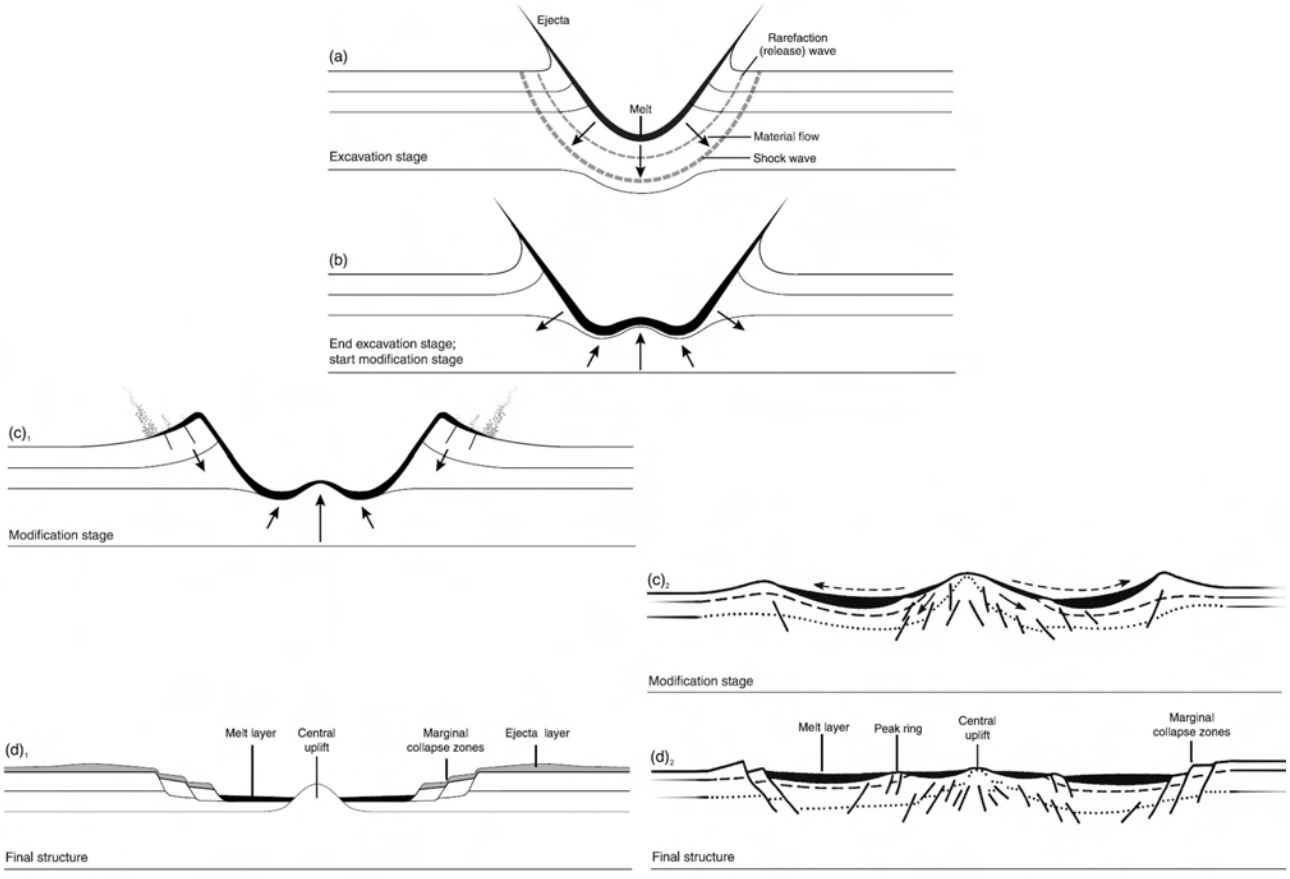

Figure 2. The formation of complex craters. Note the normal faulting on the rims. Compare with Fig. 1. (a–d$_1$ after French, 1998; c$_2$–d$_2$ adapted from Grieve et al., 1981, and Hörz et al., 1991)

The most striking feature of larger complex craters – especially when one is dealing with craters on other planets and not the terrestrial heavily eroded and buried impact structures – is the presence of central uplift that forms a well-defined topographic central peak or a group of peaks (Dence, 1964; Fig. 3b). The mechanism of the central uplift formation is still somewhat unclear, but apparently a means to temporarily reduce the strength of the rocks is necessary (see Chapter 9.8 for further discussion about the strength reduction). The amount of uplift can be most significant, as it is on the order of 0.1*D* (e.g. Boon & Albritton, 1937). When the diameter of the crater increases, the central uplift may also collapse (Fig. $2c_2$), giving rise first to so called central peak basins (known occasionally also as protobasins) with both a central peak and a surrounding ring of peaks (Figs. $2d_2$ and 3c), and then to peak-ring craters (or "peak-ring basins", particularly in the older literature) lacking the single central peak but having instead a central ring of peaks (Fig. 3d). Peak-ring craters are sometimes known also as two-ring, or double-ring basins. Neither central peak basins nor peak-ring craters were known before the Lunar Orbiter missions[5] photographed them on the Moon. (Hartmann & Wood, 1971; Wood & Head, 1976; Pike & Spudis, 1987; Melosh, 1989; Spudis, 1993)

In addition to the central structures, also the rims and crater floor of complex craters differ notably from simple craters. While in simple craters the rim modification is characterised by sliding of loose debris and meagre slumping, complex craters collapse in a much more magnificent manner. In complex craters almost the whole rim of the transient crater collapses, forming terraces in the inner wall of the rim. As is the case with the central uplift formation, the exact mechanism of the transient crater's rim collapse is still quite vaguely understood. The floor of a complex crater is very flat (except for the central peak formations of course), and in pristine complex craters covered by a sheet of impact melt. The rim collapse, crater floor uplift and the pooling of impact melt result in complex craters being very shallow landforms despite their dramatic appearance: their *d/D* ratios are typically far less than ~1/20. The collapse of the transient cavity is further discussed in Chapters 6.4.2 and 9.8. (e.g. Pike, 1980a, b; Grieve, 1987; Melosh, 1989; Melosh & Ivanov, 1999)

[5] For data regarding missions to the Moon, Mars, and Venus, see Appendices 1–3.

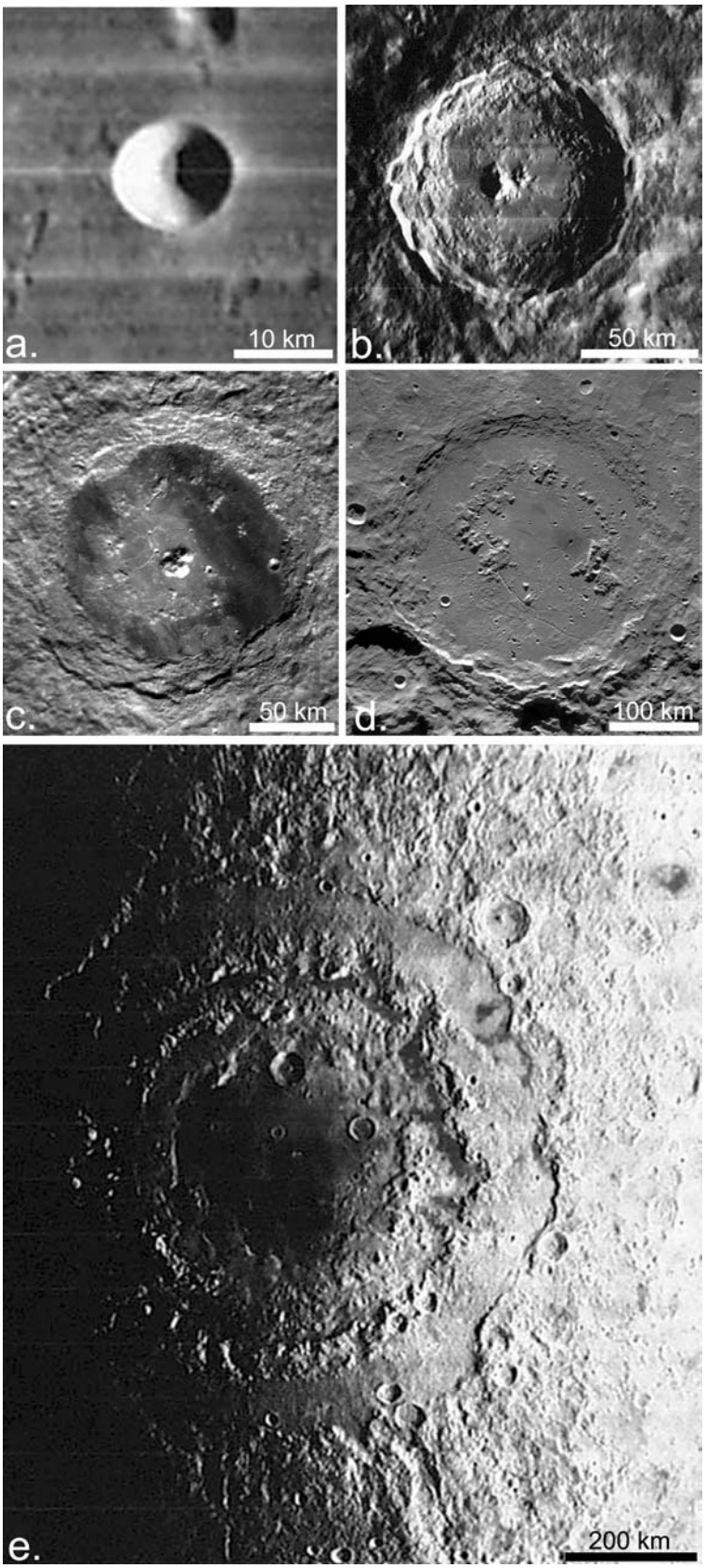

Figure 3. Morphological sequence of impact structures on the Moon. a.) Simple crater Biot, *D*=12 km (Lunar Orbiter IV 060 H1). b.) Complex crater Tycho, *D*=102 km (Lunar Orbiter IV 119 H2). c.) Central peak basin (protobasin) Compton, *D*=162 km (Clementine UVVIS). d.) Peak-ring basin (two-ring basin) Schrödinger, *D*=312 km. (Clementine UVVIS). e.) Multi-ring basin Orientale, *D*=930 km (Lunar Orbiter IV 187 M).

2.1.2 Impact basins

The largest impact structures are generally known as impact basins (Fig. 3e). The formation of impact basins, and especially of the multiple rings of the well-defined impact basins, is among the most poorly understood aspects of impact cratering (e.g. Melosh, 1989). As impact basins were in the centres of the study areas in Papers I–III and encompass the area studied in Paper VI, they are of utmost importance for this Ph.D. thesis. There are several different types of formation hypotheses for the impact basins, the most salient of which are briefly outlined in the following.

The impact basins of the Moon were first scientifically described by Grove Karl Gilbert in 1893, when he noted the so called Imbrium sculpture, i.e. radial features emanating from the Imbrium impact basin (Gilbert, 1893) seen clearly e.g. in parts of the TINN area studied in Paper VI. Especially the Imbrium sculpture is mainly caused by ejecta (Gilbert, 1893; Baldwin, 1942, 1943, 1949; Dietz, 1946; Head, 1976a), but it – as well as other similar basin features on the Moon and other heavenly bodies – also involves faults and fractures. Baldwin (1949), in addition to being fascinated by the Imbrium sculpture, described similar structures in connection with other "circular maria" too, and, importantly, noticed that the basins not only had radial features, but were also surrounded by concentric rings. As these rings are structural features, they are more persistent against subsequent degradation and obliteration than the more surficial radial features (Hartmann & Wood, 1971). (for early developments in basin studies, see also Hartmann, 1981; Hoyt, 1987; Spudis, 1993; Wilhelms, 1987, 1993)

The concept of "basin" was introduced to impact cratering studies in 1962 by Hartmann and Kuiper, initially based on their observations of the rings of the lunar Orientale basin (Hartmann, 1981). According to Hartmann and Wood (1971; see also Wood and Head, 1976), Hartmann and Kuiper's definition of a basin required the presence of both concentric rings and radial lineaments. Since then, the definition has varied very much indeed, and nowadays no generally accepted terminology exists. Essentially, the terms "basin", "impact basin", "ringed basin", "multi-ring basin", and "multi-ring impact basin" have been used almost interchangeably. On the Moon, any impact structures at least 300 km in diameter have generally been called "impact basins" (Hartmann & Wood, 1971; Wilhelms, 1987; Spudis, 1993). To add to the confusion, central-peak basins and peak-ring basins (craters) have also been called simply as "impact basins" (Grieve et al., 2008), and multi-ring impact basins merely as "craters" (Turtle et al., 2005).

However, regarding the most commonly used terms nowadays, the prefix "multi-ring" often (but certainly not always) really means observed concentric multiple ring structures, whereas mere "impact basin" can mean any very large impact structure whether or not it has observable multiple

rings. Yet, sometimes “multi-ring” can mean that the existence of rings has been inferred but not directly observed. According to an often held view, however, a true multi-ring impact basin should be characterised by at least three observable concentric rings. (Melosh, 1976, 1989; Wood & Head, 1976; Hartmann, 1981; Wilhelms, 1987, 1993)

In this thesis, the term “impact basin” refers to any very large impact structure whose assumed original diameter is clearly larger than the diameter of a peak-ring crater. A crucial distinction between peak-ring craters and multi-ring basins is that in peak-ring craters the “extra” ring forms inside the “original” transient crater, whereas in multi-ring basins they form outside it. Melosh (1989) notes that the peak-ring craters and multi-ring basins can be separated by the requirement that multi-ring basins must have at least two asymmetric escarpments, one of which may be the rim of the original crater, whereas peak-rings typically have symmetric profiles.

The volcanic modification hypothesis was among the earliest ideas for multi-ring basin formation. According to the hypothesis, the basin starts out as a large crater, but subsequently surface melting commences or an intrusion occurs beneath the crater, and subsidence along ring faults takes place. However, the greatest weakness of the hypothesis is that according to observations, the basin rings form very fast after the excavation, which clearly contradicts the hypothesis of ring formation by post-impact subsidence (model reviewed by Melosh, 1989). A slightly later model by Hartmann and Wood (1971) explains the peak-rings, as well as the inner wrinkle ridge rings of multi-ring basins as results of volcanism along ring fractures. Also this version of the volcanic modification model is generally regarded as clearly obsolete.

Unlike the volcanic modification hypothesis, the megaterrace hypothesis (Head, 1974, 1977) of basin formation does not assume any important post-impact processes. According to this view, impact basins are basically very large craters. The main difference between megaterrace basins and ordinary complex craters is that instead of the normal complex crater rim terraces, a huge megaterrace forms in the modification stage *outside* the original crater rim, when the structurally uplifted rim collapses and moves inwards, diminishing the apparent diameter of the original crater, which is assumed to be marked by the intermediate basin ring. However, this hypothesis does not adequately explain the asymmetry of the Orientale-type rings which have a steep inward-facing escarpment but a gentle backslope, nor the existence of more than one ring beyond the original crater rim. (Head, 1974, 1977; Melosh, 1989; Spudis, 1993)

Croft’s (1981a, b) basin formation hypothesis is somewhat similar to the megaterrace hypothesis. It is also an example of the so called proportional growth type of formation models. In the proportional growth models the multi-ring basins are a natural outcome of a large enough impact,

and no drastically different conditions are needed to form the basins. Thus, impact basins according to these hypotheses are merely very large complex craters, and are formed by a mechanism fundamentally similar to complex craters. (Croft, 1981a; Spudis, 1993)

The main difference between the megaterrace (Head, 1974, 1977) and Croft's hypotheses is that Croft (1981b) explains the ring formation initiating not in the uplifted rim, but notably beyond it. Croft's idea (1981a, b) suffers from the same inconsistencies with the observations as the megaterrace hypothesis (Melosh, 1989).

It can perhaps be mentioned here that personally I find Croft's (1981a, b) model difficult to accept, because an entity called "strength crater" lies at the heart of it. It is defined by a zone extending substantially beyond the final crater rim (of craters of all sizes; see e.g. Fig. 6 in Croft, 1981b), where the target rock is supposed to be "uplifted and unsupported" and "dissociated", in other words, brecciated. As rocks beyond the rims of terrestrial simple and complex craters are merely fractured but not brecciated to any major extent, Croft's (1981b) model seems unwarranted.[6] A further complication for understanding Croft's model emerges from the varying definitions (1981a, b) of the strength crater, e.g. in Croft (1981a) the "strength crater" is defined as being equal to "true crater", which generally refers to the crater form seen when the breccia lens is removed, and not something beyond the rim. These varying definitions make Croft's model (1981a, b) very difficult to follow.

The nested crater hypothesis for impact basin ring formation (Wilhelms et al., 1977; Hodges & Wilhelms, 1978) is very similar to the ideas of concentric (nested) crater formation (see below). Briefly, the hypothesis explains the basin rings as emerging from interaction between the cratering flow and the boundaries between rheologically different layers in the (Moon's) interior. Hence, the basin ring diameters are mainly dependent on the thicknesses of the layers in the lunar interior, and not proportional to the basin diameter. Thus, the long-held but highly controversial $\sqrt{2}D$ ring-spacing "rule"[7] (e.g. Hartmann & Wood, 1971; Hartmann, 1981; Pike, 1985; Pike & Spudis, 1987; Spudis, 1993, and references therein) is not explained by the nested crater hypothesis (Melosh, 1989).

The so called tsunami model, whose strongest proponent has been Ralph Baldwin (e.g. 1949, 1963, 1974, 1981; also Wilhelms, 1987), suggests as the name of the model implies that the basin rings could be likened to rather surficial massive crustal tsunami waves that have somehow "frozen" in

[6] Unless of course Croft's (1981b) "dissociated" would refer to coherent but fault-bounded blocks of bedrock several tens to hundreds of meters in diameter.
[7] According to the $\sqrt{2}D$ rule, the diameter of a basin ring is the diameter of the ring immediately inside of it multiplied by $\sqrt{2}$. Conversely, the ratios of basin ring diameters are $\sqrt{2}$ or multiples of it.

the crust. Although there are some arguments for the hypothesis – for example it may perhaps explain the $\sqrt{2}D$ "rule" – its physical plausibility is doubtful (Spudis, 1993). For example, the tsunami model (an impact into liquid mantle) would predict the presence of both concentric and radial extension features in the multi-ring basins of Ganymede and Callisto (McKinnon & Melosh, 1980). These, however, are not observed. It seems that the tsunami model does a better job in describing the crater collapse and hence the formation of peak-rings in a qualitative way, rather than in describing the formation of the rings in multi-ring basins (Melosh, 1989).

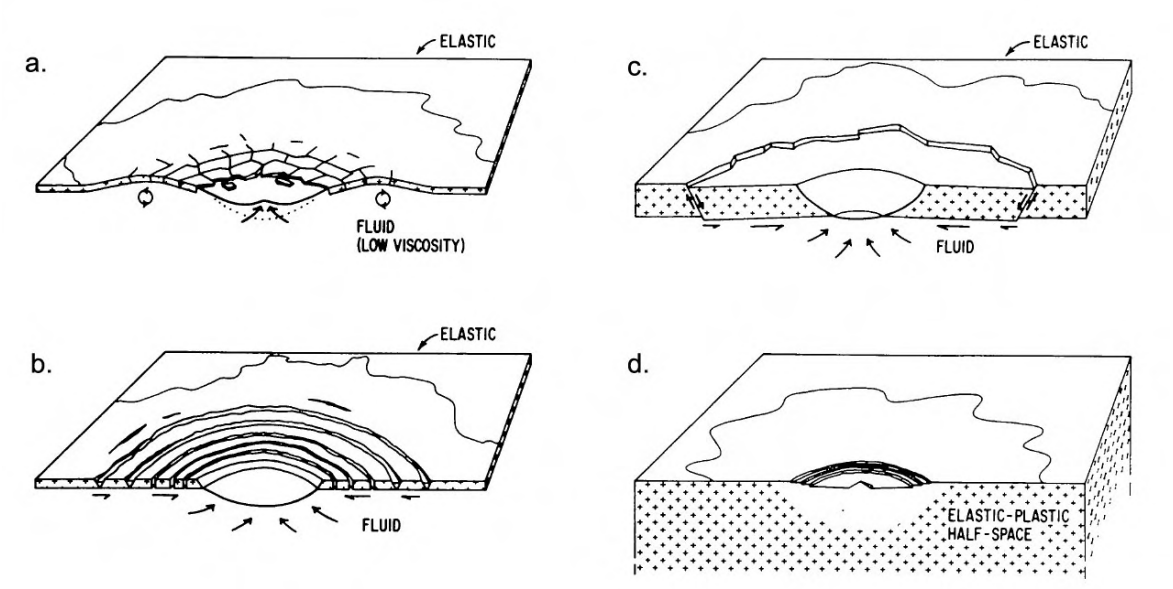

Figure 4. A schematic model of impact basin ring formation as a function of lithospheric thickness and asthenospheric viscosity. a.) Very thin lithosphere and truly liquid asthenosphere. Basin forms as oscillation of the transient cavity region (tsunami waves), probably possible only in planets with magma oceans. b.) With asthenosphere close to solidus temperature and a thin lithosphere, the lithosphere fails brittlely and/or plastically, forming multiple rings as seen on the Jovian moons Ganymede and Callisto. c.) In the case of thicker lithosphere (e.g. the Moon), only one or few rings form. d.) If the lithosphere is thick enough, normal complex crater formation takes place. After McKinnon (1981), modified from McKinnon & Melosh (1980).

The most modern and physically justified of the widely cited multi-ring impact basin formation hypotheses is the ring tectonic model (Fig. 4), developed by Melosh and McKinnon (1978; McKinnon & Melosh, 1980; McKinnon, 1981; Melosh, 1989). The basic idea of the model is a simple and realistic one. The model assumes that the target is layered so that a more rigid layer overlies a more deformable one. In practical terms, it is essentially a question of the thickness of the lithosphere overlying a more or less fluid asthenosphere. If the thickness of the lithosphere[8] is very large compared to the depth of the transient crater, nothing out of the ordinary cratering process takes place. If, however, the transient crater penetrates the lithosphere, the fluid asthenosphere

[8] In the crater collapse sense; see Melosh (1989) for a discussion.

flows inwards to partially fill the crater. This also pulls the lithosphere inwards, causing an extensional fracture to form in the lithosphere. The end result is an irregular but roughly circular asymmetric scarp, which may follow the pre-existing lines of weakness in the lithosphere. It seems that for more than one asymmetric scarp ring to form, a layer with higher viscosity must underlie the low-viscosity "channel". If the lithospheric thickness is very small compared to the depth of the transient cavity, then multi-ring basins with exceedingly many rings form. Such basins can be seen on the Jovian moons Callisto and Ganymede. (e.g. McKinnon & Melosh, 1980; McKinnon, 1981; Melosh, 1989)

Melosh (1989) doubts the existence of true multi-ring basins on Mars (and Mercury), and concludes that therefore the thickness of the Martian lithosphere at the time of the basin impacts was larger than on the Moon, Ganymede or Callisto. Although the existence or non-existence of true multi-ring basins on Mars is not really essential for this Ph.D. thesis, it ought to be noted that Mars has gone through a highly complex and active geologic history since the formation of the large impact basins, and for example erosion rates have been far greater than on the Moon. Therefore relatively subtle features like the rings of multi-ring basins are expected to be far more subdued on the surface of Mars than on the Moon. As briefly described in Chapter 4.3, many researchers who have carried out detailed mapping projects have observed several multi-ringed basins on the Martian surface, and although the suggested ring diameters sometimes vary substantially, most of those researchers agree on the reality of multiple rings in at least some of the Martian basins.

One relevant aspect of impact basins is their post-impact modification (e.g. Melosh, 1978, 1989; Freed et al., 2001). Basins are topographic lows and hence massive deposits of e.g. volcanic and fluvial material are easily accumulated in them. Especially the deposition of volcanic materials is strengthened by the presence of highly fractured crust, forming possible conduits for magma. Basically the loading of the basin causes compression in the centre of the basin and tension in the surroundings (Melosh, 1978, 1989; Freed et al., 2001). The post-impact loading of the basins and the consequent modification of the surrounding crust mainly by formation of different fractures is slightly further discussed in Paper III and below in Chapter 2.2.

Currently it seems that the ring tectonic theory is the most plausible candidate for explaining the formation of multi-ring basins. However, other theories are still worth considering, and the truth may lie in some of the theories combining aspects of the different models (e.g. Schultz et al., 1981). As Spudis (1993) pointed out, it should be kept in mind that "the formation of multi-ring basins is a complex process involving cratering mechanics, volcanism, tectonism, ballistic sedimentation, and endogenic modification. Thus, to speak of basins as 'large craters' is a vast oversimplification."

2.2 Craters, basins and fractures

Especially the Martian part of this thesis involves fractures[9] surrounding and originating from impact basins, and to notably lesser extent from somewhat smaller impact craters. The impact-induced fracturing (in a broad sense, including fractures emanating from all stages of impact crater formation and subsequent modification) is in general fairly well-known, although especially the basin-sized impacts pose a slight problem for investigations, because their fracture patterns are beyond direct field observations or experimental studies.

In impact craters the small-scale brecciation and fracturing are mostly caused by the tensional rarefaction wave, not by the shock itself (e.g. Melosh, 1989). This is simply because the tensile strength of rocks is substantially smaller than the compressive strength (e.g. Melosh, 1989). The fracture patterns surrounding the impact basins, however, stem from both the impact itself (mainly modification stage) and the post-impact loading and subsequent modification of the basins (e.g. Melosh, 1976, 1978, 1989; Freed et al., 2001; see below).

The impact-induced fractures in and surrounding terrestrial impact craters and more eroded impact structures have been observed with different methods and several highly varying scales, including direct counting and measuring from outcrops (e.g. Bischoff & Oskierski, 1988; Brandt & Reimold, 1995; Bäckström, 2005; Kumar, 2005; Kumar & Kring, 2008), visual remote sensing studies (e.g. Bischoff & Oskierski, 1988; Brandt & Reimold, 1995; Gurov & Gurova, 1982; Gurov et al., 2007), and a large selection of geophysical and petrophysical methods (reviewed in Pilkington & Grieve, 1992; see also e.g. Aaloe et al., 1976; Henkel, 1992; Brandt et al., 1998; Pesonen et al., 1999; Bäckström, 2005).

Fractures have also been observed in extraterrestrial craters: Baldwin (1978) suggested a linear dependence between the maximum length of radial fractures on the Moon and the diameter of the host crater or basin. This may or may not be close to the truth, but what is more generally accepted is that the zone of impact-induced fracturing, including the formation of larger faults as well as the smaller scale fractures, may extend up to one crater diameter away from the crater rim (e.g. Aaloe et al., 1976; Gurov & Gurova, 1982; Pilkington & Grieve, 1992; Brandt et al., 1998).

The fracture patterns surrounding impact craters are of course quite varying in detail due to local and regional differences. Some general features, however, can be seen in most cases, namely the radial and concentric fracture patterns. For example, in the 18 km diameter El'gygytgyn impact crater in Russia, straight radial fractures predominate, but concentric ones exist too (Gurov &

[9] Throughout this Ph.D. thesis the term "fractures" can mean joints, faults, fractures or any such generally roughly vertical structures of the target material, regardless of their exact characteristics or origins.

Gurova, 1982; Gurov et al., 2007). Similar results have also been obtained from the ~13 km diameter Deep Bay impact crater in Canada. There the system of concentric fractures is well developed, and an accompanying map depicts prominent radial fractures as well (Innes, 1964).

In the 23 km diameter Haughton impact structure in Canada, concentric fractures appear up to 18 km away from the crater centre (Bischoff & Oskierski, 1988), and in the heavily eroded Siljan (diameter ~52 km) impact structure in Sweden the most evident fractures in the periphery of the currently visible structure are the concentric ones (Hode et al., 2003). However, they are still actually within the rims of the original crater. In addition to natural simple and complex craters, also experimental cratering is known to result in similar radial and concentric fracture patterns surrounding the craters (e.g. Fulmer & Roberts, 1963; Curran et al., 1977; Roddy, 1977a). Thus, the presence of such patterns is well-established.

The fractures surrounding impact craters are generally rather shallow features. However, the fractures that are more essential to the topic of this thesis, i.e. those associated with impact basins, are much deeper. As was briefly mentioned in Chapter 2.1.2, the lunar basins' different fractures have been known for quite some time. Similar patterns surrounding the Martian basins are known as well, and in addition to tectonics, they have important implications for the hydrologic evolution of Mars (e.g. Schultz et al., 1982; Schultz, 1985; Wichman & Schultz, 1989; Rodríguez et al., 2005). Recent studies of the Caloris basin on Mercury indicate that even though the evolution of an impact basin can be notably different from the better known lunar basins, the radial and concentric patterns of graben are still present (Murchie et al., 2008). The following is based mainly in the studies of H. J. Melosh, and the ring tectonic model of the multi-ring basin formation in the case of "medium" lithospheric thickness (see above) is the premise of the following short discussion.

The basin-radial fractures are thought to form because of the actual impact process. Their formation, however, does take a substantial amount of time, so if "when things stop falling" (French, 1998) is taken as the end of the modification stage, then the radial fractures are a post-impact feature of the basins. However, when the modification phase of a structure as huge as a "typical" impact basin can be said to be finished is of course mainly just a matter of opinion. In any case, the basin-radial fracturing is initially induced during the early stage of the basin modification. The impact removes an enormous amount of mass, and thus a negative load is formed in the interior of the basin. To compensate for this negative load in the basin's interior, up-doming and inward flow of the astenosphere beneath the entire basin occurs. This leads to tensional hoop stresses about the basin, and consequently to the formation of radial fractures. These fractures appear as large basin-radial graben, as well as smaller joint sets, and extend several basin radii from the basin. It

should be noted that the fractures formed by this mechanism are radial only outside the basin, whereas the fractures formed inside the basin should be concentric. (Melosh, 1976, 1989).

As noted above in Chapter 2.1.2, the concentric rings that define the multi-ring basins are formed as a consequence of the astenosphere flowing inwards and pulling the lithosphere along with it. However, there is also another mechanism to form basin-concentric fractures. This is, by any definition, a post-impact process. It involves the loading of the basin by the accumulation of vast deposits of material. In the best-studied case of lunar multi-ring impact basins this material is basaltic lava, forming the mare that occupies the central part of many lunar impact basins. This accumulation of basaltic lava, sometimes accompanied by mantle uplift, results in mass concentrations (mascons), which were discovered in the late 1960s due to anomalies in the orbits of the Lunar Orbiter spacecraft (e.g. Wilhelms, 1987, 1993).

Inside a mascon basin the stresses are compressional, leading to the formation of roughly concentric wrinkle ridges in the lunar mare-filled basins. However, outside the basin the near-surface radial stress becomes extensional, and concentric normal faults (or strike-slip faults; see below) should form (Melosh 1978, 1989; Freed et al., 2001). Therefore, it seems quite clear that both impact craters and larger basins are surrounded by an extensive zone of fractures formed during different stages and by different processes, but oriented radial and concentric to the host structure.

The mechanism of basin loading responsible for the basin-concentric fracturing should, in principle, lead also to strike-slip faulting, which is essentially the same thing as the formation of a conjugate set of shear fractures (Melosh, 1978; Freed et al., 2001). According to the earlier, fairly simplified models and approximations (e.g. Melosh, 1978), the zone of conjugate shear fractures was supposed to occur inside the zone dominated by concentric fractures. Unequivocal evidence of the presence of such structures around the lunar basins has, nevertheless, been lacking. This was known as the "strike-slip faulting paradox" (Freed et al., 2001).

More recent studies have resulted in a resolution of the paradox. According to the study of Freed and co-workers (2001), the zone where the stresses required for strike-slip faulting are supposed to occur is rather narrow. The width of this zone is also dependent on the planetary radius, and the smaller the radius, the narrower the zone of the strike-slip faulting. And importantly, although the stress geometry itself would be inducive for the conjugate shear fracture formation, the stresses in large part of the zone may well be too weak to cause actual rock failure (Freed et al., 2001). Hence, it appears to be quite "normal" that convincing observational evidence for the conjugate sets of shear fractures surrounding impact basins is still lacking. The tentative hypothesis that polygonal

craters might perhaps indicate the presence of such a fracture pattern surrounding the Argyre and Hellas basins on Mars is briefly discussed in Paper III and Chapter 9.5.

2.3 Factors governing the crater shape

There are a number of parameters that affect the idealised crater formation sequence, which is based on a vertical impact of a single solid projectile into a homogenous target, as described above. Crater shape especially in geologically active planets like Mars and the Earth is also later distorted by post-impact modification – including fluvial and eolian erosion and sedimentation, mass-wasting, other impacts, volcanism, various glacial and periglacial processes, and faulting and other tectonic processes – but this falls beyond the aims of this Ph.D. thesis (see Fig. 3 in Paper II for an example of craters modified by post-impact processes). As this thesis focuses on the implications of crater morphology, a brief review of the key aspects affecting the crater shape already when the crater is formed is imperative. Some of the special morphological features characteristic of Martian and Venusian impact craters are dealt with in Chapter 5, and the effect of roughly vertical structural inhomogeneities (fractures) is discussed in some detail in Chapters 6 and 9.

2.3.1 Impact angle

Shallow impact angle (θ) is probably the most studied "deviation" from the idealised impact process. This is not surprising, as 45º is the most common impact angle (Gilbert, 1893; Shoemaker, 1962), and strictly vertical impacts don't occur in nature at all.[10] A lot of studies have focused on the distribution of ejecta in oblique impacts (e.g. Gault & Wedekind, 1978, Schultz, 1992; Anderson et al., 2003; Herrick & Forsberg-Taylor, 2003; Anderson & Schultz, 2006), which is warranted by the fact that impact's obliquity is first and most convincingly seen in the distribution of ejecta pattern. With even slightly oblique impacts, concentration of ejecta in the downrange side of the crater can be seen. When θ decreases to below 45º, a wedge-shaped "forbidden zone" where no ejecta is deposited forms first in the uprange side of the crater, then also downrange (except on Venus where the dense atmosphere complicates the matters; see Herrick & Forsberg-Taylor, 2003). This evolves into the typical butterfly pattern of ejecta in the highly oblique impacts (Fig. 5).

The changing shape of the ejecta blanket presents a relatively straightforward scenario, whereas variations in the shape of the crater itself as a function of impact angle has been the subject of much controversy (e.g. Gault & Wedekind, 1978; Schultz, 1992; Ekholm & Melosh, 2001; Herrick &

[10] Because most impacting bodies orbit the Sun nearly in the ecliptic plane (i.e. have orbits with low inclinations), the actual impact probabilities have been suggested to be skewed towards shallow incidence angles (Gault & Wedekind, 1978).

Forsberg-Taylor, 2003; see also Schultz & Lianza, 1992; Schultz et al., 1994; Bland et al., 2002; Cione et al., 2002). Currently it seems that in addition to the shape of the ejecta blanket, the only reliable indicators of obliquity are a depressed uprange crater rim (θ<~25º), a saddle-shaped crater rim with lower up- and downrange rims compared to crossrange rims (θ<~15º), and the ellipticity of the crater occurring in very shallow angle impacts (θ<~10º; Herrick & Forsberg-Taylor, 2003), as well as the "blowout" of the downrange rim in the case of extremely shallow impacts (Chappelow & Herrick, 2008). In terrestrial impact structures, it may perhaps be possible to infer the direction of the impact through a detailed structural analysis (Scherler et al., 2006; for an early notion about the importance of the structures with respect to impact angle, see Boon & Albritton, 1936), but such methods of course are not applicable to craters on other planets. Also the presence of a central ridge that sometimes forms in the most shallow angle impacts seems to reliably indicate the orientation of the projectile's trajectory (Herrick & Hessen, 2006; however, see Hale (1979) and Hale & Head (1979)).

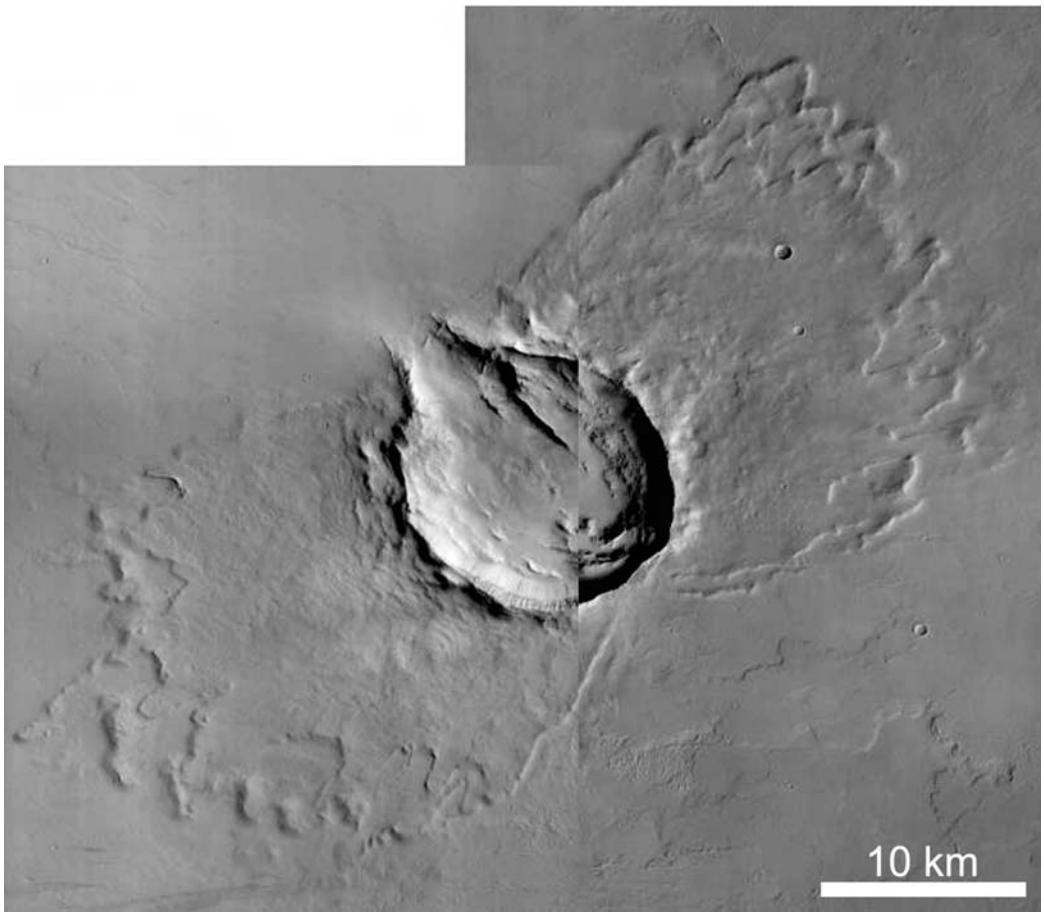

Figure 5. A Martian elliptical crater with butterfly ejecta blanket, located at 9.2°N 80.4°W. Note also that the ejecta blanket ends in ramparts (Chapter 5.4.2). A mosaic of parts of CTX images P20_008880_1915_XN_11N080W and P12_00587_1916_XN_11N080W_4. North is to the top.

Other, previously often used indicators of an oblique impact, like the shape, size and position of the central peak or peak-ring, or the steepening of the internal slope of the uprange crater rim, have been shown to have no straightforward correlation with the angle or even the direction of the impact (Ekholm & Melosh, 2001; Herrick & Forsberg-Taylor, 2003; McDonald et al., 2008; however, see the recent results by Goeritz et al., 2009). Apparently also the *d/D* ratio remains unchanged by decreasing impact angle (Gault & Wedekind, 1978; Herrick & Forsberg-Taylor, 2003), although Mars may perhaps present an exception (Herrick & Shanteau, 2001). Martian craters also maintain an elevated uprange rim even at lowest impact angles (Herrick, 2005; Herrick & Hessen, 2006), contrary to the laboratory experiments (Gault & Wedekind, 1978). Melting and vaporisation of the target material, as well as the fate of the projectile, however, are highly depended on θ (Pierazzo & Melosh, 2000a; see also Pierazzo & Melosh, 2000b).

2.3.2 Clustered impacts

The projectile itself is also one factor governing the cratering process, mostly independent of the heavenly body where this takes place. Clustered impacts caused by projectiles disrupted typically during their flight through the atmosphere, or possibly in space e.g. due to tidal forces just before the impact, produce major changes to the shape of the crater.

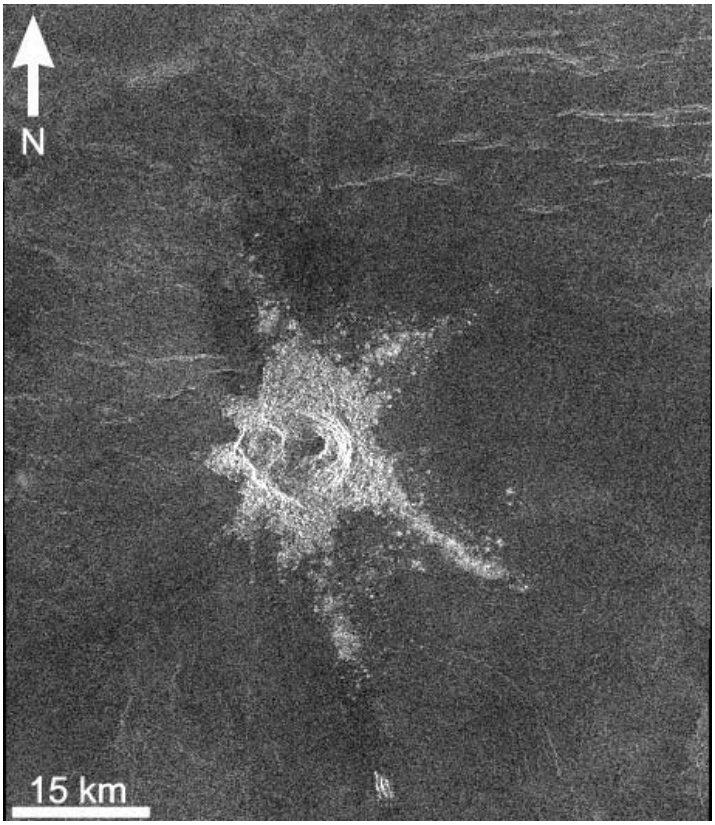

Figure 6. An irregular, non-polygonal crater Xenia on Venus (*D*=12.4 km, 30.3°S 249.2°E), formed by a clustered impact. Note also the partial dark halo surrounding the bright ejecta blanket. Magellan SAR image.

If the projectile is dispersed to only a few fragments that remain so close to each other that they are neither producing a crater field, nor impacting as a relatively tight cluster, a crater with an irregularly shaped rim may form (Fig. 6). Normally such a rim has a notably different outline than the topic of this thesis, i.e. polygonal craters (discussed more thoroughly in Chapters 6 and 9). However, in some cases of smaller craters on the surface of Venus, irregular rim caused by a loosely clustered impact can make a reliable identification of a Venusian (also known as Cytherean) polygonal crater impossible (see Chapter 7.2). This kind of a rim shape originating from a clustered impact also differs from small-scale irregularities caused by post-formational slumping of the rim. (Passey & Melosh, 1980; O'Keefe & Ahrens, 1982; Schultz & Gault, 1985a; Phillips et al., 1992)

If the projectile remains as a tighter cluster, the result can be a shallow-floored crater with a ring depression surrounding the floor. In addition to being shallow, the floor can also be hummocky and present a subtle central mound, whereas the rim may have an exaggerated relief compared to an ordinary impact with a solid projectile. Fragmented cometary projectiles can also give rise to multiple ring structures in the interior of the crater. These of course are not to be mixed with genuine multi-ring basins. Clustering also affects the ejecta pattern, as clustered impactors apparently do not produce a butterfly-shaped ejecta blanket typical for oblique single-impactor impacts (see above). Instead, oblique clustered impacts form a fan-shaped ejecta pattern that extends downrange from the crater. (O'Keefe & Ahrens, 1982; Schultz & Gault, 1985a; Phillips et al., 1992; Korycansky & Zahnle, 2004; Cochrane & Ghail, 2006)

2.3.3 Projectile velocity and shape

It is commonly assumed for simplicity that in the formation of impact craters only the amount of the projectile's kinetic energy matters, whereas its constituents, mass and velocity, are inseparable *($E_k=½mv^2$)*. However, there are some indications that the effects of impact velocity alone may actually be preserved in the shape of the crater that is formed in the impact. According to laboratory experiments, slower impact velocities (or, to be precise, longer penetration times of the projectile into the target) seem to favour the production of shallower craters (Schultz & Gault, 1986). It has also been hypothesised, that for relatively low-velocity impacts (v<15 km/s) the projectile's size could be inferred from the diameter of the "central ringed-peak",[11] and thus mass and velocity could be separable (Schultz, 1988). However, these ideas should at the moment be regarded as speculative (see e.g. Herrick & Lyons, 1998). Equally interesting, yet debatable are Schultz's (1987, 1988) ideas according to which central pit craters (see Chapter 5.3) could be due to low-velocity impacts

[11] Apparently referring to a peak-ring.

(see also Croft, 1983, for speculations about the velocity's effect on crater formation on icy satellites).

In addition to the projectile's velocity, also its shape has some relevance for the crater morphology, at least in the case of laboratory-scale low-velocity (v<2.1 km/s) impacts into granular targets. When the projectile's diameter/length ratio increases, shallower craters result (Schultz & Gault, 1985b). The projectile's shape has also been shown by 2D numerical modelling to bear notable significance to the shock pressures and temperatures experienced by the projectile: irregular shape can lead up to over 80% of the projectile to experience shock pressures under 1 GPa (Pierazzo, 1999).

2.3.4 Target effects: topographic variations and layering

Pre-existing topographic variations of the target may also significantly influence the structure and morphology of the final crater (e.g. Gifford & Maxwell, 1979; Gifford et al., 1979). Small craters tend to be elongated in the downhill direction, whereas in the uphill direction they may experience enhanced slumping. Larger craters, on the other hand, have generally been regarded as remaining fairly circular despite topographic differences. The slump terraces close to the higher topography, however, are wider than the terraces in other parts of the crater. In addition, recent studies show that asymmetries in the Chicxulub crater can be due to topographic variations (Collins et al., 2008; Gulick et al., 2008; Schultz, 2008). According to Eppler et al. (1983), the shape of about 20% of complex lunar highland craters are affected by topographic variations. Thus, the topography of the target is not a minor constituent of crater morphology. (Melosh, 1989)

The main theme of this thesis is the effect of target material's more or less *vertical* planar inhomogeneities to the crater structure and shape. This is dealt with in some detail in Chapters 6 and 9. In addition, also planar *horizontal* differences in the target clearly deviate the crater morphology from the classic simple and complex crater morphologies. Such layered targets are common both in planetary and terrestrial environments. With different relative thicknesses of a soft cover (e.g. regolith, or a layer of poorly consolidated sediments and/or water) overlying a more coherent substratum, various "aberrant" crater shapes can form. In simple craters, these shapes are craters with flat floors, craters with shallow central mounds, and so called concentric craters (Quaide & Oberbeck, 1968).

Concentric craters are also observable in the complex crater size, and they are characterised by a relatively deep inner crater, surrounded by an outer crater of notably shallower excavation (Fig. 7). An "inverted sombrero" is an often-used allegory (e.g. Melosh, 1989). Concentric craters have been

observed at least on the Moon (Quaide & Oberbeck, 1968), the Earth (e.g. Ormö & Lindström, 2000; Abels, 2004), and Mars (Gilmore, 1999; Ormö & Muinonen, 2000; Ormö et al., 2004).

Despite the fact that there are a number of different factors influencing the morphology of an impact crater, it should be stressed here that none of the processes outlined above should "normally" result in craters that would have straight segments in their rims (nevertheless, see Chapter 5.5.2 about the so called peripheral peak rings). However, in the case of some very eroded and tectonically modified impact structures a polygonal shape can be observed, but any connection to possible *primary* polygonality has been lost. A good example of such an impact structure is the ~9 km diameter Lumparn in Åland, southwestern Finland. Its present day morphology is that of a rhomboid-shaped bay, but that has been interpreted to result entirely from substantial post-impact tectonic modification[12] (Abels, 2003). In addition, when dealing with planetary data sets the lighting conditions and image resolution can cause complications (see Chapters 8.6 and 9.2), and thus, for a work like this Ph.D. thesis, it is imperative to be able to account for the "normal" variations in crater morphology.

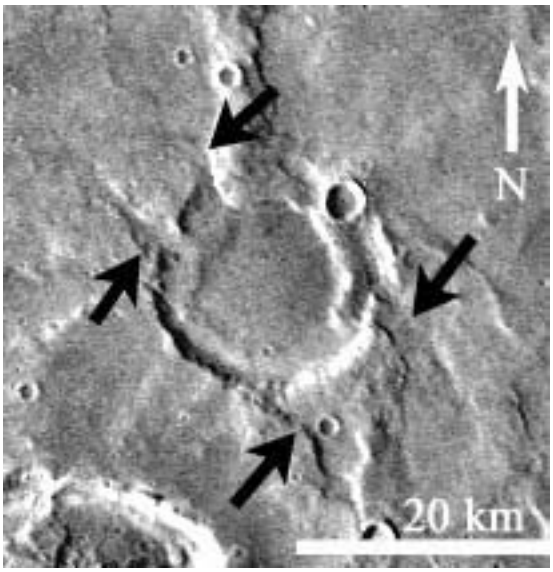

Figure 7. A Martian concentric crater, located at ~39ºN 12ºE and most likely formed when a shallow sea covered the area. Note the deeper inner crater and more shallow outer crater. The arrows point to resurge gullies, where sediment-laden water surged back to the crater, eroding the gullies. Viking MDIM 2.0 image.

[12] Dramatic non-polygonal examples of tectonically deformed impact structures include the ~54 km diameter Charlevoix, and ~250 km diameter Sudbury, both in Canada, as well as the 39 km diameter Balch crater on Venus. Charlevoix and Balch are faulted/rifted, whereas Sudbury is mainly compressed.

3 THE ENVIRONMENT OF LUNAR, VENUSIAN AND MARTIAN IMPACT CRATERING

Planetary properties like gravity, presence or absence of an atmosphere, surface temperature, and the structure and composition of the target have a major influence on the cratering process. Thus, the environment of lunar, Venusian and Martian impact cratering is briefly characterised below. A more detailed look at the geology of the main research area of this thesis – Argyre and Hellas regions of Mars – are given after the general aspects, in Chapter 4.

3.1 The Moon

The Moon is the only extraterrestrial body where manned field geological and geophysical studies have been carried out. In addition to these six Apollo landings, three unmanned Luna landers provided additional samples from the Moon (Appendix 1). These studies have been complimented by extensive remote sensing campaigns, as well as study of lunar meteorites (e.g. McSween, 1999). Thus, the Moon is by far the best-known body in our Solar System, except of course for the Earth.

The Moon was most likely formed by a collision of a roughly Mars-sized body with the proto-Earth, and the subsequent accretion of the impact debris (e.g. Cameron, 2001, and references therein). It orbits the Earth at an average distance of about 384 400 km, and as is typical for large satellites in the Solar System, the Moon revolves around its own axis in approximately the same time as it orbits around the Earth, i.e. in a month. The diameter of the Moon, 3476 km, is about a quarter of Earth's size, and the surface gravity is only a sixth of the Earth's gravitational pull. Hence, the escape velocity from the atmosphereless Moon is a mere fifth of the terrestrial one. The main planetary characteristics of the Moon, as well as Mars and Venus, are summarised in Table 1. (Lodders & Fegley, 1998)

The lunar surface is characterised by a dichotomy. Although the low-lying flat plains of dark maria constitute only 16% of the entire lunar surface, they make up 30% of the near side (Wilhelms, 1987; Vaniman et al., 1991a). Mostly the maria are located within impact basins. The basins themselves are distributed approximately randomly on the lunar globe, but the thinner crust on the near side (e.g. Zuber et al., 1994) enabled lava extrusion through the fractured basin floors, forming extensive lava flows. The sparsely cratered maria are generally basaltic in composition, and were derived from partial melting of the lunar mantle. Major basaltic volcanism lasted at least from 3.9 Ga to 3.1 Ga, and since about 3 Ga ago the Moon has been volcanically practically inactive. (Hörz et al., 1991)

Based on studies of partially flooded craters, the thickness of the maria is on average about 400 m, but it varies a lot (De Hon, 1979). DeHon and Waskom (1976) found that for example in the northern part of mascon-hosting Nectaris basin the mare is about 1000–1250 m thick with the central areas possibly having even up to 3–4 km of mare basalts, whereas much of Tranquillitatis lavas are on average less than 500 m thick. Similarly, large parts of Mare Nubium lavas are less than 500 m thick, but thicken to 500–1000 m towards south (DeHon, 1979; see also Hörz et al., 1991).

Table 1. Average values of some key planetary properties of the Earth, Mars, Venus, and the Moon. Most values are taken from Lodders & Fegley (1998), other references may give slightly varying values of some properties. Some lunar data are taken from Vaniman et al. (1991b). Impact velocities (often highly variable depending on the reference) are from Bottke & Melosh (1996), Bottke et al. (1994, cit. Bottke et al., 2000), and Ivanov (2001). The reported ± distance of the Moon is its distance from the Earth, and its orbital velocity is the velocity with respect to Earth.

	Earth	Mars	Venus	Moon
Equatorial diameter [km]	12 756	6 794	12 104	3 476
[Earth=1]	1	0.53	0.95	0.27
Distance [AU]	1	1.52	0.72	1 ± 0.0026
Orbital velocity [km/s]	29.8	24.1	35.0	1.023
Escape velocity [km/s]	11.2	5.0	10.4	2.38
Surface gravity (g) [m/s^2]	9.8	3.7	8.9	1.62
[Earth=1]	1	0.38	0.90	0.17
Asteroidal impact velocity [km/s]	17.2	13.6	19	16.2
Surface temperature [°C]	15	-59	460	-153 / 107
Surface pressure [hPa]	1013	6	92 000	~ 0
Atmospheric composition	78.1% N_2 21.0% O_2 0.9% Ar	95.3% CO_2 2.7% N_2 1.6% Ar	96.5% CO_2 3.5% N_2	(Ne, H_2, He, Ar)

The lunar highlands, or terrae, are notably different from the maria. The highland crust probably formed 4.6–4.3 Ga ago (Taylor et al., 1991) when plagioclase-rich rocks floated on top of lunar magma ocean (Vaniman et al., 1991a). The most significant highland rock types are ferroan anorthosites, and various Mg-rich rocks from dunites to sodic ferrogabbros (Taylor et al., 1991). One consequential aspect of the lunar rocks, also for impact processes, is their total lack of water (e.g. Taylor et al., 1991).

As there is no atmosphere to stop the projectiles of any sizes, the lunar rocks, especially the highland varieties, are commonly heavily brecciated. The brecciation leads to the formation of regolith, which is only a few metres thick on maria, and seldom exceeds 10–20 m in the highlands

(Taylor et al., 1991). However, regolith in underlain by megaregolith, which is essentially impact basin ejecta. It is generally believed to be at least 2–3 km thick, and fracturing and brecciation in highlands can reach the depth of 10 km or even more. This also means that sound (P-wave) velocities are highly reduced in the upper lunar crust, being <0.5 km/s in the uppermost regolith and reaching constant ~7 km/s at the depth of about 25 km. (e.g. Head, 1976b; Hörz et al., 1991, and references therein)

Based on recent radar studies of crater ejecta, there is a marked change in the thickness of megaregolith in the southern near-side highlands. At around 48°S, the thickness changes from about 1.5 km in the north, to about a kilometre more in the south. This change, attributed to ejecta deposits from Solar System's largest and deepest generally accepted impact basin, the South Pole – Aitken basin (e.g. Spudis et al., 1994), almost concurs with the southern border of the TINN area studied in this thesis. (Thompson et al., 2009)

3.2 Venus

Venus is the brightest object in the sky after the Sun and the Moon, and has often been regarded as Earth's sister planet. It circles the Sun along its highly circular orbit at about 0.72 AU, and thus is the planet that comes closest to the Earth. Venus is very close to Earth also in size-related characteristics: it has an equatorial diameter of 12 104 km (~95% of Earth), surface gravity of 8.87 m/s^2 (~90% of Earth), and escape velocity of 10.4 km/s (~93% of Earth; Lodders & Fegley, 1998). Average asteroidal impact velocity is also very similar to Earth, about 19 km/s (Bottke et al., 1994, cit. Bottke et al., 2000; McKinnon et al., 1997), and thus considerably higher[13] than on Mars.

Despite similarities with the Earth, there are some very notable peculiarities in the Venusian cratering environment. The average surface temperature of Venus is about 460°C due to the runaway greenhouse effect, and the thick CO_2-dominated (~96.5% CO_2, ~3.5% N_2) atmosphere yields an average surface pressure of 92 000 hPa (i.e. 92 bars, almost a hundred times the terrestrial surface pressure; Lodders & Fegley, 1998).

Another important difference from the terrestrial and Martian cratering environment is the practically total lack of water in the Venusian crust, at least currently. Changing the temperature from 0°C to 300°C normally reduces rock's strength by ~25% (Herrick & Phillips, 1994a). However, the elevated PT-conditions of the Venusian surface alone are not enough to make the surface material behave in a more ductile manner. On the contrary, the total lack of water in the form of hydrated minerals – induced by the high temperature – actually increases the creep strength

[13] Although the velocity itself is not that much higher, it has a major influence on the energy, because $E_k = \frac{1}{2}mv^2$.

of basaltic rocks (Mackwell et al., 1998). For comparison, the Venusian surface PT-conditions correspond to terrestrial greenschist facies metamorphism, but the lack of water and high partial pressure of CO_2 most probably make the metamorphic processes extremely slow (Barsukov, 1992). In any case, these extreme conditions are the ultimate reason for some fascinating and unique features observed in Venusian impact craters (see Chapter 5).

Venus' surface appears geologically very young when compared to the surfaces of e.g. the Moon, Mercury or Mars. It is generally believed that Venus went through a global resurfacing event or events, the latest of which ended rather suddenly ~750 (McKinnon et al., 1997), ~500 (e.g. Phillips et al., 1992; Schaber et al., 1992), or perhaps only ~300 Ma ago (Strom et al., 1994; Basilevsky et al., 1997). However, there are also studies of volcanically embayed impact craters indicating that substantial resurfacing has taken place during the last few hundred million years, and therefore a notably large part of the surface of Venus may have been resurfaced much more recently than ~500 Ma ago (Herrick & Sharpton, 2000).

Pertaining to the youthful appearance of Venus, there are two main models of the Venusian geologic history, namely the directional and non-directional models. The former supposes that there were series of epochs of vast volcanic activity, separated by stages of tectonism. These volcanic and tectonic events were global in scale, and thus similar geologic units are generally of the same age (e.g. Basilevsky et al., 1997). The latter model assumes a more complex geologic past, with various different styles of volcanism and tectonism forming the plains and tectonic structures, occurring throughout the Venusian history, but varying from place to place. Hence, this non-directional model implies that the specific age relations of the geologic units can only be applied locally, not over vast areas or globally (e.g. Guest & Stofan, 1999). The question which of these two models actually describes the "truth" more accurately remains at the moment an open question.

Despite a large number of different tectonic structures on the Venusian surface, Venus seems to completely lack Earth-like plate tectonic activity, or at least there is no evidence of it preserved (Solomon et al., 1992). Volcanism is the main process shaping the Venusian surface, and most of the planet is dominated by vast volcanic plains. This leads to the characteristically unimodal shape of the Venusian hypsometric curve, compared to the bimodal curves of the Earth (continental crust vs. the ocean floor) and Mars (southern highlands vs. the northern plains). These volcanic plains cover about 70% of the Venusian surface (Tanaka et al., 1997).

Based on *in situ* surface analyses by Venera 8, 9, 10, 13 and 14, and Vega 1 and 2 landers (see Appendix 3), the Venusian volcanic plains are known to be, in broad terms, generally basaltic in composition with some local variations, formed as partial melts of the mantle (Basilevsky et al.,

1985; Barsukov, 1992, and references therein). However, as impact-induced radar-dark parabolas (see Chapter 5.4.3) cover the Venera and Vega landing sites, it is quite possible that the geochemical analyses do not represent the surficial lavas of the landing site, but actually some material below the apparent surface, excavated by the parabola-forming impact (Basilevsky et al., 2004).

Due to the protective atmosphere, there most probably is not such an impact-induced regolith layer on Venus as on the Moon, but on several landing sites the rocks can be seen to be layered (e.g. Basilevsky et al., 1985), likely due to the air-fall beds of the dark parabolas (Basilevsky et al., 2004). At least on Venera 13 and 14 landing sites the material is also very porous, having a porosity of 50–60% (Basilevsky et al., 1985).

Venus' surface is rich in tectonic structures, and especially wrinkle ridges are highly typical on the volcanic plains. Other highly prominent manifestations of tectonism are the numerous volcano-tectonic features. In addition to volcanoes and calderas, volcano-tectonic features include coronae, novae (also known as astrae) and arachnoids (e.g. Aittola, 2003; Kostama, 2006). These are characterised by radial and concentric linear tectonic structures including graben, ridges and undifferentiated lineaments.

A target type notably different from the dominating volcanic plains is the tessera terrain. Tessera represents in general the oldest preserved Venusian surface, and it is characterised by a highly deformed material, often with at least two sets of intersecting tectonic structures (e.g. Barsukov et al., 1986; Ivanov & Head, 1996; Basilevsky et al., 1997). It covers about 8–9% of Venus' surface (Ivanov & Head, 1996; Tanaka et al., 1997). In addition to the plains, the volcano-tectonic features and tessera terrains, the Cytherean surface hosts rift valleys, fracture, ridge, and mountain belts, as well as occasional channels and dune fields (Tanaka et al., 1997). And, naturally, there is a fresh population of impact craters and other impact-related features. Their major morphologic characteristics will be briefly outlined in Chapter 5.

3.3 Mars

Mars has been extensively studied by numerous unmanned space missions, including six successful landers (see Appendix 2). These have mostly been American, but also space probes from the Soviet Union and currently also from the European Space Agency (the Mars Express mission) have provided the scientific community a wealth of data covering the whole surface of the planet, as well as its atmosphere, very weak magnetosphere and two satellites, Phobos and Deimos. The picture

that emerges from these data is one of a planet half the size of the Earth, with a geologic past that almost rivals the Earth in versatility.

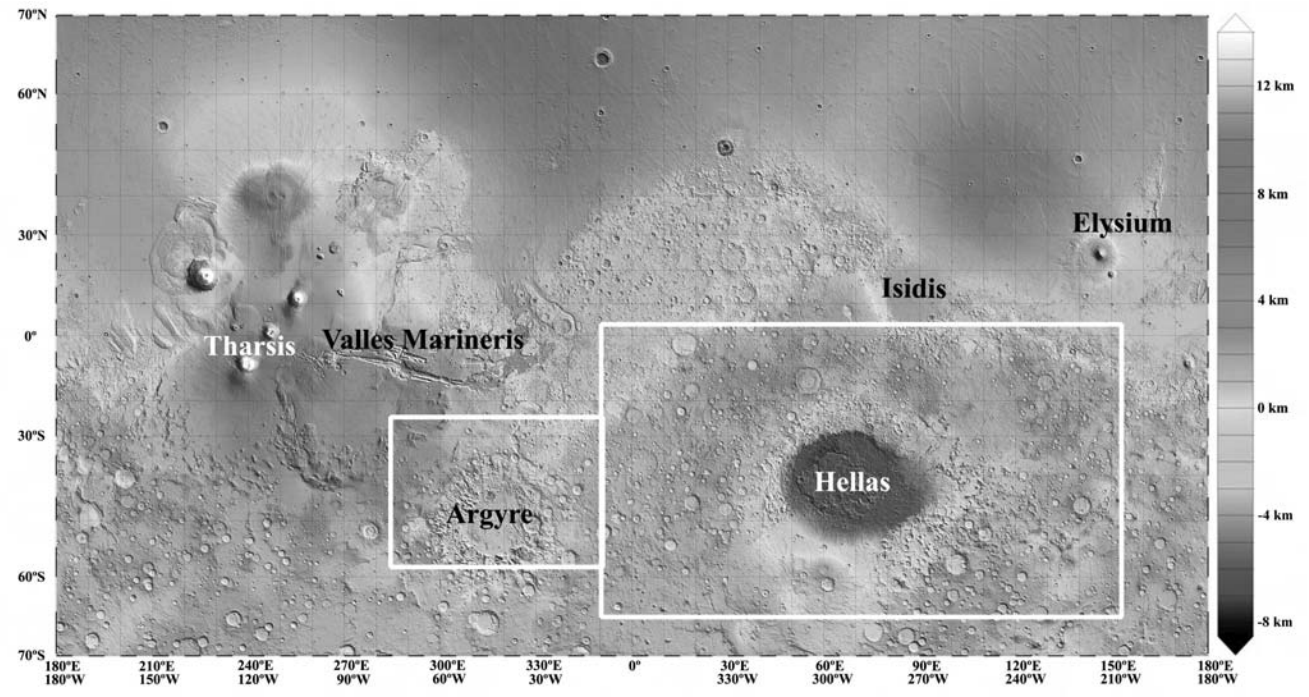

Figure 8. MOLA topography of Mars. The white boxes indicate the areas of Mars studied in this thesis. Note the crustal trichotomy of northern lowlands, heavily cratered southern highlands, and the Tharsis bulge.

Mars orbits the Sun in a quite elliptical orbit at an average distance of 1.52 AU. It has an equatorial diameter of about 6794 km and gravitational acceleration (g) of 3.69 m/s^2 – slightly more than a third of Earth's gravitational acceleration. The escape velocity of Mars is only about 5 km/s, and thus larger impacts can eject material to space, some of it reaching the Earth as Martian meteorites (e.g. McSween, 1999). (Lodders & Fegley, 1998)

Mars is currently essentially a one-plate planet, although magnetic signatures have hinted to possible primitive plate tectonics early in the planet's history (Acuña et al., 1999; Connerney et al., 1999, 2001, 2005; Purucker et al., 2000). However, the surface of Mars is far from homogenous. The most notable feature is the crustal dichotomy: the northern hemisphere is characterised by generally flat, low-lying sparsely cratered plains (but see Chapter 5.5.1 about "stealth" craters in the northern plains), whereas the southern hemisphere hosts ancient heavily cratered highlands, as well as humungous impact basins, Hellas, Isidis and Argyre basins being the most apparent ones (e.g. Wood & Head, 1976; Fig. 8). The volcanic Tharsis bulge, with the largest volcanoes in the Solar System, has prompted some authors to describe Mars as having crustal *tri*chotomy. Although Tharsis is not the only major volcanic centre of the planet, it certainly surpasses other volcanic rises, the most important of which is Elysium Mons with its surrounding Elysium Planitia. A closer look

at the main geologic features of the Argyre and Hellas regions studied in this Ph.D. thesis are given below in Chapter 4. (e.g. Carr, 1999)

The planet's smaller size and thus smaller amount of available energy is the fundamental reason why the major endogenic processes more or less ceased in Mars by the end of Early Amazonian epoch (e.g. Head et al., 2001), perhaps about 1.4–2.1 Ga ago (Hartmann & Neukum, 2001). For comparison it should be kept in mind that on Earth this means Meso–Paleoproterozoic, and that from the three main periods of Martian history, the Amazonian is the youngest. The earliest period, Noachian, was the time of the formation of the heavily cratered highlands and the impact basins. This was followed by the Hesperian period, which was dominated by volcanism and the formation of the massive outflow channels. (Tanaka et al., 1992; Head et al., 2001)

In addition to gravity and approximate impact velocity, which in the case of Mars is about 12–14 km/s for asteroidal impacts (Bottke & Melosh, 1996; Bottke et al., 1994, cit. Bottke et al., 2000), there are two major circumstances affecting the impact process that differentiate Mars from other large cratered bodies like the Moon or Mercury. These are the presence of volatile material in the crust, and the atmosphere. Although liquid water is unstable on the surface of Mars at the present day conditions – average surface temperature is about -60ºC (e.g. Lodders & Fegley, 1998; Carr, 1999), and the CO_2-based atmosphere has an average surface pressure of only ~5–6 hPa (Kieffer et al., 1992; Lodders & Fegley, 1998; about 1/200 of the average terrestrial surface pressure) – there is ample evidence that some liquid, most likely water, has flown on the surface and ponded in depressions for relatively long periods of time (e.g. Carr, 1999; Head et al., 2001, and references therein; see Chapter 4).

The Martian atmosphere has also been notably thicker, possibly even thick enough to cause rains to fall. In addition to remarkably contributing to the complexity of the impact process itself, water – both liquid and ice – and thick atmosphere affect the craters in efficiently enhancing their obliteration rate due to increased erosion. This also makes Mars an interesting object for comparative planetology, since the conditions are much closer to Earth than for instance on the Moon. By studying the Martian craters we can gain insight into the formation and structure of terrestrial impact craters that would be quite hard, or often impossible, to acquire otherwise.

The knowledge about Martian rocks is based on Martian meteorites, surface analysis by six successful landers, and abundant remote sensing data from orbiters (Appendix 2). There is regional and local variation in the composition of the Martian crust, but overall it can be described as only weakly altered basalt. However, due to areal differences, the observed range of rock types spans from ultramafic rocks to silicic dacites and granitoids. Although Mars clearly has had large amounts

of water on its surface, the subsurface aqueous alteration has been quite limited, both in intensity and duration. The dominant type of alteration on Mars has been low-pH acid-sulphate weathering, possibly preceded by a period of alteration in alkaline or neutral-pH water-rich environment. (Soderblom & Bell, 2008)

The polar regions of Mars are dominated by layered deposits tens of metres thick, as well as CO_2- and water-ice polar caps (e.g. Soderblom & Bell, 2008). Layered sedimentary rocks prevail on large areas on Mars, as seen in orbital and rover imagery (e.g. Malin & Edgett, 2000; Bell et al., 2008). Due to the complex geologic history and the shielding atmosphere, Mars probably does not have a global layer of Moon-like impact-produced regolith, and thus layered but fractured sedimentary rocks dominate large parts of the surface, instead of lunar-type fragmental impact breccias. In addition to impact cratering, the effects of weathering and eolian processes, as well as volcanism are most significant for the Martian regolith formation and evolution (Hartmann & Barlow, 2006; Taylor & Baloga, 2007; Golombek et al., 2008).

The estimates of the regolith and megaregolith thicknesses on Mars are still fairly poorly constrained. Gilmore (1999) used small concentric craters (see Chapter 2.3.4) to estimate the maximum regolith thickness to be on the order of 100 metres. Direct rover observations indicate that at least up to 10 m thick impact-generated regolith is present (Golombek et al., 2008). Martian highlands probably have a (mega)regolith ~2 km thick (Taylor & Baloga, 2007).

However, according to Hartmann and Barlow (2006), there are prominent differences in the regolith thicknesses between different areas. According to them, in the Noachian highlands, the regolith may be from 50 m to hundreds of metres thick, and is commonly consolidated or cemented by ice and evaporites. The impact-fractured zone in Noachian highlands extends from 150 m down to depths of several kilometres. In the Amazonian plains, on the other hand, the regolith is only 8–18 m thick, and the fractured zone is 24–54 m deep. This also affects the launch of secondary projectiles: all fresh craters larger than 45 km in diameter have secondary craters around them – irrespective of the target material. In the case of smaller craters, however, fresh craters in Noachian highlands with presumably thick regolith are surrounded by far less secondary craters than similar craters in younger, more competent volcanic target material. Similarly, the collection of identified Martian meteorites is strongly biased towards young, <1.3 Ga volcanic rocks (e.g. McSween, 1999; Hartmann & Barlow, 2006). It seems apparent that regolithic material cannot be launched from Mars in big enough chunks to form numerous large secondary craters or to reach Earth as Martian meteorites. Such differences in the target material are present also in Hellas and Argyre regions, outlined in the following Chapter. (Hartmann & Barlow, 2006)

4 GEOLOGIC BACKGROUND OF HELLAS AND ARGYRE REGIONS

The regions of Mars studied in this thesis are the so called greater Hellas region (2°N−66°S, 8°W−208°W; Paper I) and Argyre region (26ºS–58ºS, 10ºW–74ºW; Papers II & III). These regions cover a substantial and practically continuous portion of the heavily cratered southern highlands of Mars (Fig. 8). Thus, their geologic background is provided here as one study area. Because much more detailed studies were carried out in the Argyre region, substantially more emphasis is given to that area, although the Hellas study area is notably larger. In the following, the main geologic units, the impact basins (a major source of fracturing), as well as the principal processes affecting the study area will be briefly outlined. The focus is on the basins and the various tectonic aspects, because other processes have only minor relevance for this thesis. As the study area in the Venusian part of this Ph.D. work was the whole planet, a brief outline of the main global geologic features is given in Chapter 3.2. Some brief notes on the geology of the TINN study area of the Moon are given in Chapter 3.1.

4.1 General characteristics

The most prominent features in the study area are the Hellas and Argyre impact basins themselves, which were the reason for choosing this area for study. The sparsely cratered interiors of the basins, i.e. the plains of Argyre Planitia and Hellas Planitia cover much of the central parts of the Argyre and Hellas regions. However, most of the area can be described as old highland materials. In the west, the study area extends to Aonia Terra, and in the east it reaches Promethei Terra and the westernmost part of Terra Cimmeria. Terra Sabaea and Tyrrhena Terra represent the majority of the area north from the Hellas basin. A large portion of the study area between the Hellas and Argyre basins is covered by Noachis Terra, which is the type region of heavily cratered Noachian highlands. (Scott & Tanaka, 1986; Greeley & Guest, 1987)

The northwestern section of our study area partly covers the volcanic plains of Thaumasia and Bosporos Plana, and the central northern part our study area is on the verge of the volcanic plains of Syrtis Major Planitia. Elysium Planitia, one of the major centres of Martian volcanism, reaches the northeastern corner of our study area. The border between Elysium Planitia and Terra Cimmeria also marks the global dichotomy boundary. The type region for Hesperian period, the volcanic plains of Hesperia Planum with its paterae and outflow channels, is also within the area studied in this thesis (e.g. Tanaka et al., 1992). So is the northern part of another volcanic plains region with old paterae, Malea Planum. (Scott & Tanaka, 1986; Greeley & Guest, 1987)

Thus, although largely concentrated in the cratered highlands that superficially could be regarded as rather monotonous, the study area represents a very versatile part of the Martian surface. The study area includes indications of a complex interplay between impact cratering, volcanism, tectonism, and glacial, fluvial, lacustrine, as well as eolian processes. The versatility of the area is also manifested by the diversity of the crater morphologies, more closely described in Chapter 5 (with respect to craters in Hellas region, see e.g. Aittola et al., 2002; and Korteniemi et al., 2005, 2006).

4.2 The geologic units

The planetary-scale geologic units as defined by Scott & Tanaka (1986) and Tanaka & Scott (1987) were used in the Argyre part of this study for testing whether the target material has an influence on the polygonal crater formation. Hence, a bit closer look at these units is in order. These geologic units also give a good overview of the type of the terrain and thus the nature of the target material, therefore giving crucial perspective on understanding the distribution of polygonal craters (as well as of course impact craters in general). For the Hellas part of the study area, a rough outline of the distribution of similarly defined units (Greeley & Guest, 1987) is given for comparison. For a more detailed and recent geologic map of the Hellas region, the reader is referred to the map by Leonard and Tanaka (2001).

The oldest unit in the study area is the Noachian "hilly unit" Nplh. It is present almost exclusively on the "rim" of the Argyre and Isidis basins. The unit was formed when the basin formation uplifted old highland volcanics and impact breccia. Of approximately the same age and similar origin is the "basin-rim unit" Nh_1 which forms the rim of the Hellas basin. (Scott & Tanaka, 1986; Greeley & Guest, 1987)

Most parts of the Argyre area are covered by two heavily cratered Noachian units, Npl_1 and Npl_2. In Hellas area Npl_1 is dominates the western part, whereas the occurrence of Npl_2 is patchy. The "cratered unit" Npl_1 is actually the most widespread geologic unit in the southern highlands of Mars. It has been interpreted as materials formed during high impact flux, being most likely a mixture of lava flows, pyroclastic material and impact breccia. The younger Npl_2, or the "subdued crater unit", has been interpreted as thin lava flows and eolian deposits partly covering the rocks underneath. (Scott & Tanaka, 1986; Greeley & Guest, 1987)

"Etched unit" Nple is only present in the central part of Argyre's floor, whereas the "dissected unit" Npld forms patches here and there in the Argyre part of the study area (Fig. 9). However, in the northern part of the Hellas area, the "dissected unit" is very widespread. Both Nple and Npld are very similar to and have the same age as the "cratered unit" Npl_1, but the "dissected unit" has been

eroded by fluvial processes, and the "etched unit" by eolian and minor fluvial processes with additional decay and collapse of ground ice. (Scott & Tanaka, 1986; Greeley & Guest, 1987)

The "ridged unit" Nplr is at least partly younger than the "cratered unit" Npl_1. It is present in the eastern part of the Argyre area, continuing to the western part of the greater Hellas area. The "ridges" are interpreted mostly as normal faults, and only a minority of them are either volcanic constructs or compressional features. "Older fractured material" Nf forms only a small unit in the northwesternmost part of our study area (Melas and Nectaris Fossae), and is characterised by complexly oriented faults and destroyed crater outlines. (Scott & Tanaka, 1986; Greeley & Guest, 1987)

Hesperian units are present in the centre of the Argyre basin, in the western and northwestern part of the Argyre area, on the floor of Hellas basin, as well as of course on the type region of the Hesperian period, Hesperia Planum, located in the eastern part of the greater Hellas region. "Ridged plains material" Hr covers the volcanic plains of Hesperia, Bosporos, and Thaumasia Plana, with a minor occurrence at the floor of the Argyre basin. Like the related "ridged unit" (Nplr), the ridges in the "ridged plains material" have been interpreted as either volcanic constructs of low-viscosity lava, or tectonic features. The "smooth unit" Hpl_3 is formed by lava flows and eolian deposits covering much of the underlying rocks, and is present mainly on the floor of Argyre, as well as on its western side. (Scott & Tanaka, 1986; Greeley & Guest, 1987)

"Younger fractured material" unit Hf forms only a small patch in Melas Fossae, but it is much more widespread immediately west of our study area. The floor of the Hellas basin is mainly occupied by "ridged plains floor unit" Hh_2 and "dissected floor unit" Hh_3. Malea Planum, south from the Hellas basin, is mostly covered by the "dissected member" of the "Amphitrites Formation" (Had), which has been interpreted as ridged plains material (Hr) modified by fluvial channels. (Scott & Tanaka, 1986; Greeley & Guest, 1987)

Amazonian units are only rarely present in our study area. Their most notable occurrence is the "channeled plains rim unit" Ah_5 on the eastern rim of the Hellas basin, interpreted as eroded volcanic or eolian deposits. In addition, the deposits of the outflow channels (see below) are Amazonian in age. (Scott & Tanaka, 1986; Greeley & Guest, 1987)

4.3 The impact basins

Hellas impact basin is about 2000–2300 km in diameter and 8–9 km deep, and it has been suggested to have been caused by an oblique impact with a trajectory from northwest (e.g. Wilhelms, 1973; Wood & Head, 1976; Leonard & Tanaka, 1993, 2001; Tanaka & Leonard, 1995; Mohit & Phillips,

2007). A recent crater counting study suggests a possible age of 3.99 ± 0.01 Ga for the Hellas basin formation (Werner, 2008). The Isidis impact basin immediately to the north of and partially within our study area (e.g. Wilhelms, 1973; Wood & Head, 1976), is perhaps slightly younger, 3.96 ± 0.01 Ga (Werner, 2008). For comparison, Frey (2008) suggests about 4.1 Ga for the age of Hellas, and about 3.8 Ga for Isidis. Isidis is also somewhat smaller, with a diameter of about 1500 km, and a depth of about 3 km (Mohit & Phillips, 2007).

The more intensively studied sections of the study area surround the Argyre impact basin. The basin, with a diameter of over 1200–1500 km and a depth of about 4 km, is located southeast of the Tharsis rise and south to southeast of Valles Marineris (e.g. Wilhelms, 1973; Wood & Head, 1976; Tanaka et al., 1992; Mohit & Phillips, 2007). Argyre appears less degraded than the Hellas and Isidis basins (e.g. Spudis, 1993). Argyre has not been regarded substantially younger than Hellas or Isidis (Hiesinger & Head, 2002), and Frey (2008) dates Argyre impact at about 4 Ga. However, another recent crater dating implies that it is only 3.83 ± 0.01 Ga old, roughly 150 Ma younger than Hellas and Isidis (Werner, 2008). In addition to age, the difference in appearance may be related to the thicker crust and deeper Moho in Argyre: the crust excavated by the Argyre impact had a minimum thickness of 23.7 km, compared to only 5.8 km and 6.6 km in Isidis and Hellas basins, respectively (Neumann et al., 2004; see also Mohit & Phillips, 2007). Another difference is that in Argyre the excavation of the crust was concentrated to the centre of the basin, and the crust thickens rapidly at distances over 350 km from the centre.

Several different ring diameters have been suggested by different researchers (e.g. Wilhelms, 1973; Pike & Spudis, 1987; Schultz & Frey, 1990) for all three major impact basins in the study area, i.e. the Hellas, Argyre and Isidis basins. In these studies, the numbers and diameters of the different rings vary greatly, partly of course due to differences in the data sets used, but also because of notably different interpretations. For example, Wilhelms (1973) reports only one ring (2000 km) for Hellas, Schultz and Frey (1990) mapped three (1350–4200 km), whereas Pike and Spudis (1987) note seven different rings with diameters ranging from 840 km to 5500 km. Similar differences are present with the other basins, too.

In addition to Hellas, Isidis and Argyre, previous researchers (e.g. Schultz & Glicken, 1979; Schultz et al., 1982; Pike & Spudis, 1987; Schultz & Frey, 1990) found also other basins within or close to our study area. Holden basin (see Fig. 2 in Paper III; not to be mixed with the large, superposed Holden crater), centred at 25ºS 32ºW and having a diameter of 580 km (Schultz et al., 1982; Pike & Spudis, 1987), lies mostly inside the larger Ladon basin (see Fig. 2 in Paper III; centred at 18ºS 29ºW), which probably has a diameter of about 975 km (Schultz et al., 1982). However, Ladon's

rings as large as 1600 km and 1700 km in diameter have also been mapped (Pike & Spudis, 1987; Schultz & Frey 1990). The Ladon basin is also exceptionally deep, about 1.5 km, for an old basin of its size (however, Mohit & Phillips (2007) use a diameter of only about 440 km for the Ladon basin).

Schultz et al. (1982) identified a possible impact basin south of Hephaestus Fossae, just north of our study area's northeast corner at 10°N 233°W. If their proposed ring diameters of 500 km and 1000 km hold true, it can have implications for our study. Another large impact basin may lie in the southern part of the Hesperia Planum (32°S 255°W), where Schultz & Frey (1990) identified a basin with ring diameters of 900 and 1255 km. In addition, a large, over 1600 km hypothetical ancient impact basin located at Solis Planum west from our study area was recognized from crustal thickness data by Frey et al. (2007; Frey, 2008; see also Edgar & Frey, 2008).

Somewhat smaller basins have been mapped by Schultz et al. (1982) southeast of Hellas (273°W 45°S, ring diameters 225 km and 500 km), and in the western edge of our Hellas study area (356°W 37°S, ring diameter 430 km; Pike and Spudis (1987) mapped rings up to 640 km and 850 km). For the sake of completeness it can also be mentioned here that Schultz (1984) proposed a huge basin in Elysium (201°W 33°N) having the largest ring diameter of 1800 km. The existence of this basin, although agreed upon by Spudis (1993), is not well constrained. Similarly, if the Borealis basin suggested to be responsible for the crustal dichotomy (Wilhelms & Squyres, 1984) is real, it obviously has affected the geologic evolution of the area studied in this thesis. The most recent study (Andrews-Hanna et al., 2008; see also Marinova et al., 2008) suggests a size of ~10600×8500 km for the Borealis basin. In general, however, the existence of any particular Martian impact basin is accepted by different researchers, although the ring diameters presented may vary significantly (Spudis, 1993).

It should also be noted that in the case of the three most clearly defined Martian impact basins in this study (Hellas, Argyre and Isidis), the presence of possible antipodal impact effects have been studied. However, only the Hellas impact seems to have been energetic enough to have been able to produce deep fracturing at the antipode. This fracturing may in part account for the uniqueness of the enormous Alba Patera located at the antipode. (Peterson, 1978a; Williams & Greeley, 1994)

4.4 Tectonics

As was described above (Chapter 2.2), it is generally known that impact basins, as well as smaller impact craters, create mainly radial and concentric tectonic patterns around them (e.g. Baldwin, 1963; Melosh, 1976; Schultz et al., 1982; Wichman & Schultz, 1989; Spudis, 1993; Gurov et al.,

2007; see also Boon & Albritton, 1938). Due to the basins' far-reaching effects, mainly in the form of deep-seated zones of weakness, they may have markedly influenced the geologic evolution of our study area as well: the zones of weakness have probably controlled the location of subsequent igneous and fluvial processes (e.g. Peterson, 1978b; Schultz & Glicken, 1979; Schultz et al., 1982; Schultz, 1984; Wichman & Schultz, 1989). This can be seen especially in the distribution of chaotic terrain and channels.

Not just the later processes enabled by the basin-induced structures, but also the structures themselves have been investigated in the study area. Hodges (1980), while mapping the geology of the Argyre quadrangle, observed narrow concentric troughs, particularly in the northwest part of the area (Fig. 9). Thomas and Masson (1984) studied the tectonics of the Argyre basin, and observed many concentric escarpments. In addition, Thomas and Masson (1984) measured lineaments in the northwestern half of what they defined as the "Nereidum Formation", which approximately corresponds to Hodges' (1980) "Argyre basin rim material" unit. They found a dominance of especially basin-radial lineaments, but also lineaments tangential/concentric to the basin were ubiquitous.

Schultz (1984), and more thoroughly Wichman and Schultz (1989) studied the tectonics induced by the Hellas and Isidis basin. The mainly concentric and the substantially fewer radial features (especially around Hellas) are mainly graben and scarps. In Hellas, the Hellespontus Montes immediately west of the basin is the most prominent concentric feature, interpreted as mainly normal faults (e.g. Wichman & Schultz, 1989; Leonard & Tanaka, 2001).

Thomas and Masson (1984) found evidence for tectonism predating the Argyre impact. They observed three old tectonic lineations, with the most important one oriented NNE–NE. Other, less distinctive tectonic trends were oriented ESE and SSE (the lineaments in Fig. 9). Their conclusion was that the Argyre basin does not have any significant tectonic influence beyond an "outer scarp". Their "outer scarp" refers to Argyre Rupes situated about 1150 km southwest from the basin centre lying just beyond our study area, and smaller discontinuous escarpments along the western and northern margins of the basin (Fig. 9). However, more recent investigation indicates that the Argyre impact-induced structural fabric in the crust may have influenced the formation of the southeast part of the Thaumasia plateau (Dohm & Tanaka, 1999; Dohm et al., 2001a, b), nearly 1500 km kilometres northwest of the basin centre.

The volcanic plains of Hesperia and Malea Plana bear a rich collection of wrinkle ridges similar to lunar mare ridges (e.g. Mest & Crown, 1986; Raitala, 1988; Crown et al., 1992; Leonard & Tanaka, 2001; Ivanov et al., 2005). Many of these are induced by the paterae, but the numerous ridges radial

and concentric to Hellas imply a probable tectonic control by the basin. Some of the ridges in Hesperia Planum continue to the adjacent highland areas (Raitala, 1988). The wrinkle ridges have their origin mainly in the sinking of the Hesperia Planum, which lead to compression and faulting. The trends of the ridges are probably reflecting older crustal fractures and other similar structures (Raitala, 1988 and references therein; see also Golombek et al., 1991).

Chicarro et al. (1985) studied different types of ridges on a global scale. In general, Argyre basin region has clearly fewer basin-concentric ridges than Hellas and Isidis regions. In the Argyre region, high- and low-relief ridges (as defined by Chicarro et al., 1985) have a general NNW–NNE trend. A NNW ridge orientation is evident in old cratered plains especially west from the Argyre basin, but in younger plains the ridge orientation turns more towards NNE–NE. On the eastern side of the basin ridges on both old and younger terrain display a similar NNW strike. The importance of this orientation is emphasised by the general NNW striking ridge orientation that emerges after omitting the basin-concentric component from the data. (Chicarro et al., 1985)

After combining directions of all ridge types (except ridge rings which are most likely buried impact craters), it appears that areas west from Argyre basin are dominated by NNE striking ridges. Ridges in the eastern and northeastern surroundings of the Argyre basin are striking NNW. In the basin's northern side a broader, generally northerly ridge strike is apparent. In the areas surrounding Hellas and Isidis basins, the high- and low-relief ridges also have the general NNW direction, but especially in the area between the two basins, and also on Hellas' (south)eastern side, the high-relief ridges display varying orientations. Also the orientations of ridges in older terrains and younger plains differ clearly in the southern and eastern sections of the Hellas area. This is not surprising given the presence of Malea and Hesperia Plana and their volcanoes that dominate the local tectonics there. (Chicarro et al., 1985)

The strong and linear east–west trending magnetic anomalies that are vividly seen in Terra Cimmeria and Terra Sirenum in the southern highlands (located between our Argyre and greater Hellas study areas) have prompted hypotheses of possible early Martian plate tectonics (e.g. Acuña et al., 1999; Connerney et al., 1999; Purucker et al., 2000; Fairén et al., 2002). In Argyre region, however, the magnetic anomalies are patchy and usually weak, especially in the southern part of the region. Thus, they give no obvious signs of the possible effect of plate tectonics. In the northern part of our study area, however, more recent analysis (Connerney et al., 2005) shows somewhat stronger linear magnetic anomalies. They strike east-southeast, i.e. parallel to Valles Marineris, and also southeast. In Hellas part of our study area, the magnetic anomalies are generally stronger. Most prominent they are northwest from the Hellas basin, and on the northeastern and eastern side of the

basin. They follow the general east–west trend, but turn especially in Hellas' eastern side more towards southeast (Connerney et al., 2005).

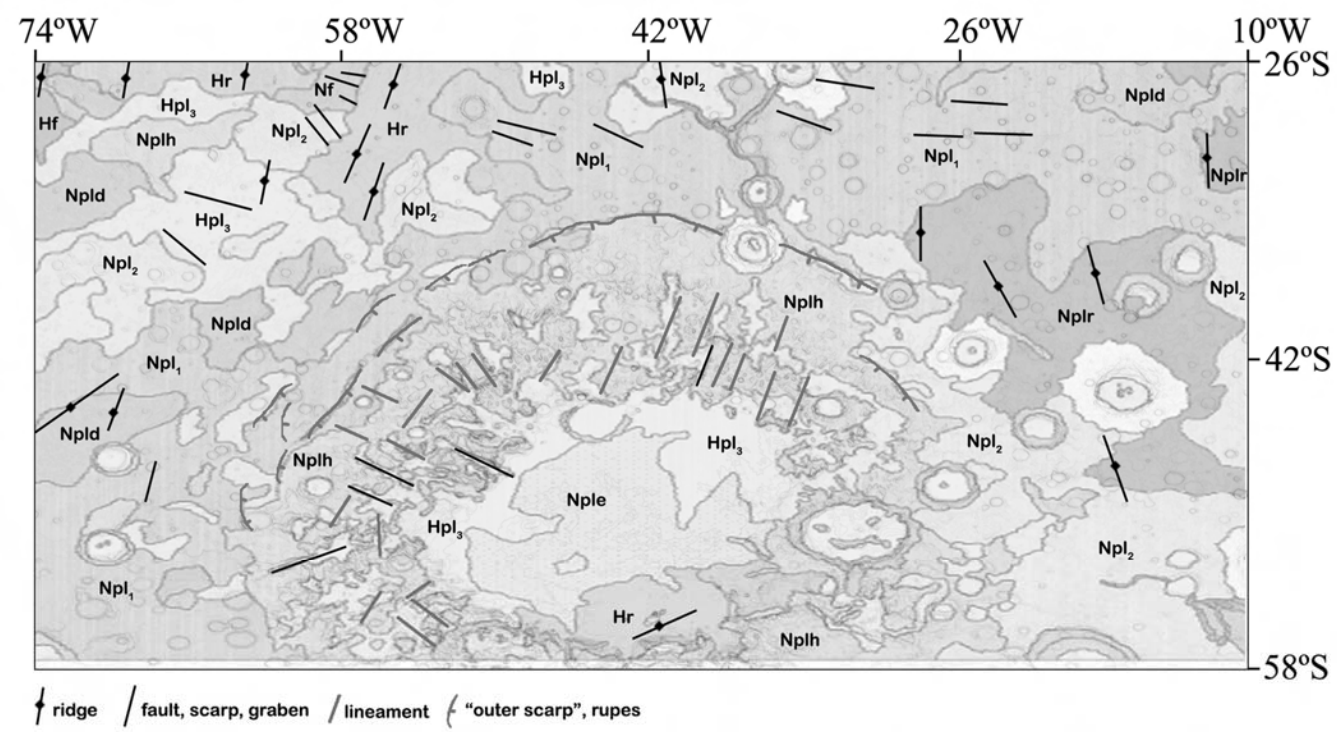

Figure 9. A sketch of the main tectonic features and the geologic units (Scott & Tanaka, 1986) in the Argyre region. Ridges, faults, scarps, and graben are simplified after Scott & Tanaka (1986), Dohm et al. (2001a), and Chicarro et al. (1985), lineaments, "outer scarp", and rupes after Thomas & Masson (1984) and Hodges (1980).

Schultz (1985) made a study of scarps, graben, and channel wall scarps in sections of the Argyre and Margaritifer Sinus regions, which partly cover our study area. His study is also noteworthy because he used a few measurements of polygonal crater rims, which gave results similar to other tectonic indicators. Schultz had only a limited number of tectonic measurements in the Argyre area, but there appears to be an orientation maximum in scarps trending N–NNE, and in graben trending E–ENE. In Margaritifer Sinus, scarps and channel-wall scarps trending NNE are dominant. In addition, some scarps have an ESE strike which parallels the main strike of the graben there. On the geologic map of the western equatorial region by Scott & Tanaka (1986), this ESE trend of graben is apparent as well. Another prominent tectonic feature in their map is the ridges trending N–NNE.

Schultz (1989) also studied strike-slip faults southeast of Valles Marineris, just on the verge of the centre part of the Argyre study area. Strike-slip faulting on Mars is regarded as a fairly rare phenomenon, but Schultz (1989) observed northeast and northwest trending *en echelon* type of strike-slip faults associated with wrinkle ridges. The Tharsis-induced strike-slip faulting predated or

overlapped the formation of the wrinkle ridges, and some of the ridges nucleated and grew as a result of the faulting. (Schultz, 1989)

Dohm and Tanaka carried out a detailed and extensive mapping (Dohm & Tanaka, 1999; Dohm et al., 2001a) of the Thaumasia region, partially covering the Argyre section of our study area. Their volcano-tectonic interpretations have major relevance for the PIC rim orientation interpretations presented in this thesis (see Chapter 9.6). The paleotectonic record of the Thaumasia region contains the Syria Planum centred radial faults and concentric wrinkle ridges marking long-lived growth of the complex volcanic area, and faults radial and concentric about the central part of Valles Marineris. These are related to the incipient development of the vast canyon system, including magmatic-driven uplift at its central part (Dohm et al., 2001a, b, 2007).

Especially in the northwestern part of our study area in the Argyre region, a sharp decline of Tharsis and Syria Planum centred normal faulting occurred during Early–Late Hesperian. During the Late Hesperian, although the rifting in Valles Marineris probably continued, Tharsis activity transitioned from mainly widely-distributed, magmatic–tectonic to concentrated volcanism to forge the giant shield volcanoes and result in local tectonism (Dohm & Tanaka, 1999; Anderson et al., 2001; Dohm et al., 2001a). The Thaumasia region may also record a pre-Tharsis phase of plate tectonism. This is indicated by the ancient mountain ranges, Thaumasia highlands and Coprates rise, marked by magnetic signatures, a generally high density of impact craters, and complex structure (Baker et al., 2007; Dohm et al., 2007). This is consistent in many respects with other ancient geologic provinces of the southern cratered highlands (Dohm et al., 2002, 2005; Fairén et al., 2002; Connerney et al., 2005; Baker et al., 2007).

Coracis Fossae, a part of the Thaumasia volcanotectonic complex, extends along the western margin of Argyre area's block A (see Figs. 2 and 4 in Paper III). Coracis Fossae tectonism is associated with mountains or small promontories that have been interpreted as volcanoes (Dohm & Tanaka, 1999; Dohm et al., 2001a; Grott et al., 2005). The extensional tectonism at Coracis Fossae that lead to the formation of the graben system trending approximately north was active from the Noachian to the Early Hesperian (Dohm & Tanaka, 1999). However, crater counts by Grott et al. (2005) place the eastern Coracis Fossae rifting at 3.5–3.9 Ga (corresponding to Middle Noachian – Late Hesperian, according to Hartmann & Neukum, 2001).

Another prominent system of graben, Claritas Fossae, almost reaches our study area just west of the Argyre block E (see Figs. 2 and 4 in Paper III). The southeasternmost graben of Claritas Fossae are generally trending NNW. Claritas Fossae –related faulting was substantially longer-lived than in

Coracis Fossae, as it commenced in Early–Middle Noachian, declined in Late Noachian and substantially diminished during the Late Hesperian or the Amazonian (Dohm & Tanaka, 1999).

In general, the previous studies suggest that the tectonics of the study area are mostly controlled by the Hellas, Isidis, Argyre and Ladon impacts and the resulting basin-radial and basin-concentric structures (and perhaps the other basins as well, mainly the large proposed basin south of Hephaestus Fossae). The long-lasting and complex tectonics related to the Tharsis bulge and Syria Planum have also made a significant overprint in the Argyre region, highlighted by the largely Tharsis-concentric ridges and generally Tharsis-radial faults and graben (Scott & Tanaka, 1986; Dohm & Tanaka, 1999; Dohm et al., 2001a, b). Especially prominent are the NW trending graben located northwest of the Argyre basin. However, in the most highly cratered terrains of the Argyre basin region, features radial to Tharsis are mostly lacking (Schultz, 1985). Similarly, in the northeastern part of the greater Hellas study area the effect of Elysium tectonism may be salient.

4.5 Volcanic, glacial, lacustrine, fluvial and eolian features

Volcanoes in the study area are only found in the Hellas region. The very shallowly sloped large volcanic edifices of Tyrrhena and Hadriaca Paterae are located east of Hellas, and Peneus and Amphitrites Paterae south of the Hellas basin (Plescia & Saunders, 1979). These paterae with highly degraded appearance of the slopes portray evidence of pyroclastic eruptions (Tanaka & Scott, 1987; Crown & Greeley, 1993; Tanaka & Leonard, 1995; Leonard & Tanaka, 2001). They are surrounded by the low-lying volcanic plains of Hesperia (e.g. Ivanov et al., 2005) and Malea Plana (e.g. Tanaka et al., 2002). The formation and the location of the paterae and the surrounding plana have been suggested to be controlled by the deformation induced by the Hellas and Isidis basins (Peterson, 1978b; Schultz, 1984; Wichman & Schultz, 1989; see also Schultz & Glicken, 1979). The eastern side of Hellas also shows evidence of dyke swarms (Korteniemi et al., 2009). Volcanic features in the Argyre region are not present as volcanoes, but as volcanic plains and geologic units interpreted to be of volcanic origin. Thus, they are briefly outlined in the previous sections about the geologic units and tectonic features.

Noachis Terra between Hellas and Argyre basins may look deceptively featureless cratered highland plains at a first glance. Unlike on the eastern side of Hellas, evidence for large-scale fluvial activity is lacking, but instead there are several indications of small-scale fluvial and glacial activity. These include channels that terminate in craters or other depressions and have apparently deposited sediments in them, as well as small mounds whose morphology and location strongly suggests that they are pingos (Aittola et al., 2006). Another indication that the Noachian highlands

in the study area have contained substantial surface and/or subsurface water reservoirs comes from the discovery of chloride-bearing materials (Osterloo et al., 2008). They are typically located in impact crater floors and other depressions, and in our study area are most common in the northwestern part of the greater Hellas region (Osterloo et al., 2008).

The boundary zone between the Hellas basin floor and the inner flank of the apparent rim displays delta formations of several large outflow channels, as well as shorelines formed in standing water body or in an ancient ice-covered lake (Moore & Wilhelms, 2001). It has been suggested that the origin for the large outflow channels in the northeastern Hellas area was due to the late-stage volcanism of Tyrrhena Patera (Leonard & Tanaka, 2001). It may have triggered collapse and outflow erosion producing the Dao, Niger and Harmakhis Vallis (Squyres et al., 1987), and may have been involved in the formation of Reull Vallis as well, although Reull seems to have had a multi-phase history (Kostama et al., 2007). The valles are roughly radial to Hellas, suggesting a possible connection to Hellas-centred tectonism, i.e. mainly basin-radial fracturing or faulting (Crown et al., 1992).

In Argyre region both Ladon and Holden basins are a part of a large, probable drainage system involving also the Uzboi Vallis, cutting the northern rim of the Argyre basin (Nereidum Montes). Uzboi Vallis is the most prominent outflow-type channel in the Argyre part of the study area (Grant & Parker, 2002). However, there are contrasting views on whether the probable water flow in the vallis has been directed to or from the Argyre basin (Parker et al., 2000; Grant & Parker, 2002; Hiesinger & Head, 2002). Other major channels include Nirgal Vallis which is a “tributary” to Uzboi Vallis, and three channels partly within the southern and southeastern edge of the study area, i.e. the Surius, Dzigai and Pallacopas Vallis. These cut through the southern part of the Argyre basin rim, i.e. Charitum Montes. (Parker et al., 2000)

Thus, similar to the Hellas region, also the Argyre region has a vast network of channels providing it with a drainage area of about 20×10^6 km^2. In addition, the Dorsa Argentea ancient polar ice deposits are located in the basin’s vicinity, giving it another possible supply of water during the melting and retreat of polar cap in the middle of Martian history (Head, 2000a, b; Head & Pratt, 2001). The basin has therefore probably been subject to filling with water to a large extent during that time. The morphology of the basin floor also suggests glacifluvial activity, mainly in the form of eskers (e.g. Kargel & Strom, 1992; Kargel, 1993).

For the Argyre basin interior’s appearance, previous studies have suggested six models of evolution: 1) mainly eolian deposition (Hodges, 1980), 2) significant volcanic activity (Scott & Tanaka, 1986), 3) emplacement of mud in large parts of Argyre after the melting of southern ice cap

(Jöns, 1987), 4) large-scale glaciation within the basin (Kargel & Strom, 1992), 5) melting of extensive southern ice cap, which resulted in the complete filling of the basin with water during Noachian (Parker et al., 2000), and 6) transport of considerable amounts of water to the floor during Hesperian (Head, 2000a, b; Head & Pratt, 2001). Most recent thorough analysis implies that the basin actually went through a complex geologic history with several geologic processes contributing to its current appearance (Hiesinger & Head, 2002). The filling and the freezing of the water body may, however, be regarded as the two major components in the evolution of the basin.

The youngest geologic units in the study area are those formed by materials transported by eolian activity, and deposited mainly as dune fields within impact craters. These eolian deposits have distinctly concentrated to the western side of the Hellas basin. The large dune fields are mostly absent in the eastern Hellas region, as well as the Argyre part of the study area. Another indication of the importance of eolian processes in the Hellas region is that the whole region has been proposed to provide material for regional and global dust storms (Martin & Zurek, 1993). This geologic diversity of the study area has resulted in the presence of uniquely Martian crater morphologies, described in the following Chapter.

5 AN OUTLINE OF IMPACT CRATER MORPHOLOGIES CHARACTERISTIC TO THE MOON, MARS AND VENUS

In addition to the "standard" sources of crater shape variation discussed above (Chapter 2.3), there are some remarkable impact features that are characteristic to Mars and Venus. These are briefly outlined below. Lunar craters are commonly regarded as "standard" craters, and were also tentatively studied in Paper VI. Hence, some of their main characteristics will be dealt with first.

5.1 Short observational history

Lunar craters were first described in "modern", scientific sense by Galileo Galilei in 1609. He noticed the topographic difference between the maria and the highlands, and observed that the highlands are peppered with craters. Although his sketches do not include a central uplift, his written descriptions clearly imply that he managed to see them, or at least one (Galilei, 1999). Perhaps the most prominent aspect of lunar impact structures – the presence of at least several true multi-ring impact basins – was not fully recognised until Lunar Orbiter IV photographs of Orientale basin in 1967 (Fig. 3e; e.g. Hartmann, 1981).

Martian impact craters were first identified from Mariner 4 images in 1965, although the largest impact basins, for example Hellas, were known for centuries from telescopic observations as albedo features. However, determining the basins' true nature of course had to wait for space missions. The first Mars missions (Mariners 4, 6, and 7; see Appendix 2) photographed mostly the southern highlands, and thus the early interpretations of the Martian impact crater population resulted in a rather lunar-like view. In contrast Mariner 9, an orbiter, provided a substantially different view with highly varying geologic environments and resulting crater morphologies, and the numerous subsequent missions with their global photographic and topographic coverage have only strengthened this view. (e.g. Carr, 1999)

Mars can be regarded as a treasure trove for anyone interested in the study of impact craters. Due to Mars' large variations in target properties during its geologic history – from dry volcanic rocks to wet sediments, probable shallow sea and ice – and the presence of a variably thick atmosphere, the surface of Mars displays a wider selection of morphologically (and thus also structurally) different impact structures than any currently known body of our Solar System. Essentially only palimpsests, ancient scars of impacts seen mainly as albedo features on the partly icy satellites of Jupiter (e.g. Croft, 1983; Jones et al., 2003), are a type of impact structures *not* seen on the surface of Mars today. Other major phenomena that are impact-related and lacking on the Martian surface, are

radar-dark parabolas and halos surrounding the ejecta blankets. These are features associated with the Venusian impact phenomenology (see below).

The impact craters on Venus were first reliably identified from the Venera 15 and 16 data (see Appendix 3) in mid-1980s, although their existence had been previously suspected – sometimes erroneously – based on Pioneer Venus 1 and Earth-based radar images (e.g. Schaber & Boyce, 1977; Ivanov et al., 1986; Basilevsky et al., 1987; Ivanov, 1990, 1992). However, the resolution provided by the Venera missions was surpassed by the Magellan mission (see Chapter 7.1.2), and thus the current view on the morphology of the Venusian impact craters is mostly based on the Magellan data.

Because of the very slow erosion rate on Venus and the geologically rather young age of the observable surface and thus of the craters, the Venusian impact crater population is quite small and the majority of the craters are very fresh (e.g. Phillips et al., 1992; Schaber et al., 1992) when compared to "average" craters on other celestial bodies. Herrick et al.'s database (1997) lists 942 impact craters, while Schaber et al.'s database (1998) has 967 craters.

The thick Venusian atmosphere prevents the formation of primary craters smaller than about 1.5–2 km in diameter (e.g. Schaber et al., 1992; Herrick & Phillips, 1994b), so all of the possible impact craters can be seen in the areas covered by Magellan imagery. Given the ~2% of Venusian surface not imaged by Magellan SAR (Ford & Plaut, 1993), it can be estimated that the whole Cytherean surface hosts approximately 950–1000 impact craters. An important fact about these craters is that their distribution on the Venusian surface is essentially random (Basilevsky et al., 1987; Phillips et al., 1992; however, compare to the initial Magellan interpretations of Phillips et al., 1991, and see the views presented by Hauck et al., 1998). Such a distribution is very different from the Martian surface, where the craters are mainly found on the southern highlands, or from the Moon where sparsely cratered maria are mostly located on the lunar near-side.

5.2 General morphology

Much of the current understanding of the general morphology of impact craters and also the cratering process is the result of a careful study of impact craters on the Moon. These general characteristics are described in Chapter 2, and therefore only some of the most conspicuous features of lunar impact structures are outlined here to provide a basis for comparison with craters on Mars and Venus.

Due to the diverse geology of the celestial bodies studied in this thesis, defining the transition diameter (D_{tr}) can be a complicated question. Some problems, especially in the past, have also been

caused by differences in definitions, i.e. some researchers have utilised the *d/D* ratios, or the diameter where first central peaks appear as D_{tr}, while others have preferred the use of rim terraces as the criterion for incipient complex crater. An interpretative combination of different features, however, leads to best results. (e.g. Pike, 1980a, b)

As mentioned previously, the diameter where the transition from simple to complex craters takes place is inversely proportional to gravitational acceleration (*g*). When the transition diameter is plotted against the *g*, the "dry planets" Moon, Venus and Mercury roughly follow a line of decreasing transition diameter with increasing *g* that is different from the other terrestrial planets. The data for Mars and the Earth – especially for craters formed in sedimentary targets, although this data is rather poorly constrained – fall notably below this line, and actually more closely follow the D_{tr}–*g* trend of the icy satellites (Fig. 10; Schenk & Sharpton, 1992; see also Herrick & Lyons, 1998). This is generally regarded as an indication of water present in Martian ground that decreases the strength of the target material during cratering.[14] These observations and ideas on Martian transition diameter are in concert with the fact that terrestrial sedimentary rocks, and thus supposedly also the Martian ones have porosities, and therefore possible water content often more than a magnitude higher than the generally dense and dry crystalline rocks. (e.g. Strom et al., 1992)

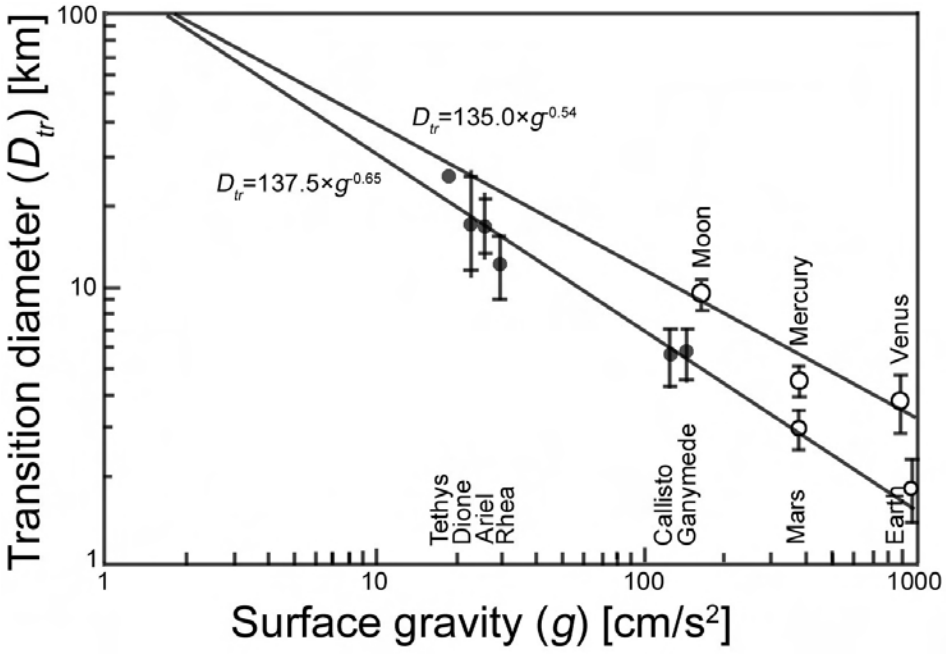

Figure 10. The transition diameter (D_{tr}) of impact craters on different heavenly bodies (open circles: rocky; closed circles: icy) as a function of surface gravitational acceleration (*g*). Venusian D_{tr} is modelled. Redrawn after Schenk & Sharpton (1992).

[14] Also other substances than water are possible, but it is for clarity from now on considered as being water and/or (ground) ice. Although for example hydrocarbons could be another possibility, envisioning them on Mars in larger quantities creates more problems than it solves.

5.2.1 The Moon

In general terms, the transition from simple to complex lunar craters is known fairly well. A good approximation for the value of the transition diameter is 15 km (e.g. Pike, 1967, 1974b, 1977; Hörz et al., 1991; Spudis, 1993). Wood and Andersson (1978) classified simple craters to those with flat floors and to those without. However, subsequent studies have shown that the two types merge into another without a clear boundary, and that both have a *d/D* ratio of 1/5 (Ravine & Grieve, 1986). Crater floors become notably flatter at about 20 km diameter (Pike, 1977), but scallops start to indicate crater wall collapse already at 13–15 km diameter range (Wood & Andersson, 1978). According to Schultz (1976), craters having an uncollapsed circular planimetric shape only seldom exceed 15 km in diameter. Also the *d–D* curve of lunar craters has its inflection point at about *D*=15 km (Pike, 1967, 1974b).

Central peaks occur rarely in lunar craters less then 10 km in diameter, although the smallest crater with a central peak has a diameter of only 2.6 km (Wood & Andersson, 1978). All fairly undegraded craters from 35 to about 100 km in diameter possess a central peak (Wood & Andersson, 1978; see also Smith & Hartnell, 1978).

As mentioned earlier, central peak basins are thought to be a transitional form between ordinary complex craters having central peaks, and peak-ring craters (e.g. Hartmann & Wood, 1971; Wood & Head, 1976). Wood and Head (1976) regarded this transition to take place in a diameter range of 140–175 km, based on two most prominent examples on the Moon. Pike (1983) and Spudis (1993) accept a value of about *D*=140–200 km for the transition. In a more recent study based on Clementine laser altimetry (LIDAR), the lunar crater *d–D* curve was extended to basin sizes, and a second inflection was observed at *D*=100–200 km, corresponding to the transition from complex craters to central peak basins (Williams & Zuber, 1998).[15] Also small but distinct ring-forming hummocks around the central peaks are present in the floors of complex craters down to roughly *D*=90–100 km (Hale & Head, 1980). However, volumetric studies of central peaks and observations of crater floor roughening imply that the central peak basin formation may actually be initiated already at about 50–80 km diameters (Hale & Grieve, 1982).

Lunar peak-ring craters span a large size distribution: the diameter range of peak-ring craters suggested by Wood and Head (1976) is 175–600 km, and Hörz et al. (1991) propose a slightly smaller range of *D*=175–450 km. The view held by Spudis (1993) is that the transition from central

[15] Note, however, that Spudis and Adkins (1996) used the same Clementine LIDAR data and studied some of the same craters/basins as Williams and Zuber (1998), and came to the opposite conclusion, i.e. that the basins' *d–D* curve is the same as determined for complex craters.

peak basins to peak-ring craters (basins) is an obscure one – like practically all transitions of impact crater morphology – but it certainly occurs between 250 and 300 km.

The variation of lunar target properties apparently causes some changes to the general crater morphology, although there does seem to be significant distinctions between different studies. For example, according to Wood and Andersson (1978) fresh simple craters on maria are ~10% deeper than in highlands, whereas the difference is negligible according to Pike (1980a). Wood and Andersson (1978) also suggest that contrary to simple craters, the 15–50 km diameter complex craters with scalloped walls are shallower on maria than their counterparts on highlands. De Hon (1980) studied craters close to the transition diameter (D=15–20 km) on both maria and highlands, and though the d/D ratios were similar, craters on the maria had a higher tendency to be shallow and flat-floored. These differences De Hon (1980) attributed to the different thickness of the megaregolith on maria and terrae. However, one should notice that his study included both simple and complex craters, and that the number of studied craters was very low indeed (17).

Smith and Hartnell (1978) noticed that on maria the details of central peaks and rim terraces are more complex than on highlands, contrary to the results of a study by Hale and Head (1979), who focused only on central peaks. Smith and Hartnell (1978) also compared craters on the central areas ("thick") and edges ("thin") of maria, and found that on "thick" maria all craters have terraces and central peaks at 25 km diameter, but the 100% level of occurrence is reached at 35 km diameter on "thin" mare. Similarly, Cintala et al. (1977) observed that in craters smaller than 40 km in diameter, mare craters have a higher abundance of central peaks than highland craters. They also noted that in the highlands, localized scallops persist as the main form of crater wall collapse to much larger crater diameters than in the maria.

In larger lunar crater and basin diameters the target properties may also be quite remarkable for the final morphology. Williams and Greeley (1997) proposed that the transition from central peaks to peak-rings is mostly controlled by crustal thickness. Their theory, based on Clementine topography and gravity data, suggests that peak-ring formation is enhanced in areas of thinner crust: peak-rings form when the transient cavity extends deeper than the crust–mantle boundary. Craters excavating only lunar crust will produce ordinary central peaks, and central peak basins (protobasins) result in the rare cases when the excavation extended approximately to the depth of the crust–mantle boundary.

According to Spudis (1995), basin's depth and age have no correlation, but the depth is probably more dependent on the crustal thickness and lithospheric conditions at the time of the impact. Crustal properties may also be pivotal for the formation of distinctive multi-ring basin rings:

Orientale basin, with its striking ring system (Fig. 3e), was the last major basin to form on the Moon (e.g. Wilhelms, 1987; Spudis, 1993 and references therein). It formed in thick crust at the time when lunar lithosphere was very much in its present-day state. This most probably promoted the ring formation (Spudis, 1993).[16] Thus, despite the fairly "simple" nature of the lunar target materials and the discrepancies between different studies, the variations of the physical properties of the target material apparently do have a real, notable effect on the cratering process, and therefore also on the final crater and basin morphology.

5.2.2 Mars

Defining the actual transition diameter for Martian impact craters is not as "easy" as in the case of lunar craters. In general, there is a consensus that on average the first signs of complexity in the shape of Martian craters – central peaks, flat floors, rim terraces, etc. – appear in the diameter range of about 5–7 km (e.g. Cintala et al., 1976; Wood et al., 1978; Pike, 1980a, b; Strom et al., 1992; Garvin et al., 2003), although for a number of craters this takes place already in the range of 3–3.5 km (Pike, 1980a). Altogether, variation in this respect is very large, since the smallest Martian impact crater with apparently a true central peak has a diameter of only 1.5 km (Mouginis-Mark, 1979), whereas some craters retain their simple morphology up to a diameter of more than 10 km, even up to 18 km (Mouginis-Mark, 1979; Pike, 1980a). For comparison, on the Earth D_{tr} is about 2 km for sedimentary targets and about 4 km for crystalline targets (e.g. Dence et al., 1977; Pike, 1980a; Grieve, 1987; Melosh, 1989; French, 1998).

Martian central peak basins were suggested to appear approximately at a fairly constant diameter of 135–150 km (Wood & Head, 1976), but subsequently it was found that they can emerge at about D=65 km, and persist to craters 160 km in diameter (Pike & Spudis, 1987; Spudis, 1993). Similarly, peak-ring craters span a very large size range, starting perhaps from craters as small as 52 km in diameter and ending in about 400 km (Pike & Spudis, 1987, Spudis, 1993) or even 470 km diameter craters (Wood & Head, 1976).

As can be seen from the large diameter ranges of morphologic transitions, there is certainly a terrain dependence on the size–morphology relationship on Mars, but different studies (e.g. Wood et al., 1978; Mouginis-Mark, 1979; Pike, 1980a) give somewhat differing results, and thus no obvious boundaries or often even trends can be set. The same, quite naturally, applies for the *d/D* ratio. The fairly recent *d/D* studies using MOLA data are to be considered the most reliable ones, and

[16] However, keep in mind that astenospheric flow is probably required for ring formation (Melosh & McKinnon, 1978; McKinnon & Melosh, 1980; McKinnon, 1981; Melosh, 1989). Further discussion on the origin of multi-ring basins and their distinctive morphological aspects can be found in Chapters 2.1.2 and 2.2.

according to them the variation is indeed large. In similar-sized simple craters, depth differences of several hundred metres are common, depending on the target lithology (Garvin et al., 2003). However, the current picture of Martian craters' *d/D* ratios is very complex with partially contradicting observations and interpretations (see, e.g., Garvin et al., 2000a, b, 2003; Boyce et al., 2003, 2004a, b; Whitehead et al., 2003; Mouginis-Mark et al., 2004). This most likely is merely an indication of the versatility of Martian geology.

Although none of the morphologic features observed in Martian impact craters are unique to Mars, several of them are present in Mars in unsurpassed quality and quantity. Practically all of these are most fluently explained by "just adding water", i.e. by the action of water during various stages of the impact process. The most striking and relevant to the cratering process of these are craters with central pits, and craters having a fluidised ejecta blanket around them, both of which will be discussed later on in a bit more detail.

5.2.3 Venus

Because the Venusian atmosphere is effectively disrupting the smaller incoming projectiles (e.g. Ivanov et al., 1986, 1997; Basilevsky et al, 1987; Ivanov, 1992; Schaber et al., 1992; Herrick & Phillips, 1994b), on Venus the transition from ordinary simple bowl-shaped craters to complex craters cannot be directly observed. However, according to calculations the D_{tr} would be in practise the same as on the Earth, about 3–4 km, if the atmosphere would not complicate the matters (Schenk & Sharpton, 1992; McKinnon et al., 1997). As was the case on the Moon and Mars, the appearance of the central peak in Venusian craters spans a fairly large diameter interval, from 8.6 km (the smallest crater with a central peak), up to 22.6 km (the largest crater without a central peak) (Herrick & Lyons, 1998; see also Ivanov, 1992). Peak-rings appear at D=40.0 km, but craters with several peaks instead of a peak-ring persist up to D=86.7 km (Herrick et al., 1997; see also Ivanov, 1992). As the target material variation on Venus is presumably not as large as it is on Mars, it is possible that the various atmospheric phenomena of impact cratering play a large role in the variation of the central peak and peak-ring onset diameter.

A surprising aspect of the Venusian impact craters, mostly induced by the nature of radar images (Chapter 7.1.2), is that their diameters are not that well constrained, although the craters themselves are generally undegraded. The problem stems from difficulties in correctly identifying the rim of the crater wall facing the radar (Herrick & Sharpton, 2000). Thus, digital elevation models (DEMs) are more suitable for accurately determining the crater diameter, as well as the depth. Diameters measured from DEMs are typically on the order of 10% larger than those reported in the Herrick et al. (1997) database (Cochrane, 2003; Cochrane & Ghail, 2006). However, DEMs are available only

for a small amount of craters. Therefore, the diameters used in this thesis are those listed in the database of Herrick et al. (1997).

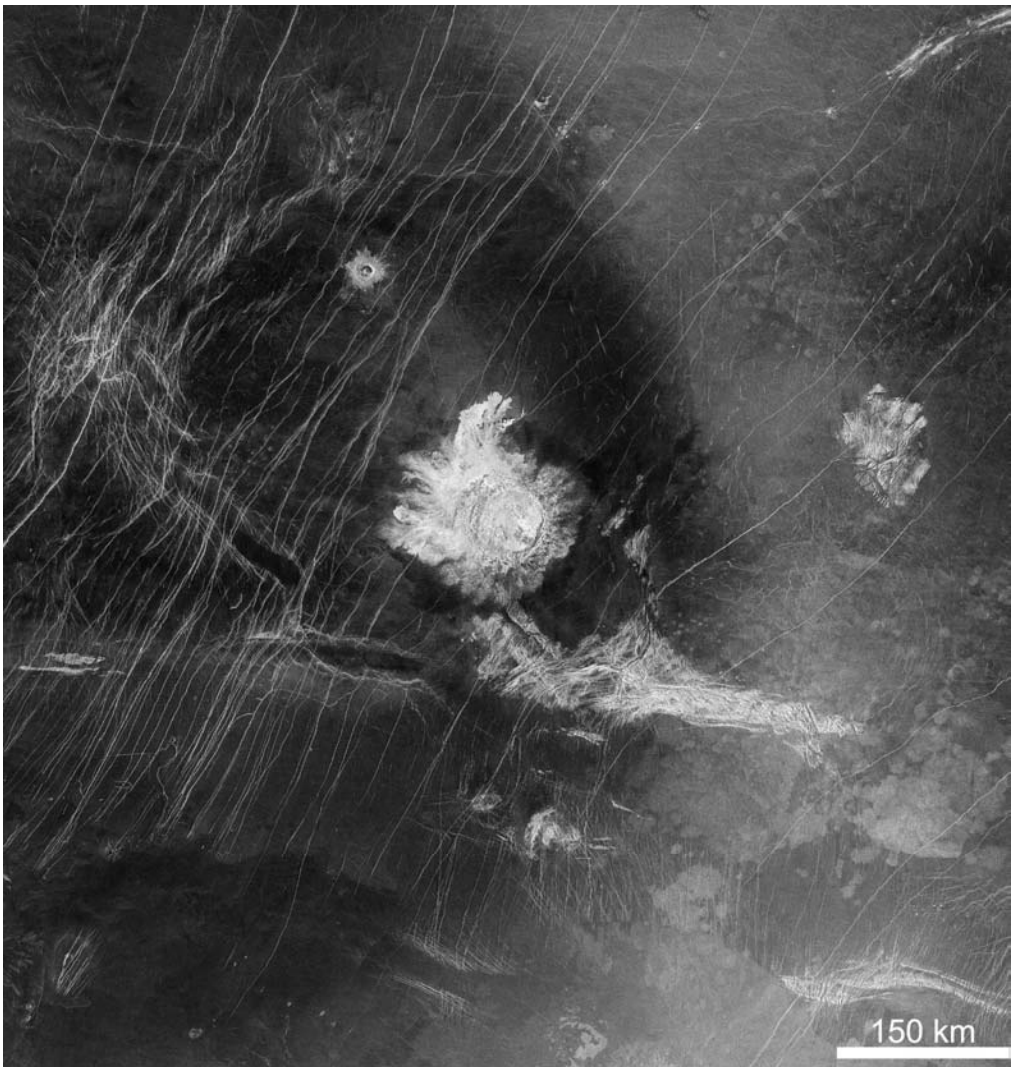

Figure 11. Venusian crater Stuart (*D*=66.6 km, 30.8°S 20.2°E) with a bright floor and dark parabola. North is to the top. Magellan SAR image.

Although the Venusian environment is in some respect less complex than the Martian one regarding the cratering phenomena, also on Venus there are some interesting features in the general morphology of the impact craters. One major division between Venusian impact craters can be made based on the brightness of the crater floor. Bright-floored craters (Fig. 11) form a minority of the craters, but they are the more interesting ones, because they are regarded as unmodified. Dark-floored craters, on the other hand, are somewhat modified by post-impact processes, namely volcanism. As the name suggests, the dark-floored craters have a floor that appears dark in radar images. More specifically, the dark crater floor material generally appears to be indistinguishable

from the material forming the volcanic plains. In addition, the dark-floored craters are shallower than the bright-floored ones. However, this is one of the relatively few clear-cut facts known about the depth of the Venusian craters. (e.g. Sharpton, 1994; Herrick & Phillips, 1994a; Herrick et al., 1997)

Already in the rather early stages of the analysis of the Magellan data, there were indications that the strict $1/g$ scaling would not hold for Venusian craters, because the craters seemed to be deeper[17] than anticipated (Sharpton, 1994). In addition, based on initial results, Schaber et al. (1992) found that Venusian d/D ratios of fresh large craters may be closer to lunar, Mercurian or Martian ones than terrestrial, although the terrestrial cratering environment is dominated by surface gravity practically inextricable from the Venusian one (the pre-erosion depths of the terrestrial impact craters are of course very difficult to estimate). Later this has gained support: the Venusian craters are deeper than expected (Herrick et al., 1997; Herrick & Sharpton, 2000), just as they supposedly are on Mercury (Pike, 1980b, 1988). However, an opposing view is held by McKinnon et al. (1997), who state that the Venusian craters are proportionally neither deeper nor shallower than the craters on the Moon or Mercury, when scaled correctly. Thus, even such a "simple" basic feature of the Venusian impact craters would benefit from further studies.

As yet unexplained is the observation that an almost flat or even decreasing trend with increasing diameter can be seen in terrain-to-floor depths of the Venusian craters (Sharpton, 1994; Herrick & Sharpton, 2000). In any case, it appears that although gravity is the most important factor contributing to a crater's depth, and that the $1/g$ scaling provides at least very good approximations, the nature of the target material – whether "dry" as on the Moon and Mercury, or "wet" as on the Earth and Mars (and the icy moons) – has a substantial effect on the overall final crater morphology.

On the larger end of the craters' size spectrum, there has been some discussion about whether or not Venus has true multi-ring basins so characteristic on the Moon (e.g. Spudis, 1993), and what are the ring diameter ratios, if true multi-ring basins really do exist (e.g. Herrick & Phillips, 1994a). The database of Herrick et al. (1997) lists ten multi-ring basins, whereas Schaber et al. (1992) suggest six possible multi-ring basins, four of which are agreed upon by Alexopoulos and McKinnon (1994). The largest of these is the largest impact crater on Venus, Mead, with a diameter of about 270–300 km (Herrick & Sharpton, 1996; Herrick et al., 1997; Schaber et al., 1992, 1998; Cochrane & Ghail, 2006).

[17] The depth of a crater always refers to the rim-to-floor depth, unless otherwise stated.

5.3 Untypical central structures

The central peaks in lunar craters are mostly very “ordinary”. After their appearance generally in 10–20 km diameter, their size increases along with growing crater diameter until about *D*=80 km, where the height of the peak has reached its maximum (Hale & Head, 1979; Hörz et al., 1991). Normally, the top of the central peak is always below the rim and the surrounding terrain. As noted above, at larger diameters the peak-rings start to form (Hale & Grieve, 1982). Morphologically, central peaks may be single massifs, ridges, or various types of clusters of peaks, but the geometry or the morphologic complexity of the peak does not appear to be related to the size of the crater. As noted above, there are contrasting views on the complexity of peaks in maria and highlands (Smith & Hartnell, 1978; Hale & Head, 1979). However, highland targets do seem to favour the formation of more linear central peaks (Hale, 1979; Hale & Head, 1979).

Instead of having a normal central uplift (a topographic central peak), many Martian complex craters were observed to have a central pit already from the Mariner 9 images (Smith, 1976; Fig. 12). However, it is somewhat dubious to call any Martian central uplift “normal”, because typically Martian central uplifts are abnormal: they are commonly larger than central uplifts in similar-sized craters on the Moon and Mercury (Hale & Head, 1981a, b; Whitehead et al., 2003). Since their discovery, the central pit craters have been one of the main points of interest in the study of Martian impact craters.

As is often the case, there are several different classifications for the central pit craters based on their morphology (see e.g. Wood et al., 1978; Barlow & Bradley, 1990; Strom et al., 1992). However, there are no distinct boundaries between various central pit types, but instead a succession of different forms. The two main types of the central pits can nevertheless be outlined. These are s*ummit pits* that are situated on top of central peaks, and *floor pits*, which sometimes can be surrounded by a low ring of peaks. The floor pits are approximately twice as common as the summit pits (Barlow & Hillman, 2006). Size range of central pit craters is fairly large, as the smallest ones are about 2–6 km in diameter (Hodges et al., 1980; Pike, 1980a), whereas the upper size limit is around 65–80 km, perhaps up to 114 km (Wood et al., 1978; Pike, 1980a; Hale, 1982; Barlow, 2006).

Central pit craters occur on various different types of terrains, but they are clearly concentrated on the southern highlands. High concentrations of central pit craters can be found for example southwest from Isidis and northwest from Hellas, whereas the surroundings of Argyre have only very few of them (Awwiller & Croft, 1986, cit. Strom et al., 1992; Barlow & Bradley, 1990; Barlow

& Dohm, 2004). Thus, there are major differences in the morphological crater populations in the various parts of the area studied in this Ph.D. thesis.

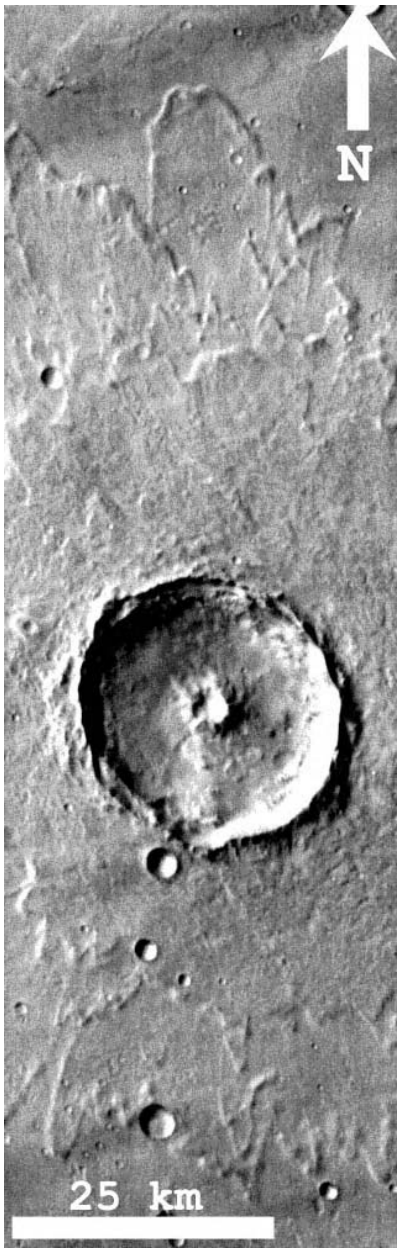

Figure 12. A Martian central pit crater at about 7.0°N 70.7°E. A part of THEMIS infrared image I03218002. Note also the ramparts at the ends of the ejecta lobes.

Despite intensive study, there is no generally accepted theory about the origin of the central pit craters. Most of theories require the presence of water in some form, and ideas involving low-velocity impacts have not received general acceptance (Schultz, 1987, 1988). The first model suggested that water and/or ice that was compressed to a high shock pressure evaporates explosively when pressure is released during the uplift of the central peak (e.g. Wood et al., 1978).

However, as Croft (1981c) noted, pressure release should occur much earlier than during the uplift, i.e. already in the excavation stage. Croft's (1981c) own idea is based on the assumption that the centre part of the central peak would be more brecciated than the peak's fringes. When the peak collapses more or less substantially, the brecciated central part would flow to the fractures below the peak and the crater floor. The ice being evaporated away from the crater floor underneath the central uplift, there should be plenty of space available for the breccia to flow into (Croft, 1981c). However, like in many other cases regarding Martian craters, it is clear that the central pit's actual formation mechanism(s) are not yet fully understood.

Also the Venusian impact craters have some unusual characteristics of the central structure: the central peaks are often very high. On other terrestrial worlds, the central peak in generally lower than the surrounding terrain. On Venus, however, the central peak often reaches the height of the surrounding area and sometimes surpasses it. The central peak height also does not increase with increasing diameter (similar to the terrain-to-floor depth; see above), in stark contrast to other planets and large satellites. These peculiar features remain as yet unexplained. (Sharpton, 1994; Herrick & Sharpton, 2000)

5.4 Ejecta blankets and other exterior phenomena

Ejecta blankets or other features located beyond the rim of an impact crater are not directly related to polygonal crater morphology. However, the ejecta blankets are easily observable indicators of the craters' age or degradational stage in general, and as such they were extensively utilised in Papers II–IV. Therefore, their most important characteristics are briefly outlined here.

5.4.1 Lunar ejecta, secondary craters and rays

The lunar ejecta blankets are well known and quite thoroughly studied. This is not surprising, as for example the ejecta ray pattern of Tycho can during full moon be seen spanning most of the near side, making it "the Metropolitan crater" of the Moon (Elger, 1895). As is the case with the actual craters, also the lunar ejecta blankets are more or less regarded as "standard". However, this is a bit of an oversimplification, as for example the lunar ray patterns are far more striking than anywhere else in the Solar System. The uniqueness of the lunar ejecta has its roots in the dry, airless relatively low-gravity lunar cratering environment described above.

Except for the concentric features of the slowest non-ballistically deposited "ejecta" immediately outside the crater rim, the lunar ejecta blankets are characterised by ballistically deposited radially patterned ejecta (e.g. Shoemaker, 1962; Wilhelms, 1987; Fig. 13). Continuous hummocky ejecta

deposits prevail generally from 0.5*D* to 2*D* from the crater rim, and grade into discontinuous deposits (e.g. Wilhelms, 1987; Hörz et al., 1991). These discontinuous ejecta deposits then grade into rays, if they are present.

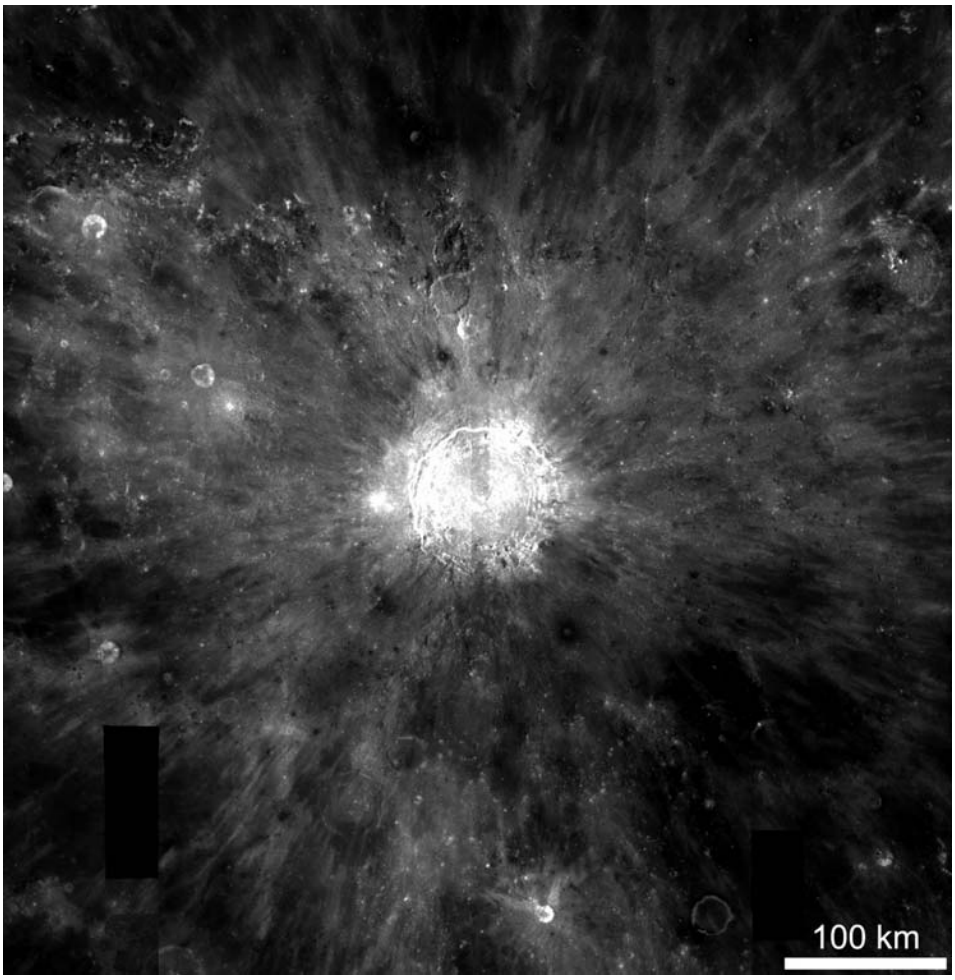

Figure 13. Lunar crater Copernicus (*D*=93 km, 9.7°N 20.1°W) with part of its ballistic ejecta deposits. Note also the straight segments of the crater rim, clearly pronounced in the northern part of the rim. North is to the top of the image. Clementine UVVIS image.

A noteworthy aspect of particularly lunar impact craters and their ejecta deposits are secondary craters. Secondaries are typically elongated, quite often somewhat irregular, shallow, and have a low or totally absent rim (Shoemaker, 1962; Wilhelms, 1987). Secondary craters are concentrated in an area 0.5–1.5*D* from the rim, and commonly occur in clusters and chains which may also form loops (Shoemaker, 1962; Wilhelms, 1976, 1987). They are often associated with a so called herringbone pattern of V-shaped ridges emerging from the secondary crater rim, with the V pointing to the host crater (Oberbeck & Morrison, 1973; Wilhelms, 1987). The ridges emerge when ejecta from two almost simultaneous secondary impacts interact with each other. The herringbone pattern apparently forms only in the case of shallow secondary impacts, where $\theta < 30°$ (Oberbeck & Morrison, 1973).

A crucial thing to remember about secondaries is that they are not formed by hypervelocity impacts: the escape velocity (v_{esc}) on the Moon is only about 2.4 km/s, and typical lunar secondary craters form with impact velocities (v) less than 1 km/s (Oberbeck & Morrison, 1973), an average sound velocity in the uppermost couple of kilometres of lunar megaregolith being about 1–2 km/s (e. g. Head, 1976b; Hörz et al., 1991). This low-velocity nature of these impacts is largely responsible for their irregular morphology.

Significant secondary cratering extends to larger crater diameters than one might intuitively think. This is because the size of the secondary-forming projectile is essentially only limited by the size of the primary impact creating it. Therefore, basin-sized impacts result in a vast number of large secondary craters. The same morphologic and spatial characteristics describe secondaries of both basins and smaller craters. It seems that at least in the case of Imbrian[18] and probably also Nectarian areas of the lunar surface, basin secondaries outnumber primary craters in the size range of 4.5–20 km in diameter, and numerous basin secondary craters up to D=30–35 km exist. (Wilhelms, 1976; Wilhelms et al., 1978; see also Ambrose, 2009)

The most distant lunar ejecta deposits are the bright ejecta rays typically radial to the host crater. They cross all types of lunar terrain, but are best visible on the dark maria. Normally they do not have any observable topographic relief, though exceptions occur (Shoemaker, 1962). The shapes and therefore the formation of at least complex crater rays are apparently determined by various inhomogeneities in the target material near the centre of the host crater, where the ray-forming particles were ejected (Shoemaker, 1962).

Rays are bright for two reasons: secondary craters of all sizes excavate fresh, optically immature material beneath the lunar surface (e.g. Oberbeck, 1971), and the composition of the ray may differ from the surroundings so that they have an albedo contrast (e.g. Hawke et al., 2004). The brightest "combination" type of rays emerge when fresh highlands material is deposited on dark mare surface. With time, cosmic ray bombardment and impact gardening effectively darken the rays. This is particularly true for "immaturity" rays. However, "compositional" rays may remain visible for extensive periods of time (McEwen et al., 1997; Hawke et al., 2004). Hence, the commonly held view that Copernican craters can be differentiated from the older Eratosthenian ones by the presence of rays (e.g. Wilhelms, 1987) is a vast oversimplification, and simply not true (Hawke et al., 2004). Interestingly, there is a spatial difference of ray craters on the Moon with respect to the orbital motion: the leading side (apex) of the Moon has more ray craters than the trailing side

[18] The current lunar time-stratigraphic division consist of Pre-Nectarian system, Nectarian system, Lower Imbrian series, Upper Imbrian series, Eratosthenian system, and Copernican system (Wilhelms, 1987).

(antapex), indicating that the recent lunar impact flux has been mainly caused by near-Earth asteroids (NEAs) rather than comets with high impact velocities (Morota & Furumoto, 2003).

5.4.2 Martian ejecta blankets

Unusual ejecta blankets are probably the most well-known "speciality" of Martian impact craters. They have inspired a lot of scientific debate, and are still the focus of many studies. The basic problem – how Martian ejecta blankets are formed – still remains somewhat open, and new theories on their origin are presented. This has also resulted in a vast number of different classifications and nomenclatures. In this thesis the nomenclature of Barlow et al. (2000) is adhered to. The peculiarities of the Martian ejecta features are attributed to the two main characteristics of the Martian cratering environment, i.e. the presence of an atmosphere and the subsurface volatiles (e.g. Barlow, 2005).

Unlike on the Moon and Mercury, fresh craters on Mars are often surrounded by an ejecta blanket that ends abruptly, rather than gradually fading away. The most studied cases are those where the ejecta forms distinct layers that terminate to a rampart rising above the remainder of the blanket and the surrounding terrain (Figs. 5 and 12). Single-layer ramparts are the most common type of ejecta on the Martian surface (Mouginis-Mark, 1979; Barlow & Bradley, 1990; Barlow & Perez, 2003), but double- and multiple-layer ramparts are certainly not a rarity (e.g. Barlow et al., 2000) and with increasing resolution their observed number is also increasing (e.g. Barlow, 2005). There appears to be a size-dependence so that multiple-layer ramparts surround larger, 20–45 km diameter craters, whereas single- and double-layer ramparts are associated with approximately 5–25 km diameter craters (e.g. Barlow, 2005 and references therein).

Rampart craters exhibit numerous features that have mostly been interpreted as indicative of a surface flow of a slurry-like substance. The ramparts themselves have been interpreted to have been formed when the outer edge of the ejecta blanket slows down and eventually stops, while material is still flowing outwards in the inner parts of the blanket (Carr et al., 1977). Thus, material would pile up on the edge of the ejecta blanket. Other features indicative of surface flow include a lobate edge of the blanket in plan view, concentric features in the interior of the blanket, and especially mesas, craters and other such obstacles around which the ejecta has been diverted, giving the obstacles an appearance of "islands" (e.g. Head & Roth, 1976; Carr et al., 1977; Strom et al., 1992).

The origin of the rampart craters is most commonly assigned to the presence of water in the form of ground ice in the target, effectively fluidising the ejecta (e.g. Carr et al., 1977; Mouginis-Mark, 1979; Kuzmin, 1980; Kuzmin et al., 1988a, b; Strom et al., 1992). It is worth mentioning, however,

that other mechanisms like impact-induced wind entraining the ejecta which is then deposited as gravity currents (Schultz & Gault, 1979), and wind erosion (McCauley, 1973, cit. Carr et al., 1977) have also been suggested to explain the appearance of rampart craters. In addition, granular flow after a ballistic deposition has been proposed as a means to create flowing ejecta without the presence of volatiles, but the current model for this mechanism does not explain the ramparts (Wada & Barnouin-Jha, 2006). As noted by, among others, Mouginis-Mark and Baloga (2006), ramparts along the sides of ejecta layers are difficult to explain with the "standard" deceleration model.

In addition to rampart craters, craters with "ordinary" radial (ballistic) ejecta, and combination morphologies, there are two other ejecta morphologies on Mars that deserve a short mention. Single-layer pancake ejecta is most commonly associated with simple craters. This ejecta type is also interpreted as fluidised, but instead of a rampart, it terminates to a concave, relatively steep slope (Mouginis-Mark, 1979; Barlow & Bradley, 1990). The more recent results obtained by using higher resolution MGS and Mars Odyssey data indicate that pancake craters might actually be just modified and degraded double-layer ejecta craters (Barlow, 2006).

Pedestal craters (Fig. 14), typically quite small and concentrated at high latitudes, are unusual among craters with preserved ejecta blankets in a sense that they are supposedly *eroded*. The ejecta blanket, originally probably of rampart or pancake type, has been protecting the immediate surroundings of the crater from erosion. As a result, the crater now stands on a massive pedestal that rises notably above the surrounding terrain (e.g. Barlow et al., 2000). One of the most recent studies (Kadish & Barlow, 2006; Barlow, 2006) implies that pedestal craters are present only where an impact occurred into an ice-rich mantling deposit. Subsequent sublimation of this ice in the surrounding area, rather than the "abrasive" actual erosion of it, would be the reason for the pedestal craters' current morphology. In any case, according to the general consensus, pedestal craters are notably degraded, and not fresh.

Another recent study (Wrobel et al., 2006) involves a more detailed mechanism for the origin of pedestals. It too requires a presence of ice-rich target. Impact-induced air blast would strip away loose material from the surface surrounding the crater, making the surface highly sensitive to the following local effects of elevated atmospheric temperature. This can lead to induration of soil by melting and migration of water which dissolves and precipitates salts. Another possibility proposed by Wrobel et al. (2006) is that the air blast and high atmospheric temperature may remove the volatiles surrounding the crater, leaving behind an armouring layer of volatile-poor dust. Overall, it is obvious that there remain several open questions in the formation mechanisms of pedestal craters.

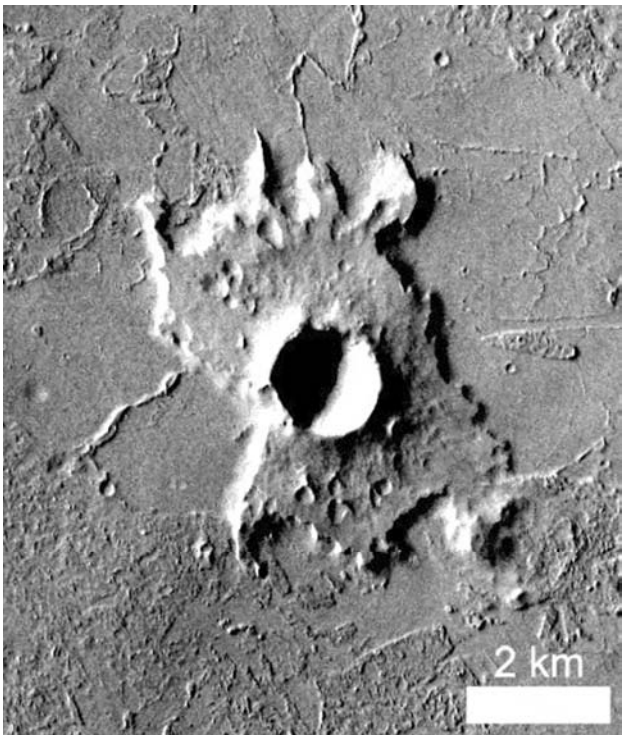

Figure 14. A Martian pedestal crater, located at about 12.6°N 203.8°E. Note also the straight segments of the western part of the rim. A part of THEMIS visual channel image V11801009. North is to the top.

Ejecta morphologies indicative of flow, often combined with studies of central pits, have often been utilised in deciphering the subsurface properties of Mars (e.g. Mouginis-Mark, 1979, 1980; Mouginis-Mark & Head, 1979; Pike, 1980a; Hale, 1982; Barlow & Bradley, 1990; Barlow & Perez, 2003; Barlow, 2004, 2005, 2006; Barlow & Dohm, 2004; Hillman & Barlow, 2005). The method certainly is applicable, but the results obtained so far have typically been somewhat contradictory. Yet, a few key aspects, summarised by Strom et al. (1992), apparently hold true: the depth to the surface of an ice-rich layer diminishes with increasing latitude, but the depth to the bottom of this layer remains relatively constant regardless of the location. Thus, closer to the poles there is a thicker ice-rich layer closer to the surface, but the bottom of this layer is roughly at a constant depth. More recent studies seem to indicate that except for the supposed sublimation of the ice in the mantling deposit in northern mid-latitudes, there has not been significant changes in the volatile content of the Martian crust during the past 3.5 billion years, and that layered ejecta morphologies are concentrated in areas where also other evidence of water or ice in the crust is present (like channels or central pit craters), as well as on the dichotomy boundary (Barlow & Perez, 2003; Barlow, 2004, 2006).

5.4.3 Ejecta and atmospheric impact phenomena on Venus

In contrast to the most highly cratered areas on the Moon and Mars, the ejecta blankets of Venusian craters are usually preserved for the most part (e.g. Herrick et al., 1997). The most surprising aspect of the ejecta blanket is the so called ejecta flows (Fig. 15; Phillips et al., 1991; Schaber et al., 1992). The mechanism to form thin, fluid-like flows that can extend hundreds of kilometres from the edge of the continuous ejecta is at present not completely understood. It may involve the more efficient production of impact melt on Venus than for example on the Moon (e.g. Vickery & Melosh, 1991; Ivanov et al., 1992), or it may be somehow related to ejecta interaction with the thick atmosphere (Phillips et al., 1991; Schultz, 1992) somewhat similar to what has been suggested for the Martian rampart craters. The main differences from Martian craters are that the Venusian ejecta flows are apparently much thinner and extend much farther, and there is no sign of a rampart.

Another uniquely Venusian ejecta-related feature are the dark parabolas (Fig. 11). They are large radar-dark parabolic areas that open towards the west, with a typically a bright-floored crater located close to the apex in the east (Arvidson et al., 1991; Campbell et al., 1992). They extend further from the crater than the ejecta flows, up to thousands of kilometres (Campbell et al., 1992; Basilevsky et al., 2004). In the Magellan emissivity data the parabolas cover even a larger area than seen in the SAR (Synthetic Aperture Radar) imagery (Bondarenko & Head, 2004). The dark parabolas are formed as fine grained ejecta is thrown high up in the Venusian atmosphere and then deposited to the surface by the prevailing easterly winds (e.g. Arvidson et al., 1991; Campbell et al., 1992; Vervack & Melosh, 1992; McKinnon et al., 1997; Basilevsky et al., 2004).

Also the dark halos (not to be confused with the “dark margins”, which may be related to the continuous ejecta blanket; About the differences between dark halos and margins, see Strom et al., 1994, and Herrick et al., 1997) that commonly surround the radar-bright ejecta blanket (see Fig. 6) are thought to be a direct result of an impact in the presence of the thick Venusian atmosphere (Phillips et al., 1991; Schaber et al., 1992; Herrick & Phillips, 1994a; Herrick et al., 1997). Sometimes the dark halo is surrounded by a radar-bright halo (McKinnon et al., 1997), and in rarer cases the halo may completely be radar-bright, or the dark halo may have a bright interior (e.g. Schaber et al., 1992).

The dark halos supposedly originate from the atmospheric shock wave impacting the surface just after the projectile itself. This air blast smoothens the surface (in the radar wavelength’s scale), and hence this area appears dark in the SAR images (e.g. Ivanov et al., 1986; Herrick et al., 1997; McKinnon et al., 1997). According to another suggested formation mechanism, the dark halos are fine grained ejecta (Schultz, 1992). Yet another proposition introduces a “back venting”

mechanism, where the gas is first pressurised and then depressurised (due to the rarefaction wave) in the pores of the soil, thus uplifting crushed soil into the atmosphere, from where it subsequently falls down (Ivanov et al., 1992; McKinnon et al., 1997).

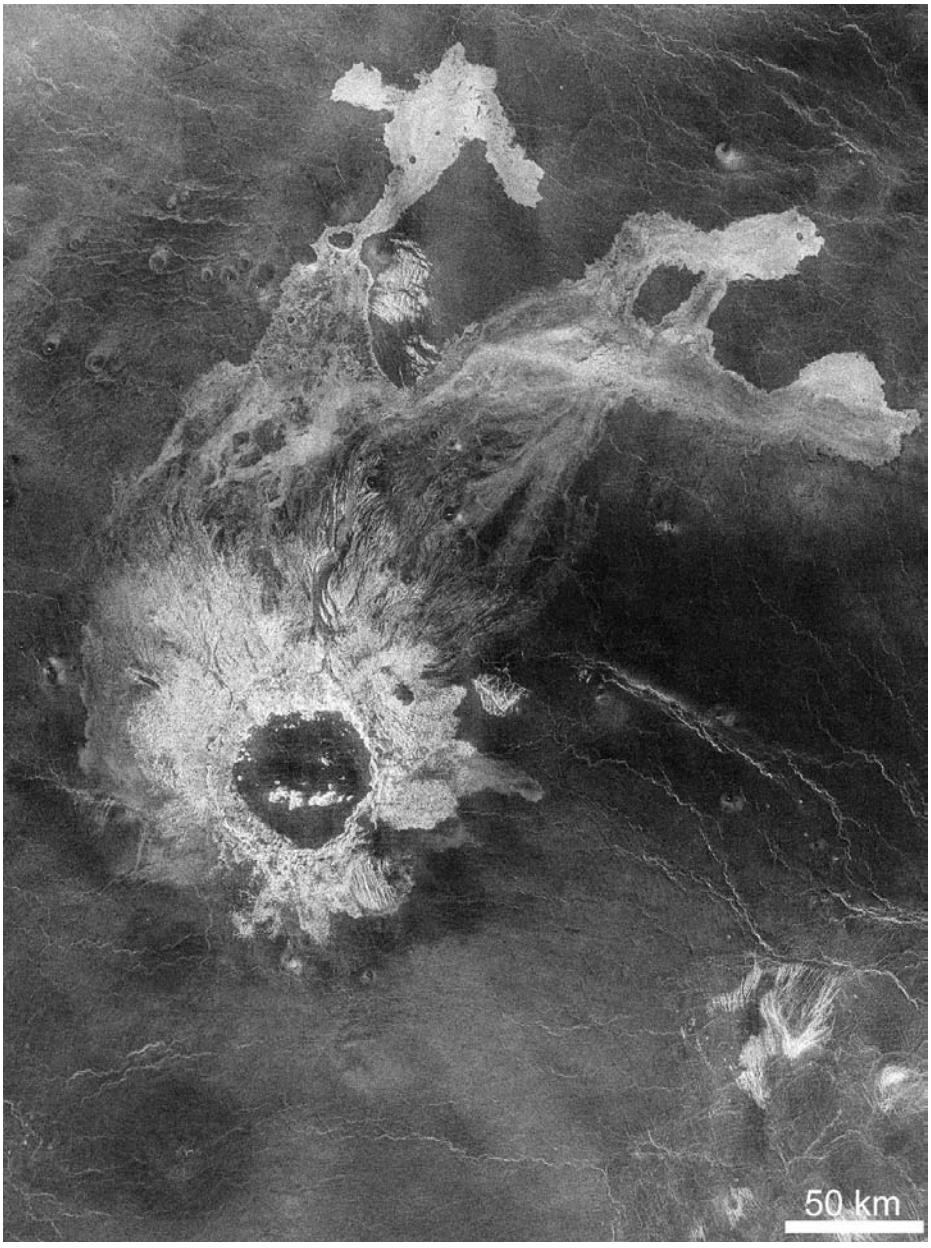

Figure 15. Venusian crater Seymour (*D*=63.9 km, 18.2°N 326.5°E) with a dark floor and extensive ejecta flows. Note also the dark splotch on lower left. North is to the top. Magellan SAR image.

According to an appealing idea, the bright halos surrounding the dark ones represent areas where the atmospheric shock wave is merely shattering and fracturing the surface, thus making it radar-bright (McKinnon et al., 1997). Another possibility is that the bright halos result from impact-induced supersonic winds cleaning the surface from finer materials, leaving behind a more

reflective surface (McKinnon et al., 1997). In any case, the dark (and bright) halos are one indication of the craters' relatively young age, although the dark halos remain with craters longer than the dark parabolas or bright floors (Herrick & Phillips, 1994a). However, in radar-bright terrains a faint or an absent halo may not indicate crater's old age (Basilevsky et al., 2003).

If the projectile is completely disrupted during the passage through the Venusian atmosphere, no crater is formed on the surface. Instead, the atmospheric shock wave creates a radar-dark "splotch" in a manner similar to the formation of the dark halos (e.g. Phillips et al., 1991; Schaber et al., 1992). Approximately 400 such splotches are identified, with diameters ranging from about 7 to 500 kilometres (Strom et al., 1994). Unlike the craters, the splotches' distribution is non-random, with heavy concentration on the low-altitude plains (Strom et al., 1994). However, caution is advisable when making interpretations based on the dark splotches, as unambiguous impact origin for all of the splotches is very difficult or even impossible to establish (Herrick et al., 1997).

5.5 Various Martian and Venusian impact oddities

5.5.1 Stealth craters and basins

Although practically global photographic coverage of Mars was obtained already by the Viking orbiters in late 1970s and early 1980s with a good resolution of about 250 m/pixel, the knowledge about Martian topography was substantially worse. This shortcoming was remedied by the MOLA instrument (Mars Orbiter Laser Altimeter) onboard the Mars Global Surveyor (MGS) spacecraft at the turn of the millennium. MOLA provided also some surprises regarding impact craters. One of the biggest was the discovery of so called stealth craters, also known as quasi-circular depressions (QCDs). These are impact structures that are not visible in ordinary photographs, but instead only seen in topographic data. The largest of them are impact basins with diameters of hundreds of kilometres, whereas the smallest ones observed are about 15 km in diameter. A large population of them is present in the northern lowlands that were previously thought to be practically devoid of larger impact craters. This clearly implies that the Late Hesperian Vastitas Borealis formation is only a thin veneer covering a substantially older surface. Although there of course is some uncertainty regarding the origin of the stealth craters and basins, impact cratering is the most plausible candidate. One of the strongest arguments for this is the very similar size–frequency distributions of stealth craters and ordinary craters. The large amount of basin-sized impacts – the total population could be a factor of four larger than the visible basins – naturally changes the ideas of the impact flux in the early Mars. (Frey et al., 1999, 2000, 2001, 2007; Kreslavsky & Head, 2001; Watters et al., 2006; Edgar & Frey, 2008)

5.5.2 Peripheral peak rings

Peripheral peak rings (PPR) are a newly discovered feature of complex craters. They have been found in the craters of Mercury and Venus (Nycz & Hildebrand, 2005), but they are best studied and apparently also best developed in Martian impact craters. The peripheral peak ring is a somewhat poor choice for the name of the feature, because it implies a link with the actual peak-ring. This, however, is not the case. PPRs form as a result of late stage "additional" slumping of the rim (i.e. slumping not directly related to the ordinary formation of terraces), either as sliding large blocks or as flowing rubble. Although Nycz and Hildebrand (2005) state that "PPR's sometimes show the same polygonal faceting as developed in crater rims", it does not become perfectly clear from the crater they are referring to (Fig. 16), what exactly do they mean. The crater in question does have some relatively short straight segments of the rim in its southern and western parts,[19] but in the southern part the orientation of the PPR does not too closely match that of the rim. Admittedly in the WNW part of the crater there is more notable parallelism between the rim segment and the PPR (Fig. 16). As yet there are no comparative studies on polygonal impact craters (as defined in this thesis) and PPR craters, so it is currently impossible to say whether or not the formation of PPRs could be affected by the same factors as the polygonal craters (see Chapter 9). However, at least in the case presented in Figure 16 it seems plausible.

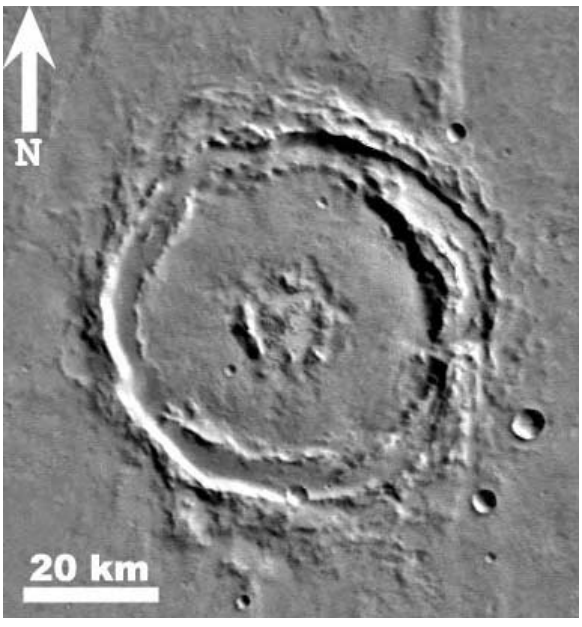

Figure 16. A Martian crater at 21.6ºS 69.1ºW, with a peripheral peak ring (PPR). Note that the PPR does not refer to the complex interior structure of the crater, but to the ring just inside the crater rim. Viking MDIM 2.0 image.

[19] However, the crater does not fulfill the criteria for polygonal craters used in this study.

What seems to be essential for the formation of PPRs is a weaker layer, for instance regolith or sediments, underlying a more competent layer, interpreted as typically being basalt. This difference in competence enhances the slumping of the rim. The extent of slumping is not arbitrary, but the ratio of the diameters of the crater rim and the peripheral peak ring is constantly about 1.3. This implies that the PPR really is an important and inextricable part of some complex craters. Because of their apparent genetic connection to specific geologic situation, their distribution on Mars is not random. The main concentration of PPR craters is the Sinai Planum southeast of Tharsis (i.e. partly in the area studied in this Ph.D. thesis). If the hypotheses regarding the origin of PPRs hold true, they provide a new tool for studying the Martian substratum. (Nycz & Hildebrand, 2003, 2005, 2006, 2007)

5.5.3 Clustered impacts and crater fields

In a study like this Ph.D. work where the crater morphology is studied, distinguishing genuinely polygonal craters (as defined in Chapter 7.2) from multiple craters and craters originating from clustered impacts (Fig. 6; Chapter 2.3.2; Schultz & Gault, 1985a) is essential. Although clustered impacts can form on any celestial body with a reasonably thick atmosphere (and rarely on other bodies too, if tidal forces cause the fragmentation of the projectile), they are best pronounced on Venus. There the thickness of the atmosphere creates ideal conditions to form craters by clustered impacts, as well as crater fields and multiple craters whose rims overlap (Herrick & Phillips, 1994b; Korycansky & Zahnle, 2004; Cochrane & Ghail, 2006).

On Venus, craters with diameters less than about 10–12 km often manifest the influence of the projectile's passage through the thick atmosphere with their irregular rims, indicating an impact of a projectile that has been disrupted (e.g. Herrick et al., 1997). In larger diameters the distinction between polygonal craters with straight rim segments and craters from clustered impacts with irregular rims is straightforward, but in smaller diameters true polygonal shape can be rather difficult to identify. Hence, the smallest craters selected for the study (in Papers IV and V) were 12 km in diameter.

As noted above in Chapter 2.3.2, a typical feature of clustered impacts is that the resulting crater is shallow (Schultz & Gault, 1985a). This is seen well in the Venusian craters. According to Cochrane and Ghail (2006), craters having diameters up to about 18 km are shallower than expected, due to a formation of a "compound crater", i.e. a crater resulting from a clustered impact. This size range corresponds to the class of "knobby base" craters in the database of Herrick et al. (1997). The Venusian knobby base (or "knobby bottom") craters were originally defined as incipient complex craters with hummocky floors (Basilevsky et al., 1987), but Cochrane and Ghail (2006) suggested

they might be a result of a clustered impact. It seems that according to this idea the genetic difference between the "multiple floor" craters and the "knobby base" craters in the database of Herrick et al. (1997) would be very small. In any case, the knobby base was used in this thesis (in Paper IV) as one variable for possibly finding differences between polygonal and non-polygonal craters.

5.6 Polygonal impact craters vs. "ordinary" impact crater morphologies

From the discussion above it becomes evident that there are several deviations from the "classic" crater shape in the impact crater populations on Mars and Venus. Mostly these deviations are the result of target properties or the atmosphere. However, as was the case with general impact processes discussed in Chapter 2.3, none of the factors and processes characteristic to Martian and Venusian craters described above produce crater shapes that would be fully compatible with the polygonal crater shapes depicted in this thesis. In some cases, however, the distinction requires a detailed study (PICs vs. craters formed by clustered impacts), and in some cases the same conditions may have contributed to the formation of two different types of crater morphology (PICs vs. peripheral peak rings formed by large sliding blocks).

Although post-impact modification and deformation of craters is not the theme if this study, it should be emphasised that such processes are equally unable to produce craters with the rims having the shapes of regular polygons (see e.g. Schultz, 1978; Grant & Schultz, 1993; Thomas & Allemand, 1993; Golombek et al., 1996; Rodríguez et al., 2005; Korteniemi et al., 2006; Paper II). As noted before, Lumparn is, however, an example indicating that polygonal apparent shapes of impact structures can be formed as a result of post-impact processes too (Abels, 2003). Yet it is worth pointing out that Lumparn's shape is rhomboid, quite unlike the partial octagon/hexagon/pentagon/square shapes encountered in this Ph.D. thesis (Chapters 6 and 9). In the case of highly eroded impact structures, both terrestrial and planetary, it is often impossible to know the relative importance of the target structures, impact processes and post-impact crater modification on the currently observable impact structure. So despite the very wide variety of different crater morphologies on Mars and Venus that have been and currently are intensively studied – most of those morphologies being very well-known but some substantially less so – polygonal plan view of the crater rim is not among them. These polygonal craters are described in further detail in the following Chapter 6.

6 THE STRUCTURAL CONTROL OF IMPACT CRATERS

The idea that various roughly vertical structures in the target material – whether they be fractures, joints, faults, folds, lithologic boundaries, foliations or the like – significantly affect the appearance of an impact crater is by no means a new conception. The resulting craters are called polygonal impact craters (PICs), "polygonal" referring here to large-scale polygonality of the apparent rim – whether fresh or degraded – of an impact crater in plan view. Thus, the common scalloped outline of a complex crater rim produced by smaller scale slumping of the crater wall does not make a crater "polygonal" in the sense of the term used here.

PICs almost never seem to get more than a brief mentioning in papers and books dealing with impact structures, especially in the more recent ones. This short introduction is not attempting to be a thorough historical review of studies or published comments concerning polygonal craters, but merely aims to show that they have been known throughout the impact and planetary geology communities for a long time, especially in the 1960s and to a lesser extent in the 1970s.

Although this Ph.D. thesis deals with the structural weaknesses in the target, it is well worth remembering that also the target's topography has a remarkable effect on the cratering process, as was described above. Therefore it also has major consequences for the final morphology of the crater (e.g. Gifford & Maxwell, 1979; Gifford et al., 1979; Eppler et al., 1983; Melosh, 1989; Collins et al., 2008; Gulick et al., 2008; Schultz, 2008). Further discussion of this, however, lies beyond the scope of this thesis. The same applies for the alleged structural control of the location of the central peaks (Chapman & Fielder, 1964; Guest, 1971) and their elongation or (polygonal) morphology (e.g. Hale, 1979; Antoine et al., 1990; Wieland et al., 2004), as well as for the structural control of ejecta formation and distribution (e.g. Shoemaker, 1962; Gault et al., 1968; Morrison, 1984). Thus, when discussing the structural control of impact craters, it is assumed in this thesis that the discussion refers to the planimetric shape of the crater rim and its formation by planes of weakness in the target material.

6.1 Previous studies on planetary polygonal impact craters

6.1.1 Lunar PICs

The Moon is quite naturally the heavenly body whose surface has received most attention during the history of planetary geology. Thus it is no surprise that the majority of studies involving PICs are about lunar geology. Without delving too deeply into the fascinating history of impact science, it is easy to find out that lunar PICs (Fig. 17e) have been known at least for more than a century, as

they were observed and discussed by Wilhelm Prinz in 1893, Thomas Gwyn Elger in 1895, and Pierre Puiseux in 1908 (Elger, 1895; Fielder, 1961; Kopal, 1966; Davydov, 1968). Given the fact that in some of lunar craters the rims' polygonality is quite obvious – even a few of the large well-known craters like Aristoteles, Metius, Encke (Green, 1965a), Ptolemaeus (Elger, 1895; Wood, 2003), and Copernicus (Fig. 13; Elger, 1895; Shoemaker, 1962; Morrison, 1984) have a polygonal shape – it is likely that the polygonal outline of some craters was discovered in the very early days of telescopic lunar observations.

Fielder (1961) gave a brief review of the late 19th to mid-20th century studies on lunar craters' polygonality. Prinz, in his study from 1893, had noted the polygonal shape of several terrestrial volcanic craters and calderas, and argued that the polygonal (hexagonal) shape of lunar craters would have a similar origin. After Prinz, Elger, and Puiseux, Graff discussed the polygonality in 1929, and suggested that either compression or tension had altered the shape of the craters during cooling, leading to the observed polygonal shapes of the (presumed volcanic) lunar craters (Fielder, 1961). Citing an obscure reference,[20] Fielder (1961) also mentions another possible formation mechanism: rectilinear dykes, swarms of which were said to be typical in the lunar highlands, appear to have limited the development of the craters, thus giving them polygonal outlines.

The early part of the 20th century, until the 1950s to 1960s, to some extent up to the mid-1970s, was the time of debate regarding the impact vs. volcanic origin of lunar (and Martian) craters, often intertwined with discussion about the alleged lunar global tectonic grid. In 1945 Josiah Edward Spurr, according to Green (1965a), had recognized the existence of the lunar grid system of fractures[21] that control the crater shapes, good examples of this control being craters Ptolemaeus and Arzachel. Similar observation of the connection between polygonal shape of craters and the surrounding structures was apparently made by A. V. Khabakov in 1949 (Davydov, 1968).[22] Spurr's model for polygonal crater formation was that they result from the collapse of volcanic bubbles that are bounded by pre-existing faults (Wood, 2003). Also during these decades the planimetric shape of crater rims, mainly their circularity or non-circularity, occasionally also polygonality, was regarded as one possible mechanism of telling a difference between impact craters and volcanic calderas (e.g. Murray & Guest, 1970; Oberbeck et al., 1972; Pike, 1974a).

[20] Fielder (1961, p. 182) cites a passage from *L'Annulaire pour 1956*, but I have been unable to clarify what that reference actually is.

[21] The existence of a global lunar tectonic grid is nowadays generally declined (e.g. Baldwin, 1963; Wilhelms, 1987, 1993; see also Hörz et al., 1991). Larger scale tectonic structures are due to the formation and modification of the impact basins (see Chapter 2.2), and much of the lineaments are due to basin ejecta (e.g. Baldwin, 1963).

Alter wrote a series of papers describing the surface of the Moon (e.g. 1956a, b, 1957, 1958). Usually polygonal craters are dealt with only in passing (Alter, 1956a, 1957, 1958), but his paper on lunar "walled plains" describes them in more detail (Alter, 1956b). By "walled plains" he meant, as was common for the time, impact craters having normally a diameter of about 80 to 240 km. He noted that they are typically hexagonal, although squares are common as well. He stressed that they are not formed by explosions – neither external (impact) nor internal (volcanic) – but instead are graben-like features formed by the collapse of large gas- or steam-filled domes. Interestingly, he was convinced that small craters at or near the rims of the walled plains indicated sinking along fault lines (Alter, 1956b). These craters he likened to terrestrial blowholes in a sense that they were supposedly lying along fractures.

It became apparent at the latest by mid-1960s that four-, five-, eight- and particularly six-sided polygonal craters on the Moon are common, or that at least the craters often have three or four straight sides forming a partial polygon. It was also clear that the directions of the straight rim segments of the polygonal craters, even somewhat buried ones, often are parallel with other tectonic lineaments, both in the immediate vicinity of the craters and in a regional scale. (e.g. Fielder, 1961, 1965; Baldwin, 1963, 1964; Fulmer & Roberts, 1963; Green, 1965b; Miyamoto, 1965; Kopal, 1966; Guest & Fielder, 1968; Davydov, 1968)

Gilbert Fielder (1961, 1965) was a strong proponent of lunar craters' volcanic origin, as well as the existence of the lunar tectonic grid (for background on Fielder's ideas, see Wilhelms, 1993). Hence, many of his conclusions should not be regarded as valid anymore, but some of his observations are most interesting. He noted that craters larger than 20 km in diameter are in general polygonal, and craters less than 20 km circular (Fielder, 1961). When studying the relationship between the "polygonal structures" and other topographic features, he saw no evidence for the idea that once circular structures had been transformed into polygonal ones by later tectonic modification (Fielder, 1965),[23] although previously he mentioned as a possibility that craters gained their polygonal shape due to later crustal movements (Fielder, 1961). He was, however, well aware that polygonal structures can be formed by both volcanic(–tectonic) and impact processes (Fielder, 1965).

Based on his knowledge about terrestrial impact structures, especially the ~1.2 km diameter Meteor (a.k.a. Barringer) Crater[24] in Arizona (Fig. 17c; see Chapter 6.2.1), eminent lunar and impact scientist Ralph Baldwin (1963) had the important notion that it was not the later modification that

[22] This is based on the assumption that "direction of breaks" in the translation of Davydov's paper (1968) means the direction of faults or fractures.
[23] It is not quite clear whether Fielder (1965, pp. 67–68) means terrestrial or lunar polygonal structures, or both.
[24] For an early, highly influental but in its conclusions erroneous study on the Meteor Crater, see Gilbert (1896).

made some lunar craters polygonal, but it was a natural outcome of pre-existing structural lines of weakness. He did, however, also note that in addition to this process, Imbrium basin ejecta scoured crater rims so that two rim segments became rectilinear, pointing towards Imbrium. With the certitude provided by hindsight it can be noted here that Baldwin (1963) had the benefit of being correct regarding the origin of the vast majority of lunar craters, whereas other prominent lunar scientists of the 1960s, e.g. the aforementioned Gilbert Fielder (1961, 1965) and Zdeněk Kopal (1966) erroneously advocated the volcanic origin for many craters, including the polygonal ones.

Even some basin-sized impact structures, especially the Crisium basin, appear structurally controlled and distinctly polygonal when correctly projected (Kopal, 1966; Chadderton et al., 1969; see also Spudis, 1993; Chapter 2.1.2). Khodak (1965), in addition to his somewhat cryptic discussion of lunar "polygonal-annular" craters, also mentioned that V. G. Fesenkov in 1950 had noted the polygonal outlines of the lunar maria. Such observations were also done by Dauvillier (1965). According to his idea, the maria are formed by convection cells, and they have hexagonal boundaries. Tazieff (1965) had a similar hypothesis, as he stated that neither volcanic nor meteoritic origin explains the lunar craters' polygonal, frequently hexagonal contours. Craters in Tazieff's model are in fact convection cells, the size of which had been decreasing with time. This neatly "explains" the general size–age sequence of craters, i.e. that larger craters tend to be older than the smaller ones. Internal origin of PICs was shown to be possible by conducting experiments where gaseous eruptions from below created polygonal craters on the surface of viscoelastic polymer (Kaarsberg, 1969; see also Murray et al., 1969).

Another historically interesting, albeit in the light of current knowledge equally erroneous theory was based on acoustic Chladni figures, named after Ernst Florens Friedrich Chladni, who was a pioneer of both meteoritics and acoustics (e.g. Marvin, 2006, 2007). Chadderton et al. (1969) noted that polygonal craters commonly have an equal number of straight sides – four, six or eight – and that triangles never occur. They also pointed out that the sides are parallel to the lunar grid, and contrary to most other researchers, that pre-Imbrian craters are "patently polygonal" while younger craters are "undeniably round". These observations implied to Chadderton et al. (1969) that the craters as well as basins (at least Crisium) have been reshaped over extensive periods of time. Their proposed mechanism to do this was "ringing", i.e. global vibration or standing acoustic waves on the Moon. These standing waves would have been induced by violent eruptions or impacts. In a note added in proof they suggested that a similar process was responsible for polygonal craters on Mars too. (Chadderton et al., 1969)

Davydov (1968) presented observations that agreed with previous results: partial hexagons, more rarely pentagons, are common on the Moon, whereas square or triangular shapes are rare. His theory for their formation, however, seems in some respects quite unique in the history of PIC research: he attributed the polygonal shape to the anisotropy of the shock wave forming the crater. This anisotropy was introduced very early in the cratering process by the mostly hexa- and pentagonal columnar jointing of basalt, whose existence on the Moon had just gained a lot of support from Luna 10 gamma spectrometry (see Appendix 1). To the best of my knowledge, this or similar ideas for PIC formation have not been discussed since. (Davydov, 1968)

A good example of how widely known the craters' sometimes polygonal shape was in the mid-1960s is evidenced by the papers in an important conference proceedings volume called Geological Problems in Lunar Research (1965). There are at least 11 papers in the volume that mention or discuss the polygonal shape of either lunar or terrestrial craters. Most commonly polygonal outline of lunar craters was interpreted as an indication of their volcanic origin. In addition to the papers already cited above, for example von Bülow (1965) noted that the polygonal outlines of many craters, including large ones, prove the tectonic dependence of the lunar volcanism. McCall (1965) stated that lunar impact structures, which he called "cirques", may be circular, polygonal, oval, rhombohedral, or irregular, and strongly argued that lunar craters are analogous to terrestrial calderas. He included the polygonal shape of crater rims, especially when associated with ridges, as evidence for the craters' endogenic, non-explosive origin.

Another indirect indication of the apparently rather general awareness in the 1960s that impact craters can sometimes be polygonal can be deduced e.g. from Öpik's (Wells et al., 1967) and Binder's (1969) comments. They wrote about issues not related to polygonal impact craters as such, but both noted in passing that although generally craters are circular, they can sometimes be polygonal. Even such brief comments, not to mention more detailed views, are totally absent from more recent accounts on impact craters.

One of the few papers in the Geological Problems in Lunar Research volume that favoured the impact origin of polygonal craters was by Quaide and co-workers (1965). According to them, lunar craters larger than 20 km in diameter are more often polygonal than the smaller ones. They also stated that most of the terraced craters are polygonal, and that it may be a feature of bedrock control as it is in the Meteor Crater. Quaide et al. (1965) held a quite modern view also regarding the origin of complex PICs: gravity sliding, probably along ring fractures produced during impact, may among other things account for the greater frequency of polygonal outlines of larger craters. Rather similar idea had actually previously been presented by Shoemaker (1962), who had noted that the

normal slump faulting which makes the Copernicus crater "somewhat polygonal" (see Fig. 13) has been controlled by pre-existing target structure.

Fulmer and Roberts (1963) made valuable contributions to the understanding of the origin of polygonal impact structures. They conducted impact experiments in fractured targets (see Chapter 6.3 for further discussion), and studied lunar polygonal craters. They discovered that often polygonal lunar craters tend to be larger ones, and that they can be located on both the lunar maria as well as on the highlands. For the pertinent question of why some craters are polygonal and some are not, Fulmer and Roberts (1963) offered one very plausible explanation: in layered targets the craters that are formed in a weakly fractured surface layer are not influenced by the structure of the deeper layer having a dominating fracture pattern. They also stressed the significance of the fracture spacing, and pointed out the basic fact that erosion should soften the polygonal outline of craters, not enhance it. Thus, the "modern" researchers of (lunar) PICs, Baldwin (1963), Shoemaker (1962, see also 1960), and Fulmer and Roberts (1963) came up with quite similar ideas at about the same time. From these, the least known, i.e. Fulmer and Roberts (1963), made what in many respects can be regarded as the most important and detailed contributions to the understanding of polygonal impact craters.

Ronca and Salisbury (1966), later followed by Adler and Salisbury (1969), discussed the circularity of lunar craters. Although neither of these works uses the word "polygonal" to describe the craters they studied, it is clear that at least the "angular" craters listed in Ronca and Salisbury (1966) are polygonal craters in the sense of the word used in this thesis.[25] Ronca and Salisbury (1966) pondered upon the possibility of jointed target distorting the crater shape, but considered it to be unlikely based on the observation that circular and "subcircular" craters can be found located immediately next to each other. Instead, Ronca and Salisbury explained their "subcircular" craters as a result of deformation during a period of compressive stress in the lunar crust. They also suggested that younger craters are more circular than older ones, which was agreed upon by Adler and Salisbury (1969; see also Eppler et al., 1982, 1983).

Adler and Salisbury (1969), however, opposed the idea of compressive stress, but agreed that "subcircular" craters that they found concentrated around the maria (~impact basins[26]), were originally circular and became later modified by the basins' extensive radial and concentric fracture systems and the stresses related to the maria formation. Melosh (1976), who studied such basin-

[25] It is rather safe to assume that also the craters discussed by Adler and Salisbury (1969) are polygonal craters. This same conclusion has been reached also by Schultz (1976).
[26] The concept of "impact basin" was not yet fully developed in the late 1960s, and "mare" was used, among other words, almost as a synonym for what currently would be referred to as an impact basin. See Wilhelms (1993) for some further details.

induced fracturing (Chapter 2.2), noted that the pre-existing fractures may give rise to polygonal rims of subsequently formed craters, thus contradicting Adler and Salisbury's (1969) view that polygonality is due to post-impact modification.

Saunders et al. (1970) mainly reviewed Alfred Wegener's work in early 1920s on crater morphology (Wegener, 1975) and modern research at the time, but actually held slightly different views from other researchers, when it comes to lunar PIC formation models. Simple craters may become sometimes polygonal by "slipping or flowing of loose material down slopes", whereas complex polygonal craters result either from excavation along pre-existing joint surfaces like in Meteor Crater, or by "mass wasting resulting in selective terrace formation" (Saunders et al., 1970). They also mentioned that most craters 20–40 km in diameter are "not precisely circular" regardless of their age, and that young craters over 40 km in diameter are not polygonal, whereas older craters of the same size may be.[27]

Five Lunar Orbiter missions (1966–1967) provided a high-resolution, practically global photographic coverage of the Moon (Appendix 1). Lunar Orbiter imagery is still for many purposes by far the best dataset available. Trask and Rowan (1967) noted that many very small (D≈50–300 m) lunar craters are markedly polygonal. Elston et al. (1971) did a much more detailed work with respect to PICs when they studied the lunar near-side tectonics from a substantial area including both highlands and maria, covered by Lunar Orbiter IV imagery. They made almost 1500 measurements of polygonal crater wall segments, and the results matched very well with those obtained from straight rilles and highland and mare ridges. They attributed the origin of polygonal craters, as well as other tectonic indicators, to N–S compression and E–W tension, which lasted most of the history of the Moon.

Scott et al. (1977) used a substantially smaller, yet a significant number (235) of polygonal crater rim strike measurements in their tectonic study of the entire lunar farside. Their results from PIC rim segment directions are almost perfectly compatible with the results from faults, ridges and other lineaments. Their directional data indicated a NE–SW and NW–SE tectonic grid, similar to the one reported to have been observed on the near-side. They also emphasised that the gaps in their diagrams were not caused by illumination effects, but were due to real geologic phenomena (Scott et al., 1977).

Among the most interesting lunar studies regarding polygonal craters is the one by Pohn and Offield (1970). Their extensive study divided craters in three size–morphology classes according to

[27] It is not quite clear if these observations are taken from a work by Pohn and Offield that preceded their subsequent study (Pohn & Offield, 1970, see below), or if these are results by Saunders et al. (1970) themselves.

the planimetric shape of the "young" crater rims. Complex craters larger than 45 km in diameter were round with distinct rim crenulations, and simple craters in the size range of 8–20 km were round. However, complex craters having a diameter between 16 km to 48 km (rounded to 20–45 km) were classified as polygonal.

Pohn and Offield (1970) actually observed polygonal craters in all size classes, but they were the most dominant in the 20–45 km size range. In that class polygonal craters were present in all of their seven[28] morphologic stages that corresponded to the craters' relative ages. The freshest polygonal craters were "commonly hexagonal". Craters in this size range of 20–45 km were formed as polygonal and remained as such through subsequent modification. Because Pohn and Offield (1970) classified as polygonal craters also the ones that were modified by superposed craters, their observation that in the 20–45 km size range the craters were polygonal already from the beginning is important for the ideas regarding their formation mechanism(s).

In Pohn and Offield's (1970) class of the largest craters, polygonal craters were also quite ubiquitous, but absent in the most degraded morphological stages. In the smallest size class they interpreted that craters were formed as circular, but then developed polygonality as they degraded to the mid-scale morphologic stages.

For the issues relevant to this thesis, Pohn and Offield's (1970) results indicate two highly consequential things: generally polygonality is *not* more pronounced in the older (and hence more degraded) craters, but craters can be formed polygonal, and there also appears to be a size range "preferred" by the polygonal craters.

In mid-1970s, Head discussed lunar polygonal craters in several studies (1976a, b, 1977). He (1976a) studied the orientations and lengths of linear rim segments of 24 post-Imbrium craters (D>30 km) surrounding the basin. He found no major rim orientation related to the radial Imbrium sculpture, and thus concluded that the radial texture does not extend to depth and therefore is sedimentary (i.e. basin ejecta) and not structural in origin. However, he measured from 12 to 37 straight rim segments from each crater. A polygon with that many straight segments starts to be a reasonably good approximation of a circle. Thus, although Head (1976a) apparently weighed the orientations with their respective lengths, one might wonder if a perfectly natural outcome from a study of orientations measured from fairly circular structures (i.e. his polygonal craters) spread over a fairly circular area (i.e. around Imbrium basin) is indeed a fairly random pattern as revealed by his results.

[28] Actually eight, but the oldest (most degraded) age group has no observable diagnostic crater features like polygonality, rays, or rim terraces.

Head's study (1976a) is interesting regarding PIC formation mechanisms: he noted that slumping of the crater walls occurs preferentially along regional lineaments, but contrary to most other researchers, he stated that the slumping prefers an orientation *normal* to the structural trend of the area too. In another study (Head, 1976b) he only mentions basal wall failure along pre-existing fractures or joints as a PIC-formation mechanism. In the same study he notes that one characteristic feature of flat-floored craters is their polygonal outline, and that the onset of polygonality coincides with the appearance of rim terraces. Straight rim segments usually parallel straight segments of the terraces (Head, 1976b). A typical diameter range for these flat-floored, terraced and central-peaked polygonal craters is 20–140 km (Head, 1976b).

In a later study (Head, 1977) he did not discuss polygonal craters in any detail, but included "polygonal outline" in his figure of major morphologic features in lunar impact craters and basins with respect to diameter, revising the PIC diameter range from his earlier study. It seems that according to Head's (1977) study, the polygonal outline is most dominant in the diameter range from 40 km to 1000 km, and at least present down to craters 20 km in diameter. Thus, his results (1977) clearly differ from those of Pohn and Offield (1970).

Schultz (1976) made a remarkable study of lunar morphology, and polygonal craters were among the landforms he studied. Like other researchers, he noted that the directions indicated by PICs correlated with other lineament data. According to his study, polygonal craters that are less than 15 km in diameter are not slumped (so in essence they are simple craters), but instead structurally controlled in the excavation stage (see Chapter 6.4.1). He also observed that craters larger than 15 km in diameter are typically either scalloped or polygonal in plan view. However, his concluding comment on craters larger than 15 km, where scalloped outline would be caused by structurally controlled modification, whereas a polygonal outline results from non-structurally controlled slumping, must certainly be a typographic mistake. The opposite must be what Schultz (1976) actually means. This is because in other parts of his book where he discusses polygonality, he clearly points out the connection between polygonal segments of crater rims and the orientations of structural weaknesses in the lunar crust.

From a methodological point of view it is noteworthy that Schultz (1976) stressed how lighting conditions may play an important role in classifying a crater either as scalloped or polygonal. It is also interesting to note that Schultz (1976) classified the Tsiolkovsky crater (basin) as a polygonal crater, while Guest and Murray (1969) emphasised its strong circularity, although they admitted that "the slight polygonality of the crater shows some influence of regional structure". Later, however,

Guest (1971) took a somewhat stronger opinion, and stated that straight parts of the crater rim are due to faulting along regional planes of weakness, specifically the global lunar tectonic grid.

Pike (1977) studied fresh lunar crater morphometry, and presented a concise review of the studies concerning lunar craters' circularity, non-circularity, and polygonality. Pike's own data (Pike, 1976) revealed (Pike, 1977) that craters about 10 km in diameter are the most circular ones, circularity diminishing in both smaller and larger sizes. However, his earlier study (1968, cit. Pike, 1977) implied that the frequency of polygonality as well as the "strength of polygonality" increases with increasing diameter.

Although non-circularity and polygonality of a crater are not the same thing, one can conclude as a general trend from Pike's (1977) review and the aforementioned earlier studies of lunar craters (especially the results obtained by Fielder (1961), Quaide et al. (1965), Pohn and Offield (1970) and Schultz (1976) are very consistent), that the size does matter: larger craters tend to be polygonal more often than smaller ones. More specifically, it seems rather obvious that small to mid-sized complex craters have a strong tendency to be polygonal rather than circular.

The PIC *formation models* by Eppler et al. (1983) that were developed based on their research on the planimetric shape of lunar craters (Eppler et al., 1977) will be further discussed below in Chapter 6.4, but it is appropriate to cover some of their *observations* also here. They studied 716 near-side craters larger than 15 km in diameter (so they were mostly, but not solely of the complex crater size) and utilised Fourier shape analysis. Regarding crater size with respect to shape, Eppler et al. (1977) appear to be somewhat self-contradictory, because while describing their results, they state twice that larger craters are more circular than smaller ones (and make a similar comment in the abstract), but nevertheless conclude that craters' size does not affect their planimetric shape.

It is noteworthy that like numerous authors before them (see above), Eppler et al. (1977) speculate on the possibility of regional structural patterns affecting the craters' planimetric shape, although this was discussed more thoroughly in their subsequent work (Eppler et al., 1983). For instance, Eppler et al.'s (1977) finding that mare craters are more circular than highland craters was attributed to highland crust's greater lithological and structural complexity. Interestingly, Eppler et al. (1977) state that their 11th order harmonic[29] that characterises the small-scale irregularities of the crater rim may be controlled by the properties of the bedrock. In other words, they did not assign the overall crater shape, but instead the somewhat smaller scale unevenness of the planimetric rim outline to bedrock properties.

[29] In practise the number of the harmonic indicates the number of corners in a polygon; see Eppler et al., 1983.

In agreement with the results obtained by Ronca and Salisbury (1966), Eppler et al. (1977, 1982, 1983) found that the craters' planimetric shape becomes more irregular with increasing age. This irregularity is characterised by relatively minor post-formational slumps. In contrast, major slumps that are responsible for the large-scale polygonality of the crater, take place during the formation of the crater, and they are also a long-lasting feature of craters (Eppler et al., 1983; see Chapter 6.4).

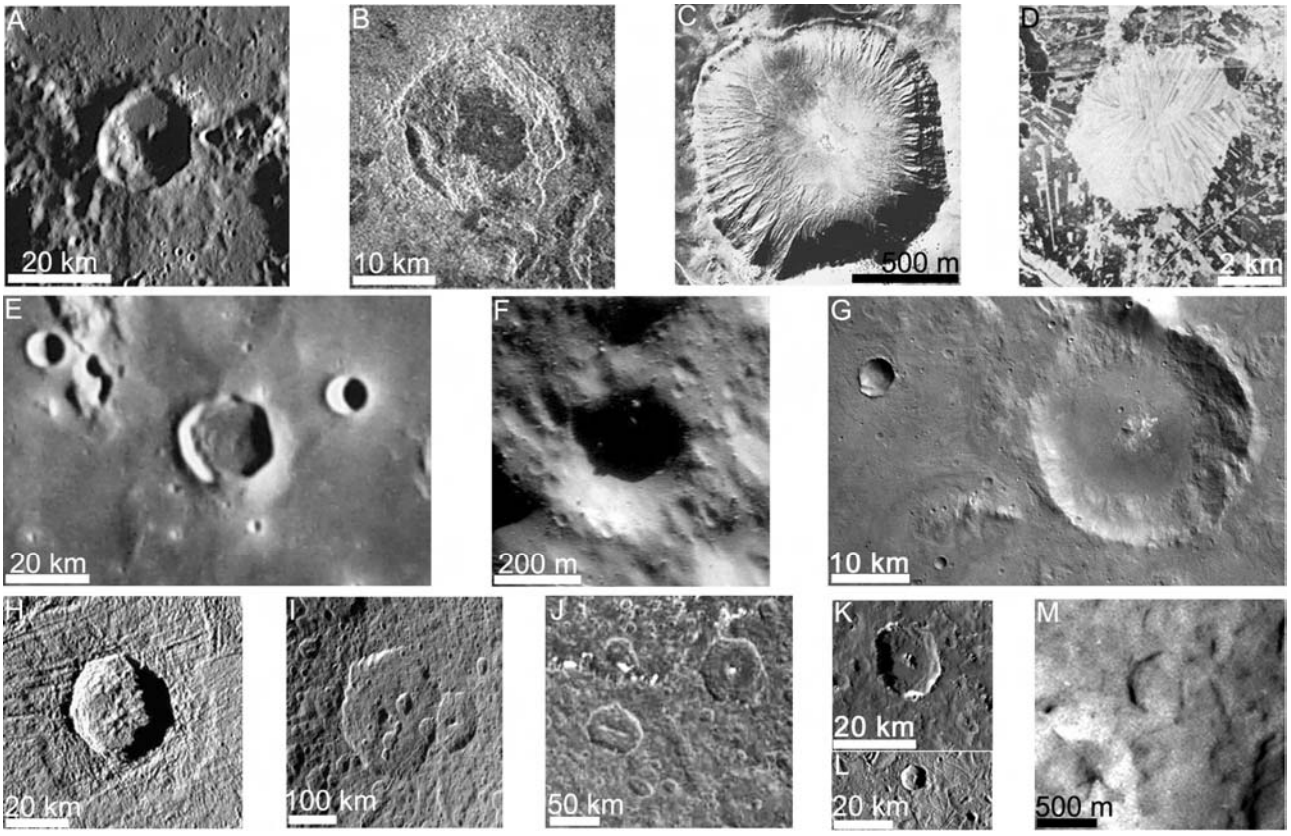

Figure 17. PICs on different bodies of the Solar System. a.) Mercury (~5°N 100°E; MESSENGER MDIS NAC image EN0108827037M; NASA/Johns Hopkins University Applied Physics Laboratory/Carnegie Institution of Washington). b.) Venus, Galina crater (Magellan SAR image; NASA/JPL). c.) Earth, Meteor Crater (sedimentary target; Baldwin, 1963). d.) Earth, Söderfjärden impact structure (crystalline target; the apparent hexagonal shape of the crater floor is enhanced by agricultural modification; Laurén et al., 1978). e.) Moon, Janssen crater (note the circularity of the adjacent "normal" simple craters; Kuiper et al., 1967). f.) Eros (NEAR-Shoemaker image PIA03131; NASA/Johns Hopkins University Applied Physics Laboratory). g.) Mars (28.2°S 283.2°W; note the partially similar polygonality of the largest hexagonal complex crater and the crater of transitional size on the left, compared to the circularity of the small simple crater at lower left; Mars Express HRSC image 0411_0000_ND2; ESA/DLR/FU Berlin/G. Neukum). h.) Ganymede, Achelous crater (Galileo image PIA01660; NASA/JPL/DLR). i.) Rhea (Cassini image PIA08173; NASA/JPL). j.) Iapetus (Cassini image PIA06166; NASA/JPL). k.) Callisto (7.4°S 6.6°W; Galileo image PIA00745; NASA/JPL). l.) Europa, Brigid crater (Galileo image; NASA/JPL). m.) P/Wild-2 (Stardust image PIA06285; NASA/JPL-Caltech). Scale bar precision is only approximate.

Since the study of Eppler et al. (1983), there was, at least according to my knowledge, a lengthy gap in lunar PIC studies. That seems to be still ongoing. Quite recently, however, Ambrose (2009)

studied the secondary craters around Nectaris basin, i.e. partially in the TINN area studied in this thesis too. As briefly discussed in Chapter 5.4.1, secondary craters typically have irregular planimetric shapes. Ambrose (2009) noted that the shallow, narrow-rimmed Nectaris secondaries range in diameter from 10 to 35 km, and are polygonal in outline. However, it is not clear if he is actually referring to the "normal" irregularity of secondary craters, or if he means the large scale regular type of polygonality with relatively long straight rim segments, as in this thesis.

To summarise, the presence of polygonal impact craters on the Moon is well-established, but apparently they haven't been studied much since early 1980s. They are most commonly partially hexagonal in plan view, although other polygonal shapes occur as well. From early on it was clear that there is at least some correlation between the orientations of tectonic structures in the vicinity of the PIC and the straight segments of the PIC rim. The size distribution of PICs spans from small simple craters less than a hundred meters in diameter to a basin-size of hundreds of kilometres. There is significant variation between different studies regarding the most "favourable" PIC formation size, but the most convincing arguments seem to imply a preference to small to mid-sized complex craters. PICs are found among both young and old lunar craters, and thus it appears to be clear that some craters are formed polygonal, and are not the result of later modification or degradation. Until late 1960s most researches believed PICs to be of internal origin, whereas later studies have made it practically undeniable that the most likely reason for PIC formation on the Moon is the effect of target material's structural inhomogeneities in impact cratering processes.

6.1.2 Martian PICs

Martian polygonal impact craters (Figs. 17g & 18) were identified already from the first flyby images obtained by Mariner 4 spacecraft in 1965 (Binder & McCarthy, 1972). Mariners 6 and 7 provided more data, and polygonal craters were studied to some extent by Binder and McCarthy (1972) for investigating the lineament systems of Mars. Lineaments that are concentric and radial with respect to Hellas impact basin (see Chapter 4) were identified already in this early study. Importantly, Binder and McCarthy noted that the results of their lineament measurements – large but unspecified amount of which were made from straight polygonal crater rim segments – were not consequentially affected by the digitising process, solar illumination effects, or from the use of different resolutions.

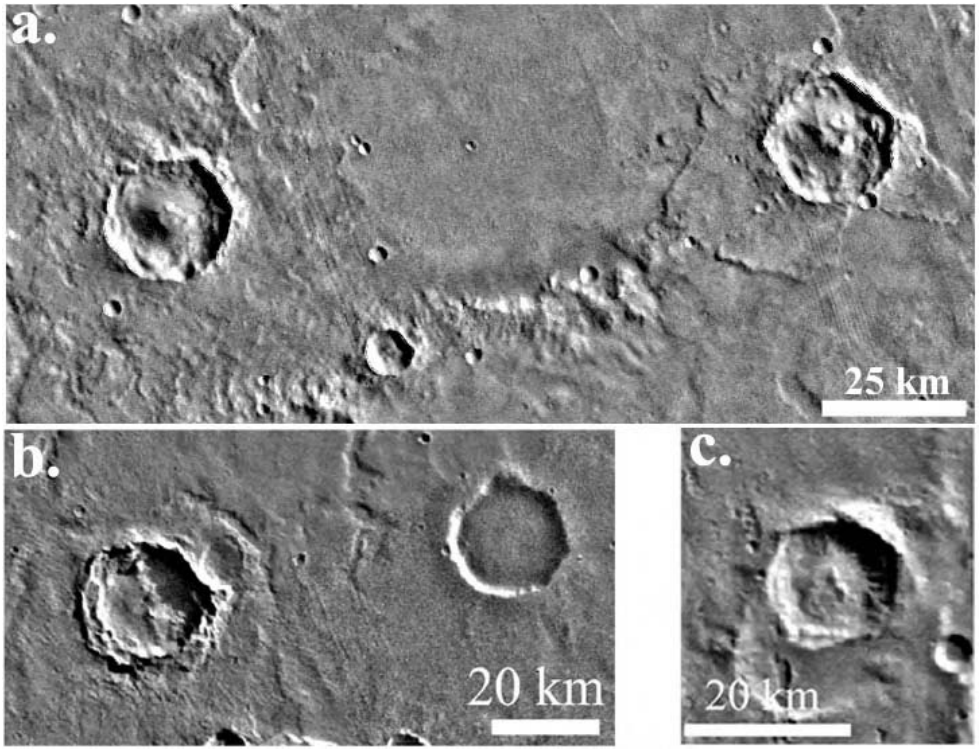

Figure 18. Examples of Martian polygonal craters as seen in the Viking MDIM 2.0 mosaic. a.) Three PICs north from the Hellas basin (2.8ºS 298ºW). Note the roughly parallel strikes of e.g. the rim segments in the northeastern parts of the craters, quite possibly enhanced by lighting geometry. b.) A fresh (left) and a degraded (right) PIC northeast from the Argyre basin (29.5ºS 22.5ºW). c.) A PIC northeast from the Argyre basin depicting strong tendency towards a hexagonal shape (30.2ºS 24.5ºW). North is up in all images.

Leighton et al. (1969) also used photographs from Mariner 6 and 7 missions. In their preliminary study they stated that craters in Meridiani Sinus[30] "have more marked polygonal outlines" than craters in some other areas imaged by Mariners 6 and 7. Polygonal craters on Mars were also identified by Pike (1971) using the same early Mariner images. However, at the time he merely stated that small Martian craters are usually simple in shape, whereas craters larger than 10–15 km tend to have typical features of complex craters and polygonal outlines. In his later study (Pike, 1980b), PICs receive even a shorter mention in connection with an image of a rather poorly-defined polygonal simple crater.

In his study of ancient Mars tectonics, Schultz (1985) used a few measurements from polygonal crater wall scarps that concur with other tectonic data, but didn't give any further details. Thomas and Allemand (1993) studied the extensional tectonics of the Tharsis bulge,[31] and mention polygonal craters as being caused by an impact into faulted target. However, in addition they state that some of the polygonal craters are also elliptical, due to easier excavation along fault planes.

[30] Meridiani Sinus (i.e. Sinus Meridiani) was later named Terra Meridiani, but both names are now abandoned. Currently accepted name Meridiani Planum covers a section of Terra Meridiani, and it is partly within the greater Hellas study area dealt with in Paper I.

The easy excavation along fault planes was suggested by Eppler et al. (1983) as a way to create elliptical craters, but such craters were not polygonal in their model, merely elongated. Thus, it remains somewhat unclear from Thomas and Allemand's (1993) study, how such a polygonal–elliptic crater should actually look like, and how it could be differentiated from ordinary polygonal or elliptic craters.

A highly interesting new approach to Martian polygonal crater studies has been initiated by Watters (Watters, 2006; Watters & Zuber, 2007, 2009). His study uses a machine vision approach and Fourier shape analysis, thus effectively removing subjectivity in the classification and measuring process. The system has so far been mainly applied to small simple craters in Meridiani Planum, especially the polygonal Endurance (D=150 m) crater intensively studied by the Mars Exploration Rover Opportunity (Watters, 2006). Watters' results imply that where fracture systems are visible, the polygonal crater corners are frequently intersected by fractures.

The most recent results (Watters & Zuber, 2009) are also the most intriguing. According to them, the small simple craters that form in targets having "clearly-expressed systematic joints", or in "non-lava targets" (referring to debris- and sedimentary-dominated targets) have a larger tendency to be square-shaped than craters in other types of target materials. Another very significant result regarding the PICs is that simple craters larger than about 150–250 m in diameter are more circular than smaller craters, possibly related to the change from strength- to gravity-dominated cratering regime (Watters & Zuber, 2009). These first preliminary results hold great promise for future implementation of the system for studying the interplay between cratering and tectonic structures.

6.1.3 PICs on Mercury

The innermost and smallest planet of our Solar System, Mercury, is a rather poorly studied planet compared to Venus, Mars, Jupiter or Saturn. Only two space missions have investigated the planet: Mariner 10 more than three decades ago, and MESSENGER (Mercury Surface, Space Environment, Geochemistry and Ranging) on its first flyby on January 14th 2008, and the second on October 6th, 2008. Because Mariner 10 was not an orbiter but instead performed three flybys, it was able to photograph less than half of the planet's surface (e.g. Vilas, 1999). Now (December 2008), about 95% of the surface has been imaged by a spacecraft. MESSENGER's data from the first two flybys has obviously not yet been studied in great detail, so despite some new interesting results (e.g. Murchie et al., 2008; Strom et al., 2008), the so far published knowledge about the Mercurian surface is still based almost entirely on Mariner 10 imagery.

[31] For another study in the same region, with significantly differing results, see Golombek et al., 1996.

Polygonal impact craters are also present on Mercury (Fig. 17a), but their study has apparently been rather limited in scope. The only studies even briefly discussing Mercurian polygonal craters that I am aware of, are a comparative study on crater degradation by Wood et al. (1977), research on Mercurian global tectonics carried out by Dzurisin (1978) and Melosh and Dzurisin (1978; for a pre-MESSENGER update on the tectonics of Mercury, see Melosh and McKinnon, 1988), and the geologic map of the Bach region by Strom et al. (1990; see also Strom & Sprague, 2003). However, in otherwise comprehensive reviews of Mercurian cratering and crater morphology (e.g. Gault et al., 1975; Pike, 1988; Schultz, 1988), polygonal craters are conspicuously missing.

The first study on Mercurian PICs is in many ways also the most fascinating. Wood et al. (1977) found that 13% of craters with a continuous and sharp rim over 30 km in diameter are "quasipolygonal", and 3% "strongly polygonal". Unfortunately no definitions or figures accompany these classifications. In any case, altogether 16% of fresh craters display at least some level of polygonality. In the class of most degraded craters where the craterform is not easily recognised, only 3% of craters (D>30 km) are classified as having any polygonal features. Although Wood et al. (1977) do not specifically state it themselves, this is a clear indication that crater degradation is not the cause for the polygonal outline of crater rim. Another salient general conclusion of their study was that the polygonal shape of Mercurian craters is not as well developed or conspicuous as it is on the Moon, and that there does not seem to be any systematic orientations of the straight rim segments. No data, however, is presented to support this. (Wood et al., 1977)

Melosh and Dzurisin (1978) included in their lineament study an unspecified but apparently a small number of linear segments of crater rims that Dzurisin (1978) had mapped. Dzurisin (1978) already noted that many Mercurian craters are distinctly polygonal, and Melosh and Dzurisin (1978) presumed that "crater polygonalization" is caused by the structural control of pre-existing fractures. Also Strom et al. (1990) mention PICs with other lineaments like ridges and scarps. According to their study, "joint-controlled mass movements are most likely responsible for the polygonal crater-wall segments". As Strom and co-workers (1990) observed straight crater rim segments as long as 100 km, they concluded that the fractures controlling their formation extend deep into the lithosphere. In addition to being deep, at least some of these fractures are also very old, probably older than the oldest craters and basins (Strom et al., 1990). Strom and Sprague (2003) complemented the Strom et al. (1990) study by adding that straight rims occur on both degraded and fresh craters, and that also preferential excavation along zones of weakness may be causing the polygonal outline. In addition, the earlier orientation results by Wood et al. (1977) are contradicted by Strom and Sprague (2003): PIC rims and "linear ridge-like structures" trend mainly northeast and northwest, with a weaker north–south orientation.

Having gone through global shrinking and an immense impact creating the Caloris basin with its marked antipodal effects, Mercury certainly has a fascinating geologic history from a structural point of view, albeit it is apparently not a tectonically active planet anymore (e.g. Melosh and McKinnon, 1988; Murchie et al., 2008; Solomon et al., 2008). Thus a detailed analysis of Mercurian PICs – the abundance of which has been attested not only by the Mariner 10 images but also by the first two MESSENGER flyby PR image sets – could quite possibly reveal fascinating new aspects of the geology of Mercury even before MESSENGER starts the detailed mapping of the planet's surface in 2011, hopefully followed by the European BepiColombo mission in 2019.

6.1.4 Venusian PICs

As described earlier (Chapter 3.2), Earth's "sister planet" Venus has a surface dominated by volcanic and (volcano–)tectonic features. Its impact crater population is rather small, comprising only less than a thousand impact craters (Herrick et al., 1997; Schaber et al., 1998). As the planet's surface is geologically young (Phillips et al., 1992; Schaber et al., 1992; Strom et al., 1994; Basilevsky et al., 1997), the impact craters are generally quite pristine and so the fresh crater morphology can be studied. Venus' very dense atmosphere has made it impossible to study the surface by photographic means. Hence radar images, primarily obtained by the Magellan mission during the early 1990s, are the data source for Venusian craters, naturally thus complicating some aspects of impact studies. (e.g. Phillips et al., 1992; Weitz, 1993; see below)

Herrick et al. (1997) reviewed the morphology of the Venusian impact craters. They do not mention polygonal craters as a distinct crater class in their review. However, their accompanying database does have twelve impact craters classified as polygonal.[32] Almost all of them are polygonal also according to our definition. To my knowledge, that is the only instance before this thesis (first noted in Paper I), where the polygonality of Venusian impact craters has even been mentioned.

In summary, PICs have been identified on Mars, Mercury and Venus immediately after high-resolution images from the surface became available. Their study has been most advanced in the case of Mars, where they to small extent have been used as a tool in mapping paleotectonics, whereas Venusian PICs haven't been studied at all before this Ph.D. thesis. The most recent studies of small Martian PICs imply a possibility of a noticeable variation between different types of target material in their tendency to promote PIC formation. Results gained from the study of Mercurian PICs clearly seem to indicate that PICs are controlled by deep, ancient structures in the lithosphere.

[32] Paper IV is somewhat imprecise about this. According to Paper IV, Herrick et al.'s (1997) database has only four polygonal craters. However, there are twelve polygonal craters altogether in the database, but only four in the size range studied in Papers IV and V.

6.1.5 PICs on other heavenly bodies

The Jovian and Saturnian systems have been studied by several space missions, most recently by Galileo and Cassini spacecraft, the latter currently orbiting Saturn. As can be seen in Figs. 17h–17l, several moons in these systems host PICs on their surfaces, regardless of the fact that many of these surfaces are rich in ice(s); for example Europa's sparsely cratered surface is almost completely made out of water ice (e.g. Greenberg & Geissler, 2002).

To my admittedly limited knowledge about the research regarding the geology and impact craters of these intriguing worlds, very few remarks have been made about polygonal craters. Saturn's satellite Rhea hosts a large population of impact craters on its surface, and a substantial portion of them are strikingly polygonal. This was noticed already from the images provided by the Voyager 1 flyby mission in 1981 (Smith et al., 1981). However, this observation by Smith et al. (1981) led them to suggest that a rubble zone makes up the upper crust. This can hold for the many irregular craters on Rhea's surface, but it is in contrast with ideas and conclusions drawn by several other research groups regarding the origin of polygonal craters, and that are also promoted in this Ph.D. thesis. Another possibility is that the rubble Smith et al. (1981) are referring to, has a very large "grain size" compared to the diameters of the craters.

Subsequent studies give even less input to the story of polygonal impact craters on the moons of the outer Solar System. Thomas et al. (1998) mention in passing that the crater Nergal on Ganymede is polygonal. Porco et al. (2005) and Denk et al. (2005) noticed that at least two large impact basins on Iapetus are polygonal, whereas Helfenstein et al. (2005) observed that some of the viscously relaxed craters on Enceladus are polygonal. More emphasis in Enceladus studies has been given to the observation that pre-existing impact craters control the orientations of the subsequently forming fractures (e.g. Miller et al., 2007).

A bit more can be said about the studies concerning polygonal craters on the surfaces of asteroids. Asteroid 243 Ida was imaged by the Galileo spacecraft en route to Jupiter. It is apparently the first asteroid where PICs were identified (Belton et al., 1994). PICs on the surface of Ida were interpreted to suggest a formation in a fractured surface layer, or in a strong enough pre-existing stress field (Belton et al., 1994).

The NEAR–Shoemaker (Near Earth Asteroid Rendezvous) spacecraft orbited around, and eventually even landed on the asteroid 433 Eros (measuring 34×11×11 km) at the turn of the millennium, providing a wealth of data. Among the data were highly detailed photographs of Eros' surface features, including numerous impact craters. Many of these are polygonal (Zuber et al., 2000) and most commonly square-shaped simple craters like the Meteor Crater, as noted and briefly

discussed by Prockter et al. (2002; Fig. 17f). According to Prockter et al. (2002), only craters of "optimum" size are affected by the structural control, i.e. too small craters have diameters less than the average spacing of fractures so they are not affected by the fractures, just as was suggested by Fulmer and Roberts (1963; see Chapters 6.1.1 and 6.3). The fact that also craters larger than the "optimum" size are less distinctly polygonal may be connected to the depth of fracturing (Prockter et al., 2002).

In addition to Ida and Eros, also asteroid 253 Mathilde hosts polygonal impact craters on its surface. Like Eros, also Mathilde was photographed by the NEAR–Shoemaker spacecraft. Veverka et al. (1997) noted that craters larger than five kilometres in diameter are markedly polygonal. They interpreted this as an indication of structural control, possibly by pre-existing fractures. However, the PICs do not reveal a continuous structural fabric across Mathilde (Thomas et al., 1999). On Mathilde, the PICs are the only indication of the asteroid's fractured structure, underlining the importance of polygonal craters in the studies of small Solar System bodies. (Veverka et al., 1997; Thomas et al., 1999; see also Cheng, 2002, 2004a, b)

Besides asteroids, also comets may host impact craters on their surfaces. Most of the craters on the nucleus of comet 81P/Wild-2 (Fig. 17m) are circular, but some of the flat-floored craters are polygonal, as was noted by Basilevsky and Keller (2006). In addition to PICs, there are also other indications of the structural control of the surface features on Wild-2. These observations enabled them to conclude that either the inner structure of Wild-2 is not that of a "rubble pile" (see e.g. Asphaug et al., 2002), or at least the size of the fragments must be in a specific size range (Basilevsky & Keller, 2006).

Thus, all in all, PICs can fairly safely be concluded to be a common feature among the smaller bodies of the Solar System, whether they be (icy) moons, asteroids, or even comets. On the surfaces of the smallest of these bodies they serve as prominent indicators of significant crustal strength.

6.2 Studies of terrestrial polygonal and structurally controlled craters

6.2.1 Simple craters

The 1960s was an important decade also for ground-truth data of PICs. Baldwin (1963, 1964) noted that often terrestrial impact craters (e.g. Meteor Crater, Aouelloul, and Wolfe Creek) tend to have polygonal shapes rather than being circular. In concert with his conclusions about lunar craters, Baldwin (1963) was also convinced that the polygonality of the Meteor and Aouelloul craters was a

primary feature. Regarding the Meteor Crater he also suggested that "the form of the crater may have been affected by structural weakness in the rock" (Baldwin, 1963).

However, it was mainly Eugene Shoemaker's work (1960, 1963,[33] see also 1962) on the Meteor Crater in Arizona, USA, which made it finally clear that this meteorite impact crater certainly is not circular, but much more resembles a square. The square shape had been observed at least already in the late 1940s (Zimmerman, 1948, cit. Fielder, 1961; Baldwin, 1949), but before Shoemaker's work there had been claims that the square shape is merely apparent rather than being real (Baldwin, 1963).

The significance of two perpendicular regional joint sets in the target rocks (mainly sandstones) was strongly pointed out by Shoemaker (1960, 1963; see also 1962), and subsequent work by Roddy (1978) further emphasised their critical role in forming the squarish outline. The works by Shoemaker and Roddy also asserted that the straight segments of the Meteor Crater wall are a primary feature of the crater, and not a product of erosion (see Chapter 6.4).

One of the highly consequential observations about the Meteor Crater was that the diagonals of the crater are essentially parallel to the main regional joint sets in the target rock (Shoemaker, 1960, 1962, 1963; Roddy, 1978). Interestingly, Baldwin (1963) pointed out that originally Shoemaker had regarded the joint sets in the Meteor Crater being parallel to the sides of the square, not the diagonals. Recent field work in the Meteor Crater has provided observations and interpretations for both dominating diagonal fractures (Poelchau et al., 2008, 2009), as well as dominant rim-parallel fractures (Kumar & Kring, 2008). These issues, most relevant for polygonal crater formation models, are further discussed in Chapter 6.4.1.

Another proven (or perhaps "accepted" would be a more suitable term) terrestrial impact structure in the simple crater size range, where a notable influence by pre-existing structures has been suggested, is the small, heavily degraded and tectonically modified Saarijärvi impact structure in northern Finland.[34] Due to the substantial erosion, infilling and glacial overburden cover of Saarijärvi, the polygonal (roughly pentagonal or hexagonal) shape of the structure can most easily be seen in the electromagnetic anomalies. (Öhman, 2002; Öhman et al., 2003; see also Öhman, 2007b)

[33] Shoemaker (1963) is actually very much a word by word copy of his earlier work (Shoemaker, 1960), particularly the section dealing with the Meteor Crater.

[34] The influence of pre-existing target weaknesses in Saarijärvi is certainly not proven, as it is possible that at least partly the polygonality is due to the heavy post-impact tectonic modification of the structure. The original diameter of Saarijärvi may have been close to the average simple-to-complex transition diameter in crystalline rocks, i.e. 4 km.

The 1.13 km diameter Tswaing[35] crater in South Africa appears hexagonal in a satellite image (Reimold et al., 1996). However, this has been deemed "a result of the combination between radial faulting and the effect of shadow" (Reimold et al., 1996). The crater has been described as being highly circular (Brandt & Reimold, 1995; Reimold et al., 1996), and no conclusions have been drawn on the possible effects of the regional joints on the crater formation (Brandt & Reimold, 1995). Nevertheless, on a cursory level it is interesting to note that on the geologic map of the crater (Brandt & Reimold, 1995) the western rim of the structure appears very straight indeed, and that its orientation exactly parallels a prominent joint orientation of the target rocks (Brandt & Reimold, 1995).

6.2.2 Complex craters

The accounts of larger terrestrial impact structures possibly being polygonal and/or morphologically affected by pre-existing target structures are typically not too specific in their description of possible effect of the target structures, a good example being Morrison's (1984) mentioning and a sketch of Charlevoix's (D=54 km) polygonality. Exceptions include the Wells Creek (see below), Lappajärvi, and Söderfjärden (Fig. 17d) impact structures, where somewhat more detailed studies are available. The Söderfjärden structure in western Finland, having a present day rim-to-rim diameter of about 6.6 km (Abels, 2003), is actually a prime example of a small terrestrial complex crater with a distinctly hexagonal rim shape. The target rocks (mainly migmatitic granitoids) in Söderfjärden have two regional approximately orthogonal fracture directions (Abels, 2003; see also Talvitie et al., 1975, and Raitala, 1985). The third dominating structural trend comes from the metamorphic fabric bisecting the fracture trends roughly in an angle of 45º (Raitala, 1985; Abels, 2003). All these three directions can readily be seen in the present day topographic appearance of this notably hexagonal impact structure, as well as in its geophysical signature (Abels, 2003). Thus, in Söderfjärden the match between the rim strikes and regional structural directions is clearly manifested (Abels, 2003; see also Laurén et al., 1978; Raitala, 1985; and Öhman & Raitala, 2005).

Similar observations and conclusions have been made also regarding the target fractures' and schistosity's effect on the polygonality of magnetic, electromagnetic and gravity anomalies in the ~22 km diameter[36] Lappajärvi impact structure, also located in western Finland (Elo et al., 1992; Abels, 2003). Elo et al. (1992) clearly conclude that the sharp straight edges of the aeroelectromagnetic anomalies – which are parallel to bedrock structures – imply that two

[35] Previously known as Pretoria Saltpan.
[36] ~22 km is the estimated average original rim-crest diameter (Abels, 2003).

orthogonal pre-existing sets of faults and deep fractures controlled the formation of the Lappajärvi impact structure.

Another rather well-known case is the Bigach impact structure (D≅7–8 km) in Kazakhstan, which has been described as a polygonal rimmed structure by Grieve et al. (1988). Its slightly angular shape has been ascribed to the structure of the target rocks, selective erosion (Kiselev & Korotushenko, 1986, cit. Masaitis, 1999), and neotectonic block movements (Masaitis, 1999). According to Roddy (1977a), the notably straight western "crudely terraced" walls of the 3.8 km diameter Flynn Creek impact structure[37] seem to follow the regional joint pattern, although it is possible that the present form is enhanced by erosion (see also Roddy, 1977b).

In their remote sensing study, Garvin et al. (1992, 1995) describe Bosumtwi impact structure (D=10.5 km) in Ghana as having a "quasipolygonal" outline. They identify northeast and north-northeast striking regional structural trends, but state that the shape of the crater is "clearly independent" of these regional trends (Garvin et al., 1992). According to them, major slumping of the inner wall of the crater (without structural influence) is the mechanism responsible for the crater shape. However, at least a partial match of some straight segments of the rim with regional fault trends can easily be seen for example in the simplified geologic map by Reimold et al. (1998). Also, Garvin et al.'s (1992) somewhat indirect and unclear reasoning that the independence of the regional structures and the polygonal shape of Bosumtwi would gain support from studies of planetary impact craters seems unfounded, as has been shown above.

The polygonality of the Crooked Creek (D=7 km) and Decaturville (D=6 km) complex impact structures, both in Missouri, USA, were studied in some detail in the mid-1960s. At the time of the works by Amstutz (1965) and Zimmermann & Amstutz (1965) their origin was unclear. These authors preferred an endogenic origin, and the structures' shapes were explained by many periods of faulting and folding associated with long-lasting diapiric movements (Amstutz, 1965; Zimmermann & Amstutz, 1965;[38] for a more recent tectonic study regarding Crooked Creek, see Kenkmann, 2002). In any case, these impact structures are located in an area of two major regional fault systems (Amstutz, 1965), so their effect to the impact process does not seem too far-fetched. It is interesting to note that Amstutz (1965) mentions the Weaubleau structure – nowadays regarded as a probable impact site – as a polygonal area, although in modern studies (e.g. Evans et al., 2003, 2006) it is considered as a circular structure.

[37] Despite its small size, Flynn Creek is a complex impact structure with a well-pronounced central uplift, most likely due to the sedimentary target rocks.
[38] In addition, see the brief discussion by Papunen (1973), whose work in some extent compares Sääksjärvi impact structure in Finland to e.g. Crooked Creek and Decaturville.

In addition to Weaubleau, other probable or possible impact structures that have been described as being polygonal include Temimichat (D=700 m) in Mauritania, whose hexagonal outline has been interpreted to be caused by preferential erosion of gabbroic dykes on the crater rim compared to the more competent granitoid bedrock (Rossi et al., 2003; polygonality was already noted by Baldwin, 1964). Other possible terrestrial polygonal impact structures are Ramgarh in India, and Umm al Binni in Iraq. The former, about 3 km (Master & Pandit, 1999) to 5.5 km diameter (Grieve et al., 1988) structure has a shape of a square with rounded corners (Master & Pandit, 1999), and the latter ~3.4 km diameter structure – possibly of late Holocene origin – has a southern part that forms half of a hexagon (Master, 2001; Master & Woldai, 2004). However, the origin of these structures and thus also the origin of their polygonal shape remains highly speculative.

Also one of the largest of the currently known impact structures on the Earth appears to be structurally controlled. Manicouagan impact structure (D=100 km) in Canada was described as "a remarkable octagonal feature" already by Currie in 1965. Manicouagan's polygonality is not seen in the structure's actual rim, which of course has long since been totally eroded, but in the crater's peripheral trough now flooded by a reservoir. It is seen even better in the original distribution of the non-flooded lakes and rivers (Morrison, 1984). In other words, the structure's polygonal outline is defined by deeper levels of the inner wall of the crater rim. According to Floran and Dence (1976) and Trenc et al. (1999), the peripheral trough's straight segments follow regional fault and fracture orientations, and the downfaulting took place along these pre-existing planes of weakness.

For the sake of completeness, as well as clarity, it should mentioned that also other very large terrestrial impact structures, the Sudbury structure (D≅250 km) in Canada, the Chicxulub structure (D≅195 km) in (the Gulf of) Mexico, and the extremely eroded Vredefort structure (D≅300 km?) in South Africa, were probably affected by pre-existing target heterogeneities during the crater formation. In the case of Sudbury, Spray et al. (2004) proposed that two regionally dominant sets of basement faults affected the modification stage of the crater, as well as influenced post-impact isostatic adjustments. Morrison (1984) even suggested that Sudbury could have originally been a polygonal impact crater very much like the Copernicus crater on the Moon. According to his idea, most of the Sudbury's world-class Cu–Ni–PGE ores are related to troughs that are located in the corners of the original polygonal-shaped crater. However, given the extreme deformation of the Sudbury structure since its formation ~1.85 Ga ago, Morrison's (1984) idea about reconstructing the original polygonal morphology should be regarded merely as an interesting, yet highly speculative hypothesis.

Grieve et al. (2008) also noted the influence of pre-existing structures in the formation of Sudbury, but the similar effect is more pronounced in Vredefort, mainly because there more structural data is available. Re-activation of the pre-existing structures, related both to the excavation and the modification stages, is evidenced as thrusts and strike-slip faults (Grieve et al., 2008; see also Brink et al., 1997).

To avoid any ambiguities it is worth noting here that the Vredefort structure possesses some well-known polygonality. However, the polygonal shape can be seen in the central uplift (e.g. Antoine et al., 1990; Wieland et al., 2004), not anywhere near the rim (the location of which is debated and basically cannot be defined anymore due to the very heavy erosion), and therefore although being an extremely interesting phenomenon as such, it does not fall within the scope of this Ph.D. thesis.

Also the case of Chicxulub falls beyond the main topic of this thesis, but should be mentioned briefly. As the Chicxulub structure is fully covered by post-impact sediments, structural observations and reconstructions similar to the ones regarding Sudbury and Vredefort are not possible. Nevertheless, Gulick et al. (2008; see also Collins et al., 2008; and Schultz, 2008) mention the importance of target heterogeneity in the formation of the impact structure. However, they interpret that the observed asymmetries in Chicxulub, based on the new seismic data, are mainly due to the varying bathymetry (i.e. target topography), not faults or other similar planes of weakness. Thus, the case is similar to the ones observed in some lunar craters (e.g. Gifford & Maxwell, 1979; Gifford et al., 1979).

Possible implications for polygonal complex crater formation that are significantly different from many other works cited above can be found in the impressive book by Wilson and Stearns (1968; main results are summarised in Stearns et al., 1968). Their work is one of the most detailed studies ever carried out on the structural geology of an impact structure. They investigated the origin of the Wells Creek structure (D=12 km) in Tennessee, USA, by combining their studies on stratigraphy, structure, and brecciation, augmented by geophysical data. Morphologically the structure is characterised by an outer graben, horst, inner graben and a central block. According to the work of Wilson and Stearns (1968), the Wells Creek structure is essentially circular in plan view, but there are clear deviations from the circularity, caused by pre-existing target fractures. Concentric faults of the structure are straight for substantial parts of their circumferences. Similar structural control can also be observed in the radial faults. The Marable Hollow fault, which marks the boundary between Wilson and Stearns' (1968) horst and inner graben, delineates a square-shaped inner part of the impact structure. The two, roughly orthogonal pre-existing joint sets are parallel to the diagonals of this square.

In the Wilson and Stearns (1968) model (their Fig. 67) the Wells Creek structure had an original rim-to-rim diameter of about 5 km, and the rim crest was located in the inner part of the current inner graben. However, if we accept the diameter of 12 km (as cited in the Earth Impact Database[39]), which was also Wilson and Stearns' maximum diameter, the crater rim would be somewhere in their outer graben, rather close to the horst. Thus the Marable Hollow fault approximately marks the inner part of the crater wall.

Wilson and Stearns (1968) made a rather direct comparison between the roughly square planimetric shapes of the interior of the Wells Creek structure (i.e. the area bounded by the Marable Hollow fault) and the Meteor Crater. This seems rather unwarranted, because in their favoured model the Marable Hollow fault lies outside the crater rim. The currently accepted diameter (Wilson and Stearns' maximum diameter) would make the comparison somewhat more justified. However, Wells Creek clearly is a complex crater, and thus the currently favoured formation models of polygonal complex craters (Chapter 6.4.2) should be applied. The Marable Hollow fault forming an angle of about 45° with the two pre-existing orientations of weakness in the target rock obviously is a misfit to the ideas presented both previously (Eppler et al., 1983) and in this Ph.D. thesis.

To summarise, it appears to be quite common that – with a handful of exceptions described above – either the polygonal shape of a terrestrial impact structure (whether it be proven or proposed) is merely mentioned, but its origin is not discussed in detail, or that the polygonal outline is explained as resulting from post-impact erosional or tectonic modification. The connection between target structures and terrestrial PICs is, however, shown to exist in several cases, but detailed studies have only been carried out in Meteor Crater and, to some extent, with remote sensing methods in Söderfjärden. Even in Meteor Crater both old and new published studies give surprisingly varying results and conclusions. Despite these shortcomings, it is clear that many terrestrial impact structures exhibit at least some degree of real, structural polygonality. This can be visible either in their morphology, or in their geophysical anomalies that often represent the structures' true shape much better than their present day eroded morphological appearance.[40]

[39] http://www.unb.ca/passc/ImpactDatabase/index.html, last accessed January 7th, 2009.

[40] Currently my unpublished list of terrestrial polygonal impact craters or impact structures influenced by target fractures includes 34 proven or generally accepted impact structures that show at least some notable polygonality, or have been described in literature as such, plus seven probable or possible polygonal impact structures, and three structures where the central uplift is polygonal. Whether the polygonality of all of these structures is primary and structurally controlled is, however, entirely another question.

6.3 Impact and explosion experiments concerning polygonal craters

In addition to detailed field work on natural impact structures, the 1960s saw the rise of experimental impact and explosion cratering studies. A few of them dealt with polygonal impact craters as well. The work conducted by Gault et al. (1968) at the NASA Ames Vertical Gun Range showed that while the Meteor Crater displays a fairly simple and elegant case,[41] one cannot assume that two perpendicular joint sets would always give rise to a square-shaped crater whose diagonals parallel the joints: with two perpendicular joint sets, also a hexagonal crater was produced. Unfortunately Gault et al. (1968) did not specify the relationships between the joint sets and the straight rim segment strikes of the small hexagonal impact crater that resulted from their experiment.

Similar problems occurred with the reports of polygonal craters resulting from experiments with high explosives carried out in the Nevada test site (Johnson, 1962, cit. Fulmer & Roberts, 1963). In their own smaller explosion experiments, however, Fulmer and Roberts (1963) noted that there are joints parallel both to polygonal craters' rims and to their diagonals. Combining their experimental studies and observational work on lunar PICs, Fulmer and Roberts concluded that distinctly polygonal craters result when impact occurs in target material that is rigid and has a well-developed simple fracture pattern. When the rigid target material has a complex set of closely spaced fractures, or when the fractures are very widely spaced or even non-existent, the impact results in a dominantly circular crater. The same occurs when the target material is fairly "soft" (non-cohesive), like loosely or non-compacted sediments.

Roddy and Davis (1977) studied shatter cones formed in small-scale explosion craters (a diameter of a few metres), but briefly noted also the effect of target joints and fractures on the crater shape. The fracture sets in the target tonalite were approximately orthogonal, and at least in one case the result was a somewhat square-shaped crater, "due to the effects of the vertical joints". In addition, in one case Roddy and Davis (1977) mention that "complex jointing caused a very irregular crater", but it is not quite clear whether they mean the planimetric shape of the crater rim, or the morphology of the crater floor. It can be mentioned here, despite the fact that it appears not to have been discussed in previous studies (e.g. Roddy, 1976, 1977a), that the innermost ring of the multi-ringed 500 ton TNT explosion crater Prairie Flat is strikingly hexagonal, well illustrated for example in Fig. 8b in Roddy (1977a).

Numerical studies of the effect of target fractures on the cratering mechanism have so far been very much lacking. Although the importance of target structure, including fractures, is acknowledged,

the research efforts have been mainly aimed at understanding the effect of target granularity to the shock wave and the cratering process. (Barnouin-Jha et al., 2003)

What becomes painfully obvious from the published studies of impact and explosion experiments regarding PICs is that more experimental work is definitely needed. And most importantly, the structures and other properties of the target material must be carefully described before and after the experiment, and the observed structures of the resulting crater must be correlated with them. The experimental studies carried out so far have implied that the interplay between cratering mechanics and target structures is complex, but the details and the crucial question of why it is so complex need to be answered by more rigorously implemented experiments in the future.

6.4 Modern models of PIC formation mechanisms

From the aforementioned studies it becomes apparent that some of the key points presented in this Ph.D. thesis (see Chapters 9 and 10) – that polygonal impact craters are common, their origin is not degradational or caused by illumination effects, and that the straight rim segments often (but not always; see Chapter 9.6) parallel the apparent regional tectonic trends – have been known and also published for decades. Despite this the importance of PICs, or even their existence beyond the Meteor Crater, is generally quite poorly known among the impact research community. The fundamental reason for this is unknown, but one can reasonably speculate that the lack of a generally accepted and concisely presented unifying theory of how exactly such craters form is one contributing factor. An attempt towards such a theory has, however, been presented, and its pros and cons will be dealt with next.

6.4.1 Simple PICs and crater excavation

Eppler et al. (1983; summarised in their preceding work Eppler et al., 1982; see also Eppler et al., 1977) presented two models to account for the polygonal shape of simple and complex lunar craters. According to their (Eppler et al., 1983) Model 1, “excavation of the crater cavity proceeds preferentially along directions of crustal weakness. The cavity is enlarged in directions parallel to the trends of crustal structure.” Therefore the straight segments of the crater rim bisect the strike of the structural weakness in an angle that in the case of the Meteor Crater is about 45º. It is worth stressing that in this model, the polygonal shape of the crater originates already from the excavation stage of the crater, and is thus indeed a very primary feature of the crater.

[41] However, see chapter 6.4.1 about the problems in understanding the structural origin of the Meteor Crater.

This model owes a lot to previous works mainly by Shoemaker[42] (1960, 1963; see also 1962) and Roddy (1978; preceded by Roddy et al., 1975) as well as Schultz (1976), and in some extent also to experimental works for example by Gault et al. (1968). So obviously Model 1 has its roots in the field evidence from the Meteor Crater.

Poelchau et al. (2008, 2009) restudied the pre-impact and impact-induced structures of the Meteor Crater, and presented a slightly more detailed view on how the square-shaped morphology actually forms. According to them, the two dominant pre-impact fracture sets (however, the fracture data was taken from Roddy, 1978) are forming diagonals across the current square-shaped crater. In their approach the target material is approximated by cubes bound by the two joint sets and the bedding planes. When the excavation flow field is directed parallel to the joint sets, a smaller surface area of each cube is exposed to the flow field than in the case where the excavation flow is at an angle of 45° to the joint sets. When the excavation flow is parallel to the joints, the shear stress is exerted only on one surface of the cube, not on two as in the latter case. Hence, the excavation flow "feels" less resistance in the orientation parallel to the joint sets, and thus the excavation propagates faster and further when the excavation flow is parallel to the joints. According to their model, it should be $\sqrt{2}$ times easier to excavate the crater in the direction parallel to the joints than in an angle of 45° to them. Whether it is a coincidence or a ground truth validation of this simplified model, but the diameter of the Meteor Crater is $\sqrt{2}$ times larger measured from the corners than from the sides of the crater (Poelchau et al., 2009).

Another result of major consequence in the study of Poelchau et al. (2009) is that the heterogeneities (orthogonal joint sets) in the target do not only influence the plan view of the crater, but also the rim uplift becomes differential: the rim uplift is notably enhanced in the corners of the crater. This can readily be seen in the Meteor Crater. The enhanced uplift in the corners seems to be accompanied by the opening of gaps between the weaker interbeds, which then become filled with so called interthrust wedges. Obviously the target structure is not of importance for crater formation in the early stages of the excavation when the stresses greatly exceed the strength of the target material, but it becomes dominating near the end of the excavation phase (Poelchau et al., 2008, 2009).

The model by Poelchau et al. (2008, 2009) is clearly the most detailed model developed so far for PIC formation, and it seems to fit the observations in the simple Meteor Crater very well. Yet, somewhat surprisingly, significantly differing observations were made and conclusions drawn by

[42] Despite an apparently commonly held belief (e.g. Saunders et al., 1970), Shoemaker (1960, 1962, 1963) does *not* mention preferred excavation as a cause for the square shape of Meteor Crater. He merely points out the structural

Kumar and Kring (2008). According to them, instead of just two sets of fractures, there are three prominent sets of pre-impact target fractures, and the majority of them are parallel to the sides of the square-shaped crater, not its diagonals (i.e. similar to Shoemaker's original opinion, according to Baldwin, 1963). They suggested that the square shape resulted when the excavation flow preferentially overturned material along the fractures, and/or the slumping of the crater took place along them (see Model 2 by Eppler et al. (1983) below). Thus, it appears that although the Meteor Crater is one of the most thoroughly studied impact craters in the world, there are still large uncertainties regarding even the very basic geologic facts of the crater.

The PIC formation models involving enhanced excavation parallel to fractures (Eppler et al., 1983; Poelchau et al., 2008, 2009), although having been documented by case studies in the Meteor Crater, fail to account for the observations made from impact and explosion experiments by Gault et al. (1968) and Fulmer and Roberts (1963) described above. Of course one may argue that results obtained from small-scale impact and explosion experiments, producing craters from about 10 cm in diameter up to craters having a diameter of a few tens of metres, are not necessarily fully applicable to craters in the size range of kilometres. Nevertheless, the problem of scaling is almost always inherent in many cratering studies, and thus simply cannot be avoided.

To summarise the results from the field studies of simple crater sized PICs – and also experimental work – it can be said that based only on remote sensing studies without some other supporting evidence or further studies, it seems currently impossible to decipher with any reasonable certainty the relationship between the orientations of fractures in the target and the straight rim segments of any single simple polygonal impact crater. Further work is clearly needed.

6.4.2 Complex PICs and the crater modification stage

Model 2 presented by Eppler et al. (1983) is an attempt to explain the formation of polygonal craters that are in the size range of complex craters. In this model, which was outlined already by for example Schultz (1976), the walls of the transient cavity fail in the modification stage along pre-existing structures of the target. Thus, "the transient cavity is enlarged in directions perpendicular to the trends of crustal structure" (Eppler et al., 1983). This is in stark contrast to the scenario presented in Model 1. However, it is an advantage for the mapping of the crustal structures, because in this case the straight segments of the crater rim are parallel to the faults, fractures or joints or other such planes of weakness.

---

control, but does *not* say anything about the actual mechanism.

It should be emphasised that Eppler et al. (1983) clearly differentiate between large-scale polygonality, characterised by their low order harmonics, and the smaller-scale erratic irregularities that are described by their 11^{th} and other higher order harmonics. The large-scale shape of the rim remains relatively unchanged by later degradational processes. This is at least in part a reflection of the fact that the formation of large-scale polygonality requires more energy than is needed to generate the irregularities in the crater rim. (Eppler et al., 1983; cf. Eppler et al., 1977)

There is also some observational geological and geophysical data from the complex terrestrial impact structures supporting Eppler et al.'s (1983) Model 2, as discussed above. Despite all these field evidence it is currently not yet perfectly clear how, from a mechanical point of view, the formation of PICs according to Model 2 should actually take place.

The study of lunar crater rim terraces, typical for complex craters, has shown that at least the near-surface part of the rims' inner walls behave like a perfectly plastic material with negligible internal friction in the final moments of the modification stage (Pearce & Melosh, 1986; Melosh, 1989; see also McKinnon, 1978). On the other hand, the modification of the deeper levels of the crater centre, especially the formation of the central uplift, require a fluid-like behaviour of the target material (e.g. Melosh, 1989; Melosh & Ivanov, 1999). As noted by Melosh (1989), viscous fluid behaviour and perfectly plastic behaviour of target material seem contradictory. A combination of these two types of behaviour is not achieved by any classic rock mechanics. However, a substance known as a Bingham fluid is a material that supports applied stresses until a certain plastic yield strength is exceeded, after which the material behaves like a viscous fluid (Melosh, 1989). One way to make rocks behave like a Bingham fluid is through the process of so called acoustic fluidisation (e.g. Melosh, 1979; Melosh, 1989).

The basic idea behind the concept of acoustic fluidisation is that the impact-induced strong, short wavelength seismic (i.e. acoustic) shaking of rocks substantially lowers their strength, making the rock debris in a sense analogous to liquid (e.g. Melosh & Gaffney, 1983). The acoustic fluidisation probably works in practice as oscillating separate fault-bounded blocks, so the rocks do not deform as a plastic continuum, but the deformation is strongly localised (Ivanov & Kostuchenko, 1997; Melosh & Ivanov, 1999; Kenkmann et al., 2000).

Acoustic fluidisation hypothesis manages to explain several otherwise very problematic phenomena, most notably perhaps the formation of the central uplift. It works especially well with numerical modelling, while it must be said that also other ideas of strength degradation (e.g. thermal weakening and extensional failure at densities below normal; see O'Keefe & Ahrens, 1993, 1999) incorporated into the numerical models manage to produce – at least to some extent – simulated

craters with properties similar to what can be observed. However, the modification stage of the complex craters (e.g. Melosh & Ivanov, 1999 and references therein) is rather poorly understood at the moment. Even though it is commonly assumed that in addition to the forming central peak, the rim of the transient cavity must be substantially strengthless while it first collapses in the modification stage (e.g. McKinnon, 1978; Melosh & Ivanov, 1999), it often appears to be somewhat unclear how long in the modification stage this strengthlessness prevails, or how far laterally it extends from the point of impact.

The acoustic fluidisation hypothesis or other similar ideas that require large proportions of the transient crater material to be substantially strengthless,[43] bear notable significance to the Model 2 of polygonal impact crater formation presented by Eppler et al. (1983). The Model 2 requires that crater rim has a kind of a "memory" about the target properties, i.e. that the crater rim "knows" somehow where in the target there is a weaker direction, along which it can then collapse. If the rim material in the final moments of the modification stage is still in a substantially strengthless state, or if the strengthless region has at any point destroyed the pre-existing structures of the target, it is impossible for the rim to retain such a "memory". So if the necessarily somewhat simplified two-dimensional numerical models by, for example, Wünnemann and Ivanov (2003), where fluidised region extends far beyond the rim of both transient and final craters' rim (see Fig. 7 in Wünnemann & Ivanov, 2003), would be taken strictly literally and without understanding the geologic context or the resolution of the simulations, any effect of the target structures on the final crater morphology would be impossible. Target properties in the context of polygonal craters are further discussed in Chapters 9.6 and 9.11.

The theory for formation of complex PICs is simple as a concept. It has substantial support from mainly remote sensing studies of terrestrial complex craters, as well as planetary research. Therefore, although direct observational evidence for PIC formation according to Model 2 is lacking, the model is at least a very good working hypothesis, supported by a mass of indirect observations. It seems clear that complex craters have a tendency to collapse along a pre-existing plane of weakness. Thus, the straight segments of complex PIC rims are generally parallel to some pre-existing structural inhomogeneity of the target material. A possibility of a third PIC formation mechanism is discussed in Chapter 9.9.

[43] It is worth noting that there has fairly recently been a tentative attempt to explain the late-stage collapse mechanisms without any substantial loss of strength, but any further details of this approach are as yet lacking (Holsapple, 2004).

7 DATA AND METHODS

7.1 Image datasets

7.1.1 Martian data

The primary dataset used throughout the Martian part of this thesis is the digital Viking MDIM 2.0 photomosaic with a nominal resolution of 231.4 m/pixel at the equator (Kirk et al., 2000). In addition to the adequate resolution, it has a favourable illumination geometry and continuous global coverage. However, a downside of the MDIM 2.0 is that the resolution gets substantially poorer in higher latitudes. This significantly hampers the identification of the PICs, as well as the measuring of the straight rim strikes. Therefore, it introduces an inevitable bias to the data, because smaller PICs become increasingly difficult to recognise in the southern parts of the study area. This must be kept in mind when inspecting the areal distribution of PICs.

In Paper II, also Mars Global Surveyor's wide angle images taken with Mars Observer Camera (MOC-WA, the resolution of the modified image mosaic used was 231.5 m/px) were used for comparison after being reprojected to conformal Mercator projection also used in MDIM 2.0. The Viking dataset is much better than MOC-WA for this kind of study due to its lower incidence angle that makes the detection of topographic features like crater rims easier. The comparison between Viking imagery having variable incidence angle and MOC-WA with generally quite unchanged incidence angle was paramount for determining the effect of illumination geometry on the craters' apparent polygonality, and especially its effect on the rim strike distribution of a larger population of polygonal craters.[44] Also onboard the Mars Global Surveyor was the Mars Orbiter Laser Altimeter (MOLA). MOLA data was only used for creating reference or background images.

In Paper I, the relatively scarce (at the time of the writing of Paper I) Mars Odyssey THEMIS (Thermal Emission Imaging System) night-time infrared images (~100 m/px) were used to show that polygonality can be seen in other resolutions and wavelengths as well. THEMIS dataset was more extensively used in Paper III, when the morphology of the polygonal craters in the Argyre region was studied by classifying them as either simple or complex craters. The simple/complex classification was based on THEMIS infrared and the higher resolution visual channel images (17–35 m/px). Mars Reconnaissance Orbiter's HiRISE images (High Resolution Imaging Science

[44] See the brief comments in e.g. Fielder, 1961, p. 161; Fulmer & Roberts, 1963, p. 461; Binder & McCarthy, 1972, p. 280; and Schultz, 1976, p. 28 on the importance of the illumination geometry.

Experiment; 0.25 m/px) were used to look for small simple PICs with a clear-cut relationship with the tectonic structures of the target.

For practical reasons, mainly in order to limit the file sizes, both of the research areas on Mars were divided arbitrarily into several "blocks" defined by latitude and longitude boundaries. This block division was used as a basis for the directional analysis of the PIC rim strikes. In the greater Hellas region (Paper I), however, strike measurements were done only in part of the blocks due to the size of the area, although their distribution was studied in the whole research area.

For some further details regarding the Mars missions whose data was used directly as datasets or indirectly (i.e. used by previous researchers dealing with Martian polygonal craters; see Chapter 6.1.2) in this Ph.D. thesis, see Appendix 2.

7.1.2 Venusian data

Due to the thick Venusian atmosphere (see Chapter 3.2), the Venusian dataset used in this study is of a different nature than the very "normal" looking, mainly visible light images obtained from the Martian surface. The dataset was produced by the Magellan spacecraft, which orbited Venus from 1990 to 1994. Magellan images are synthetic aperture radar (SAR) images, i.e. the movement of the orbiting spacecraft creates a synthetic aperture much larger than the aperture of the radar antenna itself, thus increasing the resolution. Magellan radar, working on the wavelength of 12.6 cm, was side-looking, i.e. the radar was not imaging the area directly below the spacecraft, but either left or right.[45] Due to mission requirements, the incidence angle varied from ~15° to ~45°. Because of this, and because of the elliptical orbit, the Magellan SAR data is not of uniform quality. (Ford et al., 1993)

The primary dataset used from the variety of Magellan image products were the full-resolution mosaicked image data records (FMIDR) that have a resolution of ~ 75 m /px. These were used for the measurements and analyses. Additionally, once compressed mosaics (C1-MIDR) with 225 m/px resolution were used occasionally when FMIDRs were not available. C1-MIDRs were also used for the tectonic mapping of the areas that were used as examples (Paper V). The Magellan altimeter data with a "footprint" of 10–30 km was used sometimes for additional insight into the morphology of larger craters, as well as for mapping purposes. (Ford et al., 1993)

The radar images obviously do not depict the surface like the visible light imagery does. The stronger the backscatter of the radar signal, the brighter the image is. Thus, the radar imagery is

[45] Thus, in the Magellan terminology, "left-looking" images are the ones were the radar is actually "looking" towards right, and hence the surface is "illuminated" from the left.

very sensitive to slopes, as well as surface roughness (on the scale of the radar wavelength). Rough surface produces bright radar image, whereas smooth surfaces, like the volcanic plains, produce a relatively dark radar image. (Ford et al., 1993)

7.1.3 Lunar data

The dataset used for lunar PIC studies was the oblique-illumination photographs of the digital version of the Consolidated Lunar Atlas (CLA; Kuiper et al., 1967), which were taken with the 61 inch NASA Telescope at the Catalina Observatory. One of the reasons for choosing the study area (10°W–40°E, 10°N–50°S, Fig. 19) – covering parts of Tranquillitatis, Insularum, Nubium and Nectaris basins (TINN for short), as well as the less pronounced Werner–Airy and Mutus–Vlacq basins (Spudis, 1993) – was to have good CLA coverage of the area. As the study area, dominated by the Lower Imbrian and older Nectarian basin materials[46] (Wilhelms, 1987), is in the central near-side of the Moon, CLA provides several images with different illumination geometries of each surface feature.

The selection and minor editing of the subset of the CLA imagery that was used in Paper VI and Öhman et al. (2007, 2008a, b) was done by Mr. M. Kallo. He also did a preliminary selection of possible PICs that was used in Öhman et al. (2007). However, in Paper VI and Öhman et al. (2008a) his selection was used merely for "informative" purposes, and the actual classification of craters to polygonal and non-polygonal ones was done by me. Thus, the requirement for the agreement of two researchers (see below) was in this case not put into effect.

The identification of the observed polygonal craters was done using the Atlas and Gazetteer of the Near Side of the Moon (Gutschewski et al., 1971), Virtual Moon Atlas Pro 3.5 software (Legrand & Chevalley, 2006), and in rare cases the 1:1 Million-Scale Color-Coded Topography and Shaded Relief Maps of the Moon (in essence the Lunar Aeronautical Charts, or LACs) available from the United States Geological Survey's (USGS) website. The coordinates and diameters of the craters were taken from the compilation by McDowell (2004; an update of Andersson & Whitaker, 1982), available from the USGS Planetary GIS Web Server (PIGWAD), except for the seven unnamed polygonal craters and one obvious mistake in McDowell (2004). In these cases the diameters were measured using the Virtual Moon Atlas.

[46] Though unknown at the time of the selection of the study area, the southern boundary of the TINN area fortuitously roughly concurs with a major change in megaregolith thickness (Thompson et al., 2009). Thus, in this respect, the highland parts of the study area can be regarded as being quite homogenous.

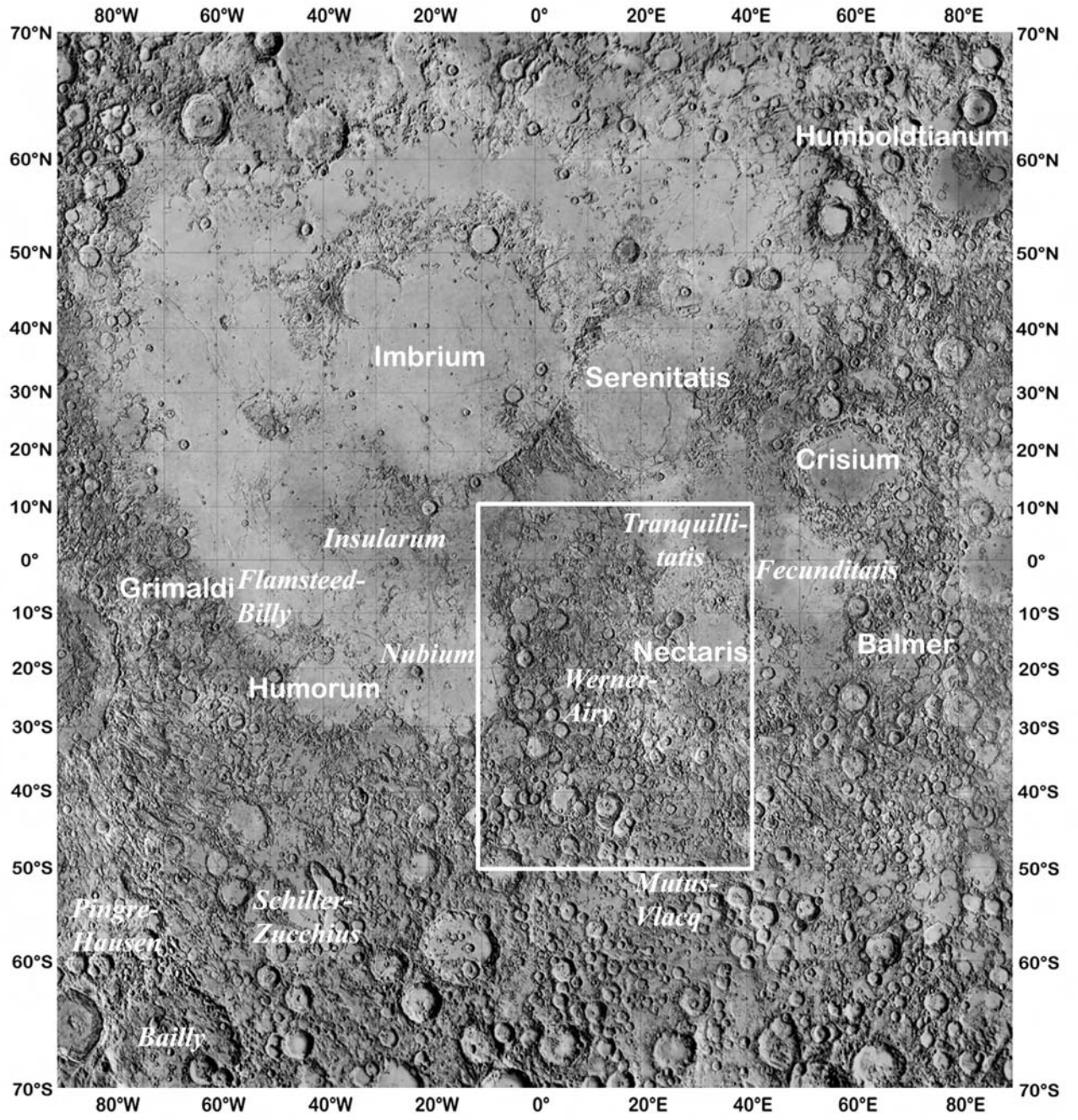

Figure 19. The location of the study area (white box, 10°W–40°E, 10°N–50°S) in the near-side of the Moon, plotted on Clementine lidar topographic data, and the approximate locations of the main impact basins. True multi-ring impact basins are written in roman letters, whereas smaller or older basins with less than three observable rings are written in italics (Spudis, 1993).

7.2 Definitions and classifications

One of the crucial aspects for this study is to decide which craters actually are polygonal and which are not. An objective method, like the Fourier shape analysis applied for digitised crater rims (Eppler et al., 1977, 1983) or the modern machine vision approach (Watters, 2006; Watters & Zuber, 2007) would be ideal if such a method would not be so laborious for vast areas like in the present work. Therefore, in this work another approach, based on thorough visual inspection of

images was chosen. Regarding Mars, the polygonal/non-polygonal classification was made based on MDIM 2.0. Also the craters that were classified as simple craters using THEMIS imagery were first classified as PICs using MDIM 2.0.

The definition of a polygonal crater is a pivotal matter, as no "official" definition or terminology exists. In this study, by definition, a polygonal crater has to have at least two adjacent straight segments of the crater rim with a clearly discernible angle between them. Thus a crater having for instance two parallel and straight rim segments on the opposite sides of the crater would not make the crater polygonal, since the straight parts would be connected by more or less circular segments of the rim. However, it must be noted that not all of the straight rim segments need to have a clear-cut angle between them: two is enough to make the craters polygonal in this classification, and other straight segments may even be isolated from the rest.

Admittedly the selection of PICs based on the somewhat arbitrary definition described above is subjective. An initial attempt to decrease this subjectivity was made by accepting only those PICs that were defined as such by two independent researchers. This was done regarding the greater Hellas region (Paper I). Although in general the classifications by the three researchers – each mapping about two thirds of the greater Hellas area – are in agreement, different combinations of their independent PIC classifications may lead to small systematic bias in the PIC distribution.

Encouraged by the generally good match of two researchers' independent selections in the greater Hellas region, it was decided that for the Argyre region, as well as for Venus, it is sufficient if the general requirement of the independency of the selections is left out. Thus, for the PIC datasets used in Papers II–V, a preliminary selection was made by one researcher, and the final selection of PICs was based on this (as acknowledged in the statement of authorship). In Paper VI, as noted above, the selection of the PICs was done solely by me. Because of the fairly strict criteria for classifying craters as polygonal, the amount of PICs found in this Ph.D. work represents the minimum number of polygonal craters in the area, and only a relatively small fraction of all craters which have straight segments of the rim.

In Papers II and III the PICs from Argyre region were classified according to their degradational stage. The selected classification scheme was a fairly crude one: only three classes were chosen. These were 1) "fresh" craters having a preserved ejecta blanket,[47] 2) "rimmed" craters that do not have any visible ejecta blanket left but still have a clearly discernible topographic rim, and 3) "degraded" craters whose rim has been substantially or completely degraded. The classification is

[47] Note that in the case of pedestal craters the ejecta does *not* indicate the crater's relatively young age (see Chapter 5.4.2). No pedestal craters, however, were observed in the study area.

notably uneven, as usually the rimmed craters are by far the most abundant type. This was, however, necessary due to the statistical approach, because with a larger number of classes there would have been very many cases where the number of measurements in each class would have been zero or very small, thus making reliable statistical investigation impossible. The basis of this classification is essentially similar to the one defined by Herrick et al. (1997) and used for the Venusian craters in Paper IV, i.e. 1) pristine with ejecta, 2) no ejecta, and 3) highly degraded.

The diameter and location data of PICs and non-polygonal craters on Mars was taken from Barlow's (2003) Catalog of Large Martian Impact Craters. The diameters and coordinates of the craters smaller than 5 km in diameter or otherwise absent from Barlow's catalogue were measured from the USGS's shaded relief hard-copy maps, and/or using data in PIGWAD. The geologic units used in Paper III and described in Chapter 4.2 were determined from USGS's 1:15,000,000 scale geologic maps that cover extensive areas and therefore have consistent nomenclature (Scott & Tanaka, 1986; Greeley & Guest, 1987; Tanaka & Scott, 1987).

In the case of Venus (Papers IV and V), the craters' diameters and other data (mainly the degradation stage, floor reflectance, presence of a dark parabola, geologic environment, morphologic class, and wall terracing that were used in Paper IV as discriminating factors) were taken from the Venus Crater Database by Herrick et al. (1997). In larger craters it is rather easy to differentiate polygonal craters having straight rim segments from craters created by clustered impacts (see Chapters 2.3.2 and 5.5.3). However, in the case of smaller diameters the true polygonal shape can be more difficult to identify reliably. Hence, the smallest Venusian craters selected for the study were 12 km in diameter. Approximately 12 km is also the size when Venusian craters start to have a significant flat part on the crater floor, so the distinction between dark and bright floors becomes meaningful (Herrick & Sharpton, 2000).

As was discussed before, the transition from simple to complex crater morphology is not abrupt and thus does not depend solely on the surface gravity ($1/g$), but is affected also by the target properties. In Paper VI, commonly accepted average values for the transition diameter (D_{tr}) were used for different planets. These were 7 km for Mars (e.g. Cintala et al., 1976; Wood et al., 1978; Pike, 1980a, b; Strom et al., 1992; Garvin et al., 2003), 4 km for Venus (e.g. Schenk & Sharpton, 1992; McKinnon et al., 1997), and 15 km for the Moon (e.g. Pike, 1967, 1974b, 1977; Hörz et al., 1991).

7.3 Measuring methods

All the strike measurements of the polygonal crater rims and the tectonic structures were done on-screen using Adobe Photoshop, and measurements in Photoshop's coordinate system were then

simply recalculated to actual geographic directions. Although no formal tests of the precision of the measurements were carried out, repeated measurements clearly imply that the precision is on the order of ±5º, often better. Thus the representation of the data using diagrams with 10º or 15º bins (class widths) is validated. The measurement of tectonic lineaments in the Argyre region (graben, ridges and small channels) used in Paper III was carried out in a similar fashion, but the precision of the ridge and channel measurements is poorer due to their somewhat sinuous nature. Measurements were made from the rectilinear parts of the ridges or channels. Several measurements of each tectonic structure were made in cases where the orientation of the structure changed appreciably (around 15º).

The same general principles hold for the measurements of the tectonic orientations on the Venusian surface (Paper V) as well. In addition, a few other restrictions were applied. The maximum of tectonic measurements was limited to three, because from some tectonic structures, especially wrinkle ridges and tessera terrain, numerous minor orientations could be measured. The orientations that were always measured were the main trend of the tectonic structure in question, and the orientation closest to the polygonal crater, which of course could be the same orientation.

Moreover, in Paper V, the different tectonic structures (wrinkle ridges, old and young rift zones, tessera terrain, mountain belts, radial and concentric components to volcano-tectonic features, and undifferentiated lineaments) were further divided into two classes based on their distance from the polygonal crater. The structures were either located “close” (less than two crater diameters), or “far” (more than two but less than ten crater diameters) from the polygonal crater in question. In addition, when it was unambiguously achievable by direct cross-cutting relationships, the age relations between the crater and the tectonic structures were defined. This, however, was possible only on rather rare occasions.

Due to the sinuosity of the tectonic structures (and sometimes ambiguity, especially in the case of the tessera terrain) and the inevitable small errors in the actual measuring process, PIC rim orientations and tectonic orientations were regarded as matching if the tectonic orientation was within ±7.5° of a direction measured from the crater rim. It should be emphasised that one correlating PIC rim and tectonic orientation was enough to qualify as a “match” (see Chapter 7.4), even if several non-correlating measurements from each PIC and tectonic structure were made. Unlike in Paper III, in Paper V the measurements of the polygonal crater rim orientations and the tectonic orientations were made by different researchers, enhancing the objectivity of the study.

Because of the nature of the side-looking Magellan SAR-imagery, linear tectonic structures and crater rims oriented approximately east–west are very difficult and usually impossible to reliably

even see, not to mention measuring their directions. This becomes evident, for example, in Figure 20 that displays all the Venusian polygonal crater rim orientation measurements, including both left- and right-looking data. The ~30°–40° gap in the diagram around east–west direction certainly does not represent the actual geologic situation on the Venusian surface, but it is merely an artefact of the dataset. It is quite possible that the relative scarcity of PIC rim orientations a few tens of degrees further than the apparent gap is also due to the same effect. Because of this, all measurements (both crater rims and tectonic structures) between 075° and 105° (255°–285°) were omitted from the correlation study in Paper V.

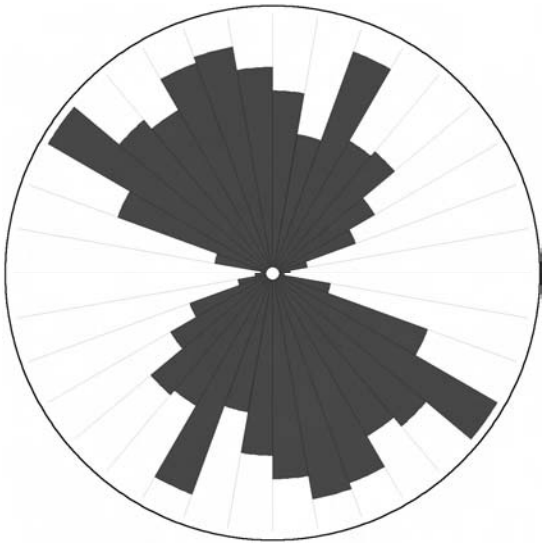

Figure 20. A rose diagram including all measurements of Venusian PIC rim strikes. The practically complete lack of ~E–W oriented PIC rim segments is most probably an indication of the nature of the Magellan SAR data, unless an unknown and unlikely geologic reason prohibits the formation of ~E–W oriented straight crater rim segments everywhere on Venus. The class width is 10°, and the circle represents 10%.

One important aspect of the measurements from Venusian polygonal crater rims was that both left- and right-looking images were used whenever they were available. There are often major differences in the measurements from left- and right-looking images from the same crater, which is not surprising given the nature of the Magellan SAR data. As with the Martian craters, the straight rim segment measurements were made from the rim crest if it was discernible. However, as a bit further discussed in Chapter 5.2.3, the exact location of the rim crest of a Venusian crater is typically rather difficult to say, and thus it is highly likely that some, or probably most of our measurements are not from the actual rim crest, but a bit further inside. Thus, the Venusian PIC rim orientation measurements probably mostly indicate the orientation of the uppermost crater wall, or

the orientation of the head scarp of the uppermost rim terrace. Thus, the left- and right-looking radar images usually cannot reveal exactly the same parts of the crater.

7.4 Data presentation and statistical methods

In the geostatistical community it is well known that a normal rose diagram that is plotted based on the radius of each sector is not an ideal tool for representing strike data, due to its tendency to overemphasise the preferred orientation (e.g. Cheeney, 1983). A more sound choice would be to use true circular histograms that are based on the area of each class, not the radius. I am aware of this problem, as well as the general tendency of histograms being prone to notable changes in their appearance depending on the width of classes and the position of the class boundaries.

The common radius-based rose diagram was used in this work, however, for several reasons. One of the main reasons is that it is – perhaps unfortunately – so widely used in geosciences, so it is familiar and easily interpreted. It gets the message through, so to speak. In addition, such diagrams could be plotted using the available software, and therefore they are substantially less laborious and less prone to errors than circular histograms drawn by hand. In the data used in this thesis there are also usually several main directional trends instead of just one, so these can be regarded as being not so prone to the overemphasis of the preferred orientation. In addition, a large portion of the data was also analysed using normal histograms that are based on the area of the classes, and this had no effect on the main conclusions. As explained in more detail in Paper II, several different class widths were also tested, and while this had a small effect in the statistical analysis in Paper II, it had no impact on the geologic implications. The positions of the class boundaries were always the same, i.e. the first class boundary is at 0º (north). Due to the highly variable number of PIC rim strike measurements, and for the ease of comparison, the data in Papers I and III was presented as percentages in the same scale. The rose diagrams were drawn using the RockWare Inc. RockWorks 2004 software (revision 5.6.6. in the most part of this Ph.D. work), except for the hand-drawn (Adobe Photoshop) diagrams in Paper I.

The concepts of “match” and “correlation”, as used in this connection (Paper V), should be clarified. Mostly the term “match” is used, and “correlation” should not be understood in a rigorously statistical sense, but only as a way to avoid excessive repetition. As noted above, the PIC rim and tectonic orientations were said to “match” if they were within ±7.5°, this being essentially an arbitrary value. The probability of a match occurring by chance can be determined by simple calculations, the easiest way being the binomial expansion (Cole & King, 1968). If the probability of an event (match) occurring is p and the alternative is q, (i.e., $p+q=1$), the formula for the problem

studied in this thesis takes the form of $3q^2p$. When three random PIC rim orientations are measured and compared to three tectonic orientations covering the largest possible azimuthal range (45°, i.e. 2×7.5°+2×7.5°+2×7.5°), the probability of a match (i.e. one PIC rim orientation being within ±7.5° with one of the tectonic orientations) is:

$$3\times\left(1-\frac{45^\circ}{180^\circ}\right)^2\times\frac{45^\circ}{180^\circ}\approx 42\%$$

Because most of the tectonic orientations clearly are not entirely random and independent of each other, but usually measured from linear structures spanning a fairly narrow azimuthal range, the actual "random" percentage against which the "match" percentages should be compared is notably smaller. If, for example, the three tectonic measurements would be separated by only one degree (thus making a 17° span of possible "matching" orientations), the probability of a match would be 23%. Thus, if the orientations of the PIC rims and the surrounding tectonic features would be independent and basically random, the match percentages in the case of three PIC rim and three tectonic measurements would lie somewhere between 23% and 42%. It is noteworthy, however, that less than three PIC rim and tectonic orientation measurements was a common scenario. For example, each of the radial and concentric components of volcano-tectonic features is just a single orientation. Therefore, the random probabilities of a match are often even smaller than 23%–42%.

The statistical analysis in Papers II and III was conducted mainly by using two-tailed Kolmogorov–Smirnov (K–S) two-sample test in 95% confidence level. This test elucidates whether or not two samples are drawn from identical populations. In practise this means that the test checks if the rim strike distributions of the two batches of measurements – for instance rim strike measurements from the same area, but measured from craters of two different degradational stages (paired as fresh–rimmed, rimmed–degraded or fresh–degraded), or from two datasets (Viking – MOC-WA) – are similar or not. The K–S test is far superior to the common χ^2 test (which was also used in few occasions in Papers II and III for verification of the results given by the K–S test), because it is valid for cases where the samples have highly different or small number of measurements, and it can easily be used for data having classes with zero values. In addition, one of the K–S test's strong points is that it is independent of any assumptions about the distribution of the population. (Cheeney, 1983; Davis, 2002; Sheskin, 2004)

In this study the null hypothesis to be tested is the one of "no change", i.e. the hypothesis that the two samples under scrutiny are drawn from identical populations. This is in accordance with common practise. The K–S test is constructed by first classifying the data and then compiling cumulative sum-frequency curves. The two curves are compared and the largest difference (D-

value) of the curves is calculated. The D-value is then compared to the critical value (D_{crit}).[48] If the D-value is greater than the critical value, the null hypothesis is rejected. Thus, in the case when $D>D_{crit}$, the null hypothesis can be rejected in the selected confidence level (95% throughout this work), and the samples can be regarded as being drawn from different populations. In the opposite case the null hypotheses cannot be rejected, and thus the samples cannot be said to be statistically significantly different. (Cheeney, 1983; Davis, 2002; Sheskin, 2004)

[48] The critical values are somewhat different depending on the reference used. In this study critical values are mainly derived from Davis (2002). However, for cases with a large number of measurements ($n_1+n_2>100$) the approximate critical values are calculated, using the formula given by Cheeney (1983).

8 RESULTS

8.1 Distribution and abundance of PICs

Altogether 1863 PICs were identified in this study. Most (1306) of them are located in the greater Hellas region of Mars. However, PICs on Venus (121) and in the Argyre region (269) of Mars were studied more profoundly. PICs in the TINN study area of the Moon (167) have so far only been identified, and studied with respect to their size distribution (see below). The identified PICs from the Argyre region, Venus, and the TINN area of the Moon are listed in Appendices 4–6.

In the case of Martian data, one general feature of the PIC distribution should be remembered. Because the resolution of the Viking dataset diminishes in higher latitudes, the slight apparent decrease of the amount of PICs in the southernmost parts of the Hellas and Argyre study areas probably does not reflect reality, but is merely caused by the observational bias.

Although no formal tests of spatial statistics were done, it seems clear that based on the data gathered in this Ph.D. thesis, the areal distribution of polygonal impact craters closely follows the distribution of impact craters in general: in areas with lots of craters, there are also plenty of PICs (see Figs. 21–23 for the distribution maps). Thus, heavily cratered areas in Martian and lunar highlands are the places where the highest absolute numbers of PICs can be found. Some places seem to, however, have a slightly higher number of PICs than other, otherwise very similar areas. For example, in Hellespontus Montes immediately west from the Hellas basin, and the part of Tyrrhena Terra southwest from the Isidis basin, there seem to be small concentrations of PICs (Fig. 21). Similarly, in the lunar data (Fig. 23) there appears to be some clustering of PICs for instance southwest from the Nectaris basin (in the central area of the Werner–Airy basin). The general trend of PIC distribution does, nevertheless, seem to follow that of the non-polygonal craters.

To get a better understanding of the distribution of PICs, relative abundances rather than the absolute numbers of PICs need to be studied. This was studied in the Argyre region (Paper III), using the geologic units defined Scott and Tanaka (1986), and Tanaka and Scott (1987) as age references for the different terrains. The results are summarised in Table 2. The highest relative abundance (PICs' percentage of the entire crater population over 7 km in diameter) can be found west from the basin in areas dominated by the old cratered unit Npl_1. There the PIC percentage is about 22%, whereas in areas where the younger units prevail the PIC percentages are notably lower, about 13%–15%. So despite the general spatial coincidence of PIC and non-polygonal crater

distributions, there appears to be some preference of PIC formation in certain areas: the older terrains seem to have relatively more PICs than younger terrains.

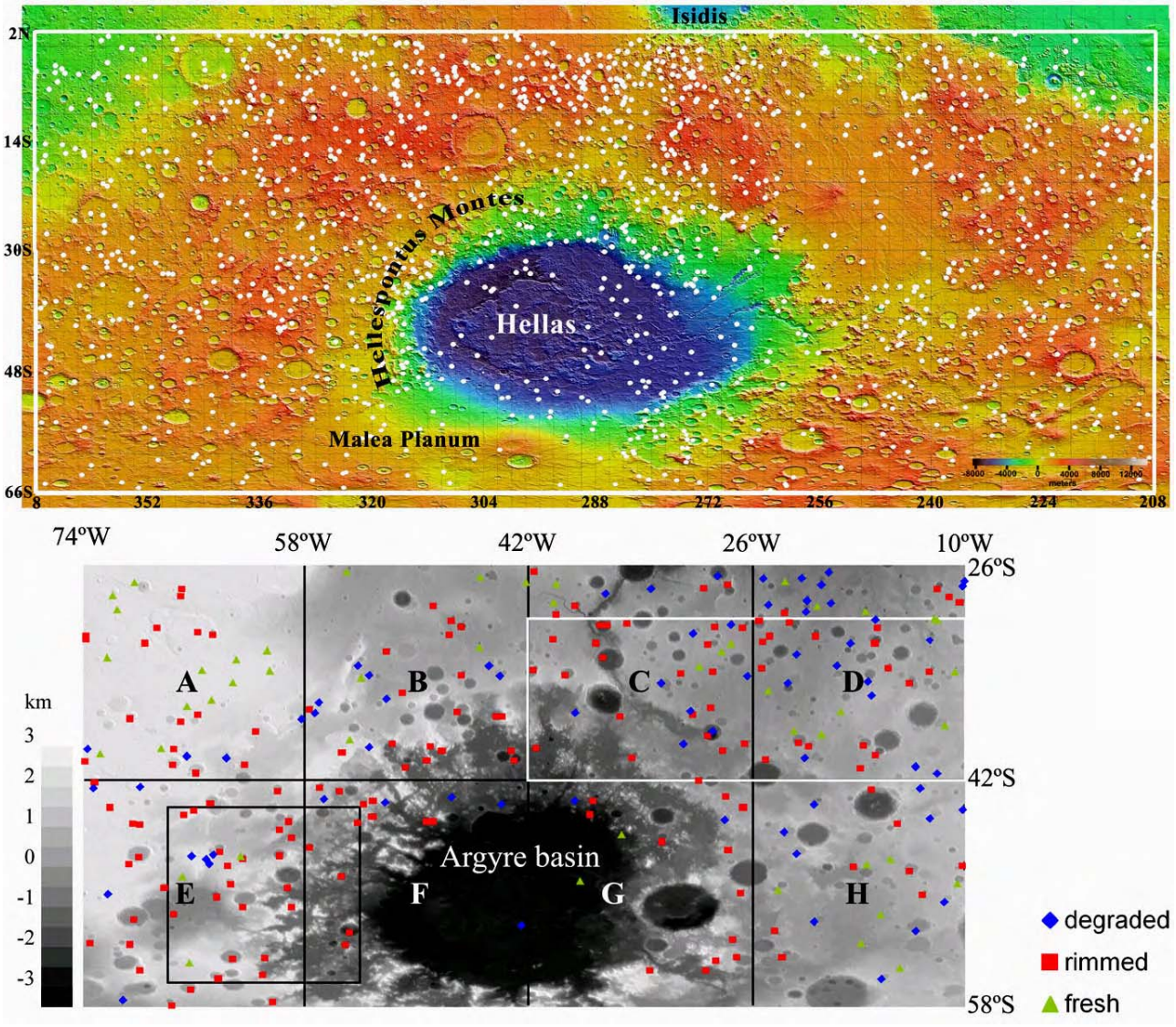

Figure 21. The distribution of Martian PICs in the greater Hellas (upper) and Argyre (lower) regions, plotted on MOLA topography. In the Argyre region also the degradation stage of the PICs is indicated, as well as the block division. The white box indicates the area where the effect of different illumination geometries (MDIM vs. MOC-WA) was tested (note that the location of the white box in Paper II is erroneous), and the black box in blocks E and F indicates the area whose PIC orientations were compared to the ones west from the Hellas basin (see Paper III). For a colour version of the figure, see the electronic version of the thesis.

The observation that spatially PICs generally follow the "normal" crater distribution is emphasised by their distribution on the surface of Venus: just like the distribution of all craters on Venus, the distribution of Venusian PICs (Fig. 22) appears to be random (although no formal tests of randomness have been carried out). Thus, on a global Venusian scale, no connection was observed with the location of PICs and the geologic provinces (Paper IV).

Table 2. The relative abundances of PICs in the Argyre region, and the absolute numbers of craters over 7 km in diameter, as well as the main geologic units in the different blocks (see Fig. 21) of the study area.

Block	PICs %	PICs	Others[1]	Total	Main units[2]
A	15%	26	144	170	Hpl_3, Npl_2, Hr
B	14%	29	185	214	Npl_1, Hr, Nplh
C	17%	33	161	194	Npl_1, Nplh
D	19%	51	216	267	Npl_1, Nplr
E	22%	44	152	196	Npl_1, Nplh
F	16%	14	73	87	Nple, Hpl_3, Nplh
G	16%	15	79	94	Hpl_3, Nplh, Nple
H	13%	24	158	182	Npl_2, Nplr
Mean / Total	17%	236	1168	1404	

[1]Taken from Barlow's catalogue (2003).
[2]Taken from Scott and Tanaka (1986) and Tanaka and Scott (1987).

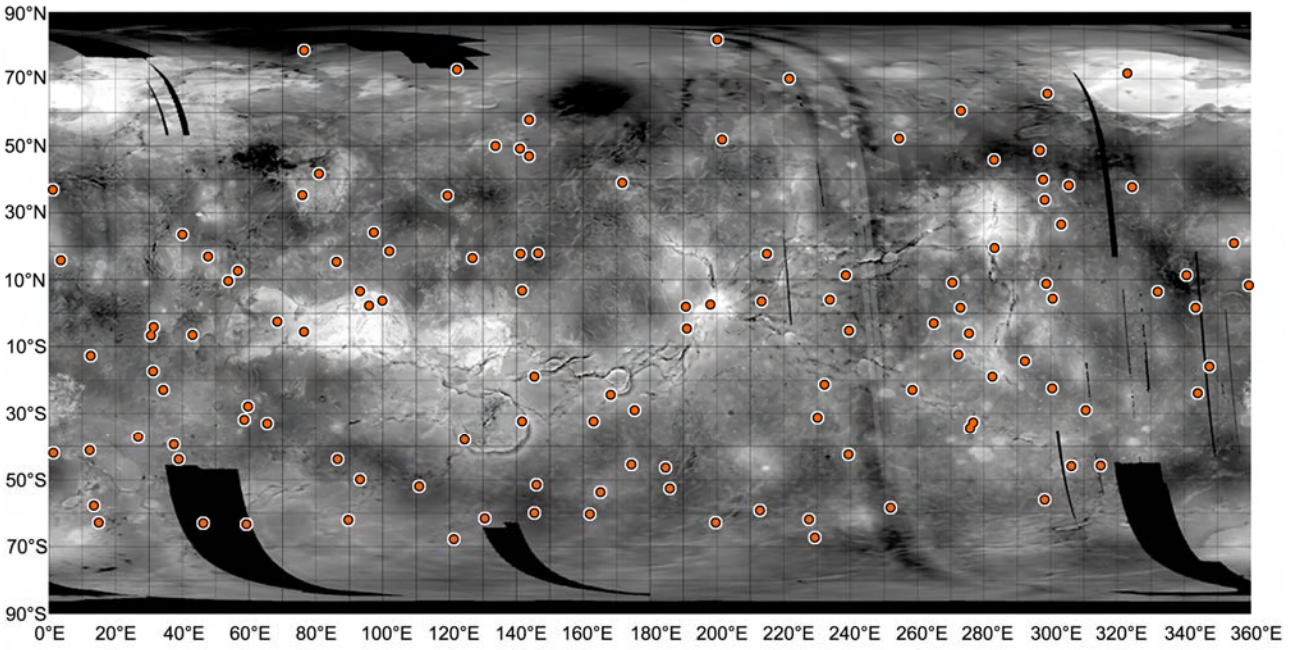

Figure 22. The distribution of Venusian PICs, plotted on Magellan topography. Brighter areas are higher.

The relative PIC abundance on Venus is quite similar to the one on the Martian surface. 121 PICs (revised from initial number of 131 in Paper IV) make 22%[49] of the whole crater population at least 12 km in diameter (according to Herrick et al.'s (1997) database). In the lunar study area, 160 named (+7 unnamed) polygonal craters larger than 10 km in diameter were identified. The area holds also 656 non-polygonal named craters, thus resulting in the relative PIC abundance being about 20%. The ~20% is apparently a good estimate of the approximate PIC percentage of all craters in the study area, because most of the lunar near-side craters whose "crater-like"

[49] The 13% mentioned in Paper IV refers to a minimum percentage, although this was not explicitly stated. The number of PICs over 12 km in diameter was compared to the total number of *all* craters, because of problems in reliably identifying polygonal craters in smaller diameters. Hence, ~13% is the minimum.

morphology has been preserved have been named. Thus, of the impact craters on the surfaces of all three celestial bodies studied in this thesis, roughly 20% are polygonal ones.

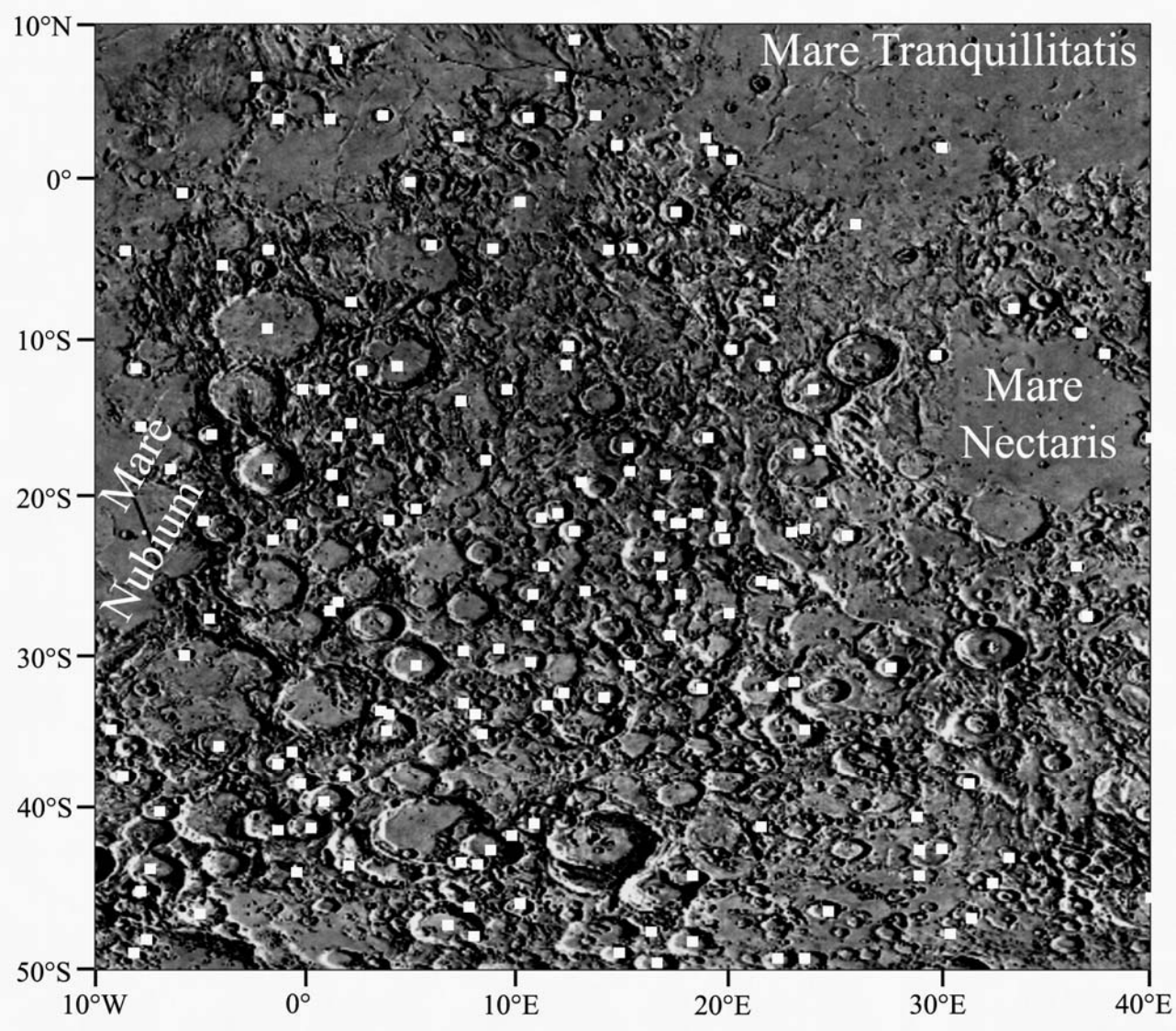

Figure 23. The distribution of the PICs in the TINN study area of the Moon, plotted on the Clementine shaded relief map.

8.2 General morphology and polygonality

The morphologic aspects of Venusian PICs were studied by using the morphologic classes defined by Herrick et al. (1997), and comparing the PICs' and "normal", non-polygonal craters' relative abundances in those classes (multi-ring, peak-ring, several peaks, central peak, knobby base, and flat floor craters). The results (Fig. 24, Paper IV) indicate small differences, yet they are fairly straightforward. Non-polygonal craters are more common in the classes of peak-ringed and multiple peak craters, whereas in the case of central peak and knobby base craters the situation is reversed.

Apparently the PICs seem to "prefer" particular morphologic classes of craters that are associated with smaller diameter.

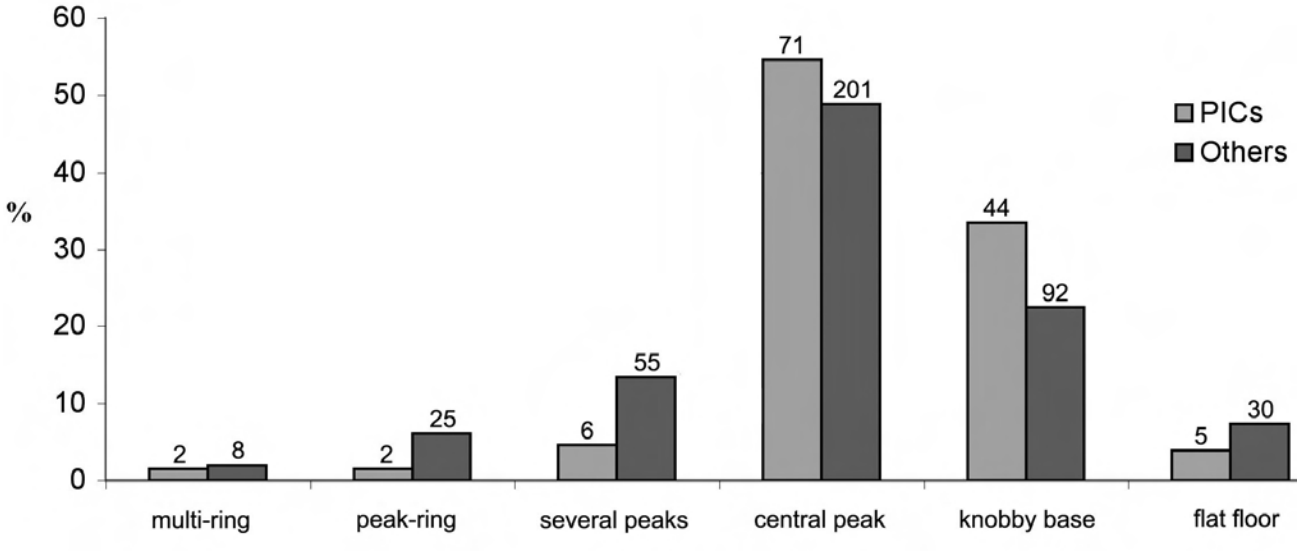

Figure 24. The relative abundances of Venusian PICs and non-polygonal craters ("others") in the different morphologic classes of Herrick et al. (1997). Note that the absolute numbers (on top of the bars) in some classes are very small, and that this data includes 130 PICs as in Paper IV (one PIC lacking a morphologic classification).

The vast majority of the PICs had a tendency to form a part of a regular polygon, a partial hexagon being the most typical plan form. The polygonality, or the number of straight segments measured from each impact crater classified as a PIC, can be compared against various other crater characteristics. An obvious one is the size. The results from Mars and Venus, however, seem to differ. In the case of Mars (Argyre region), there seems to be an obvious trend: the larger the crater, the larger the number of straight rim segments (Fig. 25). The Venusian data seems more monotonous, as no obvious trends are visible. This is most likely a result caused by the resolution of the data sets used. It is difficult to reliably see more than two straight rim segments in small Martian craters, whereas the smallest craters in the Venusian dataset are fairly large compared to the resolution, and thus several measurements can be made.

Polygonality compared to the geologic units of the Argyre region (see Fig. 5 in Paper III) on the other hand, does not show any apparent trends. Typically a polygonal impact crater in the Argyre region has three straight rim segments, regardless of the geologic unit that now hosts the crater. In other words, the percentages of each individual polygonality class are approximately the same in all of the geologic units (note that all Hesperian and some of the Noachian units were combined). Polygonality was also compared with the degradational stages of PICs (see below; Paper II).

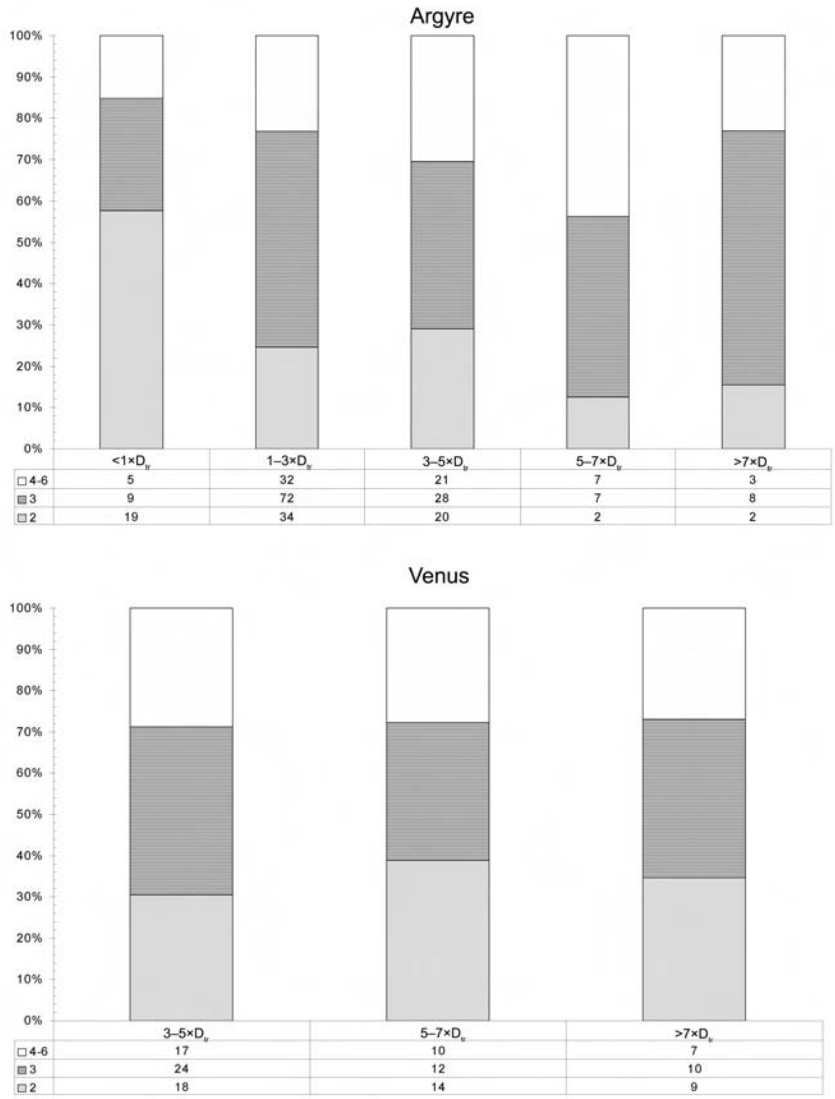

Figure 25. The numbers of PICs with 2, 3, or 4–6 straight rim segment measurements in the Argyre region, and Venus (the maximum number of straight rim segments seen either in left- or right-looking data) in different size classes. Transition diameters (D_{tr}) used were 7 km for Mars and 4 km for Venus. Note the increasing trend of measurements with increasing size in the case of Argyre, and the lack thereof in the Venusian data. The tables present the absolute numbers of PICs (altogether 121 PICs on Venus in this case, 269 in Argyre region).

8.3 Degradational stages

The effect of crater degradation and its influence on the polygonal craters and their straight rim strike orientations were studied using data from the Argyre region (Paper II) and Venus (Paper IV). Of the 269 PICs that were recognised and analysed in the Argyre region, "rimmed" craters were the most common ones (152), with less than half that amount (70) being "degraded". Only 47 PICs were classified as "fresh", mostly located on the volcanic plains. PICs that are located in the same area but having gone through different levels of degradation were not generally observed to have statistically significant differences in their rim strike orientations (Table 3, see also Fig. 26). The

few exceptions usually occurred when the number of measurements was rather low. It should be noted here that, as mentioned in Chapter 5.4.2, the pedestal craters' ejecta blankets do not imply relatively young ages or little degradation of the craters. However, no pedestal PICs were observed in the Argyre region, and thus the "fresh" PICs with preserved ejecta blankets should represent the youngest and most undegraded PICs in the region.

Table 3 shows the results of the K–S test of the rim strikes of PICs in same areas having different degradational stages (Paper II). From the results it becomes evident that in general the statistical match (in 95% confidence level) of the rim strikes is very good. From the 36 different comparisons (fresh–rimmed, fresh–degraded, rimmed–degraded; each of the six blocks was tested using both 10º and 15º divisions), 28 showed that in 95% confidence level the samples were drawn from the same (identical) population. From the remaining eight comparisons, only three showed that the samples were clearly from different populations, while in five comparisons the samples were in practise drawn from the same population even though the statistical criteria were not exactly fulfilled.[50] In practical terms, the rim strikes of, for example, degraded PICs in block D are generally the same as the rim strikes of fresh PICs in the same area. This is exemplified by Figure 26.

Table 3. The results of Kolmogorov-Smirnov test of the rim strikes of PICs in same blocks (see Fig. 21), but having different degradational stages. Each block (centre coordinates are given; blocks F and G are omitted due to low number of measurements) was tested using both 10° and 15° divisions.

Block	Division	Degraded – Rimmed	Degraded – Fresh	Rimmed – Fresh	n_d	n_r	n_f
A	10º	×	–	+	10	55	41
34ºS 066ºW	15º	×	+	+			
B	10º	+	×	+	26	60	14
34ºS 050ºW	15º	+	×	+			
C	10º	+	+	+	33	86	15
34ºS 034ºW	15º	+	+	+			
D	10º	+	+	+	71	67	29
34ºS 018ºW	15º	+	+	+			
E	10º	+	+	+	22	107	11
50ºS 066ºW	15º	+	+	+			
H	10º	+	–	×	31	25	24
50ºS 018ºW	15º	+	–	+			
Total					193	400	134

+ Samples are similar, i.e., drawn from the same population in the 95% confidence level.
× Samples are practically similar, i.e., drawn from the same population in almost 95% confidence level.
– Samples are dissimilar, i.e., drawn from different populations in the 95% confidence level.
The abbreviations n_d, n_r, and n_f refer to the number of rim strike measurements from degraded, rimmed, and fresh PICs, respectively.

[50] In Table 3 the symbol "x" and the description "practically similar" refer to the fact that in these cases the difference of D and D_{crit} was on the order 0.01, so quite small indeed. So for instance using a different reference with slightly varying D_{crit}-values could have changed the result to samples being drawn from the same population. Hence the somewhat arbitrary "practically similar" classification.

In the case of Venus, the crater degradation classification by Herrick et al. (1997) was used (Paper IV). The results are quite similar to the ones obtained regarding Mars. PICs and non-polygonal craters are equally abundant in the different degradational stages (Fig. 27a). The same holds when other indicators of crater degradation, the presence of a parabolic feature (Fig. 27b) or the floor reflectance (Fig. 27c), is studied. In general, both on Mars and Venus, more degraded craters do not have a tendency to be more polygonal, or vice versa.

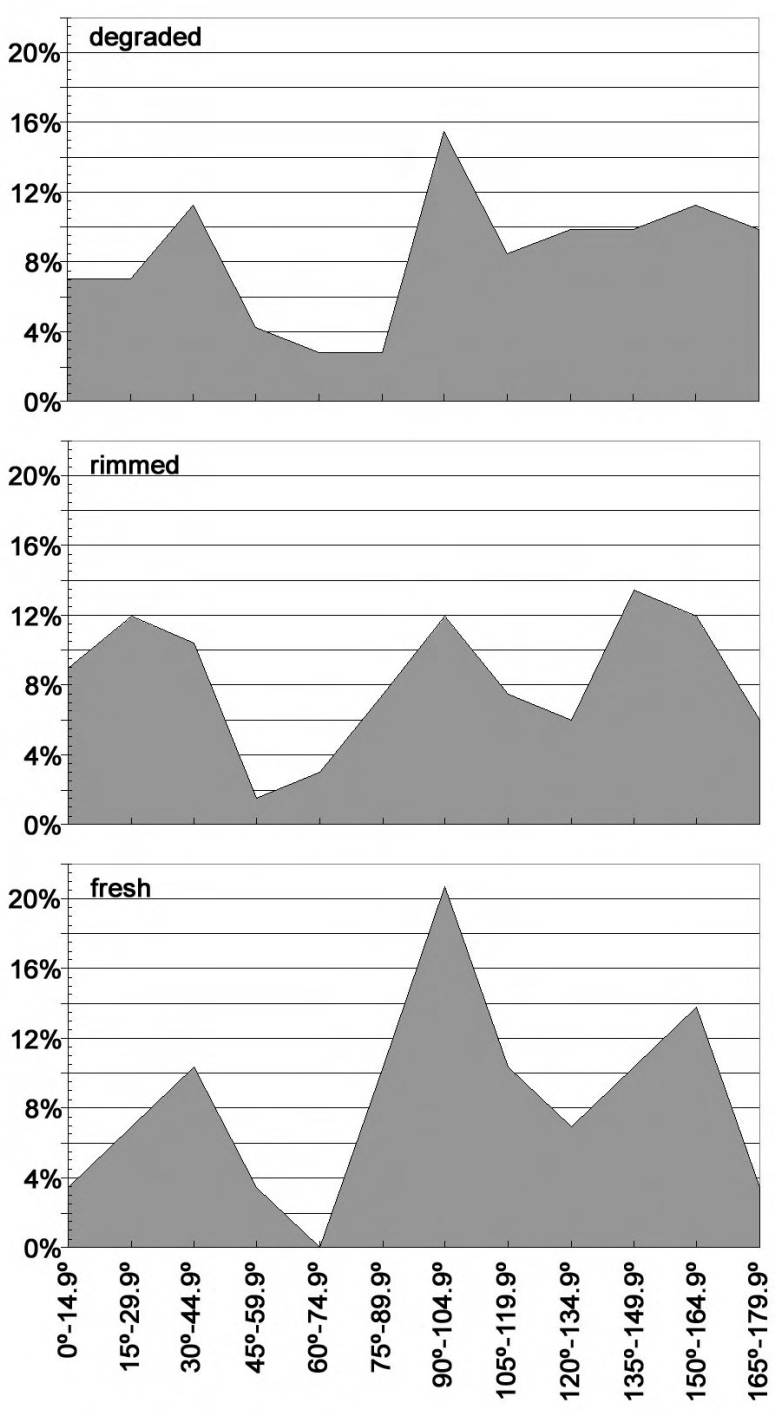

Figure 26. Histograms of the straight PIC rim segment strikes in block D, northeast of the Argyre basin. The total number of measurements is 71 for degraded, 67 for rimmed, and 29 for fresh PICs.

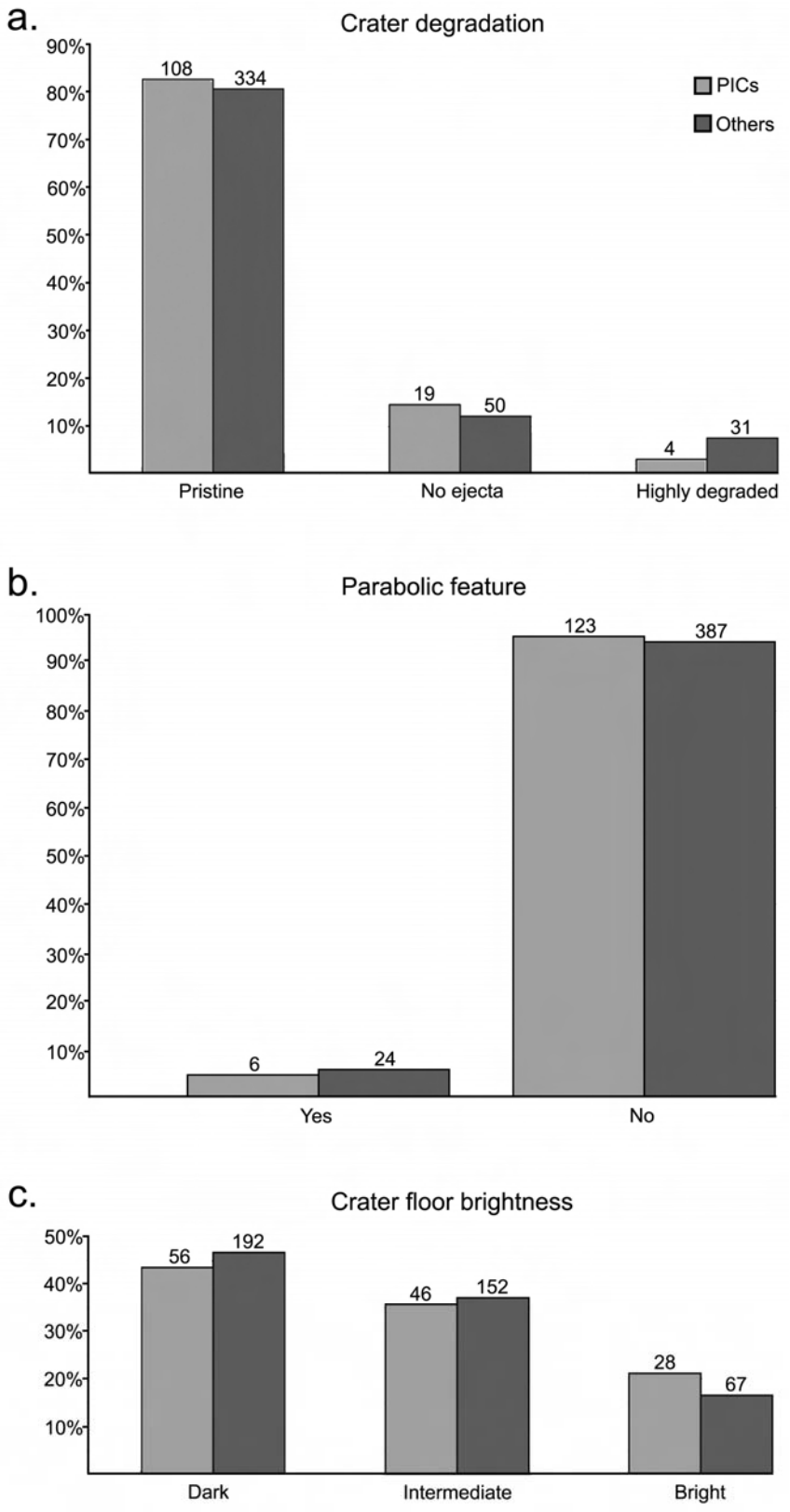

Figure 27. The relative abundances of 131 Venusian PICs and 418 non-polygonal craters ("others") in different classes of crater modification indicative of the age of the crater, i.e. a.) the crater degradation, b.) the presence of a (dark) parabolic feature, and c.) the crater floor brightness. PICs and non-polygonal craters are in practise equally abundant in all the different classes, implying that crater erosion/modification is not the cause of the crater polygonality. Numbers on top of the bars indicate the absolute numbers of craters (not all craters had features classified). Classifications based on data from the impact crater database of Herrick et al. (1997).

8.4 Diameter

The diameters of the Martian (Argyre region), Venusian and lunar PICs were compared to the diameters of non-polygonal craters in the respective study areas. In all of the cases there was a distinct discrepancy between the polygonal and non-polygonal crater size distributions. Figures 28 and 29 summarise these results, normalised to the average transition diameter (D_{tr}) on each planet (4 km, 7 km, and 15 km, for Venus, Mars and the Moon, respectively; see Chapters 5.2 and 7.2). The Venusian data (D≥12 km) is perhaps the most straightforward one. Clearly, the PICs prefer the smaller end of the size distribution, as there are relatively more PICs in the size classes from 3–4×D_{tr} to about 6–7×D_{tr} (~12–28 km in diameter). The Martian data (D≥5 km) shows similar general results, but as the usable dataset extends to smaller sizes (both in relative and absolute terms), some differences also occur. The "preferred" PIC size appears to be approximately 2–5×D_{tr} (~14–35 km in diameter). The sudden drop of both the PIC and non-polygonal crater curves at the <1×D_{tr} is an effect of the class widths (i.e. size selection, the smallest class covering a diameter range of only 2 km compared to 7 km in other classes), and at least for the most part not a real feature.

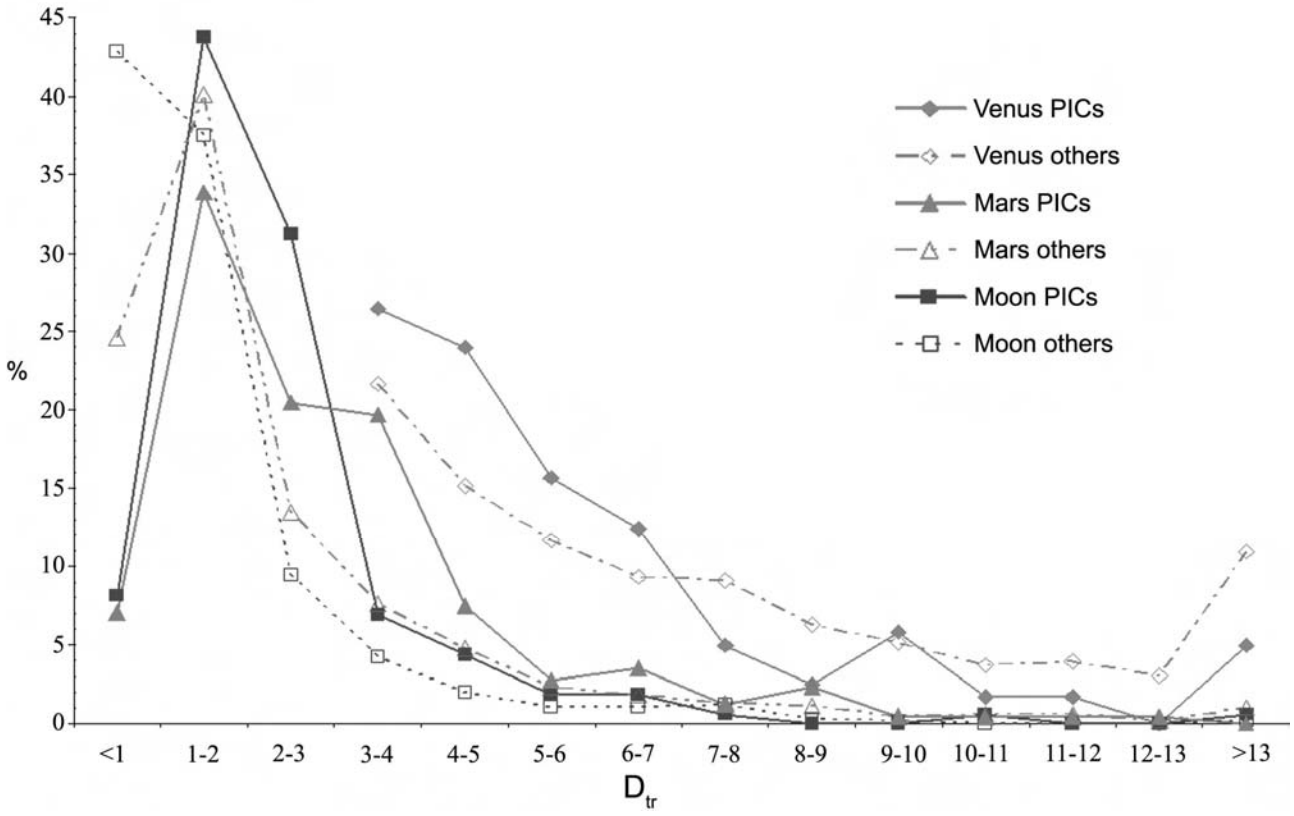

Figure 28. The normalised size distributions of lunar, Martian, and Venusian PICs and non-polygonal craters ("others"). Simple-to-complex transition diameters (D_{tr}) were 15 km, 7 km, and 4 km, for lunar, Martian, and Venusian craters, respectively. The deficiency of Martian simple craters (<1×D_{tr}) is due to the limited diameter range (5–7 km) of the smallest size class. See text for details, and compare with Fig. 29.

The lunar data (D≥10 km) presents perhaps the most interesting case: ~1.3–3×D_{tr} (~20–45 km) is clearly the most "favourable" PIC formation size (Paper VI). At D<1×D_{tr} the percentage of PICs drops rapidly, whereas the percentage of non-polygonal craters increases. In contrast to the Martian data, this is not a result of class widths (as can be seen in the increasing number of non-polygonal craters) and it is not a result of the resolution either, as the planimetric shapes of craters having a diameter of ~10 km are quite easily seen in CLA imagery. This observation and its manifold implications are further discussed in Chapter 9.10.

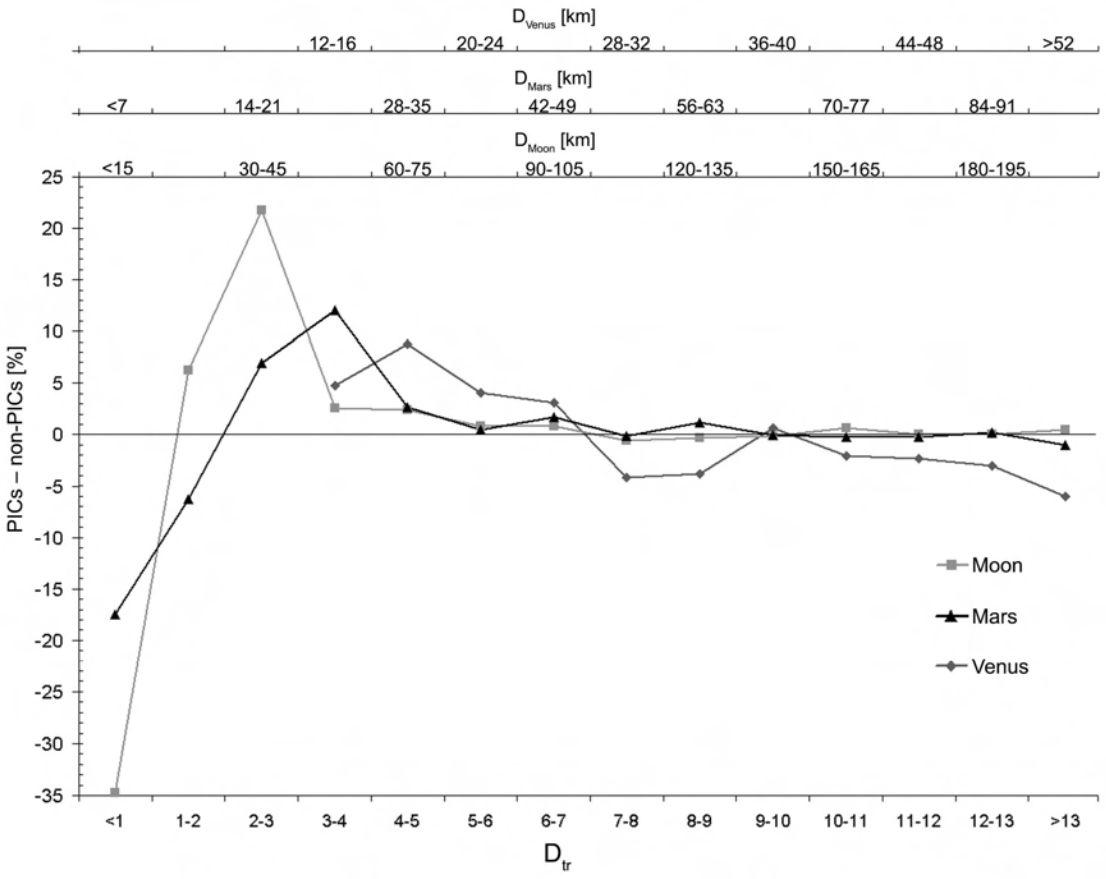

Figure 29. The differences of the relative abundances of PICs and non-polygonal craters on the Moon, Mars, and Venus in different size classes. Simple-to-complex transition diameters (D_{tr}) were 15 km, 7 km, and 4 km, for lunar, Martian, and Venusian craters, respectively. Note the deficiency of simple PICs (<1×D_{tr}) and the dominance of small complex (~2–5×D_{tr}) PICs. Compare with Fig. 28.

8.5 Simple and complex PIC rim strike orientations and other tectonic structures

The orientations of the PIC straight rim segments, and their relations to impact basins as well as tectonic structures like graben and ridges is among the main topics of this Ph.D. thesis. Paper I gives an outline of the results and conclusions in the greater Hellas region without delving too much into detailed analysis. Paper III, on the other hand, describes the relations between PIC straight rim segment strikes and other tectonic structures in the Argyre region of Mars (with some implications for the greater Hellas region as well) in more detail. Paper V focuses on such relations on Venus.

More detailed accounts on the results can be found in the respective papers, and merely the main points of the results are given here. The PIC rim strike measurements can be found in Appendices 4a, 4b and 5a.

In the rose diagrams used in this thesis to depict the Martian PIC rim orientations, data from both simple and complex PICs are combined. Thus, it is crucial to know if that data is a combination of two different sets of data, or if they present samples drawn from identical populations. In practise, are the rim strike distributions of simple and complex PICs different, as would be expected if they are formed by different mechanisms (see Chapter 6.4)? This was studied using data from the Argyre region. Due to the low number of simple PICs (42 simple PICs out of the total of 269 PICs), it was essential to combine two blocks to have a meaningful number of rim strike measurements. Hence, the straight rim segment strikes of simple and complex PICs were studied from four combined blocks. The results are presented in Figure 30. The straight rim orientation distributions of simple and complex PICs appear to be very similar. This similarity was also verified by the K–S test: in the 95% confidence level, there were no statistically significant differences in the rim strike distributions. The result in the combined blocks A and B was also corroborated by the χ^2 test. Thus, it is justified to present orientation data from both simple and complex polygonal craters in one combined diagram.

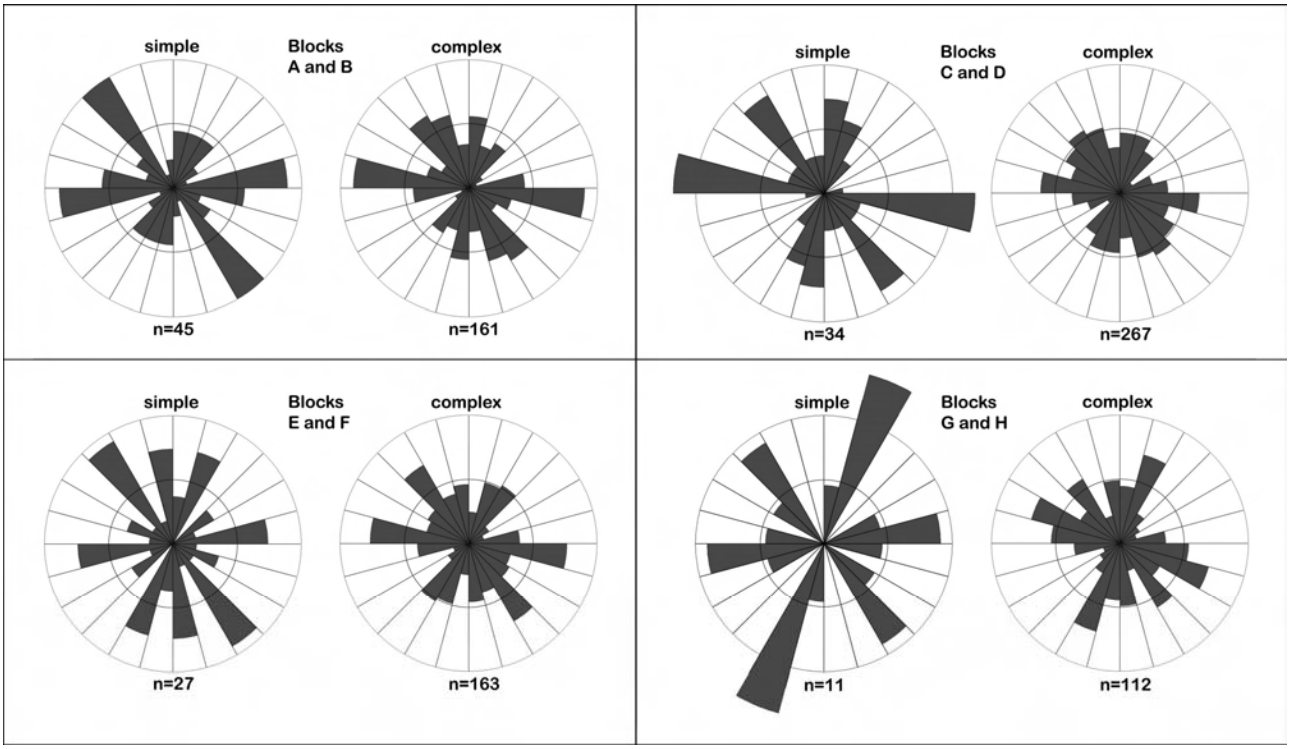

Figure 30. Simple and complex PIC rim orientations in combined blocks (see Fig. 21) in the Argyre region, Mars. Note that despite large differences in the numbers of measurements, the peaks and gaps of the rose diagrams are in the same orientations. No statistically significant differences between simple and complex PICs were found.

The PIC rim strike orientation results from the greater Hellas region are summarised in Figure 31 (for individual diagrams, see Paper I). One of the most striking features is the basin-radial fracturing, seen in areas west of Hellas and south of Isidis. Concentric fracturing is also evident around both basins, and in the block immediately west from Hellas it is noteworthy that the roughly N–S trending PIC rims are generally parallel to the main tectonic orientations in Hellespontus Montes, which is characterised by graben-like features and adjoining higher ground. Further west from Hellas it is notable that the concentric component loses its significance, with the radial component becoming more dominant. Also other important orientation components are present in the diagrams (see Paper III and Chapters 9.5 and 9.6). In the northeastern part of the greater Hellas region, partly on Elysium Planitia, a component roughly radial to Elysium Mons (NNE from the study area) is also apparent. In Hesperia Planum some of the most obvious trends (E–W and NNW–SSE) of the wrinkle ridges (Raitala, 1988) are parallel to the directions indicated by PICs.

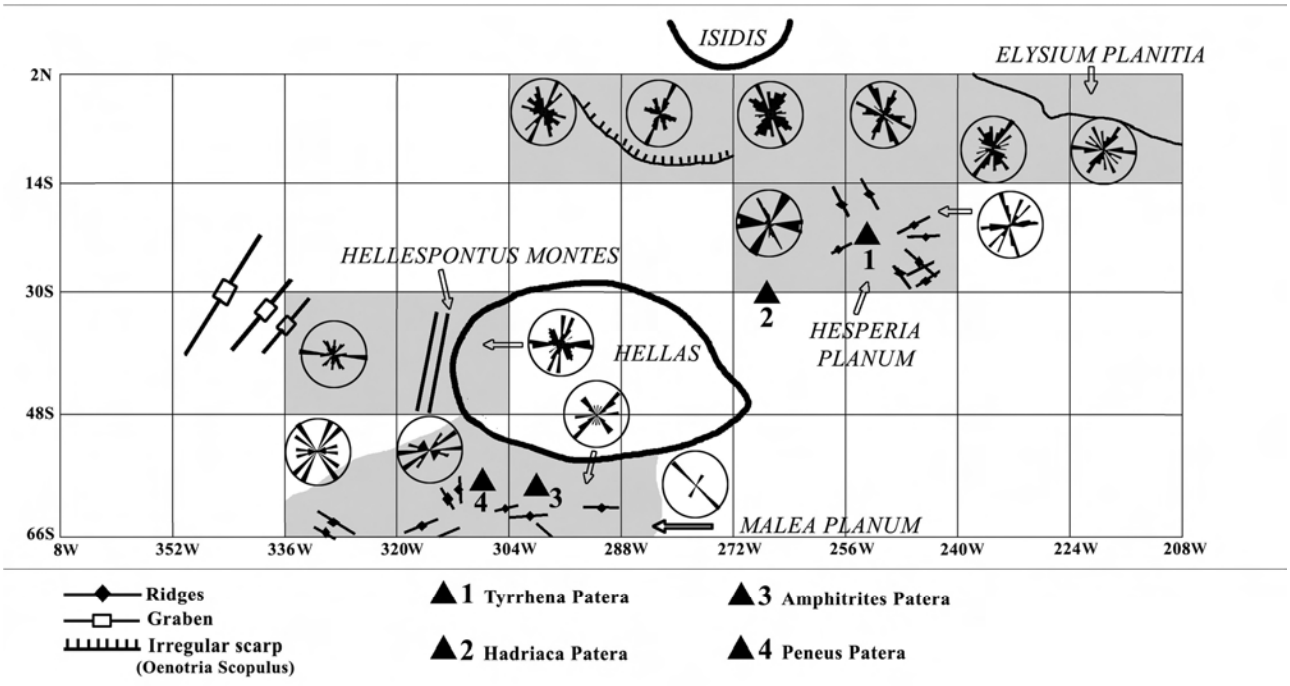

Figure 31. A summary sketch of the PIC rim orientations and other tectonic indicators in the greater Hellas region. The shading indicates the areas where the rim strike measurements were made. For better resolution images of the rose diagrams, see Paper I.

Figures 32 and 33 hold the bulk of the tectonic information collected from the Argyre region. Ridges are present in the northern part of the study area, and their orientations are tightly clustered. A systematic anti-clockwise turn can be seen in the ridge orientations from blocks A to D. A similar shift can be seen in the graben orientations. Ridges are clearly concentric to Tharsis, while graben are radial to it. Graben also often tend to approximately follow the main strike of Valles Marineris. The channels are closely connected to graben particularly in the northwestern part, while in other

areas they usually tend to follow the general topographic slope without a visible connection to a graben (note that the smallest, clearly very surficial channels that can be seen e.g. on the rims of craters were not included in the study).

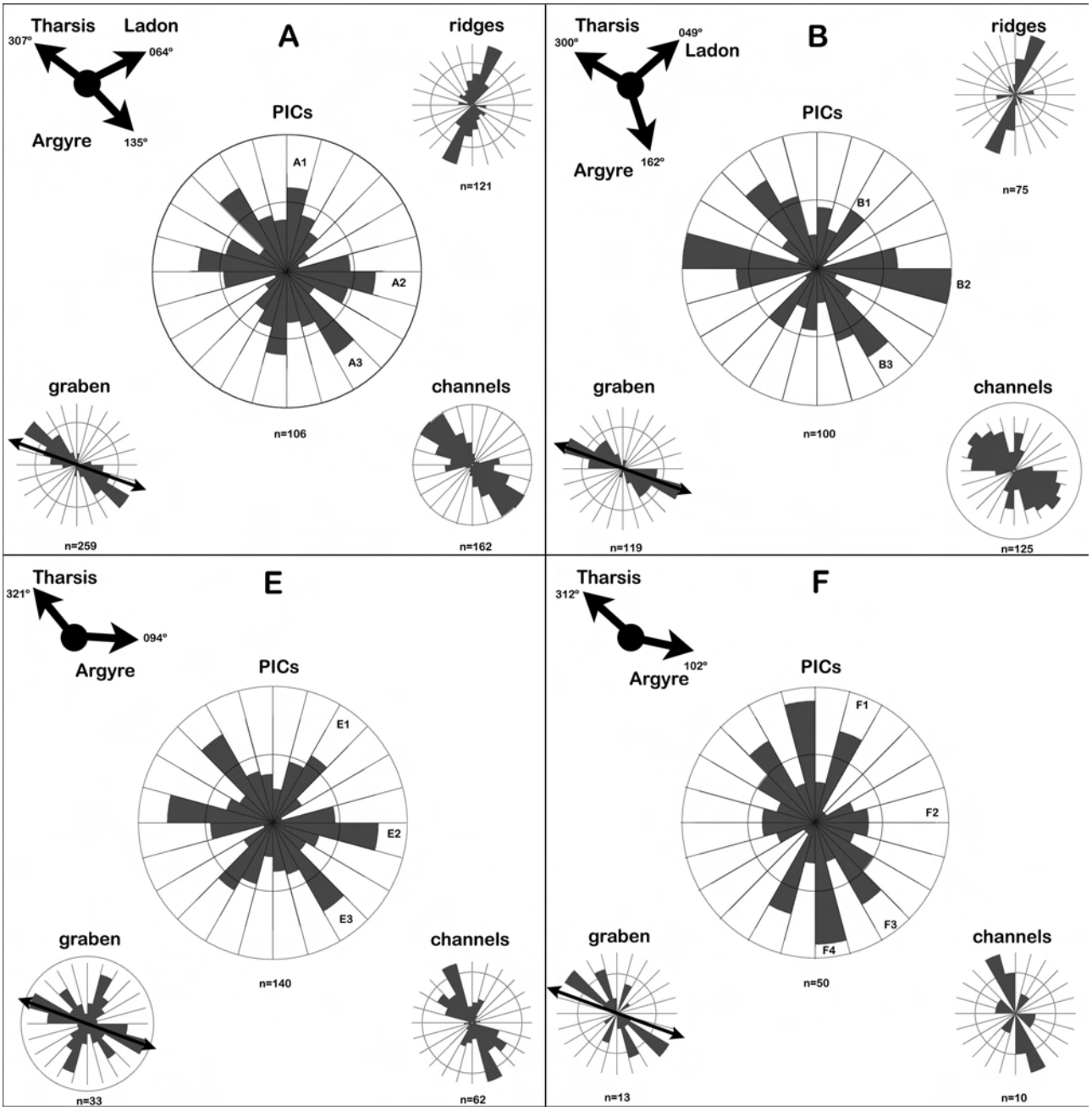

Figure 32. Structural data from the blocks in the western half of the Argyre study area (see Fig. 21). All the rose diagrams in Figs. 32 and 33 are plotted using 15° class intervals. The inner and outer circles in PIC diagrams denote 10% and 20% of the total, respectively. In the ridge, graben, and channel diagrams, the circles mark 20% of the total. In the upper left corner of the set of diagrams, arrows pointing to the centres of the Argyre basin and the Tharsis bulge (the latter taken to be the caldera of Pavonis Mons; see, e.g., Dohm & Tanaka, 1999) are also included for reference, as well as the direction to the Ladon basin in some of the blocks located closest to it. The general trend of the Valles Marineris is displayed as a double-headed arrow in the graben diagrams. The peak numbering refers to Table 5.

The PIC rim strikes in the Argyre region reveal interesting orientation patterns (Figs. 32 and 33). One of the most striking features is that in the northern half of the study area, an E–W component is ever-present. Throughout the entire area (except in block G), a NW–SE component can also be seen in the diagrams. As further discussed in Chapters 9.5 and 9.6, it seems probable that several different factors contribute to these and other major orientation peaks in the rose diagrams.

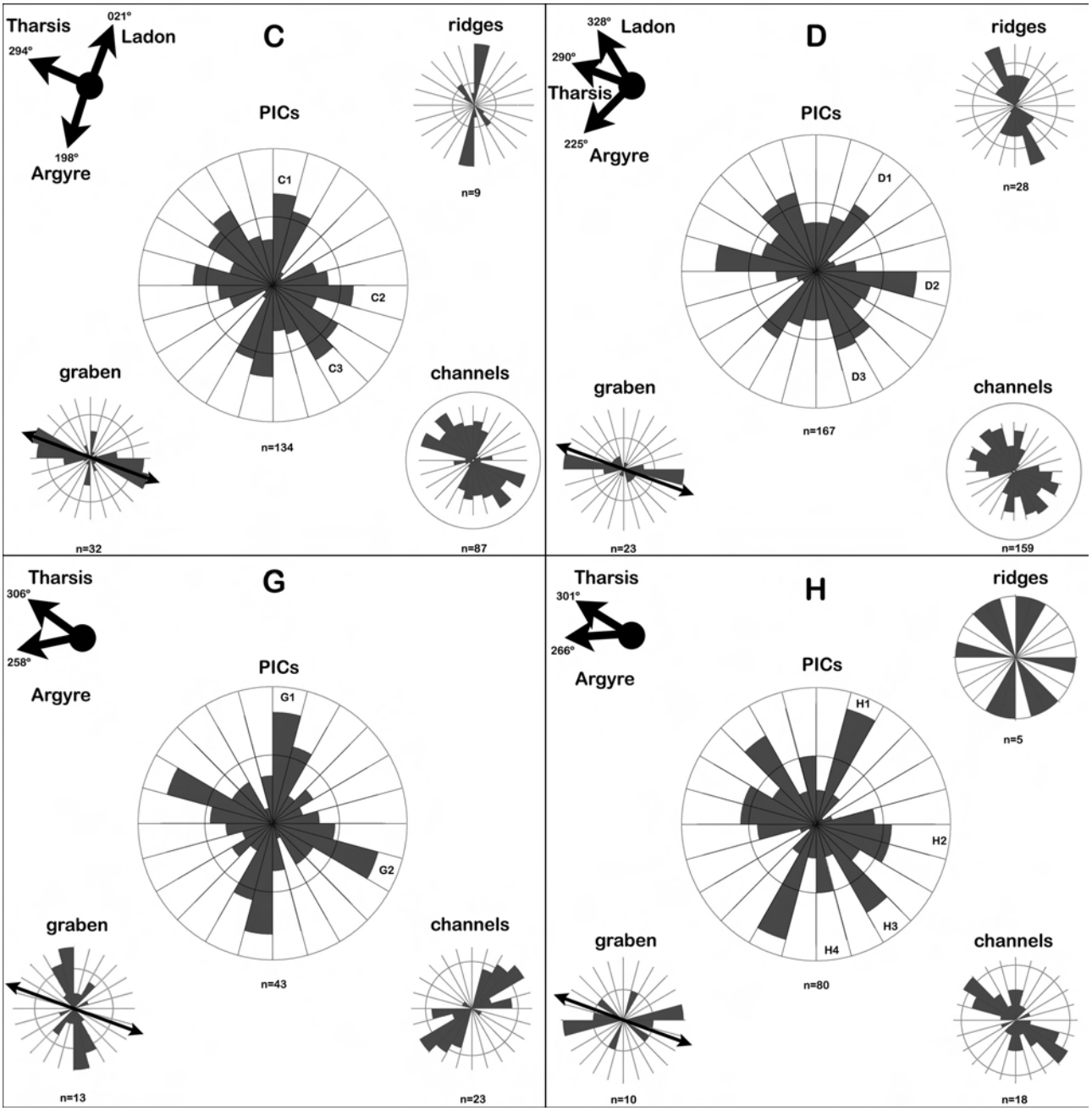

Figure 33. Structural data from the eastern half of the Argyre study area (see Fig. 21). For the explanations of the diagrams, see Fig. 32.

One fascinating feature seen in Figures 32 and 33 is that the orientations of straight PIC rim segments and ridges, graben and channels in the Argyre region very often do *not* coincide. However, when ridge orientations in block A are compared with the fresh PIC rim orientations, a

clear match is observed. Perhaps a similar match can be seen in block B, but the low number of fresh PIC rim strike measurements (n=14) prohibits reliable comparisons.

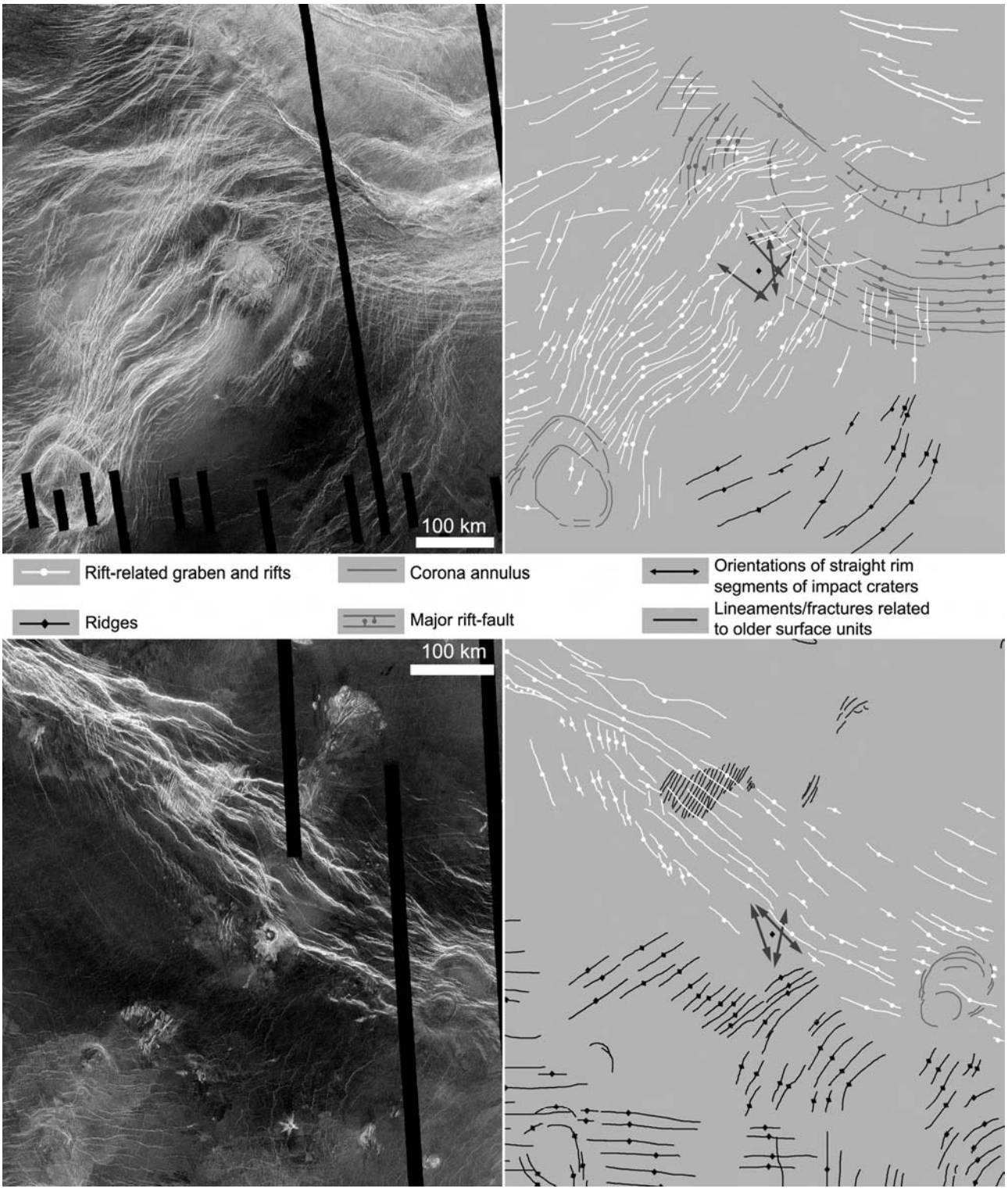

Figure 34. Tectonic sketch maps of features surrounding Venusian PICs, based on Magellan SAR imagery. The upper image pair shows crater Austen (D=42.9 km, 25.0°S 168.5°E), the lower one is Devorguilla (D=23.1 km, 15.3°N 4.0°E).

The results regarding Venus must be viewed slightly differently from the Martian ones. This is because of the low number of Venusian PICs and impact craters in general (see Chapter 5.1). Because no statistically meaningful areal studies of PICs can be made, rose diagrams or other similar methods of describing the results are only useful for exemplifying for instance the limitations of the radar data (Fig. 20). Therefore, the Venusian PICs and their relations with the surrounding tectonic features must be studied one by one. Examples of individual cases are shown in Figure 34.

The matches between PIC straight rims and tectonic orientations are compiled in Table 4. Some observations are worth taking a closer look. Particularly the tectonic orientations measured from tessera terrains, young rift zones, and the concentric component of volcano-tectonic features (mainly coronae) have a strong positive correlation with the PIC straight rim segment orientations. In the case of tessera terrain, the match percentages are the highest, about 83% (<2*D*) and 57% (2–10*D*). For young rift zones and the concentric component of volcano-tectonic features the match percentages are about 76%/42%, and 75%/43%, respectively. The match percent between wrinkle ridges near the PICs is the lowest of all (36%). More distant ridges would yield a huge variety of orientations and, hence, were not taken into consideration. Despite the numerous strong positive correlations, not all PICs have straight rim segments parallel to surrounding tectonic structures: 22, or about 18% of the identified PICs had no match with any of the tectonic orientations measured in their vicinity.

Table 4. The numbers of tectonic measurements, and the match percentages between PICs and the tectonic structures close (<2 PIC diameters) and far (2–10 PIC diameters) from the PIC.

	<2D		2D–10D	
Structure type	Match %	*n*	Match %	*n*
tessera	83%	12	57%	7
young rift zone	76%	21	42%	12
volcano-tectonic, concentric	75%	16	43%	23
old rift zone	54%	26	28%	18
mountain belt	50%	18	21%	14
lineament	47%	32	24%	17
volcano-tectonic, radial	39%	23	24%	21
wrinkle ridge	36%	64	62%	13
total		212		125

Matches between PIC rims and tectonic structures can also be viewed with respect to crater size. Figure 35 depicts the relative abundances of PICs with rim orientations that match or do not match

with some presumably deeper-seated tectonic structure (structures in tessera terrain, rift zones, volcano-tectonic features, and mountain belts; PICs that match only with lineaments or wrinkle ridges are excluded) orientations in three different diameter classes. Although there are some small differences, the low number of craters makes it doubtful that these slight differences are truly significant. Rather the implication is the size does not seem to be an important factor for the matches.

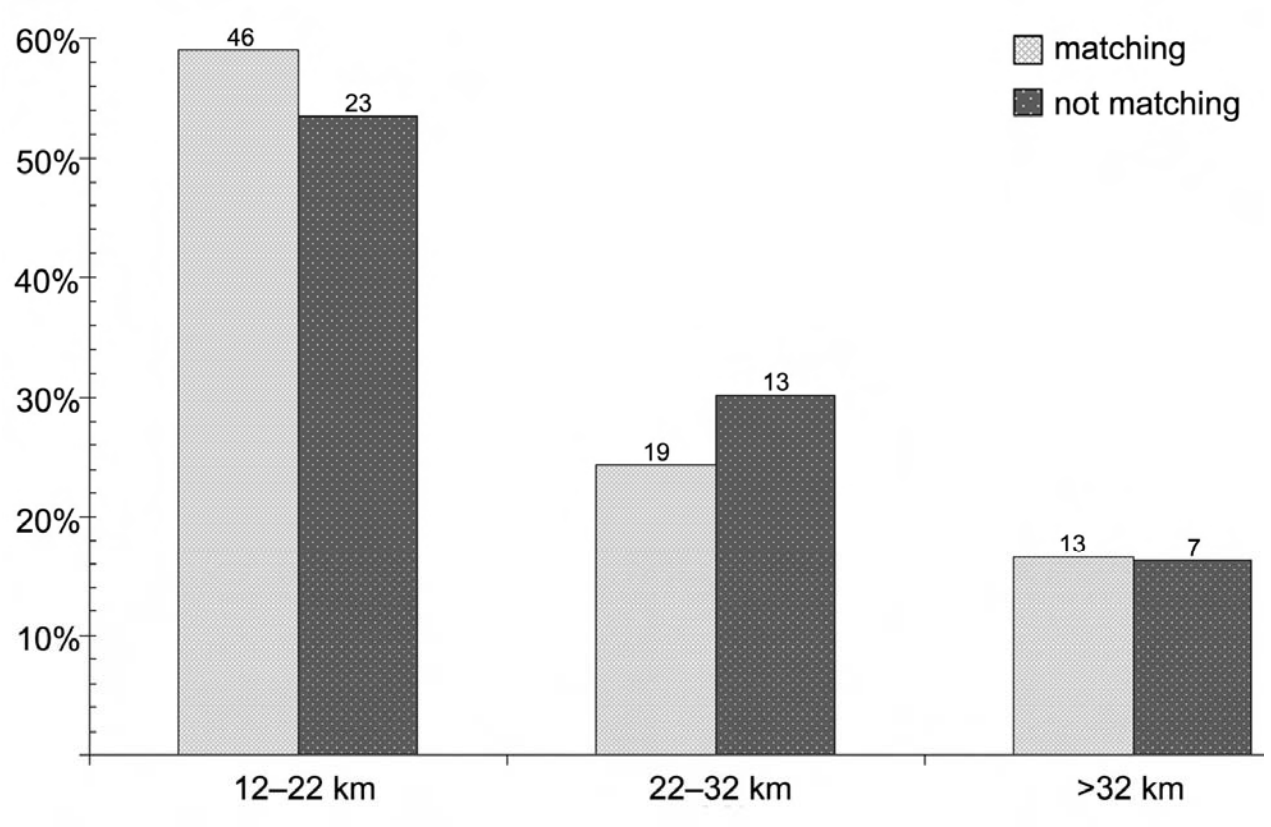

Figure 35. The relative abundances of PICs that have matching rim orientations with the surrounding presumably "deeper" tectonic structures (tessera terrain, rift zones, volcano-tectonic features, and mountain belts) in different diameter classes. The numbers on top of the bars indicate the absolute numbers. The total number of "matching" PICs is 78 and that of the "not matching" ones is 43.

8.6 The effect of illumination geometry

As implied by some of the results presented above, the effects of the selection of the dataset, especially the illumination geometry as well as the resolution, should not be neglected when considering the results obtained by studying PICs. In the case of both photographic datasets (Martian and lunar data), it is clear that when any single crater is studied, the illumination geometry can have a distinct effect on whether or not the crater is classified as polygonal. However, when a larger number of craters are studied, the effect of the illumination geometry seems to become

inconsequential with respect to the conclusions drawn about the “big picture”. In the case of Mars, due to lower incidence angle, PICs are more easily recognised from the MDIM 2.0 dataset than from the MOC-WA mosaic (Fig. 36). Commonly, though far from always, the polygonality is more pronounced on the sunward side of the crater (i.e. if the crater is illuminated from the right, polygonality is often easier to see on the right side of the crater).

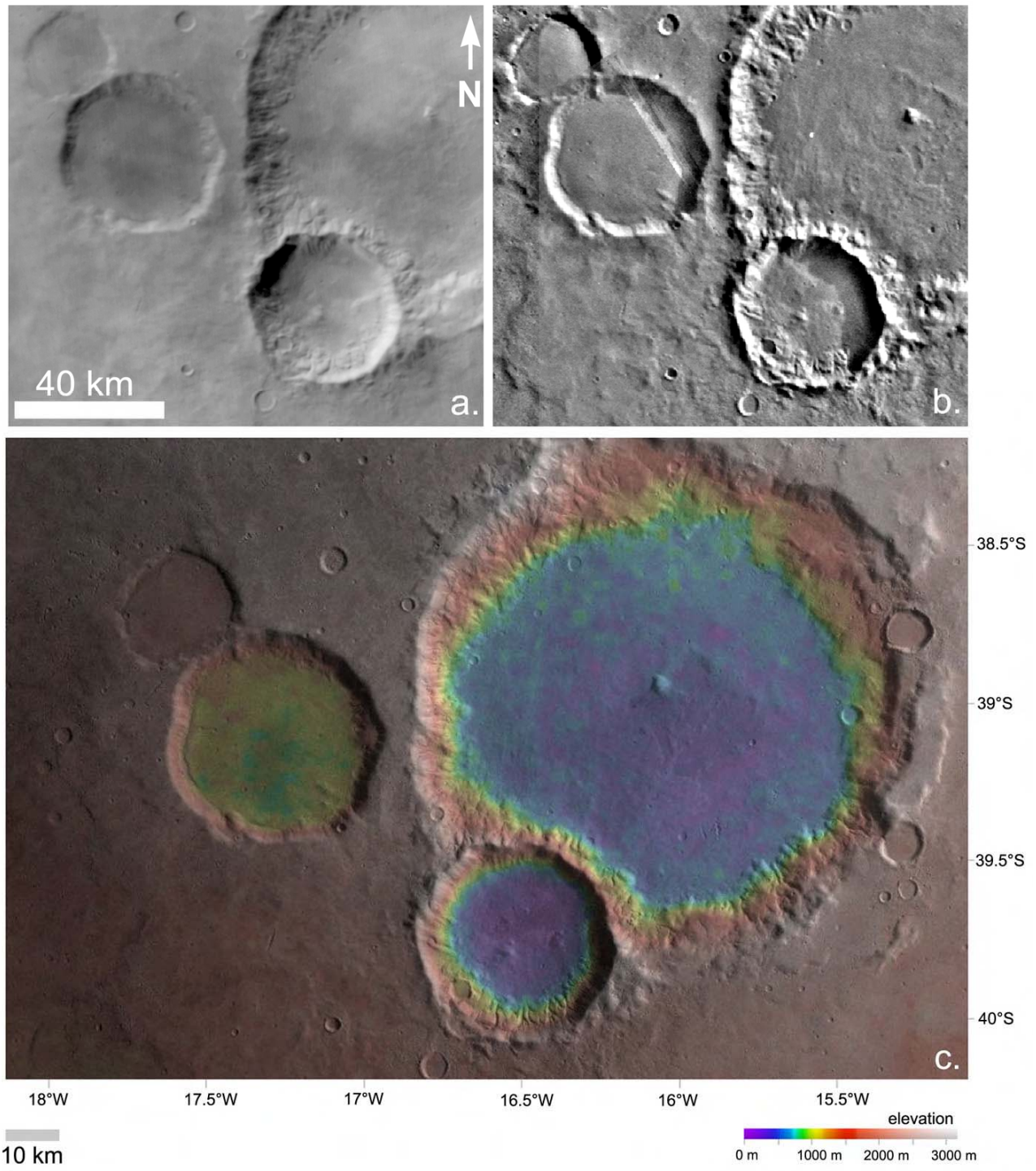

Figure 36. The effect of the illumination geometry on the apparent polygonality of impact craters northeast of the Argyre basin. a.) MOC-WA, b.) Viking MDIM 2.0, c.) HRSC DTM (2687_0000 nadir image). For a colour version of the DTM, see the thesis cover, or the electronic version of the thesis.

To examine the effect of the illumination geometry more closely, an area northeast from the Argyre basin (30°S–42°S, 10°W–42°W; Note that in Paper II the longitude is incorrect, as is the marked location of the area in the accompanying Fig. 1 in the Paper. See Fig. 21 for the correct location.) was studied by using both MDIM 2.0 and MOC-WA photomosaics, having notably different incidence angles (see Chapter 7.1.1 and Paper II). Figure 36 exemplifies the differences between MDIM and MOC-WA, accompanied by an HRSC DTM (digital terrain model) for comparison and topographic reference. The straight rim segment strikes of 30 craters that were classified as PICs using MDIM 2.0 were also measured from the MOC-WA imagery. The resulting straight rim segment orientations from the Viking and MOC-WA datasets are presented in Figure 37. The main features of the diagrams seem similar, and statistically (K–S test in the 95% confidence level) no significant difference could be found.

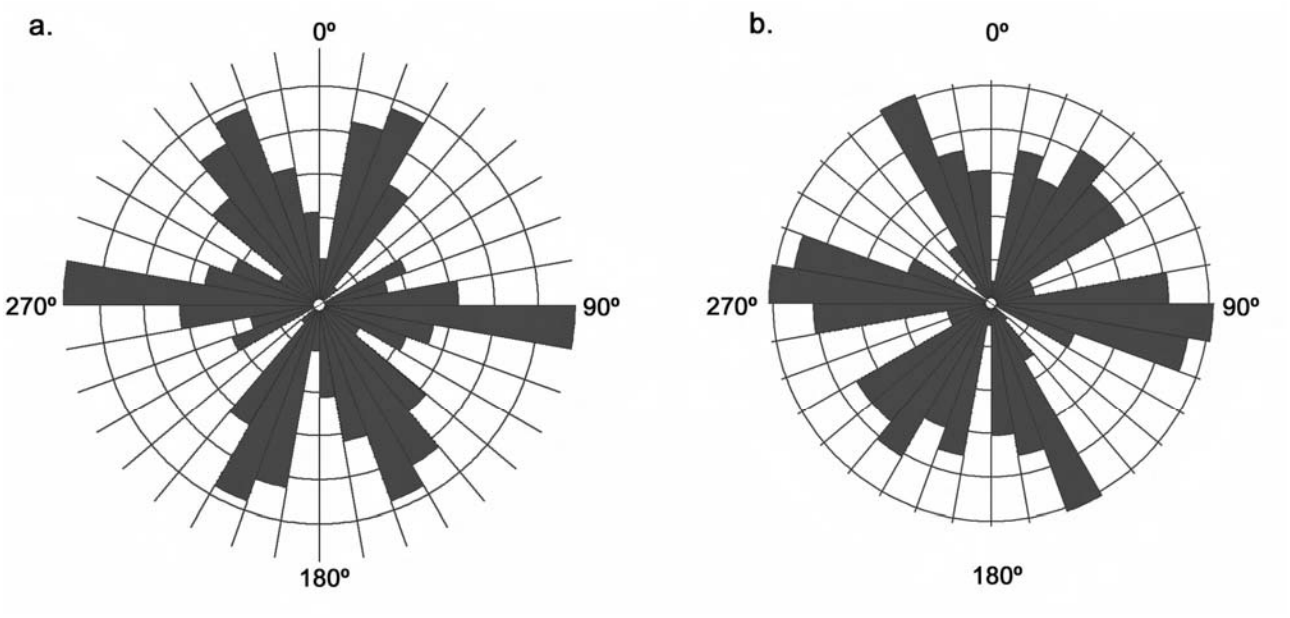

Figure 37. Rose diagrams of the percentages of Martian PIC straight rim segment strikes northeast from the Argyre basin (10°W–42°W, 30°S–42°S; see Fig. 21) in 10° classes, based on a.) Viking MDIM 2.0 mosaic and b.) MOC-WA mosaic. Despite some discrepancies, the overall match of the peaks and gaps is apparent, and no statistically significant differences were found. The circle spacing is 2%, with the outermost circles representing 10%. The number of measurements is 94 for MDIM and 98 for MOC-WA, and the number of PICs included was 15.

In the case of Venusian PICs, the dataset has an even more pronounced effect. Due to the nature of the data (see Chapter 7.1.2), structures oriented approximately east–west are exceedingly difficult to see. Occasionally structures in E–W directions are visible, but the norm is that nothing reliable can be said about them. The ~30°–40° gap in Figure 20 depicting all the PIC rim orientation measurements (both left- and right-looking images) made from the 121 Venusian PICs clearly demonstrates this.

Figure 38 indicates another notable feature of the Venusian PIC rim orientation data. In Figure 38 only measurements from those 42 PICs that have both left- and right-looking images are included. In contrast to the illumination geometry data from the Argyre region (Fig. 37), these diagrams are distinctly different from each other. This emphasises that both left- and right-looking data are needed to see all the straight rim segments (with the ever-present exception of ~E–W oriented rim segments) of a Venusian PIC. This is not surprising given the limitations of the radar data: the same part of the rim cannot be seen in both left- and right-looking images. Typically, a part of the rim crest may be clearly discernible in the left-looking image, whereas the right-looking image of the same part of the crater rim may depict actually some inner structure of rim instead. Thus, left- and right-looking images complement – not contradict – each other.

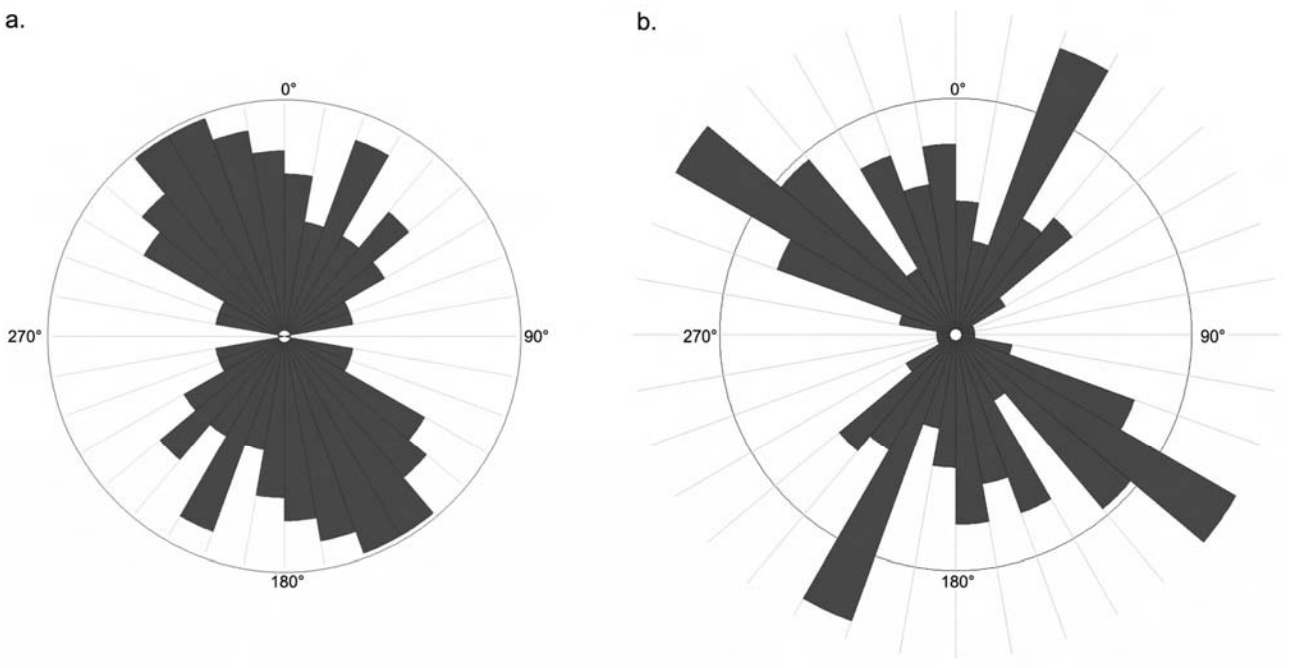

Figure 38. Rose diagrams of the percentages of Venusian PIC straight rim segment strikes (D>12 km), based on a.) right-looking, and b.) left-looking Magellan SAR data, in 10° classes. Only measurements from the 42 PICs that had both left- and right-looking data are included. The circle represents 10%, and the number of measurements was 102 for the right-looking, and 124 for the left-looking data.

The nature of the SAR data also presents a possible source of error in the observations. Topographically uneven crater rim may lead to false identification of straight crater rim segments due to the distortion of the radar image. For example, if there is a topographic high in the eastern rim of the crater, in the left-looking image it would be shifted westward. In principle, this could lead to an erroneous identification of an angle and a straight rim segment. As the resolution of the Magellan altimetry data is not sufficient for distinguishing such small-scale features, it is currently

very difficult to estimate the possible effect of this bias. However, this effect probably is not of major importance. In addition, Poelchau et al. (2009) showed that the corners of square-shaped Meteor Crater are topographically higher than the straight rim segments. If the same applies to Venusian PICs, the apparent shift in the SAR image would merely enhance an existing feature and not create a false identification of a PIC.

9 DISCUSSION

The previous Chapters have described what impact craters are and how they are formed (Chapters 2 and 5), how different cratering environments (Chapter 3) and target properties (Chapters 3 and 4) affect the cratering process (Chapter 5), reviewed earlier studies on polygonal impact craters (Chapter 6), and summarised the methods used (Chapter 7) and results gained (Chapter 8) in this Ph.D. thesis. In this Chapter, synthesising all this into a coherent view on the most important aspects of PICs is attempted. Topics dealt with include the ubiquity of PICs (Chapter 9.1), the consequential effects of the dataset (mainly illumination geometry) in identifying PICs (Chapter 9.2), the centuries old problem of why particularly a partially hexagonal crater shape appears to be the most common one seen in PICs (Chapter 9.3), and the significance of particularly basin-induced fracturing (Chapters 9.4 and 9.5). The origin of PICs is viewed from two perspectives: what is apparently not causing them (Chapter 9.7), and what are the favoured ideas for their formation (Chapter 9.9). Some emphasis is also given to the crater modification stage with respect to PICs (Chapter 9.8). These issues very much form the core of the "theory" part of this thesis, most relevant for impact cratering mechanics. The question of size distribution (Chapter 9.10) is relevant for cratering mechanics, but it prompts applications as well. Discussions on the relation between other tectonic structures and PICs (Chapter 9.6), and PICs as a possible tool in target material classification (Chapter 9.11) belong firmly to the "application" part of the thesis. So do the speculations on further ways to use PICs in planetary studies (Chapter 9.12).

9.1 The universality of polygonal impact craters

It is apparent that polygonal craters were recognised and their origin was pondered on very early in the lunar crater research. The problem of why polygonal craters for the most part then disappeared from the scene of impact and planetary research for decades is an interesting one, but largely a subject of the history of science as well as observational psychology, and thus does not fall within the framework of this thesis. One might, however, speculate that first the lack of a simply-stated theory of how PICs should form was a hindrance to their study, although the importance of pre-existing fractures was incorporated in a number of writings (e.g. Baldwin, 1963; Fulmer & Roberts, 1963; Fielder, 1965; Adler & Salisbury, 1969). Also the fact that many studies from the 1960s implied at least partly a volcanic origin for polygonal craters (e.g. Fielder, 1965; Kopal, 1966; Ronca & Salisbury, 1966; most PIC-papers in the Geological Problems in Lunar Research volume) may perhaps have given polygonal craters a "bad reputation" that may have driven impact geologists off of their study, especially after the impact origin for the vast majority of (lunar) craters

became canonical in the early 1970s. Once the topic had lost its appeal it was hard to redeem it, and the ideas presented by Eppler et al. (1983) were just generally overlooked for one reason or another.

Despite the lack of previous systematic studies about polygonal impact craters it is, and largely has been for quite some time, clear and apparent that PICs are present and often even common on the surfaces of all terrestrial planets (Mercury, Venus, Earth, Mars), as well as on moons (e.g. the Moon, Europa, Ganymede, Callisto, Rhea, Iapetus), asteroids (e.g. 433 Eros and 253 Mathilde) and possibly even a cometary nucleus (P/Wild-2) (e.g. Paper I and references therein; Schultz, 1976; Roddy, 1978; Strom et al., 1990; Prockter et al., 2002; Abels, 2003; Denk et al., 2005; Basilevsky & Keller, 2006; see Chapter 6.1 and Fig. 17). In the study areas of Argyre region, Venus, and TINN area of the Moon, about 15%–20% of the craters are classified as PICs.[51] It is also noteworthy that Wood et al. (1977) observed 16% of Mercurian craters to show at least some level of polygonality. Clearly, polygonal impact craters are not a rare phenomenon.

Although formal classifications and tests are yet to be made, based on current knowledge and preliminary comparisons with impact crater databases, it appears that polygonal craters are present in all main types of Martian and Venusian crater (e.g. with or without central pit) and ejecta (e.g. single layer, multiple layer, or ballistic) morphologies. If this would turn out to be true, it would imply that none of the processes responsible for creating the observed morphologies significantly affect the craters' polygonality. However, detailed studies are in order, as for example in the case of Mars the correlation studies of layered ejecta morphologies or the peripheral peak ring and polygonality could give further indications of the properties of the target material.

As noticed, the polygonal plan view of impact craters is an inseparable part of craters formed in a huge variety of different conditions, it therefore must be dealt with when considering the formation mechanisms of impact craters. Also this "universality" of PICs implies that the fracturing creating the pre-requisite for PIC formation needs not to be related to large-scale tectonic processes like impact basin formation, the build-up of volcanic edifices, or plate tectonics.

9.2 The illumination geometry and its effects

Before the origin of polygonal craters can be studied, and before the apparent tectonic patterns revealed by them should be utilised in deciphering the tectonic history of the study area, it is of utmost importance to be sure the PICs themselves and the orientations indicated by them are real,

[51] It can be noted that also the percentage of terrestrial structurally controlled impact craters in my unpublished list falls in this same ~15%–20% interval. However, given the high uncertainties involved in the identification of possible structural control in the heavily eroded and modified terrestrial impact craters (or structures), this may be purely coincidental.

and not an artefact of illumination geometry, resolution or wavelength of the dataset used. It is well-known among planetary geologists that the illumination geometry can enhance some features that in other lighting conditions could be almost indistinguishable (e.g. Schultz, 1976). The wavelength and resolution of the dataset used has not been the focus of this study, but the preliminary results presented in Papers I and III indicate that although there are important differences in the appearance of craters seen by Viking (visual) and THEMIS (both visual and infrared), polygonality can be observed in both wavelengths, as is to be expected. The same applies for the use of images having different resolutions (Binder & McCarthy, 1972).

Regarding the illumination geometry, the Kolmogorov–Smirnov test based on PICs northeast from the Argyre basin (Fig. 37) clearly indicates that in 95% confidence level the two samples (rim strikes of PICs measured from Viking MDIM 2.0 and MOC-WA images, see Fig. 36 for an example) are drawn from identical populations. Thus, on a regional scale the different incidence angle of the two datasets has no relevance to the geologic implications of the data (Paper II). With respect to any individual crater, however, it has major significance, as a crater appearing to be polygonal in Viking data may look circular in MOC data, and vice versa. These results on the negligible effect of illumination geometry in a regional scale concur perfectly with those briefly reported by Binder and McCarthy (1972) and Scott et al. (1977).

The problem of illumination geometry could perhaps be partially overcome by using topographic data like MOLA, although even for a highly typical Martian PIC about 20 km in diameter, the resolution of the MOLA data is too coarse to allow reliable identification of straight rim segments, and therefore it could only be used for the more scarce, larger PICs. Hence, it has become clear that from the current selection of available datasets,[52] the polygonality of Martian impact craters that are studied over extensive areas is easiest to see using Viking MDIM.

The Venusian PICs are more sensitive to the illumination geometry, i.e. to the looking direction of the Magellan radar. East–west oriented structures cannot usually be seen at all (Fig. 20). Because left- and right-looking radar images reveal slightly different parts of the crater rim (Fig. 38; Fig. 1 in Paper IV), both images should be used whenever possible in order to be able to see as much of the true rim polygonality or circularity as possible.

[52] Currently relevant to this study are data from Mariner (9), Viking (MDIM), MOC-WA, MOC-NA, THEMIS, HRSC, HiRISE, CTX, and to some extent also MOLA.

9.3 The number of straight rim segments and their mutual angles

Pike's (1968, cit. 1977) comment on the statistical increase of the "frequency" and "strength" of polygonality with increasing crater size is interesting. Unfortunately Pike (1977) does not describe his earlier methods or definitions. It can, however, be conjectured that the number of straight rim segments used in this Ph.D. work could be a close proxy of Pike's frequency and strength of polygonality.

In the case of Martian PICs, there is a straightforward apparent trend in agreement with Pike's results (1968, cit. 1977): the bigger the crater, the larger number of straight rim segments it has (Fig. 25). This could be interpreted merely as an indication of resolution, i.e. it is easier to see more straight rim segments in a large crater than in a small one. The Venusian data, on the other hand, does not reveal a similar trend (Fig. 25). It should be emphasised, however, that the smallest craters in the Venusian dataset are fairly large compared to the resolution, and thus several rim strike measurements can be reliably made even of the smallest Venusian PICs if straight rim segments are present.

Typically only a part of the crater rim is polygonal, while the remainder of the rim more or less follows the sector of a circle. This observation also demands a brief discussion. Most likely it reflects the uneven vertical or lateral distribution of dominating inhomogeneities in the target. The formation of both simple and complex PICs requires some *preferred orientations* of weakness. Thus, if the target is heavily fractured in various directions, it can be regarded as homogenous in this context. The same, of course, applies if the target has no or only weakly pronounced fractures (see Fulmer & Roberts, 1963).

The fundamental reason why a partial hexagon appears to be the most common PIC shape, also noted among others by Alter (1956b), Kopal (1966), Davydov (1968) and Leonardi (1976)[53] regarding lunar PICs, is currently unknown. As a bit of an exception to the "rule" it can be noted here that Morrison (1984) did not emphasise the 60° (120°) angle, but instead stressed the 15° (and its multiples) difference between the straight rim segments (60° of course being a multiple of 15°). In any case, fault or fracture patterns promoting a hexagonal shape are rather easily developed in terrestrial crustal rocks during shearing. For instance, in strike-slip faulting, under compressive stress, two sets of faults develop at about an angle of 30º with respect to the maximum stress axis σ_1 that bisects the two fault sets. The intersection of the fault planes is parallel to intermediate stress axis σ_2 (e.g. Park, 1997). Thus, in a target rock with a typical conjugate shear fracture pattern

[53] Leonardi (1976) made an interesting, yet somewhat ambiguous and vague remark that the importance of the polygonality of lunar craters may be exaggerated by some researchers because of "theoretic opportuneness".

developed in strike-slip faulting, the fractures or faults form a "grid" with angles of about 60° (120º) between the two sets. In the case of Mars, wrinkle ridges and associated *en echelon* type strike-slip faults have been observed with a 120° angle between the ridge and fault strikes (Schultz, 1989). In such a target, a partial hexagon is a natural shape for a structurally controlled polygonal impact crater.

Riedel shearing is another common process for creating fracture sets with angles of about 60º (120º) between the sets. Riedel shear fractures typically form at angles of 15º (low angle Riedel, R) and 75º (high angle Riedel, R') with respect to the general trend of a shear zone, so the angle between low and high angle shears is 60º (e.g. Bursnall, 1989; Hodgson, 1989). Although it can be very difficult to infer the true origin of the fracturing and therefore the orientation of the principal stress axes σ_1–σ_3 on a planetary surface, it could be done with meticulous regional mapping, aided by and combined with the new very high resolution datasets (HiRISE in particular). Therefore, a detailed analysis of PICs combined with other tectonic indicators in relation to the stress and strain created by, for instance, the impact basins and volcanic rises, as well as the possible early plate tectonics on Mars, may prove to be useful for understanding the evolution of a planet's crust.

To summarise, only tentative conclusions on the questions of the number of straight rim segments and their mutual angles can be drawn. The Martian trend of more straight rim segments with increasing PIC diameter may well be just a spurious trend induced by resolution of the dataset used. If, however, the trend is real and not just apparent, a possible explanation would be that the spacing of the structures causing the polygonality is large, and hence the smaller PICs have a larger probability of hitting, in this sense, a homogenous target. The observation that partially hexagonal shapes in particular are "preferred" among PICs, apparently known for centuries, still remains somewhat elusive. A possible solution could be that typical rock materials commonly fracture with 60° (120°) angles between the fracture sets under conditions of strike-slip faulting or Riedel shearing. Such a fracture pattern in the target material would clearly promote the formation of a hexagonal PIC.

9.4 The importance of target fracturing

Polygonal, instead of circular or ellipsoidal crater rim shape indicates dominating inhomogeneities of probably considerable vertical extent in the target material. On average, those inhomogeneities must be separated by a distance less than the crater's apparent diameter in order to affect the crater rim in a way demonstrated by PICs. This may be relevant especially in experimental craters, but

also in the very smallest simple PICs. As speculated above, it may perhaps affect the number of straight rim segments in somewhat larger PICs too.

Geologically long lasting fractures and faults that extend rather deep into the crust are the most plausible cause for these inhomogeneities in the areas studied in this thesis. Similar observations and conclusions were previously made regarding lunar (Fielder, 1965) and Mercurian (Strom et al., 1990; Strom & Sprague, 2003) polygonal craters. Deep-seated fractures may also be reactivated later on, and can affect surficial layers of previously brecciated material, as is probably the case with the PICs in figure 2 in Paper II. Sometimes, however, PICs may perhaps indicate also slightly more shallow structures like wrinkle ridges (see below).

The fact that PICs reflect areally widespread structures of the target material is also evidenced by the distribution pattern of PIC rim strikes: if it weren't for the dominating fracture orientations, the rim strike distribution pattern would be more even (random), and the notable peaks and gaps in the directional diagrams (e.g. Figs. 32 and 33) would be absent or at least less pronounced. In addition, the PIC rim strikes typically parallel the predicted (and sometimes also observed) fracture patterns of impact basins (Papers I and III) as well as the directions of tectonic structures like graben (Papers I and especially V; However, this certainly is not always the case, as noted in Paper III.). This would be hard to conceive if PIC formation would be independent of the target structure.

9.5 Basin-induced fracturing and PICs

The origin of the main target structures affecting the formation of PICs studied in this work seems, for the most part at least, to be relatively straightforward. The main source of fracturing in the case of the Martian and lunar study areas is most likely the formation and subsequent modification of the impact basins. Impact basins and large complex craters are known to have extensive radial and concentric fracture patterns surrounding them, created at the time of the impact but also significantly enhanced during the later basin modification and infilling (e.g. Melosh, 1976, 1978; Curran et al., 1977; Schultz et al., 1982; Wichman & Schultz, 1989; Spudis, 1993; Freed et al., 2001; Rodríguez et al., 2005; Gurov et al., 2007; see Chapter 2.2). These fracture patterns become evident in the dominating radially and concentrically oriented peaks in PIC rim strikes especially south of Isidis, west of Hellas (Fig. 31; Papers I and III) and west of Argyre (Fig. 32; Table 5; Paper III). The Ladon basin apparently has induced similar fracture patterns, partly overlapping the fractures created by the smaller Holden basin located within Ladon.

Although Wichman and Schultz (1989) mention Hellas-radial tectonic patterns, they do not recognise them as a major tectonic feature. Instead, they noted five Hellas-induced concentric

structures with different distances from the basin. With this background, it seems even more interesting that on the western side of the Hellas basin the polygonal craters imply the dominance of a radial, not concentric system of structural weakness. In the case of Isidis, however, Wichman & Schultz (1989) do notice the importance of the basin-radial fracturing.

Thus, the basin-radial and concentric fractures are well-known, and also evident in the PIC data gathered in this thesis. However, the basin-induced conjugate shear fractures have been a bit of an enigma, and their formation around lunar impact basins has been deemed improbable (Chapter 2.2; Freed et al., 2001). Nevertheless, as discussed in more detail in Paper III, the Martian PIC data includes prominent rim strike maxima, whose orientation with respect to the basin fits the hypothetical basin-induced conjugate shear fracture sets, and which are not readily explained otherwise (see Table 5). In addition to areas west of both Argyre and Hellas basins, the shear fractures might be visible in the PIC data south from Isidis basin as well. However, the idea of Martian basin-induced conjugate shear fractures is presented here merely as a hypothesis worth taking a closer look at in the future. A more detailed study of the reality of the hypothesis, involving the lithospheric thickness, the basins' infilling history, and their gravity anomalies, lies beyond the scope of this Ph.D. thesis.

In addition to the well-known basins of Hellas, Isidis, Argyre and Ladon, PICs may give credence to other suggested basins too. The up to 1000 km diameter ancient impact basin at 233°W 10°S ("south of Hephaestus Fossae") suggested by Schultz et al. (1982) seems quite plausible in the light of PIC data (Öhman et al., 2008b): the three northeasternmost blocks studied in the Hellas area indicate PIC rim orientations that would parallel basin radial and concentric components, partly enhanced by matching orientations with Isidis (not forgetting the possible influence of Elysium). The Solis Planum basin suggested by Frey et al. (2007) is a highly hypothetical one, but some of the otherwise relatively poorly explained PIC rim strike clusters in the northwestern part of the Argyre region could be due to this basin-induced fracturing.

9.6 PICs and other tectonic indicators

Other tectonic indicators, graben being good examples, may concur with the results obtained from the study of PICs. This has been observed regarding lunar PICs (e.g. Schultz, 1976; Scott et al., 1977), and on a very preliminary level also in this thesis (Paper I). Nevertheless, as discussed in more detail in Paper III, PICs and tectonic structures may also indicate different tectonic developments.

In addition to impact basins, other probable major sources of fracturing in the studied parts of the Martian surface include the Tharsis bulge and the genetically related canyon complex of Valles Marineris, the volcanic centre of Elysium Mons, and the ancient paterae in Hesperia and Malea Plana. Their tectonic effects on the surrounding regions are easily seen e.g. as ridges and graben. In the Argyre region their orientations are controlled by the Tharsis bulge, as can be seen in Figures 32 and 33. Ridges are concentric to Tharsis, while the graben (and the associated channels in the northwestern part of the study area) are radial to it.

In Paper I it was noted that some of the dominating ridge orientations in Hesperia Planum, probably reflecting older structures (Raitala, 1988), are parallel to PIC rim orientations. A more detailed scenario can be seen in the northwestern part of the Argyre region (block A), in Thaumasia and Bosporos Plana. There one of the maxima in the fresh (and thus small and rather shallow) PIC rim strike distributions parallels the ridge strike. When all degradational stages of PICs are combined, this orientation ceases to be important. This is a possible indication that while rimmed (and the very rare degraded) polygonal craters display some other, probably older structures of the target, the fresh PICs and ridges both record a younger tectonic phase in the region's geologic evolution.

The complexity of the geologic evolution in block A in the northwestern Argyre region may also be manifested in the fact that the statistical match between the rim strike orientations of different degradational stages is worse than usually in the study area, although the low number of measurements may also be the sole contributor to this discrepancy (Table 3). In any case, it seems that although the fresh PICs and ridges give compatible results in block A (and perhaps B), the majority of the PIC rim strikes in the Argyre region record earlier phases of the tectonic evolution than the ridges (or graben). As summarised in Table 5, these phases appear to be for a large extent basin-related, although pre-Argyre tectonics (Thomas & Masson, 1984) are quite possible as well.

An interesting direction present in the PIC rim data of the Argyre region is also the N–S peak (A1) in block A (Fig. 32; Table 5). One possible explanation might be that it is related to the same tectonism, which has caused the prominent N–S trending graben in Coracis Fossae, located just west of block A. So the old (Dohm & Tanaka, 1999; Dohm et al., 2001a) tectonic orientations indicated by the graben of Coracis Fossae are seen in PIC data, whereas the younger WNW oriented and Tharsis-centred graben that are so distinct in our study area do not have a counterpart in the PIC rim orientations.

If the weak linear magnetic anomalies are interpreted as an indication of plate tectonics in primitive Mars (e.g. Acuña et al., 1999; Connerney et al., 1999, 2001, 2005; Purucker et al., 2000), then in the area between Argyre basin and Valles Marineris the PICs having rim strikes identical with weak

magnetic anomalies may even reveal the imprint of this early fracturing (Paper II). However, this remains highly speculative, because on the southwestern side of Isidis basin the magnetic anomalies are somewhat stronger, but a similarly oriented PIC rim strike pattern is absent from the data.

Table 5. Possible contributing factors to help explain the PIC rim strike orientations in the Argyre region. For the block division, see Figure 21.

Block	Peak no.[1]	Orientation	Possible contributing factors[2]
A	A1	000º–015º	Coracis Fossae
	A2	075º–120º	medium pre-Argyre
	A3	135º–150º	Argyre radial, minor pre-Argyre
B	B1	(000º)–045º	major pre-Argyre, Ladon radial
	B2	075º–090º	Argyre concentric, medium pre-Argyre
	B3	135º–150º	Argyre radial, Ladon concentric
C	C1	000º–030º	Argyre radial, Ladon radial, Holden radial
	C2	090º–105º	Argyre concentric, medium pre-Argyre
	C3	120º–150º	Ladon concentric
D	D1	(015º)–045º	Argyre radial, Ladon concentric, major pre-Argyre
	D2	090º–105º	medium pre-Argyre
	D3	135º–165º	Ladon radial, Argyre concentric, minor pre-Argyre
E	E1	015º–045º	Argyre conjugate, major pre-Argyre
	E2	075º–105º	Argyre radial
	E3	135º–150º	Argyre conjugate, Claritas Fossae, minor pre-Argyre
F	F1	015º–030º	Argyre conjugate, major pre-Argyre
	F2	075º–105º	Argyre radial
	F3	120º–150º	Argyre conjugate, minor pre-Argyre
	F4	165º–180º	Argyre concentric
G	G1	000º–030º	Argyre concentric
	G2	090º–120º	Argyre radial
H	H1	015º–030º	Argyre conjugate, major pre-Argyre
	H2	075º–120º	Argyre radial
	H3	135º–150º	Argyre conjugate, minor pre-Argyre
	H4	165º–180º	Argyre concentric
“EF”	EF1	020º–040º	Argyre conjugate, major pre-Argyre
	EF2	080º–100º	Argyre radial
	EF3	130º–150º	Argyre conjugate, Claritas Fossae, minor pre-Argyre
	EF4	170º–180º	Argyre concentric

[1] Peak numbering refers to Figs. 32–33.
[2] Note that these should not be considered as the only solutions, as there are diverse and complex factors that contribute to PIC morphology.

The relatively young Venusian surface lacks or at least has very few true impact basins (Chapter 5.2.3). Tectonic features, however, are common, and thus there are plenty of sources for relatively deep fractures. It is interesting that the tectonic orientations measured from the young rift zones, tessera terrain and the concentric component of the volcano-tectonic features (mainly coronae; no arachnoids or volcanoes, and no novae without an associated corona) yield the strongest matches

with the PIC rim orientations. Possible reasons for why these particular structures are apparently reflected in the PIC rim orientations are worth a bit closer look (Paper V).

Young rift zones are among the youngest tectonic features on the Venusian surface. It seems plausible that rifting is such a powerful process that it effectively erases most of the previously existing structural fabrics from the crust, both in the rift zone itself, as well as in the immediate vicinity. Thus, the dominating structural orientations are mostly those originating from the rifting, and hence the match between the young rift and PIC rim orientations is strong. The substantially lower percentage of matches between PIC rims and old rift zones or fracture belts may be due to other, later tectonic events destroying the dominating structural fabric that probably was present surrounding the still visible old tectonic features. Thus, the situation may originally have been similar to what now can be seen surrounding the young rift zones.

Coronae form a group of highly complex volcano-tectonic structures with a broad and vague morphologic definition. According to the most commonly held view, the coronae are circular to elongate structures that have a concentric annulus consisting of mostly extensional fractures but sometimes also of ridges, and they are often associated with lava flows or volcanic cones or shields. Coronae are typically located close to the equatorial rift zones, and they, like other volcano-tectonic features, are proposed to be formed by mantle upwelling. (Barsukov et al., 1986; for further discussion, see Aittola, 2003, and Kostama, 2006)

Unlike the arachnoids, novae and corona-novae, the coronae lack a significant radial structural component, although radial dykes are probably present (Barsukov et al., 1986; Grosfils & Head, 1995; Aittola, 2003; Kostama, 2006, and references therein; cf. Cyr & Melosh, 1993). Hence, it is not surprising that PICs have a strong positive correlation with the concentric, but not the radial component of the coronae. Furthermore, the radial stresses are dominant in the first, uplift stage of the corona formation, whereas the concentric deformation occurs in the latter stages of the long-lasting process (Cyr & Melosh, 1993; Koch & Manga, 1996; Aittola, 2003; Kostama, 2006). Thus, the concentric structures are likely to dominate the corona surroundings. Interesting is that even beyond two PIC diameters the match between the PIC rim orientations and the concentric component of the coronae is a fairly strong one (~43%). This implies that the coronae have had a major deformational influence on the crust much further than the mere apparent corona annulus would suggest.

Orientations measured from the tessera terrain were observed in this thesis (Paper V) to have the strongest positive correlations (~83% close to PICs and ~57% further away) with the Venusian PIC rim orientations. This may perhaps be readily explained. Tessera terrain is generally regarded as

being older than all the surrounding geologic units (e.g. Ivanov & Head, 1996; Basilevsky et al., 1997). Hence, it is apparent that the tessera terrain extends far under the surrounding geologic units (e.g. Ivanov & Head, 1996; Hansen & López, 2009), and either affects the formation of the subsequent tectonic structures, or the PICs reflect directly the orientations of the tessera. This latter option would imply that the thickness of the surficial unit covering the tessera is quite small, further speculated below in Chapter 9.10.1. This is actually closely related to the observation that the wrinkle ridges have *relatively* the lowest matches with PIC rims (as ridges are so ubiquitous, and several measurements can be made from them, the absolute number of PIC–ridge matches is high; see Paper V).

Although the match between measured Venusian PIC rim orientations and tectonic orientations have been emphasised here, it should not be forgotten that some (22, or about 18%) of the identified PICs had no correlation with any of the tectonic orientations measured for that crater. Another notable point is that commonly several measurements (e.g., on average 2.9 measurements per a Venusian PIC in the left-looking data) were made from the straight PIC rims, and positive correlations with the tectonic orientations were found in perhaps only one or two of the straight rim segments. So although the apparent tectonic structures provide a possible and even a probable explanation to the presence and rim orientations of many of the PICs, a considerable portion of them obviously reflect some yet unidentified tectonic events, or a lesser component of an identified tectonic event.

With higher resolution more straight rim segments are likely to appear, and also to match with the surrounding tectonic orientations. However, such small-scale features are not the focus of this Ph.D. study, as they do not contribute to the overall polygonal shape of the craters. Also, with the current data of the Venusian surface, reliable identification and measurement of such features would be difficult, if not utterly impossible (see Chapter 9.10).

Two further aspects of the match between the Venusian PIC rim and the tectonic structure orientations are also worth a short note. These are the effects of the crater's size on the correlations, and the age relations of the crater and the tectonism. The age relations between the crater and the tectonic structures are sometimes difficult to determine unambiguously, as typically no direct cross-cutting relationships occur. In most of the cases where unambiguous cross-cutting relations could be determined, the tectonism was older than the craters, in accordance with the general Venusian geologic history (e.g. Basilevsky et al., 1997). Two cases, where the polygonal crater is older than the tectonic structures having matching orientations with the PIC rims, can be mere coincidences (and there were other tectonic structures that could "explain" the PIC rim orientations). In addition,

there were a few instances where the PIC was older than the tectonism, but there the orientations were not matching. Hence, the idea of pre-existing crustal structures and not later tectonic deformation controlling the PIC rim orientations gets support from the age relation studies, although statistically convincing studies are impossible (Paper V).

Poor statistics hamper to some extent also the study of the crater size's effect on the rim segment orientation matching with tectonics. When the size distribution of 78 PICs that have a matching rim segment orientation with the surrounding, presumably "deeper" tectonic structures (i.e. tessera terrain, rift zones, volcano-tectonic features, and mountain belts, excluding the PICs that match only with lineaments or wrinkle ridges) is compared to the size distribution of the 43 PICs that have not, very similar distributions appear (Fig. 35). The distributions are also similar to the general PIC size distribution. More detailed analysis of the size–match data is, unfortunately, practically impossible due to the low number of Venusian PICs. In any case, it appears that although the size of the crater is very important for the probability of a crater being a PIC or not (as can be seen in the different size distributions of PICs and non-polygonal craters; Figs. 28 and 29), it is not a major factor for the match between the orientations of the straight PIC rim segments and the tectonic structures on Venus: a PIC rim orientation either matches with the "deeper" tectonic structures or it does not, irrespective of the size of the crater.

9.7 Crater degradation as the origin of polygonal craters?

Despite a quite extensive literature study, only a few references were found to promote, or even comment on various degradational processes as a means to explain the polygonal outline of some terrestrial impact structures (Kiselev & Korotushenko, 1986, cit. Masaitis, 1999; Rossi et al., 2003; briefly discussed by Abels, 2003, and mentioned by Laurén et al., 1978). As was noted by Shoemaker (1960, 1963) and Roddy (1978), and shown by Pohn and Offield (1970) and Eppler et al. (1983), polygonality is a primary feature of craters and not affected by later degradational processes to any major extent, at least in the cases of the square-shaped Meteor Crater and the lunar polygonal craters. However, based on my discussions with various geoscientists, it appears that the idea of some kind of preferential erosion being the cause of polygonality is rather popular. In this Ph.D. thesis, one of the key issues is to resolve and verify by statistical analysis if degradation of the Martian or Venusian craters can cause any observable variation to the amount of polygonality of craters, or especially to the strikes revealed by PICs of different degradational stages.

When the polygonality (the amount of straight rim segments) of PICs in the Argyre region is compared to their state of degradation, an unchanged distribution appears: in each of the four

polygonality classes, degraded PICs make about 20%–30%, rimmed PICs about 55%–65%, and fresh PICs about 15%–20% of the whole number (Fig. 4 in Paper II). In the case of Venus a similar study does not give statistically robust results as the vast majority of the PICs are classified as pristine (101) and only three as degraded, but a similar unchanging distribution is implied. When the percentages of PICs and non-polygonal craters in the three degradational classes are compared, it is also clear that the distributions are similar (Fig. 27; Paper IV; Note, however, that the low number of highly degraded PICs hampers the reliability also here.). The same can be seen when other indications of crater's age, i.e. the floor reflectivity and the presence of a dark parabola (see Chapter 5), are studied.

This kind of constantly similar distribution is to be expected if polygonality is a primary and permanent feature of some impact craters. If degradational processes would be the cause of polygonality, a distribution where the classes of highly polygonal (e.g. ≥4 straight rim segments) PICs would include a larger proportion of degraded craters would be expected. As this is not the case, it can quite safely be deduced that at least in the light of the current study, the degradation of craters does not enhance their polygonality.

This result is further emphasised by another point of view. The straight rim segment strikes of polygonal craters of different degradational stages can be compared using the K–S test (or in some cases the "standard" χ^2 test). The results of the K–S test carried out with the data from the Argyre region (Table 3, see also Fig. 26) show that in the vast majority of comparisons, the samples were drawn (practically in 95% confidence level) from the same (identical) populations. Thus, the directional patterns of fresh, rimmed and degraded polygonal craters in the same area are, in practice, identical. This suggests that for the most part of the Argyre region, all the PICs regardless of their age have been affected by the same structural elements of the target material during their formation. Hence, the dominating fracture sets in that part of the Martian crust that are evidenced by PICs have been present for a geologically significant time. A directional distribution like this would be more difficult to explain by a degradational origin of polygonality, especially as the directions revealed by PICs often are "expected" based on PICs' location with respect to impact basins or major tectonic structures.

Although the low number of measurements currently complicates reliable statistical analyses of PIC rim strikes in areas having a complex geologic history and a relatively young surface age, for example in block A northwest from Argyre basin (see Fig. 21), there are some indications that in such areas the basic scenario of identical rim orientations in different degradational classes described above does not hold true. In block A (and perhaps in block B) there is a match between

the dominant ridge orientation and one of the fresh PIC rim strike maxima. This orientation is not evident when the data from all degradational stages of PICs are combined. Therefore, in complex areas PICs of different degradational stages (and thus, in practise, of different ages), may reveal orientations of structural weakness that have been present in different times. In such a case the depth of the crater, and thus the older target material where the crater is excavated in, may become an important factor (this is further discussed below in Chapter 9.10).

In the greater Hellas region (Paper I) the situation seems to be slightly different (although one should note that this subject has not been dealt with as thoroughly in the greater Hellas as it was in the Argyre region). Ridge orientations (Raitala, 1988) have a match in the rim strikes of PICs (PICs of all degradational stages included). This result can be seen as giving support to Raitala's (1988) conclusion that the wrinkle ridges in Hesperia Planum are reflecting older crustal fractures and other similar structures.

The spatial distribution of Venusian PICs (Fig. 22) gives further emphasis to the idea that post-impact degradation and modification are not important for creating the polygonal plan view. The distribution of tectonised and volcanically embayed impact craters on Venus is localised to the vicinity of rift zones[54] (Herrick & Phillips, 1994a; Stefanick & Jurdy, 1996). No such concentrations can be seen in the case of PICs (see Fig. 3 in Paper IV). No analyses of spatial statistics have been carried out, but based on a mere visual inspection it appears that PICs follow the general distribution of impact craters on Venus, as well as on Mars and the Moon, giving indirect support to the idea that polygonality is not caused by crater degradation or post-impact modification.

9.8 Crater modification stage and polygonal impact craters

In the modification stage of complex impact craters (see Chapter 2.1 and Fig. 2), most cratering models assume some mechanism for decreasing the strength of the material in order to explain the observed uplift of the central peak and the probable collapse of the deep transient cavity (e.g. Melosh, 1979, 1989; O'Keefe & Ahrens, 1993; Melosh & Ivanov, 1999). It is commonly assumed that the collapsing transient crater rim behaves as a viscous fluid, i.e. it is essentially strengthless (McKinnon, 1978; Melosh, 1989; Melosh & Ivanov, 1999). However, as has been indicated by the studies of lunar crater rim terraces, at least the near surface rocks of the inner wall of apparent crater rim do possess substantial strength in the final stages of the crater modification (Melosh, 1989; see also Pearce & Melosh, 1986).

These ideas are corroborated by the analysis of polygonal crater data. Specifically, PICs imply that probably brittle faulting has been the main process creating the polygonal outline of larger complex craters' rims. The fractures in the target most likely affect the complex crater formation already in the excavation stage, just as they do in simple craters. Thus, the excavation has proceeded faster parallel to the strike of the fractures (Model 1 by Eppler et al., 1983). According to current ideas, this early stage polygonality should probably not be seen in the final complex crater, because of the modification of the crater after the excavation.[55] In the modification stage of complex craters the fractures cause the crater to expand in the direction perpendicular to the fractures' strike by normal faulting (probably turning into listric faulting and low-angle detachment zones with increasing depth; see e.g. Kenkmann et al., 2000) along pre-existing fracture planes in the uplifted rim material (Model 2 by Eppler et al., 1983). However, this late modification stage faulting may affect only the inner wall of the crater rim, as has been suggested by Reimold et al. (1998; see also the comments regarding Manicouagan by Floran & Dence (1976) and Trenc et al. (1999), already referred to in Chapter 6.2.2). As the modification stage has no obvious end, the late-stage re-adjusting and modification of the rim by small-scale faulting may take place long after the actual formation of the crater. However, as was suggested by Eppler et al. (1983), this very late modification probably does not considerably change the large-scale planimetric morphology of the crater.

As was observed in Paper IV, the rim terraces of craters are practically equally common in Venusian PICs and non-polygonal craters. Thus, the faulting associated with the terraces is probably mostly independent of the faulting (or thrusting; see below) that causes the polygonal plan view of the rim crest (or, as can be seen in the case of Venusian PICs, perhaps the uppermost inner wall of the crater). The terracing is likely a very late stage phenomenon of the cratering process (Pike, 1980b; see also e.g. Herrick & Lyons, 1998), and apparently also occurs in a somewhat more damaged rock mass than the earlier PIC rim formation.

In any case it is worth stressing that the simplified (out of computational necessity), and perhaps in a *merely visual sense* rather extreme numerical models (e.g. Wünnemann & Ivanov, 2003) with acoustically fluidised zone of target material – supposedly analogous to liquid (Melosh & Gaffney, 1983) – extending from the surface to more than twice the depth of the transient cavity and laterally far beyond the rim of the final crater, are not to be taken as absolute geologic truths, and especially not as describing the rheological properties of any essentially "small" piece of rock. This is simply because if the fluidisation would be so extreme, all the pre-existing target structures would be

[54] However, note that initially the number of volcanically embayed craters was underestimated (Herrick & Sharpton, 2000).
[55] However, see the next chapter for a discussion on the PIC formation mechanisms.

demolished and thus could not have any effect on the crater shape, contrary to the vast number of observations presented not only in this thesis, but also in the literature (see the references mentioned above). Of course the original fabric of the rocks would in such a case also be destroyed, again opposite to the observations.

The acoustic fluidisation, therefore, most likely behaves in practise as suggested by the so called block oscillation model (Ivanov & Kostuchenko, 1997), and these oscillating fault-bounded blocks (e.g. Kenkmann et al., 2000) do not completely destroy the pre-existing structure of the target. On the contrary, it would seem tempting to assume that the locations of the faults bounding these oscillating blocks would favour the pre-existing structures of the target. The existence and ubiquity of polygonal craters would thus seem to support the acoustic fluidisation – block oscillation model of crater modification, or at least it is not in contrast with it.

9.9 An accompanying PIC formation mechanism?

In one of the extremely few of the existing, fairly detailed structural analyses of a rim of a notably *well-preserved* terrestrial complex crater, Bosumtwi in Ghana,[56] Reimold et al. (1998) noted dominant thrust faulting in the inner and outer walls of the rim. According to them, this was related to the early stages of the cratering process. As a relatively slightly degraded impact structure, Bosumtwi provides the closest terrestrial analogue to the small and mid-sized complex craters on Mars, Venus and the Moon studied in this thesis. As the thrusts are the dominant structural feature (which is not surprising: the crater rims are, after all, uplifted landforms, not depressions), it is quite possible that the current models of polygonal crater formation (Eppler et al., 1983) adhered to in this thesis, emphasising the normal faulting of the rim in the case of complex PIC formation (Eppler et al.'s (1983) Model 2), might actually be partially incorrect. Complex PICs may, in fact, sometimes be the result of not normal faulting in the modification stage, but thrusting (or reverse faulting) in the excavation stage (Fig. 39; Öhman, 2007a; Öhman et al., 2007). In this scenario, the thrusting would utilise the pre-existing structures of the target in a similar manner as the normal faulting in Eppler et al.'s (1983) Model 2. Therefore, the orientation of the straight rim segments would be the same as in the normal faulting scenario, i.e. parallel to the fractures. There is also some observational support for this, as faulting has been noted to be controlled, at least occasionally, by the pre-existing jointing e.g. on the rim of the Meteor Crater (Roddy, 1977a; see also Kring, 2007). Figure 39 highlights the differences between the aforementioned different formation models.

[56] The 10.5 km diameter Bosumtwi impact structure actually appears to have relatively straight segments of the crater rim, as mentioned in Chapter 6.2.2.

Currently it is impossible to tell which of the two possibilities, normal faulting in the modification stage or the thrusting in the excavation stage, depicts the formation mechanism of complex PICs better. In any case it should be kept in mind that there can be major differences in the tectonic evolution of the crater rim in different parts of the crater (Osinski & Spray, 2005; see also Bischoff & Oskierski, 1988): some parts of the crater rim may be deformed mainly by anticlinal folding (thus likely leading to more circular rim segment), whereas in other parts faulting may be more important (Roddy, 1977b, 1979; see also Lana et al., 2006, 2007). The styles of the rim deformation can also change within one outcrop, as exemplified by Figure 40.

As thrusting of course takes place in simple crater rims as well (e.g. Shoemaker, 1963; Roddy, 1978; Brandt & Reimold, 1995; Kring, 2007; Poelchau et al., 2008, 2009; Kumar & Kring, 2008), it is quite possible that also the mechanics of simple PIC formation involves sometimes thrusting (Öhman, 2007a; Öhman et al., 2007; see also Kumar & Kring, 2008). Thrusting was also observed in the cratering experiments by Gault et al. (1968), carried out in a fractured target: "The presence of such fractures also influences the style of deformation in that true overthrusts rather than reverse faults tend to develop high in the stratigraphic sequence, with blocks between fractures moving radially from the crater centre." They also noted that in unfractured targets the rim formed mainly by "upwarping" (anticlinal folding), whereas in fractured targets thrusting takes place.

It was highly unfortunate that Gault and co-workers (1968) did not describe in detail the relations between the fractures and the rims of their experimentally produced polygonal craters (see Chapter 6.3), but merely noted that in the square-shaped crater the orthogonal fractures formed diagonals across the crater. Therefore it remains purely speculative, if the hexagonal crater created in orthogonally fractured target[57] could be formed for example as a combination of enhanced propagation of the excavation flow parallel to the strike of the fractures (Eppler et al.'s (1983) Model 1), and thrusting perpendicular to the fracture's strike (the above-mentioned "reversed" version of Eppler et al.'s (1983) Model 2).

[57] Note also the varying straight rim segment – joint strike relationships reported by Fulmer and Roberts (1963).

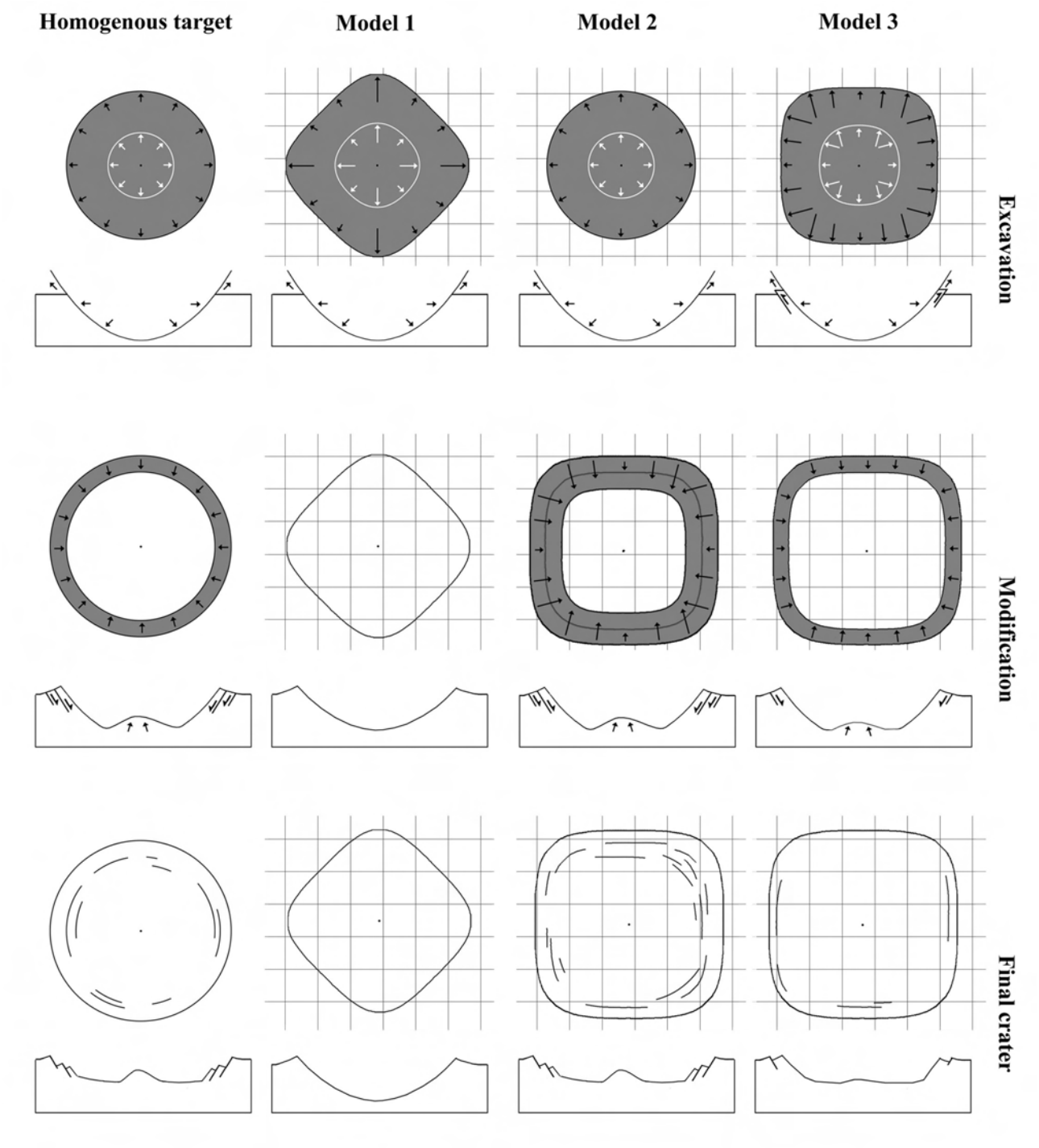

Figure 39. A sketch of the plan views and profiles of the models for polygonal impact crater formation in an orthogonally fractured target (the background grid in Models 1–3). The excavation stage of large complex craters (Model 2) may be structurally controlled according either to Model 1 or Model 3, but the structurally controlled slumping in the modification stage overshadows this. Simple craters (Models 1 and 3) and small complex craters (Model 3) do not slump significantly, and thus the polygonal morphology obtained at the excavation stage prevails. The shading and the lengths of the arrows indicate the expansion of the crater. The concepts of Models 1 and 2 are after Eppler et al. (1983).

Figure 40. The granitic southeastern rim of the simple Tswaing (*D*=1.13 km) impact crater in South Africa. Faulting (probably thrusting) dominates the right part of the outcrop, whereas anticlinal folding can be seen on the left. The crater centre is to the right. The shaft of the hammer is about 72 cm long. See Brandt & Reimold (1995) for further details. For a colour image, see the electronic version of the thesis.

There is also some indirect evidence in favour of the proposed thrusting model. Figure 12 in Paper III is a very high-resolution image taken by the HiRISE camera onboard the MRO spacecraft. Prominent northeast–southwest oriented faults are parallel to the rim segments in the two very small simple craters in the lower left and upper right of the image. As it is very hard to see clear-cut angles in the rims, these craters would not have been classified as true polygonal craters in this study, but nevertheless strongly hint towards structural influence that is different from the "classic" Meteor Crater type (Eppler et al.'s (1983) Model 1; However, it is in agreement with the results and conclusions of Kumar and Kring's study (2008) of the Meteor Crater). At least in the original image it can be seen that in the crater at upper right, both the upper left and lower right rim segments are straight and parallel to each other, and are oriented parallel to the faults. So is the upper left rim segment of the crater at lower left in Figure 12 in Paper III. Note that solar illumination from approximately northwest may partly enhance the appearance of these straight rim segments.

Based on the results presented in the accompanying Papers and a rather extensive literature study summarised above, it therefore feels justified to suggest that there are three mechanisms which produce polygonal impact craters:

1. Preferential excavation of the crater in a direction parallel to fractures. The fracture orientations would bisect the straight segments of the crater rim. Possibly applicable only to simple craters. (Eppler et al.'s (1983) Model 1)

2. Slumping of complex crater rim along fractures during the modification stage. The fracture orientations would be parallel to the straight rim segments. Applicable only to (large) complex craters. (Eppler et al.'s (1983) Model 2)

3. Thrusting along fractures in the late excavation stage. The fracture orientations would be parallel to the straight rim segments. Applicable to both simple and (small to mid-sized) complex craters.

Whether or not the polygonality introduced by the new Model 3 (Öhman, 2007a; Öhman et al., 2007) would be visible in the final crater depends on the amount of slumping of the rim. In a very large terrestrial polygonal crater like the Manicouagan, Model 2 probably is the main cause for the polygonality of the inner rim as has been suggested (Floran & Dence, 1976; Trenc et al., 1999). However, in simple craters and in small and moderate-sized complex craters where slumping is not so prominent, Model 3 may be important. At least in simple craters this could very well operate in conjunction with Model 1, the relative importance of each formation mechanism depending on the exact geologic situation. Similarly, some craters may reflect both Models 1 and 2, as was already suggested by Eppler et al. (1983).

9.10 Size distribution

The diameters of PICs were compared to the diameters of non-polygonal craters in the Argyre region of Mars (Paper III), Venus (Paper IV), and the TINN study area of the Moon (Paper VI). The results from each heavenly body are interesting in their own right, but an even more fascinating picture emerges when all of the results are combined, and viewed in the same scale, i.e. with diameter presented as multiples of the transition diameter (D_{tr}) (Figs. 28 and 29; Paper VI). As many different viewpoints presented in earlier studies and in this thesis imply that polygonality should be a "normal" feature of impact craters, one would be inclined to think that also the size distributions of polygonal and non-polygonal impact craters would be similar.

However, as becomes evident from, for example, Figures 28 and 29, this is not the case. All three study areas indicate a similar general trend in the PIC size distribution: there is a specific size range where PICs are relatively more common than the non-polygonal craters. In the case of lunar and Martian data where the diameter range of the studied craters extends to smaller diameters than for Venus, it is apparent that simple craters (<1D_{tr}) do not have a strong tendency to be polygonal, but the "preferred" PIC formation size range starts from small complex craters. The lunar and Martian PICs are relatively most common at around 2–4×D_{tr}. The Venusian data extends the "preferred" PIC size range to a diameter of about 6×D_{tr}. This preference is also seen in the morphology (Paper IV): PICs "favour" central peak and knobby base craters to peak-ring craters. Although there is discrepancy in the specific location of the "excess" PICs between the different heavenly bodies, a general trend, however, is obvious: PICs "prefer" small to mid-sized complex craters. As the transition diameters are variable both on the Moon and especially on Mars, and as the Venusian transition diameter cannot be known but is modelled, some differences are to be expected.

Although this type of a study to my knowledge has not been done before (see Chapter 6), some comparisons to earlier studies are still possible, particularly in the case of the lunar PICs. If the lunar crater distribution curves are examined slightly closer (see Fig. 5 in Paper VI), it becomes evident that the PICs are relatively more abundant than the non-polygonal craters in the size range of about 20–50 km. This is virtually the same as the 16–48 km (rounded to 20–45 km) size range that Pohn and Offield (1970) classified as polygonal. A strong indication for the reality and "speciality" of this diameter range 20–50 km is that Pohn and Offield (1970) used a dataset (Lunar Orbiter imagery) completely different from the CLA imagery used in this thesis. Two independent studies with different datasets but the same result leaves little doubt about the reality of the observations. In addition, the results by Fielder (1961), Quaide et al. (1965), and Schultz (1976) are also in general agreement with this.

Some tentative support is also available regarding Mars. Pike (1971) noted that the Martian impact craters 10–15 km in diameter (i.e. generally small complex craters) tend to be polygonal, whereas the smaller ones do not. This is compatible with the results obtained in this Ph.D. thesis. Therefore, there really is a size range where PICs have a stronger tendency to form than in other sizes, and with respect to the transition diameter, this size range seems to be roughly the same on the Moon and Mars, and with slightly larger error margins, also on Venus.

The observation of this "preferred" PIC size range is quite clear, but the reason(s) why it exists remains much more speculative. As neither almost no slumping of simple craters, nor the extreme slumping of the largest complex craters (Melosh & Ivanov, 1999) does not seem to be beneficial for

PIC formation, the reason must lie somewhere in the formation mechanism of small to mid-sized complex craters.

The notably lower relative number of simple PICs may perhaps be related to the fact that they excavate only a fairly shallow portion of the crust, which has been effectively fractured by previous impacts of all sizes. Hence, *dominating* structural orientations may be scarce, and from the point of view of the cratering flow, the target is homogenous. In the other end of the size scale, the major slumping of the larger complex craters may be such a high-energy process that the ordinary inhomogeneities of the target become unimportant. Or, as dominant orientations of structural weakness are a pre-requisite for PIC formation in all sizes, perhaps the cratering flow in the "preferred" size range for some reason gets more easily affected by the target structures? This might involve a PIC formation process different from the simple PICs (Eppler et al.'s (1983) Model 1) or the largest complex PICs (Eppler et al.'s (1983) Model 2), as was discussed above in Chapter 9.9.

These issues can be approached in a somewhat more quantitative way too. The absolute maximum depth of a structure that can possibly have any significant effect in the formation of an impact crater is the depth of the transient cavity. This depth can be estimated using the equation derived by Croft (1985). According to Croft's (1985) equation, the diameter of the transient cavity (D_t) can be approximated from the final crater diameter (D), and the simple-to-complex transition diameter (D_{tr}):

$$D_t \approx D_{tr}^{\,0.15\pm0.04} D^{0.85\pm0.04} \tag{1}$$

The depth of the transient cavity (d_t) is about one third of the transient diameter (Melosh, 1989):

$$d_t \approx (0.28 \pm 0.04) D_t \approx \frac{1}{3} D_t \tag{2}$$

However, in the cratering process, the deeper parts of the transient cavity are merely pushed downwards and outwards (e.g. Dence et al., 1977; Melosh, 1989). Hence, the lower parts of the transient cavity are quite unlikely to affect the shape of the crater rim. The depth of excavation (d_e) can thus provide a more realistic maximum depth of a structure possibly playing a major role in the formation of the crater rim. Because the excavation flow streamtubes reach the ground surface from the depth of excavation (i.e. material gets thrown out of the crater from d_e and higher, but not from below), the d_e effectively defines the maximum depth of a structure affecting the formation of the crater's rim. The depth of excavation, defining the so called excavation cavity, is only about a third of the depth of the transient cavity, or about one tenth of transient diameter (Dence et al., 1977; Croft, 1980; Melosh, 1989; Spudis, 1993):

$$d_e \approx (0.1 \pm 0.02) D_t \approx \frac{1}{3} d_t \quad (3)$$

With equations 1, 2, and 3 the approximate excavation depths of craters forming the "PIC peaks" in the size distribution curves can be estimated. In the case of the Moon, 20–50 km diameter craters excavate to about a depth of 1.9–4.2 km, whereas Martian PICs 14–35 km in diameter excavate material from a depth of about 1.3–2.8 km. The 12–28 km diameter PICs on Venus have even more shallow excavation depths, only about 1–2.1 km. Thus, the larger the body, more shallow the excavation depth of the craters forming the "PIC peak". The excavation depths for craters of transitional size, i.e. those that do not have such a high probability of being polygonal, are 1.5 km and 0.7 km for the Moon and Mars, respectively.

These values can be compared to estimates of megaregolith thickness. In the TINN study area of the Moon the megaregolith is, according to Thompson et al. (2009), about 2.5 km thick. As discussed in Chapter 3.3, the Martian megaregolith thickness is poorly constrained, but in the highlands it may be around 2 km (Taylor & Baloga, 2007). Although the error margins are very large, it would be appealing to suggest that there is a causal link between crater polygonality and the depth of excavation: small craters both on the Moon and Mars excavate only heavily brecciated megaregolith that lacks a dominating fracture pattern. Larger craters, those that form the "PIC peak" in the size distribution diagrams, have greater excavation depths, extending to the more coherent bedrock that possesses a fairly simple pattern of planes of structural weakness. This pattern is then "inherited" in the rim structure of PICs. The depth of excavation and its implications in the case of Venus are more closely discussed below in Chapter 9.10.1.

Also another intriguing hypothesis emerges from the observation, best seen in Figure 29, that the "PIC peak" actually does not seem to be set at a constant transition diameter, but it appears to shift to larger *relative* diameters (i.e. with respect to D_{tr}) with increasing surface gravity. As the amount of data is not really sufficient for a reliable analysis, this remains pure speculation at the moment. However, if this would turn out to be true, one possible explanation would be that in the presence of a fractured target, on a fundamental level, it is the gravity that "dictates" if a forming crater has a high tendency to become polygonal or not. The inclusion of smaller Venusian craters (where the Magellan data quality allows) in the study would give further constraints to the hypothesis, as would the investigation of PICs on the surface of another heavenly body. Mercury would be a tempting option for further studies in this respect too, given its similar surface gravity to Mars, but somewhat different and notably less complex target material properties (i.e. the probable lack of volatiles and "soft" sedimentary rocks; e.g. Strom & Sprague, 2003). In this context one should also

remember the observation by Watters and Zuber (2009) that the smallest of Martian simple craters are less circular than larger ones, and that this may be connected to the shift to gravity-controlled cratering regime. Interplanetary comparisons also in this case would be most welcome.

The shift of the "PIC peak" could also have other, more plausible origins. Perhaps in a specific size range (with respect to D_{tr}) a certain PIC formation mechanism is more "efficient" than in other sizes, or maybe more than one mechanism is "active" in that size: Model 1 might mainly explain the smallest simple craters and Model 2 the largest complex craters, whereas the mid-sized craters can be formed by both of the mechanisms, and possibly also by a third mechanism (Model 3), as suggested in Chapter 9.9. The exact mechanism, or combination of mechanisms, would depend on the specific situation.

Another, more mundane point of view should also be briefly discussed. The importance of the scale at which the craters are studied has already been mentioned regarding the number of observed straight rim segments. With ever higher and higher resolution, more and more straight rim segments would become visible, and thus more and more craters could be seen to be influenced by the structures of the target. However, although this would increase the number of identified structurally controlled impact craters, these craters would not be classified as PICs as defined in this study, because the polygonality refers to the large-scale polygonality of the crater rim. This polygonality is seen quite adequately in the datasets used in this thesis, even in the case of the smallest craters studied. Thus, the lack of small PICs is not dependent on the resolution. The question of scale does not help in explaining the relative scarcity of the largest PICs either. Therefore, the ultimate reason why PICs "favour" this particular size range of small to mid-sized complex craters apparently has nothing to do with the dataset, and thus must be related to the cratering process itself.

All in all, PIC diameter data can lead to different hypotheses regarding the origin of the "PIC peak" and its apparent – whether it is real or not – shift to larger relative diameters with increasing gravity. Although there is no solid evidence one way or the other, one could suppose that the most plausible and robust hypotheses are the effect of excavation depth vs. the thickness of heavily brecciated megaregolith, and a combination of different PIC-forming mechanisms in a certain size range. Some currently unknown process of "direct" gravity control would be scientifically the most interesting, but also by far the most hypothetical.

9.10.1 PICs and Venusian plains

As discussed above, the study of polygonal impact craters can reveal interesting nuances of the impact cratering processes. Another consequential aspect of PIC studies is, as also shown above,

that they can be used as an additional means to study planetary paleotectonics. This was also noted already by Eppler et al. (1983). Especially important the PICs are in revealing older and/or deeper tectonic patterns than can be seen in ridges or graben.

There is also at least one more way the polygonal impact craters can be utilised in planetary geology quite feasibly. If we accept the premise held in this thesis that impact crater rims occasionally reflect the structure of the substratum, the polygonal craters can be used to estimate the approximate maximum thickness of the surficial layer that is not significantly affecting the cratering process.

As an example one can study the regional volcanic plains of Venus. According to Schaber et al. (1992), Phillips et al. (1992) made a rough model assuming that the Venusian regional plains have a uniform thickness of 2 km.[58] As mentioned earlier, the regional plains overlie the tessera terrain (e.g. Ivanov & Head, 1996; Basilevsky et al., 1997). In Paper V it was found that many polygonal craters have straight sections in their rims that match the tectonic orientations of the nearby tessera, but do not match the orientations of the wrinkle ridges on the plains. Thus, the wrinkle ridges either post-date the formation of the craters (which, in many cases, can be true; see e.g. Basilevsky & Head, 2006), and/or the deposit with ridges and reverse or thrust faults most likely underlying them (e.g. Golombek et al., 1991; McGill, 1993) is relatively thin. In any case, it is obvious that the structures of the underlying tessera terrain (or at least some planes of weakness caused by similar forces that created the parallelly oriented structures in tessera) do have an effect in the cratering process. Therefore, it is obvious that the regional plains cannot be thicker than the depth of excavation of a polygonal crater that has straight rim segments parallel to the tectonic orientations observed in the nearby tessera terrain.

With equations 1, 2 and 3 it can be calculated that the depth of excavation of a Venusian crater 20 km in diameter is about 1.6 km. As there are polygonal craters in this size range (e.g. Toklas D=17.2 km, Quimby D=22.9 km) that have matching tessera orientations, it is quite obvious that the thickness of the regional plains cannot be 2 km as, according to Schaber et al. (1992), was used in the model by Phillips et al. (1992). Their model has been criticised on other grounds as well (Schaber et al., 1992), but the PICs provide another way to test the tenability of their (or any other similar) model.

It should be noted here that a more modern estimate of the regional plains' thickness is on the order of a few hundred metres (Kreslavsky & Head, 1999), although Basilevsky and Head (2006) state

[58] Note, however, that such an assumption cannot be directly found in the paper by Phillips et al. (1992), but it is only implied by Schaber et al. (1992).

that the thickness of the volcanics involved in the resurfacing is poorly constrained. If the estimate of a few hundred metres of regional plains' thickness is correct, it is too shallow to be tested using the polygonal craters used in our study (for a D=12 km crater, the d_e is about 1 km). Another aspect that should be kept in mind is that the suggested method cannot be used for estimating the *minimum* thickness of a surficial layer. In other words, an observation that a crater (polygonal or not) does *not* reflect the orientations measured from the nearby tessera terrain, cannot be used to argue that the minimum thickness of the plains must exceed the crater's depth of excavation. This is because there are a number of reasons why a crater is not necessarily polygonal, as discussed in Chapter 6.

9.11 PICs and target material classification

As it is clear that PICs do reflect some properties of the target material, it becomes tempting to try to see whether or not PICs could be used as a tool for classifying the material units. The amount of polygonality is an obvious choice for the basis of such a study. When comparing the polygonality of PICs and the geologic units defined by Scott and Tanaka (1986), it becomes evident that at least no clear-cut correlation emerges (see Fig. 5 in Paper III). This is actually a rather expected result, as the geologic units used in planetary geology necessarily describe merely the uppermost surface of the planet (see Cintala et al. (1977) for a brief discussion on the geologic units and crater morphology). PICs, on the other hand, reveal the structure of the material somewhat beneath the surface.

For instance, a relatively thin volcanic deposit with wrinkle ridges may be juxtaposed to a similarly thin fluvial deposit having a different appearance. These deposits would of course be classified as different geologic units. When these deposits are thin compared to the excavation depth of the crater (or the depth of the transient cavity), the important thing is not the geologic unit of the surface, but what lies slightly beneath it. This underlying material beneath both deposits could, for example, be material with some dominating fracture orientations, and thus there would be no reason for the two geologic units to show any difference in the polygonality of PICs they now are hosting. However, it is noteworthy that using partially the same original geologic classification scheme of Scott and Tanaka (1986) as used in this thesis, Watters and Zuber (2009) studied smaller craters and found that square-shaped craters in targets dominated by debris- and sedimentary-based materials are more common than in lava targets. Further studies regarding also this aspect of PICs are obviously needed.

The properties of the target material may play a role in the apparently diminishing number of PICs towards the south in both Hellas and Argyre regions. On the other hand, based on the current

knowledge, this may merely be the result of the poorer resolution of the Viking MDIM closer to the polar regions, and thus may have no geologic meaning. However, it is well-known (e.g. Carr, 1999) that craters closer to poles display subdued features and in general appear more indistinct than their counterparts in the more equatorial regions, probably due to the increasing amount of volatiles in the more poleward crust. Therefore, it is quite possible that polygonal crater shape could be more difficult to develop in the higher southern latitudes, or that later creep processes effectively destroy the original polygonal outline. As said before, it would certainly be interesting to study if polygonality correlates in any way with central pits or layered ejecta blankets, both generally assumed to be caused by water in the target (Chapter 5). Such possibly latitude-dependent aspects of PICs as a possible indicator of target properties would thus be worth a further study, but would require a dataset less sensitive to the latitudinal changes than Viking MDIM. Such datasets include MEX HRSC and THEMIS.

9.12 Further possibilities for future studies regarding polygonal impact craters

In the light of the discussion above it seems fair to say that although the two models by Eppler et al. (1983) present good working hypotheses for the formation mechanisms of polygonal impact craters, they may not fully reflect what actually happens in nature. Only detailed structural studies of well-preserved terrestrial (polygonal) impact crater rims, preferably accompanied by high-resolution planetary remote sensing studies, and especially cratering experiments in fractured targets and sophisticated 3D numerical models, can solve the puzzle of polygonal impact craters' formation mechanisms. With the new HiRISE data from Mars, the lack of detailed crater imagery no longer poses a major problem. However, cratering experiments tend to be quite expensive and are generally done only in a few research facilities in the world, and despite the fast development of computers, detailed 3D modelling still consumes inconveniently lot of computing power. Hence, such PIC studies a not likely to become commonplace during the next few years. Perhaps the biggest obstacle for understanding the PIC formation in detail, however, is the lack of a well-preserved and well-exposed terrestrial complex impact craters.

Closely related to the formation of PICs are the other possible manifestations of the effect of target structures on the crater. These include the location and the (polygonal) shape of the central uplift, as well as the structural control of ejecta formation. Both major and minor features of ejecta, like loops of ejecta or secondary craters, are known to be controlled by pre-existing target structures (e.g. Shoemaker, 1962; Gault et al., 1968), but it would be interesting to study if Morrison's (1984) idea of ejecta rays emanating from the vertices of polygonal crater rims can withstand closer scrutiny. This idea has also some experimental basis, as Fulmer and Roberts (1963) observed the best-

developed rays emanating from the vertices of the square-shaped explosion crater, the rays being roughly parallel to the plane of intersection of the joint system that was controlling the crater formation. Similarly engrossing it would be to know if the strikingly hexagonal inner, continuous hummocky ejecta pattern of the Snowball 500 ton TNT explosion crater (see Fig. 7b in Roddy, 1977a) was somehow caused by some of the properties of the target consisting of unconsolidated sediments. It is clear that the target structures, the formation of PICs, and the formation of particular ejecta patterns form a closely intertwined cluster of fascinating, yet rather poorly understood phenomena.

As was hinted at before, there are several other interesting vistas for PIC studies, even if the exact formation mechanism of PICs may remain partially obscure. Terra Cimmeria and Terra Sirenum in the southern highly cratered highlands of Mars are ancient Noachian regions with fairly limited apparent tectonic influence from the surroundings. The comparison of the PIC rim orientations with the magnetic anomalies so clearly seen in these areas might give some further insight into the question of the hypothesised early Martian plate tectonics.

The planet Mercury is eventually getting its due share of the planetary scientists' interest. Given the fascinating tectonic history the planet has gone through – involving e.g. global shrinking – the PICs could have a lot to offer for the tectonic analysis of the MESSENGER and BepiColombo data. The geologic study of the Moon is also apparently awakening from its long slumber, and although the lunar PICs are the most studied ones of all PICs, a re-look might well be in order.

There are still further possibilities the polygonal craters can be used in planetary science. An interesting perspective emerges from the study of the imagery of small Solar System bodies, especially asteroids and comets. In the beginning of the 21st century there were almost 2000 known Near Earth Asteroids (NEAs) that may perhaps cause an impact threat to the Earth in some time in the future (e.g. Chapman, 2002, 2004; Stokes et al., 2002), and the number is growing fast with different search programmes finding ever smaller asteroids. In order to try to mitigate this threat, it is imperative to know the structure of these objects. Of course there are many methods to study the structure of an asteroid or a comet, but PICs provide an additional way for an initial, very rough first-hand estimate of the structure: if polygonal impact craters are present on the surface, at least the outer part of the body must have substantial strength. If the surface would have a very low strength and the internal structure resembled that of a rather loosely bound "rubble pile" (e.g. Asphaug et al., 2002), it would be unlikely to have dominating orientations of structural weakness on such a body, and thus there would be no polygonal craters either. Basilevsky and Keller (2006) found several indications of the structural control of the surface features on the nucleus of comet

81P/Wild-2 – including polygonal craters. Hence, at the time when the PICs were formed, Wild-2 was not a rubble pile (Basilevsky & Keller, 2006). Such an approach is advisable for other small Solar System body studies as well, including NEAs and other Near Earth Objects (NEOs). Thus, the PICs on the surfaces of NEAs and other NEOs could prove quite essential, if ever a quick first-hand estimate of the inner structure of an Earth-threatening object is required.

Perhaps the most promising heavenly body for further PIC studies could, however, be Venus. The PIC rim orientations are clearly not independent of some of the tectonic structures of their surroundings. Where the quality of the Magellan data permits, PICs could be studied to smaller sizes than the 12 km diameter used in Papers IV and V, hence presumably increasing their number notably. As was described in Chapter 9.10.1, the PICs can be used to give a rough estimate of the thickness of the volcanic plains. This approach could be taken a bit further. With careful analysis of the PICs and the surrounding tectonics, particularly how far the apparent effect of the tectonic structures extends, one could attempt to "strip away" the regional plains now covering most of the planet, and "see" what lies beneath them. Thus, the extent of different tectonic provinces or target materials (e.g. tessera terrain) could be estimated.

In principle such a method could be applied to the study of Martian geology as well, but in practise the highly varying ages of Martian craters and the general geotectonic complexity would probably make the attempt futile. For Venus, with almost all the impact craters being morphologically fresh and generally postdating the regional plains, the application would be notably easier. Although the method is naturally very susceptible to subjectivity and various differing interpretations, this approach could allow a new view on the geotectonic evolution of the planet, thus also possibly aiding in the planning of future planetary missions. Therefore, all in all, further studies of PICs provide possibilities to facilitate deeper understanding of some of the most fascinating aspects of planetary geology and impact crater research.

10 SUMMARY AND CONCLUSIONS

Based on the results of this Ph.D. thesis, the key aspects of the work can be summarised as follows:

- Structurally controlled polygonal impact craters (PICs) have been known for a long time, at least from the late 19th century. To some extent they have also been used in tectonic studies, especially regarding the Moon, but the interest towards their utilisation and also the apparent awareness of their existence has substantially diminished during the last few decades.

- Polygonal craters are very common in the Solar System, and they can be formed in any kind of rigid and fractured target material. The surfaces of Mars, Venus and the Moon studied in this thesis host a rich variety of such craters.

- Martian impact basins and volcanic rises are surrounded by vast regions of mainly radial and concentric fractures, as well as other tectonic structures. Such fractures affect the shape of subsequently forming impact craters.

- The only currently known geologic process described in literature, capable of producing the observed polygonal shapes of the crater rims, is the structural control of crater formation. According to current models, this is most likely taking place both in the excavation (simple craters) and modification stages (complex craters).

- Based on studies covering the Argyre region of Mars, the entire surface of Venus, and the TINN area of the Moon, about 15%–20% of all impact craters are polygonal in plan view.

- Polygonal impact craters generally appear polygonal regardless of the resolution, wavelength or illumination geometry, and thus are a real natural phenomenon and not an artefact caused by the dataset. However, all these aspects of remote sensing do have some effect on the apparent polygonality, and thus polygonality may be more pronounced for example in some lighting conditions than in others. Especially any single crater may appear notably different depending on the imaging equipment and conditions. In a regional scale, however, the illumination geometry has no statistically significant effect on the general directional pattern of the crustal weaknesses indicated by the PIC data.

- The size distributions of the polygonal and non-polygonal craters are different. The PICs are relatively more abundant than non-polygonal craters in the size range of small to mid-sized

complex craters (diameters from 1–2 to perhaps up to 5–6 times the simple-to-complex transition diameter).

- The PICs may or may not indicate the same structural orientations as e.g. graben or ridges, depending on the geotectonic situation. For example, in the Argyre region the PICs usually reflect a different tectonic component than most of the Tharsis-induced younger graben, but coincide with the direction of the oldest graben just beyond the study area. On Mars, the PIC rim orientations are generally controlled by ancient impact basins (their concentric, radial, and possibly conjugate shear fracture patterns). On Venus, PIC orientations tend to correlate very strongly with the structures of both stratigraphically old tesserae and young rift zones, as well as the concentric components of the coronae. The closer the structure is to the crater, the more likely it is to see a similarly oriented PIC rim segment.

- Directional data obtained from PICs in any particular area is generally not dependent on the degradational stage of the craters studied: in most cases craters of different degradational stages reveal statistically similar directional patterns. This is especially true in ancient highly cratered regions of Mars, whereas it seems that PICs of different degradational stages may reveal different structural patterns in younger terrains that have experienced a very complex geologic history. Even in these cases degradation itself is not important, but rather the age of the craters, i.e. PICs formed in different times may indicate different dominating structural patterns. The polygonal outline of the crater rim thus appears to be a primary feature, indicative of the structure of the target material at time of impact. It is not affected by later degradation to any major extent.

- More degraded PICs are not more polygonal than less degraded (when polygonality is measured as the number of straight rim segments). This gives further independent support to the idea that polygonality is a primary and a permanent feature, and not caused by degradation of the crater rim.

- The geologic units of the Argyre region in Mars do not correlate with the amount of polygonality. Thus, PICs alone cannot be used as an aid in interpreting the properties of the geologic unit the crater is formed in, or by which it now is surrounded. However, PICs have a tendency to be relatively more common in older geologic units.

- As PICs apparently reflect structures present in the target at the time of the impact, the near-surface material of the final, apparent crater rim must behave for the most part in a brittle

manner during the late phases of the modification stage. The orientations of some of the faults that bound the oscillating blocks of the crater rim in the acoustic fluidisation – block oscillation model quite possibly are determined by the pre-existing structures of the target.

- Polygonal impact craters can be used in regional scale structural studies, and they should be used as a remote structural mapping tool more than is currently done.

- Despite the fact that there are good working hypotheses for both simple and complex PIC formation, the actual formation mechanisms are far from being fully understood. Thrusting, either along or affected by pre-existing structures in the excavation stage may play a larger role than previously thought. Thus, in addition to detailed multidisciplinary field studies on terrestrial craters and remote sensing studies of PICs on different heavenly bodies, also impact and explosion experiments on fractured targets, as well as 3D numerical modelling of PIC formation are strongly encouraged.

The structurally controlled polygonal impact craters therefore are a fairly common natural phenomenon, occurring throughout the Solar System. They provide new insights into the complex interplay between the target material and the cratering process, and they can be used as an additional aid in understanding the geotectonic evolution of a cratered body. However, the danger of overinterpreting the PIC-data should not be forgotten. In the end, as Don Wilhelms (1993) so eloquently reminded, “the Moon and the planets are made of bedded rocks, not networks of lines.” But as long as we are unable to send geologists to study these bedded rocks, a careful investigation of such “networks of lines” may help us to better understand the most important geologic process in the Solar System, impact cratering.

11 REFERENCES

Aaloe, A., Dabizha, A., Karnaukh, B. & Starodubtsev, V., 1976. Geophysical investigations of Kaali crater. Eesti NSV Teaduste Akadeemia Toimetised, Keemia – Geoloogia 25 (1), 58–65 (in Russian, with an English abstract).

Abels, A., 2003. Investigation of impact structures in Finland (Söderfjärden, Lumparn, Lappajärvi) by digital integration of multidisciplinary geodata. Ph.D. thesis, Westfälische Wilhelms-Universität, Münster, Germany, 292 pp.

Abels, A., 2004. Impacts in two-layered targets on Earth: effects of cover thickness on crater morphostructure. Lunar and Planetary Science XXXV. Lunar and Planetary Institute, Houston, abstract #1090 (CD-ROM).

Acuña, M. H., Connerney, J. E. P., Ness, N. F., Lin, R. P., Mitchell, D., Carlson, C. W., McFadden, J., Anderson, K. A., Rème, H., Mazelle, C., Vignes, D., Wasilewski, P., & Cloutier, P., 1999. Global distribution of crustal magnetization discovered by the Mars Global Surveyor MAG/ER experiment. Science 284, 790–793.

Adler, J. E. M. & Salisbury, J. W., 1969. Circularity of lunar craters. Icarus 10, 37–52.

A'Hearn, M. F., Belton, M. J. S., Delamere, W. A., Kissel, J., Klaasen, K. P., McFadden, L. A., Meech, K. J., Melosh, H. J., Schultz, P. H., Sunshine, J. M., Thomas, P. C., Veverka, J. Yeomans, D. K., Baca, M. W., Busko, I., Crockett, C. J., Collins, S. M., Desnoyer, M., Eberhardy, C. A., Ernst, C. M., Farnham, T. L., Feaga, L., Groussin, O., Hampton, D., Ipatov, S. I., Li, J.-Y., Lindler, D., Lisse, C. M., Mastrodemos, N., Owen, W. M. Jr., Richardson, J. E., Wellnitz, D. D., & White, R. L., 2005. Deep Impact: excavating comet Tempel 1. Science 310, 258–264.

Aittola, M., 2003. Venusian novae (astra): Characteristics, classification and connection to other volcano-tectonic features. Oulu University Press, Oulu, 119 pp.

Aittola, M., Öhman, T., Kostama, V.-P. & Raitala, J., 2002. Impact craters establish geological diversity within Hellas region. Lunar and Planetary Science XXXIII. Lunar and Planetary Institute, Houston, abstract #1485 (CD-ROM).

Aittola, M., Korteniemi, J., Öhman, T., Törmänen, T. & Raitala, J., 2006. Geology of central Noachis Terra, Mars. Lunar and Planetary Science XXXIII. Lunar and Planetary Institute, Houston, abstract #1654 (CD-ROM).

Alexopoulos J. S. & McKinnon, W. B., 1994. Large impact craters and basins on Venus, with implications on the terrestrial planets. In: Dressler, B. O., Grieve, R. A. F. &

Sharpton, V. L. (Eds.), Large Meteorite Impacts and Planetary Evolution, pp. 29–50. Geological Society of America Special Paper 293.

Alter, D., 1956a. The nature of the lunar maria. Publications of the Astronomical Society of the Pacific 68 (400), 38–45.

Alter, D., 1956b. The nature of the typical lunar mountain walled plains. Publications of the Astronomical Society of the Pacific 68 (404), 437–443.

Alter, D., 1957. The explosion craters of the Moon. Publications of the Astronomical Society of the Pacific 69 (411), 533–540.

Alter, D., 1958. Peculiar features of the lunar surface. Publications of the Astronomical Society of the Pacific 70 (416), 489–494.

Alvarez, L., Alvarez, W., Asaro, F. & Michel, H. V., 1980. An extraterrestrial cause for the Cretaceous–Tertiary extinction. Science 208, 1095–1108.

Alvarez, W., 1997. T. rex and the crater of doom. Penguin Books, England, 185 pp.

Ambrose, W. A., 2009. Distribution and chronostratigraphy of asymmetric secondary craters in the Nectaris basin. Lunar and Planetary Science XXXX. Lunar and Planetary Institute, Houston, abstract #1015 (CD-ROM).

Amstutz, G. C., 1965. Tectonic and petrographic observations on polygonal structures in Missouri. Annals of the New York Academy of Sciences, 123 (2), 876–894.

Anderson, R. C., Dohm, J. M., Golombek, M. P., Haldemann, A. F. C., Franklin, B. J., Tanaka, K. L., Lias, J. & Peer, B., 2001. Primary centers and secondary concentrations of tectonic activity through time in the western hemisphere of Mars. Journal of Geophysical Research 106, 20563–20585.

Anderson, J. L. B. & Schultz, P. H., 2006. Flow-field center migration during oblique impacts: implications for curved uprange ejecta rays. Lunar and Planetary Science XXXVII. Lunar and Planetary Institute, Houston, abstract #1726 (CD-ROM).

Anderson, J. L. B., Schultz, P. H. & Heineck, J. T., 2003. Asymmetry of ejecta flow during oblique impacts using three-dimensional particle image velocimetry. Journal of Geophysical Research 108 (E8), doi:10.1029/2003JE002075.

Andersson, L. E. & Whitaker, E. A., 1982. NASA Catalogue of Lunar Nomenclature. NASA Reference Publication 1097, 183 pp.

Andrews-Hanna, J. C., Zuber, M. T & Banerdt, B., 2008. The Borealis basin and the origin of the martian crustal dichotomy. Nature 453, 1212–1215, doi:10.1038/nature07011.

Antoine, L. A. G., Nicolaysen, L. O. & Niccol, S. L., 1990. Processed and enhanced gravity and magnetic images over the Vredefort structure and their interpretation. Tectonophysics 171, 63–74.

Arvidson, R. E., Baker, V. R., Elachi, C., Saunders, R. S. & Wood, J. A., 1991. Magellan: Initial analysis of Venus surface modification. Science 252, 270–275.

Asphaug, E., Ryan, E. V. & Zuber, M. T., 2002. Asteroid interiors. In: Bottke, W., Cellino, A., Paolicchi, P. & Binzel, R. P. (Eds.), Asteroids III, pp. 463–484. Tucson, University of Arizona Press.

Bäckström, A., 2005. A study of impact fracturing and electric resistivity related to the Lockne impact structure, Sweden. In: Koeberl, C. & Henkel, H. (Eds.), Impact Tectonics, pp. 389–404. Berlin Heidelbrg, Springer-Verlag.

Baker, V. R., Maruyama, S. & Dohm, J. M., 2007. Tharsis superplume and the geological evolution of early Mars. In: Yuen, D. A, Maruyama, S., Karato S.-I. & Windley, B. F. (Eds.), Superplumes: Beyond Plate Tectonics, pp. 507–522. Dordrecht, Springer.

Baldwin, R. B., 1942. The meteoritic origin of the lunar craters. Popular Astronomy 50, 365–369.

Baldwin, R. B., 1943. The meteoritic origin of lunar structures. Popular Astronomy 51, 117–127.

Baldwin, R. B., 1949. The Face of the Moon. The University of Chicago Press, Chicago, 239 pp.

Baldwin, R. B., 1963. The Measure of the Moon. The University of Chicago Press, Chicago–London, 488 pp.

Baldwin, R. B., 1964. The Moon. Annual Review of Astronomy and Astrophysics 2, 73–94.

Baldwin, R. B., 1974. On the origin of the mare basins. Proceedings of the Fifth Lunar Conference. Geochimica et Cosmochimica Acta 1, Supplement 5, 1–10.

Baldwin, R. B., 1978. An overview of impact cratering. Meteoritics 13, 364–379.

Baldwin, R. B., 1981. On the tsunami theory of the origin of multi-ring basins. In: Schultz, P. H. & Merrill, R. B. (Eds.), Multi-ring Basins: Formation and Evolution. Proceedings of the 12th Lunar and Planetary Science Conference. Geochimica et Cosmochimica Acta, Supplement 12, part A, 275–288.

Barlow, N. G., 2003. Revision of the “Catalog of Large Martian Impact Craters”. Sixth International Conference on Mars. Lunar and Planetary Institute, Houston, abstract #3073 (CD-ROM).

Barlow, N. G., 2004. Martian subsurface volatile concentrations as a function of time: Clues from layered ejecta craters. Geophysical Research Letters 31, L05703, doi:10.1029/2003GL019075.

Barlow, N. G., 2005. A review of Martian impact crater ejecta structures and their implications for target properties. In: Kenkmann, T., Hörz, F. & Deutsch, A. (Eds.), Large Meteorite Impacts III, pp. 433–442. Geological Society of America Special Paper 384.

Barlow, N. G., 2006. Impact craters in the northern hemisphere of Mars: Layered ejecta and central pit characteristics. Meteoritics & Planetary Science 41 (10), 1425–1436.

Barlow, N. G. & Bradley, T. L., 1990. Martian impact craters: Correlations of ejecta and interior morphologies with diameter, latitude and terrain. Icarus 87, 156–179.

Barlow, N. G. & Dohm, J. M., 2004. Impact craters in Arabia Terra, Mars. Lunar and Planetary Science XXXV. Lunar and Planetary Institute, Houston, abstract #1122 (CD-ROM).

Barlow, N. G. & Hillman, E., 2006. Distributions and characteristics of Martian central pit craters. Lunar and Planetary Science XXXVII. Lunar and Planetary Institute, Houston, abstract #1253 (CD-ROM).

Barlow, N. G. & Perez, C. B., 2003. Martian impact crater ejecta morphologies as indicators of the distribution of subsurface volatiles. Journal of Geophysical Research 108 (E8), doi:10.1029/2002JE002036.

Barlow, N. G., Boyce, J. M., Costard, F. M., Craddock, R. A., Garvin, J. B., Sakimoto, S. E. H., Kuzmin, R. O., Roddy, D. J. & Soderblom, L. A., 2000. Standardizing the nomenclature of Martian impact crater ejecta morphologies. Journal of Geophysical Research 105, (E11), 26733–26738.

Barnouin-Jha, O. S., Cintala, M. J. & Crawford, D. A., 2003. Effects of pre-existing target structure on the formation of large craters. Third International Conference on Large Meteorite Impacts, August 5–7, 2003, Nördlingen, Germany, abstract #4106 (CD-ROM).

Barsukov, V. L., 1992. Venusian igneous rocks. In: Barsukov, V. L., Basilevsky, A. T., Volkov, V. P. & Zharkov, V. N. (Eds.), Venus Geology, Geochemistry, and Geophysics, pp. 165–176. Tucson, The University of Arizona Press.

Barsukov, V. L., Basilevsky, A. T., Burba, G. A., Bobinna, N. N., Kryuchkov, V. P., Kuzmin, R. O., Nikolaeva, O. V., Pronin, A. A., Ronca, L. B., Chernaya, I. M., Shashkina, V. P., Garanin, A. V., Kushky, E. R., Markov, M. S., Sukhanov, A. L.,

Kotelnikov, V. A., Rzhiga, O. N., Petrov, G. M., Alexandrov, Yu. N., Sidorenko, A. I., Bogomolov, A. F., Skrypnik, G. I., Bergman, M. Yu., Kudrin, L. V., Bokshtein, I. M., Kronrod, M. A., Chochia, P. A., Tyuflin, Yu. S., Kadnichansky, S. A., & Akim, E. L., 1986. The geology and geomorphology of the Venus surface as revealed by the radar images obtained by Veneras 15 and 16. Journal of Geophysical Research 91 (B4), D378–D398.

Basilevsky, A. T. & Head, J. W., 2006. Impact craters on regional plains on Venus: age relations with wrinkle ridges and implications for the geological evolution of Venus. Journal of Geophysical Research 111, E03006, doi:10.1029/2005JE002473.

Basilevsky, A. T. & Keller, H. U., 2006. Comet nuclei: morphology and implied processes of surface modification. Planetary and Space Science 54, 808–829, doi:10.1016/j.pss.2006.05.001.

Basilevsky, A. T., Kuzmin, R. O., Nikolaeva, O. V., Pronin, A. A., Ronca, L. B., Avduevsky, V. S., Uspensky, G. R., Cheremukhina, Z. P., Semenchenko, V. V. & Ladygin, V. M., 1985. The surface of Venus as revealed by the Venera landings: Part II. Geological Society of America Bulletin 96, 137–144.

Basilevsky, A. T., Ivanov, B. A., Burba, G. A., Chernaya, I. M., Kryuchkov, V. P., Nikolaeva, O. V., Campbell, D. B. & Ronca, L. B., 1987. Impact craters on Venus: a continuation of the analysis of data from the Venera 15 and 16 spacecraft. Journal of Geophysical Research 92 (B12), 12869–12901.

Basilevsky, A. T., Head, J. W., Schaber, G. G. & Strom, R. G., 1997. The resurfacing history of Venus. In: Bougher, S. W., Hunten, D. M. & Phillips, R. J. (Eds.), Venus II – Geology, Geophysics, Atmosphere, and Solar Wind Environment. The University of Arizona Press, Tucson, 1047–1084.

Basilevsky, A. T., Head, J. W. & Setyaeva, I. V., 2003. Venus: estimation of age of impact craters on the basis of degree of preservation of associated radar-dark deposits. Geophysical Research Letters 30 (18), 1950, doi:10.1029/2003GL017504.

Basilevsky, A. T., Head, J. W. & Abdrakhimov, A. M., 2004. Impact crater air fall deposits on the surface of Venus: Areal distribution, estimated thickness, recognition in surface panoramas, and implications for provenance of sampled surface materials. Journal of Geophysical Research 109, E12003, doi:10.1029/2004JE002307.

Bell, J. F. III, Calvin, W. M., Farrand, W. H., Greeley, R., Johnson, J. R., Jolliff, B., Morris, R. V., Sullivan, R. J., Thompson, S., Wang, A., Weitz, C. & Squyres, S. W., 2008. Mars Exploration Rover Pancam multispectral imaging of rocks, soils and dust at

Gusev crater and Meridiani Planum. In: Bell, J. (Ed.), The Martian Surface – Composition, Mineralogy, and Physical Properties, pp. 281–314. Cambridge, Cambridge University Press.

Belton, M. J. S., Chapman, C. R., Veverka, J., Klaasen, K. P., Harch, A., Greeley, R., Greenberg, R., Head, J. W., McEwen, A., Morrison, D., Thomas, P. C., Davies, M. E., Carr, M. H., Neukum, G., Fanale, F. P., Davis, D. R., Anger, C., Gierasch, P. J., Ingersoll, A. P. & Pilcher, C. B., 1994. First images of asteroid 243 Ida. Science 265, 1543–1547, doi:10.1126/science.265.5178.1543.

Binder, A. B., 1969. Martian craters: comparison of statistical counts. Science 164, 297–299.

Binder, A. B. & McCarthy, D. W. Jr., 1972. Mars: the lineament systems. Science 176, 279–281.

Bischoff, L., & Oskierski, W., 1988. The surface structure of the Haughton impact crater, Devon Island, Canada. Meteoritics 23, 209–220.

Bland, P. A., de Souza Filho, C. R., Jull, A. J. T., Kelley, S. P., Hough, R. M., Artemieva, N. A., Pierazzo, E., Coniglio, J., Pinotti, L., Evers, V. & Kearsley, A. T., 2002. A possible tektite strewn field in the Argentinian pampa. Science 296, 1109–1111.

Bondarenko, N. V. & Head, J. W., 2004. Radar-dark impact crater-related parabolas on Venus: characterization of deposits with Magellan emissivity data. Journal of Geophysical Research 109, E09004, doi:10.1029/2004JE002256.

Boon, J. D. & Albritton, C. C. Jr., 1936. Meteorite craters and their possible relationship to “cryptovolcanic structures”. Field & Laboratory 5 (1), 1–9.

Boon, J. D. & Albritton, C. C. Jr., 1937. Meteorite scars in ancient rocks. Field & Laboratory 5, 53–64.

Boon, J. D. & Albritton, C. C. Jr., 1938. Established and supposed examples of meteoritic craters and structures. Field & Laboratory 6, 44–56.

Bottke, W. F. & Melosh, H. J., 1996. Binary asteroids and the formation of doublet craters. Icarus 124, 372–391.

Bottke, W. F., Love, S. G., Tytell, D. & Glotch, T., 2000. Interpreting the elliptical crater populations on Mars, Venus, and the Moon. Icarus 145, 108–121.

Boyce, J. M., Mouginis-Mark, P. J., Garvin, J. B. & Garbeil, H., 2003. Evidence for a thick mantle of volatile-rich materials in the Utopia Basin, Mars, based on crater depth/diameter measurements. Lunar and Planetary Science XXXIV. Lunar and Planetary Institute, Houston, abstract #1967 (CD-ROM).

Boyce, J. M., Mouginis-Mark, P. & Garbeil, H., 2004a. Depth to diameter relationships of craters in the high latitudes (70º–80º) of Mars: implications for geologic history of those areas. Lunar and Planetary Science XXXV. Lunar and Planetary Institute, Houston, abstract #1129 (CD-ROM).

Boyce, J. M., Mouginis-Mark, P. & Garbeil, H., 2004b. Predicted effects of surface processes on Martian impact crater depth/diameter relationships. Lunar and Planetary Science XXXV. Lunar and Planetary Institute, Houston, abstract #1816 (CD-ROM).

Brandt, D. & Reimold, W. U., 1995. The geology of the Pretoria Saltpan impact structure and the surrounding area. South African Journal of Geology 98, 287–303.

Brandt, D., Reimold, W. U., Franzsen, A. J., Koeberl, C. & Wendorff, L., 1998. Geophysical profile of the Roter Kamm impact crater, Namibia. Meteoritics & Planetary Science 33, 447–453.

Brink, M. C., Waanders, F. B. & Bisschoff, A. A., 1997. Vredefort: a model for the anatomy of an astrobleme. Tectonophysics 270, 83–114.

von Bülow, K., 1965. Proof of the volcanic origin of most lunar craters and of tectonic maria. Geological Problems in Lunar Research. Annals of the New York Academy of Sciences 123 (2), 528–531.

Bursnall, J. T., 1989. Introduction: review of the mechanical principles, deformation mechanisms and shear zone rocks. In: Bursnall, J. T. (Ed.), Mineralization and Shear Zones. Geological Association of Canada, Short course notes 6, 1–27.

Cameron, A. G. W., 2001. From interstellar gas to the Earth–Moon system. Meteoritics & Planetary Science 36 (1), 9–22.

Campbell, D. B., Stacy, N. J. S., Newman, W. I., Arvidson, R. E., Jones, E. M., Musser, G. S., Roper, A. Y., Schaller, C., 1992. Magellan observations of extended impact crater related features on the surface of Venus. Journal of Geophysical Research 97 (E10), 16249–16277.

Carr, M. H., 1999. Mars. In: Beatty, J. K., Collins Petersen, C. & Chaikin, A. (Eds.), The New Solar System, 4th edition, pp. 141–156. Sky Publishing Corporation & Cambridge University Press.

Carr, M. H., Crumpler, L. S., Cutts, J. A, Greeley, R., Guest, J. E. & Masursky, H., 1977. Martian impact craters and emplacement of ejecta by surface flow. Journal of Geophysical Research 82, (28), 4055–4065.

Chadderton, L. T., Krajenbrink, F. G., Katz, R. & Poveda, A., 1969. Standing waves on the Moon. Nature 223 (5203), 259–263.

Chao, E. C. T., 1968. Pressure and temperature histories of impact metamorphosed rocks – based on petrographic observations. In: French, B. M. & Short, N. M. (Eds.), Shock Metamorphism of Natural Materials, pp. 135–158. Baltimore, Mono Book Corp.

Chapman, C. R., 2002. Impact lethality and risks in today's world: lessons for interpreting Earth history. In: Koeberl. C. & MacLeod, K. G. (Eds.), Catastrophic Events and Mass Extinctions: Impacts and Beyond, pp. 7–19. Geological Society of America Special Paper 356.

Chapman, C. R., 2004. The hazard of near-Earth asteroid impacts on Earth. Earth and Planetary Science Letters 222, 1–15.

Chapman, R. G. & Fielder, G., 1964. On the central peaks of lunar craters. The Observatory 84, 23–27.

Chappelow, J. E. & Herrick, R. R., 2008. On the origin of a double, oblique impact on Mars. Icarus 197, 452–457.

Cheeney, R. F., 1983. Statistical methods in geology. George Allen & Unwin, London. 169 pp.

Cheng, A. F., 2002. Implications of the NEAR mission for internal structure. In: Asphaug, E. & Samarasinha, N. (Eds.), Extended Abstracts from the NASA Workshop on Scientific Requirements for Mitigation of Hazardous Comets and Asteroids. Arlington, Virginia, USA, September 3–6, 2002.

Cheng, A. F., 2004a. Implications of the NEAR mission for internal structure of Mathilde and Eros. Advances in Space Research 33, 1558–1563.

Cheng, A. F., 2004b. Collisional evolution of the asteroid belt. Icarus 169, 357–372, doi:10.1016/j.icarus.2004.02.002.

Chicarro, A. F., Schultz P. H. & Masson, P., 1985. Global and regional ridge patterns on Mars. Icarus 63, 153–174.

Cintala, M. J., Head, J. W. & Mutch, T. A., 1976. Characteristics of fresh Martian craters as a function of diameter: comparison with the Moon and Mercury. Geophysical Research Letters 3 (3), 117–120.

Cintala, M. J., Wood, C. A. & Head, J. W., 1977. The effects of target characteristics on fresh crater morphology: Preliminary results for the moon and Mercury. Proceedings of the 8th Lunar Science Conference. Lunar and Planetary Institute, Houston, 3409–3425.

Cione, A. L., Tonni, E. P., San Cristóbal, J., Hernández, P. J., Benítez, A., Bordignon, F. & Perí, J. A., 2002. Putative meteoritic craters in Río Cuarto (central Argentina) interpreted as eolian structures. Earth, Moon, and Planets 91, 9–24.

Cochrane, C. G., 2003. Crater morphometry on Venus. Lunar and Planetary Science XXXIV. Lunar and Planetary Institute, Houston, abstract #1173 (CD-ROM).

Cochrane, C. G. & Ghail, R. C., 2006. Topographic constraints on impact crater morphology on Venus from high-resolution stereo synthetic aperture radar digital elevation models. Journal of Geophysical Research 111, E04007, doi:10.1029/2005JE002570.

Cole, J. P. & King, C. A. M., 1968. Quantitative Geography – Techniques and Theories in Geography. Glasgow, John Wiley & Sons Ltd, 692 pp.

Collins, G. S., Morgan, J., Barton, P., Christeson, G. L., Gulick, S., Urrutia, J., Warner, M. & Wünnemann, K., 2008. Dynamic modelling suggests terrace zone asymmetry in the Chicxulub crater is caused by target heterogeneity. Earth and Planetary Science Letters 270, 221–230, doi:10.1016/j.epsl.2008.03.032.

Connerney, J. E. P., Acuña, M. H., Wasilewski, P. J., Ness, N. F., Rème, H., Mazelle, C., Vignes, D., Lin, R. P., Mitchell, D. L. & Cloutier, P. A., 1999. Magnetic lineations in the ancient crust of Mars. Science 284, 794–798.

Connerney, J. E. P., Acuña, M. H., Wasilewski, M. H., Kletetschka, G., Ness, N. F., Rème, H., Lin, R. P. & Mitchell, D. L., 2001. The global magnetic field of Mars and implications for crustal evolution. Geophysical Research Letters 28, 4015–4018.

Connerney, J. E. P., Acuña, M. H., Ness, N. F., Kletetschka, G., Mitchell, D. L., Lin, R. P. & Reme, H., 2005. Tectonic implications of Mars crustal magnetism. Proceedings of the National Academy of Sciences, doi:10.1073/pnas.0507469102.

Croft, S. K., 1980. Cratering flow fields: implications for the excavation and transient expansion stages of crater formation. Proceedings of the 11th Lunar and Planetary Science Conference. Lunar and Planetary Institute, Houston, 2347–2378.

Croft, S. K., 1981a. The excavation stage of basin formation: a qualitative model. In: Schultz, P. H. & Merrill, R. B. (Eds.), Multi-ring Basins: Formation and Evolution. Proceedings of the 12th Lunar and Planetary Science Conference. Geochimica et Cosmochimica Acta, Supplement 12, part A, 207–225.

Croft, S. K., 1981b. The modification stage of basin formation: conditions of ring formation. In: Schultz, P. H. & Merrill, R. B. (Eds.), Multi-ring Basins: Formation and Evolution. Proceedings of the 12th Lunar and Planetary Science Conference. Geochimica et Cosmochimica Acta, Supplement 12, part A, 227–257.

Croft, S. K., 1981c. On the origin of pit craters. Lunar and Planetary Science XII. Lunar and Planetary Institute, Houston, 196–198.

Croft, S. K., 1983. A proposed origin for palimpsests and anomalous pit craters on Ganymede and Callisto. Proceedings of the 14th Lunar and Planetary Science Conference, part I. Journal of Geophysical Research 88, Supplement, B71–B89.

Croft, S. K., 1985. The scaling of complex craters. Proceedings of the Fifteenth Lunar and Planetary Science Conference, part 2. Journal of Geophysical Research 90, Supplement, C828–842.

Crown, D. A. & Greeley, R., 1993. Volcanic geology of Hadriaca Patera and the eastern Hellas region of Mars. Journal of Geophysical Research 98, 3431–3451.

Crown, D. A., Price, K. H. & Greeley, R., 1992. Geologic evolution of the east rim of the Hellas basin, Mars. Icarus 100, 1–25.

Curran, D. R., Shockey, D. A., Seaman, L. & Austin, M., 1977. Mechanisms and models of cratering in earth media. In: Roddy, D. J., Pepin, R. O. & Merrill, R. B. (Eds.), Impact and Explosion Cratering, pp. 1057–1087. New York, Pergamon Press.

Currie, K. L., 1965. Analogues of lunar craters on the Canadian shield. Geological Problems in Lunar Research. Annals of the New York Academy of Sciences 123 (2), 915–940.

Cyr, K. E. & Melosh, H. J., 1993. Tectonic patterns and regional stresses near Venusian coronae. Icarus 102, 175–184.

Dauvillier, A., 1965. Paleovolcanic origins of the lunar seas. Geological Problems in Lunar Research. Annals of the New York Academy of Sciences 123 (2), 516–523.

Davis, J. C., 2002. Statistics and Data Analysis in Geology, 3rd edition. John Wiley & Sons, New York, 638 pp.

Davydov, V. D., 1968. On the question of polygonality and irregularity of the shape of certain craters on the Moon. ST-LPS-LS-10697, Goddard Space Flight Center, National Aeronautics and Space Administration, 4 pp. (A translation of: K voprosu o poligonal'nosti i nepravil'nostyakh formy nekotorykh kraterov na lune. Doklady Akademii Nauk SSSR 178 (4), 797–799.)

De Hon, R. A., 1979. Thickness of the western mare basalts. Proceedings of the 10th Lunar and Planetary Science Conference. Lunar and Planetary Institute, Houston, 2935–2955.

De Hon, R. A., 1980. Variations in interior morphology of 15–20 km lunar craters: Implications for a major subsurface discontinuity. Proceedings of the 11th Lunar and Planetary Science Conference. Lunar and Planetary Institute, Houston, 2207–2219.

DeHon, R. A. & Waskom, J. D., 1976. Geologic structure of the eastern mare basins. Proceedings of the 7th Lunar Science Conference. Lunar and Planetary Institute, Houston, 2729–2746.

Dence, M. R., 1964. A comparative structural and petrographic study of probable Canadian meteorite craters. Meteoritics 2 (3), 249–270.

Dence, M. R., 1968. Shock zoning at Canadian craters: petrography and structural implications. In: French, B. M. & Short, N. M. (Eds.), Shock Metamorphism of Natural Materials, pp. 169–184. Baltimore, Mono Book Corp.

Dence, M. R., Grieve, R. A. F. & Robertson, P. B., 1977. Terrestrial impact structures: principal characteristics and energy considerations. In: Roddy, D. J., Pepin, R. O. & Merrill, R. B. (Eds.), Impact and Explosion Cratering, pp. 247–275. New York, Pergamon Press.

Denk, T., Neukum, G., Helfenstein, P., Thomas, P. C., Turtle, E. P., McEwen, A. S., Roatsch, T., Veverka, J., Johnson, T. V., Perry, J. E., Owen, W. M., Wagner, R. J., Porco, C. C., and the Cassini ISS Team, 2005. The first six months of Iapetus observations by the Cassini ISS camera. Lunar and Planetary Science XXXVI. Lunar and Planetary Institute, Houston, abstract #2262 (CD-ROM).

Dietz, R. S., 1946. The meteoritic impact origin of the Moon's surface features. The Journal of Geology 54, 359–375.

Dohm, J. M. & Tanaka, K. L., 1999. Geology of the Thaumasia region, Mars: plateau development, valley origins, and magmatic evolution. Planetary and Space Science 47, 411–431.

Dohm, J. M., Tanaka, K. L. & Hare, T. M., 2001a. Geologic, Paleotectonic, and Paleoerosional Maps of the Thaumasia Region, Mars. Geologic Investigations Series I–2650. Scale 1:5,000,000. U. S. Department of the Interior, U. S. Geological Survey.

Dohm, J. M., Ferris, J. C., Baker, V. R., Anderson, R. C., Hare, T. M., Strom, R. G., Barlow, N. G., Tanaka, K. L., Klemaszewski, J. E. & Scott, D. H., 2001b. Ancient drainage basin of the Tharsis region, Mars: potential source for outflow channel systems and putative oceans or paleolakes. Journal of Geophysical Research 106, 32943–32958.

Dohm, J. M., Maruyama, S., Baker, V. R., Anderson, R. C., Ferris, J. C. & Hare, T. M., 2002. Plate tectonism on early Mars: diverse geological and geophsical evidence (abstract #1639). Lunar and Planetary Science XXXIII. Lunar and Planetary Institute, Houston (CD-ROM).

Dohm, J. M., Kerry, K., Keller, J. M., Baker, V. R., Maruyama, S., Anderson, R. C., Ferris, J. C. & Hare, T. M., 2005. Mars geological province designations for the interpretation of GRS data (abstract #1567). Lunar and Planetary Science XXXVI. Lunar and Planetary Institute, Houston (CD-ROM).

Dohm, J. M., Baker, V. R., Maruyama, S. & Anderson, R. C., 2007. Traits and evolution of the Tharsis superplume, Mars. In: Yuen, D. A, Maruyama, S., Karato, S.-I. & Windley, B. F. (Eds.), Superplumes: Beyond Plate Tectonics, pp. 523–536. Dordrecht, Springer.

Dzurisin, D., 1978. The tectonic and volcanic history of Mercury as inferred from studies of scarps, ridges, troughs, and other lineaments. Journal of Geophysical Research 83 (B10), 4883–4906.

Edgar L. A. & Frey, H. V., 2008. Buried impact basin distribution on Mars: contributions from crustal thickness data. Geophysical Research Letters 35, L02201, doi:10.1029/2007GL031466.

Ekholm, A. G. & Melosh, H. J., 2001. Crater features diagnostic of oblique impacts: the size and position of the central peak. Geophysical Research Letters 28 (4), 623–626.

Elger, T. G., 1895. The Moon – A Full Description and Map of Its Principal Physical Features. London, George Philip & Son. EBook, http://www.gutenberg.org/etext/17712, accessed February 11th, 2009.

Elo, S., Jokinen, T. & Soininen, H., 1992. Geophysical investigations of the Lake Lappajärvi impact structure, western Finland. Tectonophysics 216, 99–109.

Elston, W. E., Laughlin, A. W. & Brower, J. A., 1971. Lunar near-side tectonic patterns from Orbiter 4 photographs. Journal of Geophysical Research 76, 5670–5674.

Eppler, D. T., Nummedal, D., Ehrlich, R., 1977. Fourier analysis of planimetric lunar crater shape – possible guide to impact history and lunar geology. In: Roddy, D. J., Pepin, R. O. & Merrill, R. B. (Eds.), Impact and Explosion Cratering, pp. 511–526. New York, Pergamon Press.

Eppler, D. T., Ehrlich, R., Nummedal, D. & Schultz, P. H., 1982. Sources of shape variation in lunar impact craters – Fourier shape analysis. Lunar and Planetary Science XIII. Lunar and Planetary Institute, Houston, 203–204.

Eppler, D. T., Ehrlich, R., Nummedal, D. & Schultz, P. H., 1983. Sources of shape variation in lunar impact craters: Fourier shape analysis. Geological Society of America Bulletin 94, 274–291.

Evans, K. R., Rovey, C. W. II, Mickus, K. L., Plymate, T. G. & Thomson, K. C., 2003. Weaubleau-Osceola structure, Missouri: deformation, event stratification, and shock

metamorphism of a Mid-Carboniferous impact site. Third International Conference on Large Meteorite Impacts. Lunar and Planetary Institute, Houston, abstract #4111 (CD-ROM).

Evans, K. R., Cox, M. R., Davis, G. R., Miller, J. F. & Rovey II, C. W., 2006. Emplacement of breccias in the Weaubleau structure, Missouri, USA: Implications for environmental disturbance in a shallow-marine carbonate setting. Impact Craters as Indicators for Planetary Environmental Evolution and Astrobiology, Östersund (Sweden), June 8–14, 2006.

Fairén, A. G., Ruiz, J. & Anguita, F., 2002. An origin for the linear magnetic anomalies on Mars through accretion of terranes: implications for dynamo timing. Icarus 160, 220–223.

Fielder, G., 1961. Structure of the Moon's Surface. Oxford – London – New York – Paris, Pergamon Press, 246 pp.

Fielder, G., 1965. Lunar Geology. London, Lutterworth Press, 184 pp.

Floran, R. J. & Dence, M. R., 1976. Morphology of the Manicouagan ring-structure, Quebec, and some comparisons with lunar basins and craters. Proceedings of the 7th Lunar Science Conference. Lunar and Planetary Institute, Houston, 2845–2865.

Ford, J. P. & Plaut, J. J., 1993. Magellan image data. In: Ford, J. P., Plaut, J. J., Weitz, C. M., Farr, T. G., Senske, D. A., Stofan, E. R., Michael, G. & Parker, T. J., Guide to Magellan Image Interpretation, JPL Publication 93-24, pp. 7–18. Pasadena, Jet Propulsion Laboratory.

Ford, J. P., Plaut, J. J., Weitz, C. M., Farr, T. G., Senske, D. A., Stofan, E. R., Michael, G. & Parker, T. J., 1993. Guide to Magellan Image Interpretation. JPL Publication 93-24. Pasadena, Jet Propulsion Laboratory, 148 pp.

Freed, A. M., Melosh, H. J. & Solomon, S. C., 2001. Tectonics of mascon loading: resolution of the strike-slip faulting paradox. Journal of Geophysical Research 106 (E9), 20603–20620.

French, B. M., 1968. Shock metamorphism as a geological process. In: French, B. M. & Short, N. M. (Eds.), Shock Metamorphism of Natural Materials, pp. 1–17. Baltimore, Mono Book Corp.

French, B. M., 1990. 25 years of the impact-volcanic controversy – is there anything new under the sun or inside the earth? EOS, Transactions of the American Geophysical Union 71 (17), 411–414.

French, B. M., 1998. Traces of Catastrophe – A Handbook of Shock-Metamorphic Effects in Terrestrial Meteorite Impact Structures. LPI Contribution no. 954. Houston, Lunar and Planetary Institute, 120 pp.

French, B. M., 2004. The importance of being cratered: the new role of meteorite impact as a normal geological process. Meteoritics & Planetary Science 39 (2), 169–197.

French, B. M. & Short, N. M. (Eds.), 1968. Shock Metamorphism of Natural Materials. Baltimore, Mono Book Corp., 644 pp.

Frey, H., 2008. Ages of very large impact basins on Mars: implications for the late heavy bombardment in the inner solar system. Geophysical Research Letters 35, L13203, doi:10.1029/2008GL033515.

Frey, H., Sakimoto, S. E. H. & Roark, J., 1999. Discovery of a 450 km diameter, multi-ring basin on Mars through analysis of MOLA topographic data. Geophysical Research Letters 26 (12), 1657–1660.

Frey, H., Hutchison, L., Sakimoto, S. E. H. & Roark, J., 2000. A large population of possible buried impact basins on Mars revealed by MOLA topographic data. Lunar and Planetary Science XXXI. Lunar and Planetary Institute, Houston, abstract #1736 (CD-ROM).

Frey, H. V., Shockey, K. M., Frey, E. L., Roark, J. H. & Sakimoto, S. E. H., 2001. A very large population of likely buried impact basins in the northern lowlands of Mars revealed by MOLA data. Lunar and Planetary Science XXXII. Lunar and Planetary Institute, Houston, abstract #1680 (CD-ROM).

Frey, H. V., Edgar, L. & Lillis, R., 2007. Very large visible and buried impact basins on Mars: Implications for internal and crustal evolution and the late heavy bombardment in the inner solar system. Seventh International Conference on Mars. Pasadena, USA, abstract #3070 (CD-ROM).

Fulmer, C. V. & Roberts, W. A., 1963. Rock induration and crater shape. Icarus 2, 452–465.

Galilei, G., 1999. Sidereus Nuncius. Tallinna, Tähtitieteellinen yhdistys Ursa ry, 295 pp. (In Finnish, translated and edited by R. Lehti. Originally published in 1610.)

Garvin, J., Schnetzler, C. C. & Grieve, R. A. F., 1992. Characteristics of large terrestrial impact structures as revealed by remote sensing studies. Tectonophysics 216, 45–62.

Garvin, J. B., Grieve, R. A. F. & Schnetzler, C. C., 1995. Satellite remote sensing signatures of impact structures. Meteoritics & Planetary Science 30 (5), Supplement, 509.

Garvin, J. B., Frawley, J. J., Sakimoto, S. E. H., & Schnetzler, C., 2000a. Global geometric properties of Martian impact craters: an assesment from Mars Orbiter Laser Altimeter (MOLA) digital elevation models. Lunar and Planetary Science XXXI. Lunar and Planetary Institute, Houston, abstract #1619 (CD-ROM).

Garvin, J. B., Sakimoto, S. E. H., Frawley, J. J., & Schnetzler, C., 2000b. North polar region craterforms on Mars: geometric characteristics from the Mars Orbiter Laser Altimeter. Icarus 144, 329–352.

Garvin, J. B., Sakimoto, S. E. H. & Frawley, J. J., 2003. Craters on Mars: global geometric properties from gridded MOLA topography. Sixth International Conference on Mars. Lunar and Planetary Institute, Houston, abstract #3277 (CD-ROM).

Gault, D. E. & Wedekind, J. A., 1978. Experimental studies of oblique impact. Proceedings of the 9th Lunar and Planetary Science Conference. Lunar and Planetary Institute, Houston, 3843–3875.

Gault, D. E., Quaide, W. L. & Oberbeck, V. R., 1968. Impact cratering mechanics and structures. In: French, B. M. & Short, N. M. (Eds.), Shock Metamorphism of Natural Materials, pp. 87–99. Baltimore, Mono Book Corp.

Gault, D. E., Guest, J. E., Murray, J. B., Dzurisin, D. & Malin, M. C., 1975. Some comparisons of impact craters on Mercury and the Moon. Journal of Geophysical Research 80 (17), 2444–2460.

Gifford, A. W. & Maxwell, T. A., 1979. Asymmetric terracing of lunar highland craters: influence of pre-impact topography and structure. Proceedings of the 10th Lunar and Planetary Science Conference. Lunar and Planetary Institute, Houston, 2597–2607.

Gifford, A. W., Maxwell, T. A. & El-Baz, F., 1979. Geology of the lunar farside crater Necho. The Moon and the Planets 21, 25–42.

Gilbert, G. K., 1893. The Moon's face: a study of the origin of its features. Philosophical Society of Washington, Bulletin 12, 241–292.

Gilbert, G. K., 1896. The origin of hypotheses, illustrated by the discussion of a topographic problem. Science 3 (53), 1–12.

Gilmore, M. S., 1999. Craters as an indicator of Martian regolith thickness. Fifth International Conference on Mars. Lunar and Planetary Institute, Houston, abstract #6228 (CD-ROM).

Glen, W. (Ed.), 1994. The Mass-Extinction Debates: How Science Works in a Crisis. Stanford, Stanford University Press, 370 pp.

Goeritz, M., Kenkmann, T., Wünnemann, K. & van Gasselt, S., 2009. Asymmetric structure of lunar impact craters due to oblique impacts? Lunar and Planetary Science XXXX. Lunar and Planetary Institute, Houston, abstract #2096 (CD-ROM).

Golombek, M. P., Plescia, J. B. & Franklin, B. J., 1991. Faulting and folding in the formation of planetary wrinkle ridges. Proceedings of Lunar and Planetary Science 21. Lunar and Planetary Institute, Houston, 679–693.

Golombek, M. P., Tanaka, K. L. & Franklin, B. J., 1996. Extension across Tempe Terra, Mars, from measurements of fault scarp widths and deformed craters. Journal of Geophysical Research 101 (E11), 26119–26130.

Golombek, M. P., Haldemann, A. F. C., Simpson, R. A., Fergason, R. L., Putzig, N. E., Arvidson, R. E., Bell, J. F. III & Mellon, M. T., 2008. Martian surface properties from joint analysis of orbital, Earth-based, and surface observations. In: Bell, J. (Ed.), The Martian Surface – Composition, Mineralogy, and Physical Properties, pp. 468–497. Cambridge, Cambridge University Press.

Grant, J. A. & Parker, T. J., 2002. Drainage evolution in the Margaritifer Sinus region, Mars. Journal of Geophysical Research 107 (E9), 5066, doi:10.1029JE001678.

Grant, J. A. & Schultz, P. H., 1993. Degradation of selected terrestrial and Martian impact craters. Journal of Geophysical Research 98, 11025–11042.

Greeley, R. & Guest, J. E., 1987. Geologic Map of the Eastern Equatorial Region of Mars. USGS Miscellaneous Investigations Series Map I-1802-B, 1:15000000. U.S. Department of the Interior, U.S. Geological Survey, USA.

Green, J., 1965a. Hookes and spurrs in selenology. Geological Problems in Lunar Research. Annals of the New York Academy of Sciences 123 (2), 373–402.

Green, J., 1965b. Summary. Geological Problems in Lunar Research. Annals of the New York Academy of Sciences 123 (2), 1236–1255.

Greenberg, R. & Geissler, P., 2002. Europa's dynamic icy crust. Meteoritics & Planetary Science 37 (12), 1685–1710.

Greene, M. T., 1998. Alfred Wegener and the origin of lunar craters. Earth Sciences History 17 (2), 111–138.

Grieve, R. A. F., 1987. Terrestrial impact structures. Annual Review of Earth and Planetary Sciences 15, 245–270.

Grieve, R. A. F., Robertson, P. B. & Dence, M. R., 1981. Constraints on the formation of ring impact structures, based on terrestrial data. In: Schultz, P. H. & Merrill, R. B. (Eds.), Multi-ring Basins: Formation and Evolution. Proceedings of the 12th Lunar and

Planetary Science Conference, Geochimica et Cosmochimica Acta, Supplement 12, part A, 37–57.

Grieve, R. A. F., Wood, C. A., Garvin, J. B., McLoughlin, G. & McHone, J. F. (Eds.), 1988. Astronaut's Guide to the Terrestrial Impact Craters. LPI Technical Report 88-03, Lunar and Planetary Institute, Houston, 89 pp.

Grieve, R. A. F., Langenhorst, F. & Stöffler, D., 1996. Shock metamorphism of quartz in nature and experiment: II. Significance in geoscience. Meteoritics & Planetary Science 31, 6–35.

Grieve, R. A. F., Reimold, W. U., Morgan, J., Riller, U. & Pilkington, M., 2008. Observations and interpretations at Vredefort, Sudbury, and Chicxulub: towards an empirical model of terrestrial impact basin formation. Meteoritics & Planetary Science 43 (5), 855–882.

Grosfils, E. B. & Head, J. W., 1995. Radiating dike swarms on Venus: evidence for emplacement at zones of neutral buoyancy. Planetary and Space Science 43 (12), 1555–1560.

Grott, M., Hauber, E., Werner, S. C., Kronberg, P. & Neukum, G., 2005. High heat flux on ancient Mars: Evidence from rift flank uplift at Coracis Fossae. Geophysical Research Letters 32, L21201, doi:10.1029/2005GL023894.

Guest, J. E., 1971. Geology of the farside crater Tsiolkovsky. In: Fielder, G. (Ed.), Geology and Physics of the Moon – a Study of Some Fundamental Problems, pp. 93–103. Elsevier Publishing Company.

Guest, J. E. & Fielder, G., 1968. Lunar ring structures and the nature of the maria. Planetary and Space Science 16, 665–673.

Guest, J. E. & Murray, J. B., 1969. Nature and origin of Tsiolkovsky crater, lunar farside. Planetary and Space Science 17, 121–141.

Guest, J. E. & Stofan, E. R., 1999. A new view of the stratigraphic history of Venus. Icarus 139, 55–66.

Gulick, S. P. S., Barton, P. J., Christeson, G. L., Morgan, J. V., McDonald, M., Mendoza-Cervantes, K., Pearson, Z. F., Surendra, A., Urrutia-Fucugauchi, J., Vermeesch, P. M. & Warner, M. R., 2008. Importance of pre-impact crustal structure for the asymmetry of the Chicxulub impact crater. Nature Geoscience 1, 131–135, doi:10.1038/ngeo103.

Gurov, E. P. & Gurova E. P., 1982. Some regularities of the areal spreading of fractures around Elgygytgyn impact crater. Lunar and Planetary Science XIII. Lunar and Planetary Institute, Houston, 291–292.

Gurov, E. P., Koeberl, C. & Yamnichenko, A., 2007. El'gygytgyn impact crater, Russia: structure, tectonics, and morphology. Meteoritics & Planetary Science 42 (3), 307–319.

Gutschewski, G. L, Kinsler, D. C. & Whitaker, E., 1971. Atlas and Gazetteer of the Near Side of the Moon. NASA SP-241. Washington, D. C., National Aeronautics and Space Administration, 538 pp.

Hale, W. S., 1979. Orientations of central peaks in lunar craters: implications for regional structural trends. In: Robertson, P. C. (Ed.), Abstracts of Papers Presented to the Conference on the Lunar Highlands Crust. November 14–16, 1979, Houston, USA. LPI Contribution 394. Lunar and Planetary Institute, Houston, 36–38.

Hale, W. S., 1982. Central pits in Martian craters: occurrence by substrate, ejecta type and rim diameter. Lunar and Planetary Science XIII. Lunar and Planetary Institute, Houston, 295–296.

Hale, W. S. & Grieve, R. A. F., 1982. Volumetric analysis of complex lunar craters: implications for basin formation. Proceedings of the Thirteenth Lunar and Planetary Science Conference, part 1. Journal of Geophysical Research 87, Supplement, A65–A76.

Hale, W. & Head, J. W., 1979. Central peaks in lunar craters: Morphology and morphometry. Proceedings of the 10th Lunar and Planetary Science Conference. Lunar and Planetary Institute, Houston, 2623–2633.

Hale, W. & Head, J. W., 1980. The origin of peak rings and the crater to basin transition. In: Merrill, R. B. & Schultz, P. H. (Eds.), Abstracts of Papers Presented to the Conference on Multi-ring Basins: Formation and Evolution. November 10–12, 1980. LPI Contribution 414. Lunar and Planetary Institute, Houston, 27–29.

Hale, W. & Head, J. W., 1981a. Central peaks in Martian craters: comparisons to the Moon and Mercury. Lunar and Planetary Science XII. Lunar and Planetary Institute, Houston, 386–388.

Hale, W. & Head, J. W., 1981b. Central structures in Martian craters: preliminary implications for substrate volatile effects. Abstracts of Papers Presented to the Third International Colloquium on Mars. Houston, Lunar and Planetary Institute, 104–106.

Hansen, V. L. & López, I., 2009. Implications of Venus evolution based on ribbon tessera terrain relations within five large regional areas. Lunar and Planetary Science XXXX, Lunar and Planetary Institute, Houston, abstract #2306 (CD-ROM).

Hartmann, W. K., 1981. Discovery of multi-ring basins: Gestalt perception in planetary science. In: Schultz, P. H. & Merrill, R. B. (Eds.), Multi-ring Basins: Formation and

Evolution. Proceedings of the 12th Lunar and Planetary Science Conference. Geochimica et Cosmochimica Acta, Supplement 12, part A, 79–90.

Hartmann, W. K. & Barlow, N. G., 2006. Nature of the Martian uplands: effect on Martian meteorite age distribution and secondary cratering. Meteoritics & Planetary Science 41 (10), 1453–1467.

Hartmann, W. K. & Neukum, G., 2001. Cratering chronology and the evolution of Mars. Space Science Reviews 96, 165–194.

Hartmann, W. K. & Wood, C. A., 1971. Moon: origin and evolution of multi-ring basins. The Moon 3, 3–78.

Hauck, S. A. II, Phillips, R. J. & Price, M. H., 1998. Venus: crater distribution and plains resurfacing models. Journal of Geophysical Research 103 (E6), 13635–13642.

Hawke, B. R., Blewett, D. T., Lucey, P. G., Smith, G. A., Bell, J. F. III, Campbell, B. A. & Robinson, M. S., 2004. The origin of lunar crater rays. Icarus 170, 1–16, doi:10.1016/j.icarus.2004.02.013.

Head, J. W., 1974. Orientale multi-ringed basin interior and implications for the petrogenesis of lunar highland samples. The Moon 11, 327–356.

Head, J. W., 1976a. Evidence for the sedimentary origin of Imbrium sculpture and lunar basin radial texture. The Moon 15, 445–462.

Head, J. W., 1976b. The significance of substrate characteristics in determining morphology and morphometry of lunar craters. Proceedings of the 7th Lunar Science Conference. Lunar and Planetary Institute, Houston, 2913–2929.

Head, J. W., 1977. Origin of outer rings in lunar multi-ringed basins: evidence from morphology and ring spacing. In: Roddy, D. J., Pepin, R. O. & Merrill, R. B. (Eds.), Impact and Explosion Cratering, pp. 563–573. New York, Pergamon Press.

Head, J. W., 2000a. Tests for ancient polar deposits on Mars: origin of esker-like sinuous ridges (Dorsa Argentea) using MOLA data. Lunar and Planetary Science XXXI. Lunar and Planetary Institute, Houston, abstract #1116 (CD-ROM).

Head, J. W., 2000b. Extensive south polar ice cap in middle Mars history? Tests using MOLA data. Lunar and Planetary Science XXXI. Lunar and Planetary Institute, Houston, abstract #1119 (CD-ROM).

Head, J. W. & Pratt, S., 2001. Extensive Hesperian-aged south polar ice sheet on Mars: evidence for massive melting and retreat, and lateral flow and ponding of meltwater. Journal of Geophysical Research 106, 12275–12299.

Head, J. W. & Roth, R., 1976. Mars pedestal crater escarpments: evidence for ejecta-related emplacement. Abstracts of Papers Presented to the Symposium on Planetary Cratering Mechanics. Lunar and Planetary Institute, Houston, 50–52.

Head, J. W., Greeley, R., Golombek, M. P., Hartmann, W. K., Hauber, E., Jaumann, R., Masson, P., Neukum, G., Nyquist, L. E. & Carr, M., 2001. Geological processes and evolution. Space Science Reviews 96, 263–292.

Helfenstein, P., Thomas, P. C., Veverka, J., Squyres, S., Rathbun, J. A., Denk, T., Neukum, G., Roatsch, T., Wagner, R., Perry, J., Turtle, E., McEwen, A. S., Johnson, T. V., Porco, C. & Cassini ISS Team, 2005. Geological features and terrains on Enceladus as seen by Cassini ISS. Bulletin of the American Astronomical Society 37 (3), abstract 36.01. 37th DPS Meeting, 4–9 September 2005, Cambridge, England.

Henkel, H., 1992. Geophysical aspects of meteorite impact craters in eroded shield environment, with special emphasis on electric resistivity. Tectonophysics 216, 63-89.

Herrick, R. R., 2005. Inferences from oblique impact craters about the role of the atmosphere and subsurface volatiles in the impact cratering process on Mars. Workshop on the Role of Volatiles and Atmospheres on Martian Impact Craters. Lunar and Planetary Institute, Houston, abstract #3019 (CD-ROM).

Herrick, R. R. & Forsberg-Taylor, N. K, 2003. The shape and appearance of craters formed by oblique impact on the Moon and Venus. Meteoritics & Planetary Science 38 (11), 1551–1578.

Herrick, R. R. & Hessen, K. K., 2006. The planforms of low-angle impact craters in the northern hemisphere of Mars. Meteoritics & Planetary Science 41 (10), 1483–1495.

Herrick, R. R. & Lyons, S. N., 1998. Inversion of crater morphometric data to gain insight on the cratering process. Meteoritics & Planetary Science 33, 131–143.

Herrick, R. R. & Phillips, R. J., 1994a. Implications of a global survey of Venusian impact craters. Icarus 111, 387–416.

Herrick, R. R. & Phillips, R. J., 1994b. Effects of the Venusian atmosphere on incoming meteoroids and the impact crater population. Icarus 112, 253–281.

Herrick, R. R. & Shanteau, R. L., 2001. The shape and appearance of oblique impact craters on Mars. Lunar and Planetary Science XXXII. Lunar and Planetary Institute, Houston, abstract #1909 (CD-ROM).

Herrick, R. R & Sharpton, V. L., 1996. Geologic history of the Mead impact basin, Venus. Geology 24 (1), 11–14.

Herrick, R. R. & Sharpton, V. L., 2000. Implications from stereo-derived topography of Venusian impact craters. Journal of Geophysical Research 105 (E8), 20245–20262.

Herrick, R. R., Sharpton, V. L., Malin, M. C., Lyons, S. N. & Feely, K., 1997. Morphology and morphometry of impact craters. In: Bougher, S. W., Hunten, D. M. & Phillips, R. J. (Eds.), Venus II – Geology, Geophysics, Atmosphere, and Solar Wind Environment, pp. 1015–1046. Tucson, The University of Arizona Press.

Hiesinger, H. & Head, J. W. III, 2002. Topography and morphology of the Argyre Basin, Mars: implications for its geologic and hydrologic history. Planetary and Space Science 50, 939–981.

Hillman, E. & Barlow, N. G., 2005. Martian central pit craters. Lunar and Planetary Science XXXVI. Lunar and Planetary Institute, Houston, abstract #1418 (CD-ROM).

Hode, T., von Dalwigk, I. & Broman, C., 2003. A hydrothermal system associated with the Siljan impact structure, Sweden – implications for the search for fossil life on Mars. Astrobiology 3 (2), 271–289.

Hodges, C. A. 1980. Geologic Map of the Argyre Quadrangle of Mars. Map I-1181 (MC-26). U.S. Geological Survey.

Hodges, C. A. & Wilhelms, D. E., 1978. Formation of lunar basin rings. Icarus 34, 294–323.

Hodges, C. A., Shew, N. B. & Clow, G., 1980. Distribution of central pit craters on Mars. Lunar and Planetary Science XI. Lunar and Planetary Institute, Houston, 450–452.

Hodgson, C. J., 1989. Patterns of mineralization. In: Bursnall, J. T. (Ed.), Mineralization and Shear Zones, pp. 51–88. Geological Association of Canada, Short course notes 6.

Holsapple, K. A., 2004. From simple to complex craters: the mechanics of late-time crater adjustments. Lunar and Planetary Science XXXV. Lunar and Planetary Institute, Houston, abstract #1937 (CD-ROM).

Hörz, F., Grieve, R., Heiken, G., Spudis, P. & Binder, A., 1991. Lunar surface processes. In: Heiken, G. H., Vaniman, D. T. & French, B. M. (Eds.), Lunar Sourcebook – a User's Guide to the Moon, pp. 61–120. Cambridge University Press.

Hoyt, W. G., 1987. Coon Mountain Controversies: Meteor Crater and the Development of Impact Theory. Tucson, University of Arizona Press, 442 pp.

Innes, M. J. S., 1964. Recent advances in meteorite crater research at the Dominion Observatory, Ottawa, Canada. Meteoritics 2 (3), 219–241.

Ivanov, B. A., 1990. Venusian impact craters on Magellan images: view from Venera 15/16. Earth, Moon, and Planets 50/51, 159–173.

Ivanov, B. A., 1992. Impact craters. In: Barsukov, V. L., Basilevsky, A. T., Volkov, V. P. & Zharkov, V. N. (Eds.), Venus Geology, Geochemistry, and Geophysics, pp. 113–128. Tucson, The University of Arizona Press.

Ivanov, B. A., 2001. Mars/Moon cratering rate ratio estimates. Space Science Reviews 96 (1–4), 87–104.

Ivanov, B. A. & Kostuchenko, V. N., 1997. Block oscillation model for impact crater collapse. Lunar and Planetary Science XXVIII. Lunar and Planetary Institute, Houston, abstract #1655 (CD-ROM).

Ivanov, B. A., Basilevsky, A. T., Kryuchkov, V. P. & Chernaya, I. M., 1986. Impact craters on Venus: analysis of Venera 15 and 16 data. Journal of Geophysical Research 91 (B4), D413–D430.

Ivanov, B. A., Nemchinov, I. V., Svetsov, V. A., Provalov, A. A., Khazins, V. M. & Phillips, R. J., 1992. Impact cratering on Venus: physical and mechanical models. Journal of Geophysical Research 97 (E10), 16167–16181.

Ivanov, B. A., Basilevsky, A. T. & Neukum, G., 1997. Atmospheric entry of large meteoroids: implication to Titan. Planetary and Space Science 45 (8), 993–1007.

Ivanov, M. & Head, J. W., 1996. Tessera terrain on Venus: a survey of the global distribution, characteristics, and relation to surrounding units from Magellan data. Journal of Geophysical Research 101 (E6), 14861–14908.

Ivanov, M., Korteniemi, J., Kostama, V.-P., Aittola, M., Raitala, J., Glamoclija, M., Marinangeli, L. & Neukum, G., 2005. Major episodes of the hydrologic history in the region of Hesperia Planum, Mars. Journal of Geophysical Research – Planets 110 (E12), doi:10.1029/2005JE002420.

Jones, K. B., Head, J. W. III, Pappalardo, R. T. & Moore, J. M., 2003. Morphology and origin of palimpsests on Ganymede based on Galileo observations. Icarus 164, 197–212.

Jöns, H.-P., 1987. Large fossil mud lakes or giant mud sheet floods in Syrtis Major (Isidis Planitia) and Mare Australe, Mars. Lunar and Planetary Science XVIII. Lunar and Planetary Institute, Houston, 470–471.

Kaarsberg, E. A., 1969. Dynamic modelling of lunar features with a viscoelastic material. EOS, Transactions of the American Geophysical Union 50 (4), 228.

Kadish, S. J. & Barlow, N. G., 2006. Pedestal crater distribution and implications for a new model of formation. Lunar and Planetary Science XXXVII. Lunar and Planetary Institute, Houston, abstract #1254 (CD-ROM).

Kargel, J. S., 1993. Geomorphic processes in the Argyre-Dorsa Argentea region of Mars. Lunar and Planetary Science XXIV. Lunar and Planetary Institute, Houston, 753–754.

Kargel, J. S. & Strom, R. G., 1992. Ancient glaciation on Mars. Geology 20, 3–7.

Kenkmann, T., 2002. Folding within seconds. Geology 30 (3), 231–234.

Kenkmann, T., Ivanov, B. A. & Stöffler, D., 2000. Identification of ancient impact structures: low-angle faults and related geological features of crater basements. In: Gilmour, I. & Koeberl, C. (Eds.), Impacts and the Early Earth. Lecture Notes in Earth Sciences, 91, pp. 279–307. Berlin Heidelberg, Springer-Verlag.

Khodak, Yu. A., 1965. Principal structural elements of the Moon and the significance of the geographic-geological approach. Geological Problems in Lunar Research. Annals of the New York Academy of Sciences 123 (2), 641–655.

Kieffer, H. H., Jakosky, B. M. & Snyder, C. W., 1992. The planet Mars: from antiquity to the present. In: Kieffer, H. H., Jakosky, B. M., Snyder, C. W. & Matthews, M. S. (Eds.), Mars, pp. 1–33. Tucson & London, The University of Arizona Press.

Kirk, R. L., Lee, E. M., Sucharski, R. M., Richie, J., Grecu, A., & Castro, S. K., 2000. MDIM 2.0: A revised global digital image mosaic of Mars. Lunar and Planetary Science XXXI. Lunar and Planetary Institute, Houston, abstract #2011 (CD-ROM).

Koch, D. M. & Manga, M., 1996. Neutrally buoyant diapirs: a model for Venus coronae. Geophysical Research Letters 23 (3), 225–228.

Koeberl, C., 2001. Craters on the Moon from Galileo to Wegener: a short history of the impact hypothesis, and implications for the study of terrestrial impact craters. Earth, Moon, and Planets 85–86, 209–224.

Kopal, Z., 1966. An Introduction to the Study of the Moon. Dordrecht, D. Reidel Publishing Company, 466 pp.

Korteniemi, J., Kostama, V.-P., Törmänen, T., Aittola, M., Öhman, T., Lahtela, H., Raitala, J. & Neukum, G., 2005. Complex geology of two large impact craters in Tyrrhena Terra, Mars: detailed analysis using MEX HRSC camera data. Journal of Geophysical Research – Planets 110 (E12), doi:10.1029/2005JE002427.

Korteniemi, J., Aittola, M., Öhman, T. & Raitala, J., 2006. Floor-fractured craters on the terrestrial planets – the Martian perspective. 40th ESLAB, First International Conference on Impact Cratering in the Solar System, Proceedings. ESA Special Publication SP-612, 193–198 (CD-ROM).

Korteniemi, J., Raitala, J., Aittola, M., Ivanov, M. A., Öhman, T., Kostama, V.-P. & Hiesinger, H., 2009. Dike indicators in the Hadriaca Patera – Promethei Terra region, Mars. Earth and Planetary Science Letters (in press).

Korycansky, D. G. & Zahnle, K. J., 2004. Atmospheric impacts, fragmentation, and small craters on Venus. Icarus 169, 287–299.

Kostama, V.-P., 2006. The crowns, spiders and stars of Venus: characterization and assessment of the geological settings of volcano-tectonic structures of Venus. Report Series in Physical Sciences, Report No. 42, University of Oulu, 104 pp.

Kostama, V.-P., Ivanov, M. A., Polit, A. T., Törmänen, T., Grosfils, E. B., Raitala, J., & Neukum, G., 2007. Topographic and morphologic characteristics of Reull Vallis, Mars: implications for the history of the Reull Vallis fluvial system. Journal of Geophysical Research 112, E11001, doi:10.1029/2006JE002848.

Kreslavsky, M. A. & Head, J. W. III, 1999. Morphometry of small shield volcanoes on Venus: implications for the thickness of regional plains. Journal of Geophysical Research 104 (E8), 18925–18932.

Kreslavsky, M. A. & Head, J. W. III, 2001. Stealth craters in the northern lowlands of Mars: evidence for a buried Early-Hesperian-aged unit. Lunar and Planetary Science XXXII. Lunar and Planetary Institute, Houston, abstract #1001 (CD-ROM).

Kring, D. A., 2007. Guidebook to the Geology of Barringer Meteorite Crater, Arizona (a.k.a. Meteor Crater). LPI Contribution No. 1355. Houston, Lunar and Planetary Institute, 150 pp.

Kuiper, G. P., Whitaker, E. A., Strom, R. G., Fountain, J. W. & Larson, S. M., 1967. Consolidated Lunar Atlas. Lunar and Planetary Laboratory, University of Arizona. Digital version by Douglass, E. & O'Dell, M. S., 2003. Houston, Lunar and Planetary Institute.

Kumar, P. S., 2005. Structural effects of meteorite impact on basalt: Evidence from Lonar crater, India. Journal of Geophysical Research 110, B12402, doi:10.1029/2005JB003662.

Kumar, P. S. & Kring, D. A., 2008. Impact fracturing and structural modification of sedimentary rocks at Meteor Crater, Arizona. Journal of Geophysical Research – Planets 113, E09009, doi:10.1029/2008JE003115.

Kuzmin, R. O., 1980. Morphology of fresh Martian craters as an indicator of the depth of the upper boundary of the ice-bearing permafrost: a photogeologic study. Lunar and Planetary Science XI. Lunar and Planetary Institute, Houston, 585–586.

Kuzmin, R. O., Bobina, N. N., Zabalueva, E. V. & Shashkina, V. P., 1988a. Inhomogeneities in the upper levels of the Martian cryolithosphere. Lunar and Planetary Science XIX. Lunar and Planetary Institute, Houston, 655–656.

Kuzmin, R. O., Bobina, N. N., Zabalueva, E. V. & Shashkina, V. P., 1988b. Mars: Estimation of the relative ice content in upper layers of the permafrost. Lunar and Planetary Science XIX. Lunar and Planetary Institute, Houston, 657–658.

Lana, C., Romano, R., Reimold, U. & Hippertt, J., 2006. Collapse of large complex impact craters: implications from the Araguainha impact structure, central Brazil. Geology 34 (1), 9–12.

Lana, C., Souza Filho, C. R., Marangoni, Y. R., Yokoyama, E., Trindade, R. I. F., Tohver, E. & Reimold, W. U., 2007. Insights into the morphology, geometry, and post-impact erosion of the Araguainha peak-ring structure, central Brazil. Geological Society of America Bulletin 119 (9/10), 1135–1150, doi:10.1130/B26142.1.

Langenhorst, F. & Deutsch, A., 1998. Minerals in terrestrial impact structures and their characteristic features. In: Marfunin, A. S. (Ed.), Advanced Mineralogy 3, pp. 95–119, Berlin Heidelberg, Springer-Verlag.

Laurén, L., Lehtovaara, J., Boström, R. & Tynni, R., 1978. On the Geology and the Cambrian Sediments of the Circular Depression at Söderfjärden, Western Finland. Geological Survey of Finland, Bulletin 297, 81 pp.

Legrand, C. & Chevalley, P., 2006. Virtual Moon Atlas, Pro Version 3.5 2006-11-4.

Leighton, R. B., Horowitz, N. H., Murray, B. C., Sharp, R. P., Herriman, A. H., Young, A. T., Smith, B. A., Davies, M. E. & Leovy, C. B., 1969. Mariner 6 and 7 television pictures: Preliminary analysis. Science 166 (3901), 49–67.

Leonard, G. J. & Tanaka, K. L., 1993. Hellas basin, Mars: formation by oblique impact. Lunar and Planetary Science XXIV. Lunar and Planetary Institute, Houston, 867–868.

Leonard, G. J. & Tanaka, K. L., 2001. Geologic Map of the Hellas Region of Mars − Map I-2694. U.S. Department of the Interior, U.S. Geological Survey.

Leonardi, P., 1976. Volcanoes and Impact Craters on the Moon and Mars. Amsterdam – Oxford – New York, Elsevier Scientific Publishing Company, 463 pp.

Lodders, K. & Fegley, B. Jr., 1998. The Planetary Scientist's Companion. New York, Oxford University Press, 371 pp.

Mackwell, S. J., Zimmerman, M. E. & Kohlstedt, D. L., 1998. High-temperature deformation of dry diabase with application to tectonics on Venus. Journal of Geophysical Research 103 (B1), 975–984.

Malin, M. C. & Edgett, K. S., 2000. Sedimentary rocks of early Mars. Science 290, 1927–1937.

Marinova, M. M., Aharonson, O. & Asphaug, E., 2008. Mega-impact formation of the Mars hemispheric dichotomy. Nature 453, 1216–1219, doi:10.1038/nature07070.

Mark, K., 1987. Meteorite Craters. Tucson, The University of Arizona Press, 288 pp.

Martin, L. J. & Zurek, R. W., 1993. An analysis of the history of dust activity on Mars. Journal of Geophysical Research 98, 3221–3246.

Marvin, U. B., 2006. Meteorites in history: an overview from the Renaissance to the 20th century. In: McCall, G. J. H., Bowden, A. J. & Howarth, R. J. (Eds.), The History of Meteoritics and Key Meteorite Collections: Fireballs, Falls and Finds, pp. 15–71. Special Publication 256. London, The Geological Society.

Marvin, U. B., 2007. Ernst Florens Friedrich Chladni (1756–1827) and the origins of modern meteorite research. Meteoritics & Planetary Science 42 (9), Supplement, B3–B68.

Masaitis, V. L., 1999. Impact structures of northeastern Eurasia: the territories of Russia and adjacent countries. Meteoritics & Planetary Science 34, 691–711.

Master, S., 2001. A possible Holocene impact structure in the Al ‘Amarah marshes near the Tigris-Eufrates confluence, southern Iraq. Meteoritics & Planetary Science 36 (9), Supplement, A124.

Master, S. & Pandit, M. K., 1999. New evidence for an impact origin of the Ramgarh structure, Rajasthan, India. Meteoritics & Planetary Science 34 (4), Supplement, A79.

Master, S. & Woldai, T., 2004. The Umm al Binni structure, in the Mesopotamian Marshlands of Southern Iraq, as a Postulated Late Holocene Meteorite Impact Crater: Geological setting and New Landsat ETM+ and Aster Satellite Imagery. Economic Geology Research Institute, Hugh Allsopp Laboratory, University of Witwatersrand, Johannesburg, Information Circular No. 382, 21 pp.

McCall, G. J. H., 1965. The caldera analogy in selenology. Geological Problems in Lunar Research. Annals of the New York Academy of Sciences 123 (2), 843–875.

McDonald, M. A., Melosh, H. J. & Gulick, S. P., 2008. Oblique impacts and peak ring position: Venus and Chicxulub. Geophysical Research Letters 35, L07203, doi:10.1029/2008GL033346.

McDowell, J., 2004. Lunar nomenclature. http://host.planet4589.org/astro/lunar/, last accessed October 30th, 2008. (an electronic and updated version of Andersson & Whitaker, 1982)

McEwen, A. S., Moore, J. M. & Shoemaker, E. M., 1997. The Phanerozoic impact cratering rate: evidence from the farside of the Moon. Journal of Geophysical Research 102 (E4), 9231–9242.

McGill, G. E., 1993. Wrinkle ridges, stress domains, and kinematics of Venusian plains. Geophysical Research Letters 20 (21), 2407–2410.

McKinnon, W. B., 1978. An investigation into the role of plastic failure in crater modification. Proceedings of the 9th Lunar and Planetary Science Conference. Lunar and Planetary Institute, Houston, 3965–3973.

McKinnon, W. B., 1981. Application of ring tectonic theory to Mercury and other solar system bodies. In: Schultz, P. H. & Merrill, R. B. (Eds.), Multi-ring Basins: Formation and Evolution. Proceedings of the 12th Lunar and Planetary Science Conference. Geochimica et Cosmochimica Acta, Supplement 12, part A, 259–273.

McKinnon, W. B. & Melosh, H. J., 1980. Evolution of planetary lithospheres: evidence from multiringed structures on Ganymede and Callisto. Icarus 44, 454–471.

McKinnon, W. B., Zahnle, K. J., Ivanov, B. A. & Melosh, H. J., 1997. Cratering on Venus: models and observations. In: Bougher, S. W., Hunten, D. M. & Phillips, R. J. (Eds.), Venus II – Geology, Geophysics, Atmosphere, and Solar Wind Environment, pp. 969–1014. Tucson, The University of Arizona Press.

McSween, H. Y. Jr., 1999. Meteorites and Their Parent Planets, 2nd edition. Cambridge University Press, 310 pp.

Melosh, H. J., 1976. On the origin of fractures radial to lunar basins. Proceedings of the 7th Lunar Science Conference. Lunar and Planetary Institute, Houston, 2967–2982.

Melosh, H. J., 1978. The tectonics of mascon loading. Proceedings of the 9th Lunar and Planetary Science Conference. Lunar and Planetary Institute, Houston, 3513–3525.

Melosh, H. J., 1979. Acoustic fluidization: a new geologic process? Journal of Geophysical Research 84, 7513–7520.

Melosh, H. J., 1989. Impact cratering: a geologic process. New York, Oxford University Press, 245 pp.

Melosh, H. J. & Dzurisin, D., 1978. Mercurian global tectonics: a consequence of tidal despinning? Icarus 35, 227–236.

Melosh, H. J. & Gaffney, E. S., 1983. Acoustic fluidization and the scale dependence of impact crater morphology. Proceedings of the 13th Lunar and Planetary Science Conference, part 2. Journal of Geophysical Research 88, Supplement, A830–A834.

Melosh, H. J. & Ivanov, B. A., 1999. Impact crater collapse. Annual Review of Earth and Planetary Sciences 27, 385–415.

Melosh, H. J. & McKinnon, W. B., 1978. The mechanics of ringed basin formation. Geophysical Research Letters 5 (11), 985–988.

Melosh, H. J. & McKinnon, W. B., 1988. The tectonics of Mercury. In: Vilas, F., Chapman, C. R. & Matthews, M. S. (Eds.), Mercury, pp. 374–400. Tucson, The University of Arizona Press.

Mest, S. C. & Crown, D. A., 1986. Relationships between wrinkle ridges and craters in Hesperia Planum: constraints on the timing of ridge formation. Lunar and Planetary Science XXVII. Lunar and Planetary Institute, Houston, 869–870.

Miller, D. J., Barnash, A. N., Bray, V. J. Turtle, E. P. Helfenstein, P., Squyres, S. W. & Rathbun, J. A., 2007. Interactions between impact craters and tectonic fractures on Enceladus and Dione. Ices, Oceans, and Fire: Satellites of the Outer Solar System. Lunar and Planetary Institute, Houston, abstract #6007 (CD-ROM).

Miyamoto, S., 1965. Morphological features of the libratory region of the Moon. Geological Problems in Lunar Research. Annals of the New York Academy of Sciences 123 (2), 776–796.

Mohit, P. S. & Phillips, R. J., 2007. Viscous relaxation on early Mars: A study of ancient impact basins. Geophysical Research Letters 34, L21204, doi:10.1029/2007GL031252.

Moore, J. M. & Wilhelms, D. E., 2001. Hellas as a possible site of ancient ice-covered lakes. Lunar and Planetary Science XXXII. Lunar and Planetary Institute, Houston, abstract #1446 (CD-ROM).

Morota, T. & Furumoto, M., 2003. Asymmetrical distribution of rayed craters on the Moon. Earth and Planetary Science Letters 206, 315–323.

Morrison, G. G., 1984. Morphological features of the Sudbury structure in relation to an impact origin. In: Pye, E. G., Naldrett, A. J. & Giblin, P. E. (Eds.), The Geology and Ore Deposits of the Sudbury Structure, pp. 513–520. Special Volume 1, Ontario Geological Survey.

Mouginis-Mark, P. J., 1979. Martian fluidized crater morphology: variations with crater size, latitude, altitude and target material. Journal of Geophysical Research 84 (B14), 8011–8022.

Mouginis-Mark, P. J., 1980. Why are there different ejecta morphologies for Martian impact craters? Lunar and Planetary Science XI. Lunar and Planetary Institute, Houston, 756–758.

Mouginis-Mark, P. J. & Baloga, S. M., 2006. Morphology and geometry of the distal ramparts of Martian impact craters. Meteoritics & Planetary Science 41 (10), 1469–1482.

Mouginis-Mark, P. J. & Head, J. W., 1979. Emplacement of Martian rampart crater ejecta blankets: a morphological analysis. Lunar and Planetary Science X. Lunar and Planetary Institute, Houston, 870–872.

Mouginis-Mark, P. J., Garbeil, H., Boyce, J. M., Ui, C. S. E. & Baloga, S. M., 2004. Geometry of Martian impact craters: first results from an interactive software package. Journal of Geophysical Research 109, E08006, doi:10.1029/2003JE002147.

Murchie, S. L., Watters, T. R., Robinson, M. S., Head, J. W., Strom, R. G., Chapman, C. R., Solomon, S. C., McClintock, W. E., Prockter, L. M, Domingue, D. L. & Blewett, D. T., 2008. Geology of the Caloris basin, Mercury: a view from MESSENGER. Science 321, 73–76.

Murray, J. B. & Guest, J. E., 1970. Circularities of craters and related structures on Earth and Moon. Modern Geology 1, 149–159.

Murray, J. D., Spiegel, E. A. & Theys, J., 1969. Fluidization on the Moon (?). Comments on Astrophysics and Space Physics 1, 165–171.

Neumann, G. A., Zuber, M. T., Wieczorek, M. A., McGovern, P. J., Lemoine, F. G., & Smith, D. E., 2004. Crustal structure of Mars from gravity and topography. Journal of Geophysical Research 109, E08002, doi:10.1029/2004JE002262.

Nycz, J. C. & Hildebrand, A. R., 2003. Martian complex impact craters: a size and morphology progression, and a newly recognized structural element, the peripheral peak ring. Meteoritics & Planetary Science 38 (7), Supplement, A132.

Nycz, J. C. & Hildebrand, A. R., 2005. The peripheral peak ring: a complex impact crater morphologic feature probably related to crater rim collapse. Lunar and Planetary Science XXXVI. Lunar and Planetary Institute, Houston, abstract #2167 (CD-ROM).

Nycz, J. & Hildebrand, A., 2006. The peripheral peak ring as an indicator of strength contrasts in near surface layering on Mars. Impact Craters as Indicators for Planetary Environmental Evolution and Astrobiology, Östersund (Sweden), June 8–14, 2006.

Nycz, J. C. & Hildebrand, A., 2007. Constraining strength properties in Martian surface layers by modelling the peripheral peak ring impact crater morphology. Bridging the Gap II: Effect of Target Properties on the Impact Cratering Process. September 22–26, 2007, Saint-Hubert, Canada, LPI Contribution No. 1360, 83–84.

Oberbeck, V. R., 1971. A mechanism for the production of lunar crater rays. The Moon 2, 263–278.

Oberbeck, V. R. & Morrison, R. H., 1973. On the formation of the lunar herringbone pattern. Proceedings of the 4th Lunar Science Conference. Geochimica et Cosmochimica Acta, Supplement 4, vol. 1, 107–123.

Oberbeck V. R., Aoyagi, M. & Murray, J. B., 1972. Circularity of Martian craters. Modern Geology 3, 195–199.

Öhman, T., 2002. The Indications of Cratering Process in Saarijärvi Impact Crater, Northern Finland. Unpublished M.Sc. thesis, Institute of Geosciences, University of Oulu, Finland, 180 pp. (In Finnish, with an extended English abstract)

Öhman, T., 2007a. The Structural Control of Polygonal Impact Craters on Mars. Unpublished Lic.Phil. thesis, Department of Geosciences, University of Oulu, Finland, 105 pp.

Öhman, T., 2007b. The origin and tectonic modification of the Saarijärvi impact structure, northern Finland. Bridging the Gap II: Effect of Target Properties on the Impact Cratering Process. September 22–26, 2007, Saint-Hubert, Canada, LPI Contribution No. 1360, 85–86.

Öhman, T. & Raitala, J., 2005. Geochemistry of the dark veinlets in the granitoids from the Söderfjärden impact structure, Finland: preliminary results. Lunar and Planetary Science XXXVI. Lunar and Planetary Institute, Houston, abstract #1738 (CD-ROM).

Öhman, T., Pesonen, L. J., Elo, S., Uutela, A., Tuisku, P, & Raitala, J., 2003. The origin and evolution of the Saarijärvi impact structure. Meteoritics & Planetary Science 38 (7), Supplement, A52.

Öhman, T., Aittola, M., Kostama, V.-P, Kallo, M., & Raitala, J., 2007. The mechanics of polygonal impact formation. Bridging the Gap II: Effect of Target Properties on the Impact Cratering Process. September 22–26, 2007, Saint-Hubert, Canada. LPI Contribution No. 1360, 87–88.

Öhman T., Aittola, M., Kostama, V.-P., Korteniemi, J., & Raitala, J., 2008a. The control of target structure on the crater morphology on the Moon, Mars, and Venus – Evidence and implications. Large Meteorite Impacts and Planetary Evolution IV, August 17–21, 2008, Vredefort Dome, South Africa. LPI Contribution No. 1423, 166–167.

Öhman, T., Aittola, M., Kostama, V.-P., & Raitala, J., 2008b. The structural control of impact craters: evidence from the terrestrial planets. The 33rd International Geological Congress, August 6–14, 2008, Oslo, Norway (CD-ROM).

O'Keefe, J. D. & Ahrens, T. J., 1982. Cometary and meteorite swarm impact on planetary surfaces. Journal of Geophysical Research 87 (B8), 6668–6680.

O'Keefe, J. D. & Ahrens, T. J., 1993. Planetary cratering mechanics. Journal of Geophysical Research 98 (E9), 17011–17028.

O'Keefe, J. D. & Ahrens, T. J., 1999. Complex craters: Relationships of stratigraphy and rings to impact conditions. Journal of Geophysical Research 104 (E11), 27091–27104.

Ormö, J. & Lindström, M., 2000. When a cosmic impact strikes the sea bed. Geological Magazine 137, 67–80.

Ormö, J. & Muinonen, P., 2000. Impact craters as indicators for oceanic phases on Mars. Lunar and Planetary Science XXXI. Lunar and Planetary Institute, Houston, abstract #1266 (CD-ROM).

Ormö, J., Dohm, J. M., Ferris, J. C., Lepinette, A. & Fairén, A. G., 2004. Marine-target craters on Mars? An assessment study. Meteoritics & Planetary Science 39 (2), 333–346.

Orton, G., A'Hearn, M., Baines, K., Deming, D., Dowling, T., Goguen, J., Griffith, C., Hammel, H., Hoffmann, W., Hunten, D., Jewitt, D., Kostiuk, T., Miller, S., Noll, K., Zahnle, K., Achilleos, N., Dayal, A., Deutsch, L., Espenak, F., Esterle, P., Friedson, J., Fast, K., Harrington, J., Hora, J., Joseph, R., Kelly, D., Knacke, R., Lacy, J., Lisse, C., Rayner, J., Sprague, A., Shure, M., Wells, K., Yanamandra-Fisher, P., Zipoy, D., Bjoraker, G., Buhl, D., Golisch, W., Griep, D., Kaminski, C., Arden, C., Chaikin, A., Goldstein, J., Gilmore, D., Fazio, G., Kanamori, T., Lam, H., Livengood, T., MacLow, M.-M., Marley, M., Momary, T., Robertson, D., Romani, P., Spitale, J., Sykes, M., Tennyson, J., Wellnitz, D. & Ying, S.-W., 1995. Collision of comet Shoemaker-Levy 9 with Jupiter observed by the NASA Infrared Telescope Facility. Science 267, 1277–1282.

Osinski, G. R. & Spray, J. G., 2003. Transient crater formation and collapse: observations at the Haughton impact structure, arctic Canada. Workshop on Impact Cratering: Bridging the Gap Between Modeling and Observations. Lunar and Planetary Institute, Houston, abstract #8010 (CD-ROM).

Osinski, G. R. & Spray, J. G. 2005. Tectonics of complex crater formation as revealed by the Haughton impact structure, Devon Island, Canadian High Arctic. Meteoritics & Planetary Science 40 (12), 1813–1834.

Osterloo, M. M., Hamilton, V. E., Bandfield, J. L., Glotch, T. D., Baldridge, A. M., Christensen, P. R., Tornabene, L. L. & Anderson, F. S., 2008. Chloride-bearing materials in the southern highlands of Mars. Science 319, 1651–1654.

Papunen, H., 1973. Chemical composition and origin of the shock metamorphic rocks of the Sääksjärvi area, Finland. Bulletin of the Geological Society of Finland, no. 45, part 1, 29–34.

Park, R. G., 1997. Foundations of Structural Geology, 3rd edition. London, Chapman & Hall, 202 pp.

Parker, T. J., Clifford, S. M. & Banerdt, W. B., 2000. Argyre Planitia and the Mars global hydrologic cycle. Lunar and Planetary Science XXXI. Lunar and Planetary Institute, Houston, abstract #2033 (CD-ROM).

Passey, Q. R. & Melosh, H. J., 1980. Effects of atmospheric breakup on crater field formation. Icarus 42, 211–233.

Pearce, S. J. & Melosh, H. J., 1986. Terrace width variations in complex lunar craters. Geophysical Research Letters 13 (13), 1419–1422.

Pesonen, L. J., Elo, S., Lehtinen, M., Jokinen, T., Puranen, R. & Kivekäs, L., 1999. Lake Karikkoselkä impact structure, central Finland: new geophysical and petrographic results. In: Dressler, B. O. & Sharpton, V. L. (Eds.), Large Meteorite Impacts and Planetary Evolution II, pp. 131–147. Geological Society of America Special Paper 339.

Peterson, J. E., 1978a. Antipodal effects of major basin-forming impacts on Mars. Lunar and Planetary Science IX. Lunar and Planetary Institute, Houston, 885–886.

Peterson, J. E., 1978b. Volcanism in the Noachis–Hellas region of Mars, 2. Proceedings of the 9th Lunar and Planetary Science Conference. Lunar and Planetary Institute, Houston, 3411–3432.

Phillips, R. J., Arvidson, R. E., Boyce, J. M., Campbell, D. B., Guest, J. E., Schaber, G. G. & Soderblom, L. A., 1991. Impact craters on Venus: initial analysis from Magellan. Science 252, 288–297.

Phillips, R. J., Raubertas, R. F., Arvidson R. E., Sarkar, I. C., Herrick, R. R., Izenberg N. & Grimm, R. E., 1992. Impact craters and Venus resurfacing history. Journal of Geophysical Research 97, 15923–15948.

Pierazzo, E., 1999. Projectile melting in impact events: shape effects. Lunar and Planetary Science XXX. Lunar and Planetary Institute, Houston, abstract #1677 (CD-ROM).

Pierazzo, E. & Melosh, H. J., 2000a. Hydrocode modeling of oblique impacts: the fate of the projectile. Meteoritics & Planetary Science 35, 117–130.

Pierazzo, E. & Melosh, H. J., 2000b. Understanding oblique impacts from experiments, observations, and modeling. Annual Reviews of Earth and Planetary Sciences 28, 141–167.

Pierazzo, E., Kring, D. A. & Melosh, H. J., 1998. Hydrocode simulation of the Chicxulub impact event and the production of climatically active gases. Journal of Geophysical Research 103 (E12), 28607–28625.

Pike, R. J., 1967. Schroeter's rule and the modification of lunar crater impact morphology. Journal of Geophysical Research 72 (8), 2099–2106.

Pike, R. J., 1971. Genetic implications of the shapes of Martian and Lunar craters. Icarus 15, 384–395.

Pike, R. J., 1974a. Craters on Earth, Moon, and Mars: multivariate classification and mode of origin. Earth and Planetary Science Letters 22, 245–255.

Pike, R. J., 1974b. Depth/diameter relations of fresh lunar craters: revision from spacecraft data. Geophysical Research Letters 1 (7), 291–294.

Pike, R. J., 1976. Crater dimensions from Apollo data and supplemental sources. The Moon 15, 463–477.

Pike, R. J., 1977. Size-dependence in the shape of fresh impact craters on the Moon. In: Roddy, D. J., Pepin, R. O. & Merrill, R. B. (Eds.), Impact and Explosion Cratering, pp. 489–509. New York, Pergamon Press.

Pike, R., 1980a. Control of crater morphology by gravity and target type: Mars, Earth, Moon. Proceedings of the 11th Lunar and Planetary Science Conference. Lunar and Planetary Institute, Houston, 2159–2189.

Pike, R. J., 1980b. Formation of complex impact craters: evidence from Mars and other planets. Icarus 43, 1–19.

Pike, R. J., 1983. Large craters or small basins on the Moon. Lunar and Planetary Science XIV. Lunar and Planetary Institute, Houston, 610–611.

Pike, R. J., 1985. Some morphologic systematics of complex impact structures. Meteoritics 20 (1), 49–68.

Pike, R. J., 1988. Geomorphology of impact craters on Mercury. In: Vilas, F., Chapman, C. R. & Matthews, M. S. (Eds.), Mercury, pp. 165–273. Tucson, The University of Arizona Press.

Pike, R. J. & Spudis, P. D., 1987. Basin-ring spacing on the Moon, Mercury and Mars. Earth, Moon, and Planets 39, 129–194.

Pilkington, M. & Grieve, R. A. F., 1992. The geophysical signature of terrestrial impact craters. Reviews of Geophysics 30 (2), 161–181.

Plescia, J. B. & Saunders, R. S., 1979. The chronology of the Martian volcanoes. Proceedings of the 10th Lunar and Planetary Science Conference. Lunar and Planetary Institute, Houston, 2841–2859.

Poelchau, M. H., Kenkmann, T. & Kring, D. A., 2008. Structural aspects of Meteor Crater and their effect on cratering. Large Meteorite Impacts and Planetary Evolution IV, August 17–21, 2008, Vredefort Dome, South Africa. LPI Contribution No. 1423, 176–177.

Poelchau, M. H., Kenkmann, T. & Kring, D. A., 2009. Rim uplift and crater shape in Meteor Crater: the effects of target heterogeneities and trajectory obliquity: Journal of Geophysical Research 114, E01006, doi:10.1029/2008JE003235.

Pohn, H. A. & Offield, T. W., 1970. Lunar crater morphology and relative-age determination of lunar geologic units – Part 1. Classification. Geological Survey Research 1970, U.S. Geological Survey Professional Paper 700-C, pp. C153–C162.

Porco, C. C., Baker, E., Barbara, J., Beurle, K., Brahic, A., Burns, J. A., Charnoz, S., Cooper, N., Dawson, D. D., Del Genio, A. D., Denk, T., Dones, L., Dyudina, U., Evans, M. W, Giese, B., Grazier, K., Helfenstein, P., Ingersoll, A. P., Jacobson, R. A., Johnson, T. V., McEwen, A., Murray, C. D., Neukum, G., Owen, W. M., Perry, J., Roatsch, T., Spitale, J., Squyres, S., Thomas, P. C., Tiscareno, M., Turtle, E., Vasavada, A. R., Veverka, J., Wagner, R. & West, R., 2005. Cassini imaging science: initial results on Phoebe and Iapetus. Science 307, 1237–1242.

Prockter, L., Thomas, P., Robinson, M., Joseph, J., Milne, A., Bussey, B., Veverka, J. & Cheng, A., 2002. Surface expressions of structural features on Eros. Icarus 155, 75–93.

Purucker, M., Ravat, D., Frey, H., Voorhies, C., Sabaka, T., & Acuña, M., 2000. An altitude-normalized magnetic map of Mars and its interpretation. Geophysical Research Letters 27, 2449–2452.

Quaide, W. L. & Oberbeck, V. R., 1968. Thickness determinations of the lunar surface layer from lunar impact craters. Journal of Geophysical Research 73 (16), 5247–5270.

Quaide, W. L., Gault, D. E. & Schmidt, R. A., 1965. Gravitative effects on lunar impact structures. Geological Problems in Lunar Research. Annals of the New York Academy of Sciences 123 (2), 641–655.

Raitala, J., 1985. The bedrock of the Vaasa circular structure, western Finland. Earth, Moon, and Planets 33, 133–155.

Raitala, J., 1988. Superposed ridges of the Hesperia Planum area on Mars. Earth, Moon, and Planets 40, 71–99.

Ravine, M. A. & Grieve, R. A. F., 1986. An analysis of morphologic variation in simple lunar craters. Proceedings of the Seventeenth Lunar and Planetary Science Conference, Part 1. Journal of Geophysical Research 91 (B13), E75–E83.

Reimold, W. U., 2003. Impact cratering comes of age. Science 300, 1889–1890.

Reimold, W. U., Brandt, D., de Jong, R. & Hancox, J., 1996. Tswaing Meteorite Crater. Council for Geoscience, Geological Survey of South Africa, Popular Geoscience Series 1, 171 pp.

Reimold, W. U., Brandt, D. & Koeberl, C., 1998. Detailed structural analysis of the rim of a large, complex impact crater: Bosumtwi crater, Ghana. Geology 26 (6), 543–546.

Roddy, D. J., 1976. High-explosive cratering analogs for bowl-shaped, central uplift, and multiring impact craters. Proceedings of the 7th Lunar Science Conference. Lunar and Planetary Institute, Houston, 3027–3056.

Roddy, D. J., 1977a. Large-scale impact and explosion craters: comparisons of morphological and structural analogs. In: Roddy, D. J., Pepin, R. O. & Merrill, R. B. (Eds.), Impact and Explosion Cratering, pp. 185–246. New York, Pergamon Press.

Roddy, D. J., 1977b. Pre-impact conditions and and craterig processes at the Flynn Creek crater, Tennessee. In: Roddy, D. J., Pepin, R. O. & Merrill, R. B. (Eds.), Impact and Explosion Cratering, pp. 277–308. New York, Pergamon Press.

Roddy, D. J., 1978. Pre-impact geologic conditions, physical properties, energy calculations, meteorite and initial crater dimensions and orientations of joints, faults and walls at Meteor Crater, Arizona. Proceedings of the 9th Lunar and Planetary Science Conference. Lunar and Planetary Institute, Houston, 3891–3930.

Roddy, D. J. 1979. Structural deformation at the Flynn Creek impact crater, Tennessee: a preliminary report on deep drilling. Proceedings of the 10th Lunar and Planetary Science Conference. Lunar and Planetary Institute, Houston, 2519–2534.

Roddy, D. J. & Davis, L. K., 1977. Shatter cones formed in large-scale experimental explosion craters. In: Roddy, D. J., Pepin, R. O. & Merril, R. B. (Eds.), Impact and Explosion Cratering, pp. 715–750. New York, Pergamon Press.

Roddy, D. J., Boyce, J. M., Colton, G. W. & Dial, A. L. Jr., 1975. Meteor Crater, Arizona, rim drilling with thickness, structural uplift, diameter, depth, volume, and mass-balance calculations. Proceedings of the 6th Lunar Science Conference. Lunar and Planetary Institute, Houston, 2621–2644.

Roddy, D. J., Pepin, R. O. & Merrill, R. B. (Eds.), 1977. Impact and Explosion Cratering. New York, Pergamon Press, 1301 pp.

Rodríguez, J. A. P., Sasaki, S., Dohm, J. M., Tanaka, K. L., Strom, B., Kargel, J., Kuzmin, R., Miyamoto, H., Spray, J. G., Fairén, A. G., Komatsu, G., Kurita, K. & Baker, V., 2005. Control of impact crater fracture systems on subsurface hydrology, ground subsidence, and collapse, Mars. Journal of Geophysical Researdch 110, E06003, doi:10.1029/2004JE002365.

Ronca, L. B. & Salisbury, J. W., 1966. Lunar history as suggested by the circularity index of lunar craters. Icarus 5, 130–138.

Rossi, A. P., Baliva, A. & Piluso, E., 2003. New evidences of an impact origin for Temimichat crater, Mauritania. Lunar and Planetary Science XXXIV. Lunar and Planetary Institute, Houston, abstract #1882 (CD-ROM).

Saunders, R. S., Haines, E. I. & Conel, J. E., 1970. Morphology and origin of lunar craters. Polarforschung 40 (1–2), 33–53.

Schaber, G. G. & Boyce, J. M., 1977. Probable distribution of large impact basins on Venus: comparison with Mercury and the Moon. In: Roddy, D. J., Pepin, R. O. & Merril, R. B. (Eds.), Impact and Explosion Cratering, pp. 603–612. New York, Pergamon Press.

Schaber, G. G., Strom, R. G., Moore, H. J., Soderblom, L. A., Kirk, R. L., Chadwick, D. J., Dawson, D. D., Gaddis, L. R., Boyce, J. M. & Russell, J., 1992. Geology and distribution of impact craters on Venus: What are they telling us? Journal of Geophysical Research 97 (E8), 13257–13301.

Schaber G. G., Kirk, R. L. & Strom, R. G., 1998. Data base of impact craters on Venus based on analysis of Magellan radar images and altimetry data. U.S. Geological Survey, Open-File Report 98–104.

Schenk, P. & Sharpton, V. L., 1992. The simple-to-complex crater transition on Venus. Lunar and Planetary Science XXIII. Lunar and Planetary Institute, Houston, 1219–1220.

Scherler, D., Kenkmann, T. & Jahn, A., 2006. Structural record of an oblique impact. Earth and Planetary Science Letters 248, 43–53.

Schultz, P. H., 1976. Moon morphology. Austin, The University of Texas Press, 626 pp.

Schultz, P. H., 1978. Martian intrusions: possible sites and implications. Geophysical Research Letters 5 (6), 457–460.

Schultz, P. H., 1984. Impact basin control of volcanic and tectonic provinces on Mars. Lunar and Planetary Science XV. Lunar and Planetary Institute, Houston, 728–729.

Schultz, P. H., 1987. Impact velocity and changes in crater shape, morphology, and statistics. Lunar and Planetary Science XVIII. Lunar and Planetary Institute, Houston, 886–887.

Schultz, P. H., 1988. Cratering on Mercury: a relook. In: Vilas, F., Chapman, C. R. & Matthews, M. S. (Eds.), Mercury, pp. 274–335. Tucson, The University of Arizona Press.

Schultz, P. H., 1992. Atmospheric effects on ejecta emplacement and crater formation on Venus from Magellan. Journal of Geophysical Research 97 (E10), 16183–16248.

Schultz, P. H., 1998. Shooting the Moon: Understanding the history of lunar impact theories. Earth Sciences History 17 (2), 92–110.

Schultz, P. H., 2008. Structural geology: The buried record of Chicxulub. Nature Geoscience 1, 90–91, doi:10.1038/ngeo120.

Schultz, P. H. & Gault, D. E., 1979. Atmospheric effects on Martian ejecta emplacement. Journal of Geophysical Research 84 (B13), 7669–7687.

Schultz, P. H. & Gault, D. E., 1985a. Clustered impacts: experiments and implications. Journal of Geophysical Research 90 (B5), 3701-3732.

Schultz, P. H. & Gault, D. E., 1985b. The effect of projectile shape in cratering efficiency and crater profile in granular targets. Lunar and Planetary Science XVI. Lunar and Planetary Institute, Houston, 742–743.

Schultz, P. H. & Gault, D. E., 1986. Experimental evidence for non-proportional growth of large craters. Lunar and Planetary Science XVII. Lunar and Planetary Institute, Houston, 777–778.

Schultz, P. H. & Glicken, H., 1979. Impact crater and basin control of igneous processes on Mars. Journal of Geophysical Research 84, 8033–8047.

Schultz, P. H. & Lianza, R. E., 1992. Recent grazing impacts on the Earth recorded in the Rio Cuarto crater field, Argentina. Nature 355, 234–237.

Schultz, P. H. & Merrill, R. B. (Eds.), 1981. Multi-ring Basins: Formation and Evolution. Proceedings of the 12th Lunar and Planetary Science Conference. Geochimica et Cosmochimica Acta, Supplement 12, part A, 295 pp.

Schultz, P. H., Orphal, D., Miller, B., Borden, W. F. & Larson, S. A., 1981. In: Schultz, P. H. & Merrill, R. B. (Eds.), Multi-ring Basins: Formation and Evolution. Proceedings of

the 12th Lunar and Planetary Science Conference. Geochimica et Cosmochimica Acta, Supplement 12, part A, 181–195.

Schultz, P. H., Schultz, R. A. & Rogers, J., 1982. The structure and evolution of ancient impact basins on Mars. Journal of Geophysical Research 87, 9803–9820.

Schultz, P. H., Koeberl, C., Bunch, T., Grant, J. & Collins, W., 1994. Ground truth for oblique impact processes: new insight from the Rio Cuarto, Argentina, crater field. Geology 22, 889–892.

Schultz, R. A., 1985. Assessment of global and regional tectonic models for faulting in the ancient terrains of Mars. Journal of Geophysical Research 90, 7849–7860.

Schultz, R. A., 1989. Strike-slip faulting of ridged plains near Valles Marineris, Mars. Nature 341, 424–426.

Schultz, R. A., & Frey, H. V., 1990. A new survey of multiring impact basins on Mars. Journal of Geophysical Research 95 (B9), 14175–14189.

Scott, D. H. & Tanaka, K. L., 1986. Geologic Map of the Western Equatorial Region of Mars. Map I-1802-A. U.S. Geological Survey.

Scott, D. H., Diaz, J. M. & Watkins, J. A., 1977. Lunar farside tectonics and volcanism. Proceedings of the 8th Lunar and Planetary Science Conference. Lunar and Planetary Institute, Houston, 1119–1130.

Sharpton, V. L., 1994. Evidence from Magellan for unexpectedly deep complex craters on Venus. In: Dressler, B. O., Grieve, R. A. F. & Sharpton, V. L. (Eds.), Large Meteorite Impacts and Planetary Evolution, pp. 19–27. Geological Society of America Special Paper 293.

Sharpton, V. L. & Dressler, B. O., 2003. Excavation flow and central peak rings: Is there a connection? Workshop on impact cratering: Bridging the Gap Between Modeling and Observations. Lunar and Planetary Institute, Houston, abstract #8059 (CD-ROM).

Sheskin, D. J., 2004. Handbook of Parametric and Nonparametric Statistical Procedures, 3rd edition. Boca Raton, Chapman & Hall / CRC, 1193 pp.

Shoemaker, E. M., 1960. Penetration mechanics of high velocity meteorites, illustrated by Meteor Crater, Arizona. In: Kvale, A. & Metzger, A. (Eds.), Report of the 21st International Geological Congress, Norden, Part XVIII, Structure of the Earth's Crust and Deformation of Rocks, pp. 418–434. Copenhagen.

Shoemaker, E. M., 1962. Interpretation of lunar craters. In: Kopal, Z. (Ed.), Physics and Astronomy of the Moon, pp. 283–359. New York and London, Academic Press.

Shoemaker, E. M., 1963. Impact mechanics at Meteor Crater, Arizona. In: Middlehurst, B. M., Kuiper, G. P. (Eds.), The Moon, Meteorites and Comets, pp. 301–336. Chicago – London, The University of Chicago Press.

Shoemaker, E. M., 1977. Why study impact craters? In: Roddy, D. J., Pepin, R. O. & Merrill, R. B. (Eds.), Impact and Explosion Cratering, pp. 1–10. New York, Pergamon Press.

Smit, J. & Hertogen, J., 1980. An extraterrestrial event at the Cretaceous–Tertiary boundary. Nature 285, 198–200.

Smith, B. A., Soderblom, L., Beebe, R., Boyce, J., Briggs, G., Bunker, A., Collins, S. A., Hansen, C. J., Johnson, T. V., Mitchell, J. L., Terrile, R. J., Carr, M., Cook, A. F. II, Cuzzi, J., Pollack, J. B., Danielson, G. E., Ingersoll, A., Davies, M. E., Hunt, G. E., Masursky, H., Shoemaker, E., Morrison, D., Owen, T., Sagan, C., Veverka, J., Strom, R., Suomi, V. E., 1981. Encounter with Saturn: Voyager 1 imaging science results. Science 212, 163-191.

Smith, E. I., 1976. Comparison of the crater morphology–size relationship for Mars, Moon, and Mercury. Icarus 28, 543–550.

Smith, E. I. & Hartnell, J. A., 1978. Crater size–shape profiles for the Moon and Mercury: terrain effects and interplanetary comparisons. The Moon and the Planets 19, 479–511.

Soderblom, L. A. & Bell, J. F. III, 2008. Exploration of the Martian surface: 1992–2007. In: Bell, J. (Ed.), The Martian Surface – Composition, Mineralogy, and Physical Properties, pp. 3–19. Cambridge, Cambridge University Press.

Solomon, S. C., Smrekar, S. E., Bindschadler, D. L., Grimm, R. E., Kaula, W. M., McGill, G. E., Phillips, R. J., Saunders, R. S., Schubert, G. & Squyres, S. W., 1992. Venus tectonics – an overview of Magellan observations. Journal of Geophysical Research 97 (E8), 13199–13255.

Solomon, S. C., McNutt, R. L. Jr., Watters, T. R., Lawrence, D. J., Feldman, W. C., Head, J. W., Krimigis, S. M., Murchie, S. L., Phillips, R. J., Slavin, J. A. & Zuber, M. T., 2008. Return to Mercury: a global perspective on MESSENGER's first Mercury flyby. Science 321, 59–62.

Spray, J. G., Butler, H. R. & Thompson, L. M., 2004. Tectonic influences on the morphometry of the Sudbury impact structure: implications for terrestrial cratering and modeling. Meteoritics & Planetary Science 39 (2), 287–301.

Spudis, P. D., 1993. The Geology of Multi-ring Impact Basins. Cambridge, Cambridge University Press, 263 pp.

Spudis, P. D., 1995. Clementine laser altimetry and multi-ring basins on the Moon. Lunar and Planetary Science XXVI. Lunar and Planetary Institute, Houston, 1337–1338.

Spudis, P. D. & Adkins, C. D., 1996. Morphometry of basins on the Moon: new results from Clementine laser altimetry. Lunar and Planetary Science XXVII. Lunar and Planetary Institute, Houston, 1253–1254.

Spudis, P. D., Reisse, R. A. & Gillis, J. J., 1994. Ancient multiring basins on the Moon revealed by Clemetine laser altimetry. Science 266 (5192), 1848–1851.

Squyres, S. W., Wilhelms, D. E. & Moosman, A. C., 1987. Large-scale volcano − ground ice interactions on Mars. Icarus 70, 385–408.

Stearns, R. G., Wilson, C. W. Jr., Tiedemann, H. A., Wilcox, J. T. & Marsh, P. S., 1968. The Wells Creek structure, Tennessee. In: French, B. M. & Short, N. M. (Eds.), Shock Metamorphism of Natural Materials, pp. 323–337. Baltimore, Mono Book Corp.

Stefanick, M. & Jurdy, D. M., 1996. Venus coronae, craters and chasmata. Journal of Geophysical Research 101 (E2), 4637–4643.

Stöffler, D., 1972. Deformation and transformation of rock-forming minerals by natural and experimental shock processes. I. Behavior of minerals under shock compression. Fortschritte der Mineralogie 49, 50–113.

Stöffler, D., 1974. Deformation and transformation of rock-forming minerals by natural and experimental shock processes. II. Physical properties of shocked minerals. Fortschritte der Mineralogie 51 (2), 256–289.

Stöffler, D. & Langenhorst, F., 1994. Shock metamorphism of quartz in nature and experiment: I. Basic observation and theory. Meteoritics 29, 155–181.

Stokes, G. H., Evans, J. B. & Larson, S. M., 2002. Near-Earth asteroid search programs. In: Bottke, W., Cellino, A., Paolicchi, P. & Binzel, R. P. (Eds.), Asteroids III, pp. 45–54. Tucson, University of Arizona Press.

Strom, R. G. & Sprague, A. L., 2003. Exploring Mercury: The Iron Planet. Berlin, Springer-Verlag & Praxis Publishing, 216 pp.

Strom, R. G., Malin, M. C. & Leake, M. A., 1990. Geologic Map of the Bach (H-15) Quadrangle of Mercury. Atlas of Mercury, USGS Miscellaneous Investigations Series Map I-2015, 1:5,000,000 Geologic series.

Strom, R. G., Croft, S. K. & Barlow, N. G., 1992. The Martian impact crater record. In: Kieffer, H. H., Jakosky, B. M., Snyder, C. W. & Matthews, M. S. (Eds.), Mars, pp. 383–423. Tucson & London, The University of Arizona Press.

Strom, R. G., Schaber, G. G. & Dawson, D. D., 1994. The global resurfacing of Venus. Journal of Geophysical Research 99 (E5), 10899–10926.

Strom, R. G., Chapman, C. R., Merline, W. J., Solomon, S. C. & Head J. W. III, 2008. Mercury cratering record viewed from MESSENGER's first flyby. Science 321, 79–81.

Talvitie, J., Pernu, T. & Raitala, J., 1975. The circular Vaasa structure in the Baltic Shield, western Finland. Contribution #59, Department of Geophysics, University of Oulu, 15 pp.

Tanaka, K. L. & Leonard, G. J., 1995. Geology and landscape evolution of the Hellas region of Mars. Journal of Geophysical Research 100, 5407–5432.

Tanaka, K. L. & Scott, D. H., 1987. Geologic Map of the Polar Regions of Mars. Map I-1802-C. Scale 1:15,000,000. Department of the Interior, U. S. Geological Survey.

Tanaka, K. L., Scott, D. H. & Greeley, R., 1992. Global stratigraphy. In: Kieffer, H. H., Jakosky, B. M., Snyder, C. W. & Matthews, M. S. (Eds.), Mars, pp. 345–382. Tucson & London, The University of Arizona Press.

Tanaka, K. L., Senske, D. A., Price, M. & Kirk, R. L., 1997. Physiography, geomorphic/geologic mapping, and stratigraphy of Venus. In: Bougher, S. W., Hunten, D. M. & Phillips, R. J. (Eds.), Venus II – Geology, Geophysics, Atmosphere, and Solar Wind Environment, pp. 667–694. Tucson, The University of Arizona Press.

Tanaka, K. L., Kargel, J. S., MacKinnon, D. J., Hare, T. M. & Hoffman, N., 2002. Catastrophic erosion of Hellas basin rim on Mars induced by magmatic intrusion into volatile-rich rocks. Geophysical Research Letters 29 (8), doi 10.1029/2001GL013885.

Taylor, G. J. & Baloga, S. M., 2007. Regolith evolution on Mars: the preservation of ancient aqueous alteration products. Lunar and Planetary Science XXXVIII. Lunar and Planetary Institute, Houston, abstract #1485 (CD-ROM).

Taylor, G. J., Warren, P., Ryder, G., Delano, J., Pieters, C. & Lofgren, G., 1991. Lunar rocks. In: Heiken, G. H., Vaniman, D. T. & French, B. M. (Eds.), Lunar Sourcebook – a User's Guide to the Moon, pp. 183–284. Cambridge University Press.

Tazieff, H., 1965. Convective origin of lunar craters. Geological Problems in Lunar Research. Annals of the New York Academy of Sciences 123 (2), 526–527.

Thomas, C., Head, J. W., and the Galileo SSI team, 1998. Morphology of Byblus Sulcus, Ganymede from Galileo SSI data. Lunar and Planetary Science XXIX. Lunar and Planetary Institute, Houston, abstract #1897 (CD-ROM).

Thomas, P. G. & Allemand, P., 1993. Quantitative analysis of the extensional tectonics of Tharsis bulge, Mars: geodynamic implications. Journal of Geophysical Research 98 (E7), 13097–13108.

Thomas, P. G. & Masson, P. H., 1984. Geology and tectonics of the Argyre area on Mars: comparisons with other basins in the solar system. Earth, Moon, and Planets 31, 25–42.

Thomas, P. C., Veverka, J., Bell, J. F. III, Clark, B. E., Carcich, B., Joseph, J., Robinson, M., McFadden, L. A., Malin, M. C., Chapman, C. R., Merline, W. & Murchie, S., 1999. Mathilde: size, shape, and geology. Icarus 140, 17–27, doi:icar.1999.6121.

Thompson, T. W., Campbell, B. A., Ghent, R. R. & Hawke, B. R., 2009. Rugged crater ejecta as a guide to megaregolith thickness in the southern nearside of the Moon. Geology 37 (7), 655–658, doi:10.1130/G25565A.1.

Trask, N. J. & Rowan, L. C., 1967. Lunar Orbiter photographs: some fundamental observations. Science 158 (3808), 1529–1535.

Trenc, N., Morgan, K. M., Donovan, R. N. & Busbey, A. B., 1999. Remote sensing analysis of selected terrestrial impact craters and a suspected impact structure in South Korea using space shuttle photographs. Geologia Croatica 52 (2), 203–215.

Turtle, E. P., Pierazzo, E., Collins, G. S., Osinski, G. R., Melosh, H. J., Morgan, J. V. & Reimold, W. U., 2005. Impact structures: What does crater diameter mean? In: Kenkmann, T., Hörz, F. & Deutsch, A. (Eds.), Large Meteorite Impacts III, pp. 1–24. Geological Society of America Special Paper 384.

Vaniman, D. T., Dietrich, J., Taylor, G. J. & Heiken, G. H., 1991a. Exploration, samples, and recent concepts of the Moon. In: Heiken, G. H., Vaniman, D. T. & French, B. M. (Eds.), Lunar Sourcebook – a User's Guide to the Moon, pp. 5–26. Cambridge University Press.

Vaniman, D. T., Reedy, R., Heiken, G. H, Olhoeft, G. & Mendell, W., 1991b. The Lunar environment. In: Heiken, G. H., Vaniman, D. T. & French, B. M. (Eds.), Lunar Sourcebook – a User's Guide to the Moon, pp. 27–60. Cambridge University Press.

Vervack, R. J. & Melosh, H. J., 1992. Wind interaction with falling ejecta: origin of the parabolic features on Venus. Geophysical Research Letters 19 (6), 525–528.

Veverka, J., Thomas, P., Harch, A., Clark, B., Bell, J. F. III, Carcich, B., Joseph, J., Chapman, C., Merline, W., Robinson, M., Malin, M., McFadden, L. A., Murchie, S., Hawkins, S. E. III, Farquhar, R., Izenberg, N. & Cheng, A., 1997. NEAR's Flyby of 253 Mathilde: images of a C Asteroid. Science 278, 2109–2114, doi:10.1126/science.278.5346.2109.

Vickery, A. M. & Melosh, H. J., 1991. Production of impact melt in craters on Venus, Earth, and the Moon. Lunar and Planetary Science XXII. Lunar and Planetary Institute, Houston, 1443–1444.

Vilas, 1999. Mercury. In: Beatty, J. K., Collins Petersen, C. & Chaikin, A. (Eds.), The New Solar System, 4th edition, pp. 87–96. Sky Publishing Corporation & Cambridge University Press.

Wada, K. & Barnouin-Jha, O. S., 2006. The formation of fluidized ejecta on Mars by granular flows. Meteoritics & Planetary Science 41 (10), 1551–1569.

Watters, T. R., Leuschen, C. J., Plaut, J. J, Picardi, G., Safaeinili, A., Clifford, S. M., Farrell, W. M., Ivanov, A. B., Phillips, R. J. & Stofan, E. R., 2006. MARSIS radar sounder evidence of buried basins in the northern lowlands of Mars. Nature 444, 905–908, doi:10.1038/nature05356.

Watters, W. A., 2006. Structure of polygonal impact craters at Meridiani Planum, Mars, and a model relating target structure to crater shape. Lunar and Planetary Science XXXVII. Lunar and Planetary Institute, Houston, abstract #2163 (CD-ROM).

Watters, W. & Zuber, M., 2007. Relating polygonal crater morphology, tectonic setting and shallow crustal structure on Mars: a machine vision approach (abstract #EGU2007-A-04664). European Geosciences Union General Assembly, Vienna, Austria, 15–20 April 2007.

Watters, W. A. & Zuber, M. T., 2009. Relating target properties to the planimetric shape of simple impact craters. Lunar and Planetary Science XXXX. Lunar and Planetary Institute, Houston, abstract #2556 (CD-ROM).

Wegener, A., 1975. The origin of lunar craters. The Moon 14, 211–236. (A translation of: Die Entstehung der Mondkrater, originally published in 1921.)

Weitz, C. M., 1993. Impact craters. In: Ford, J. P., Plaut, J. J., Weitz, C. M., Farr, T. G., Senske, D. A., Stofan, E. R., Michaels, G. & Parker, T. J., Guide to Magellan Image Interpretation, JPL Publication 93-24, pp. 75–92. Pasadena, Jet Propulsion Laboratory.

Wells, R. A., Fielder, G. & Öpik, E. J., 1967. Martian and lunar craters. Science 155, 354–356.

Werner, S. C. 2008. The early martian evolution – constraints from basin formation ages. Icarus 195, 45–60, doi:10.1016/j.icarus.2007.12.008.

Whitehead, J., Grieve, R. A. F., Garvin, J. B. & Spray, J. G., 2003. The dependence of target properties upon fresh crater morphologies on Mars. Third International

Conference on Large Meteorite Impacts. Lunar and Planetary Institute, Houston, abstract #4086 (CD-ROM).

Wichman, R. W. & Schultz, P. H., 1989. Sequence and mechanisms of deformation around the Hellas and Isidis impact basins on Mars. Journal of Geophysical Research 94, 17333–17357.

Wieland, F., Gibson, R. L. & Reimold, W. U., 2004. Field studies in the central uplift of the Vredefort impact structure. Lunar and Planetary Science XXXV. Lunar and Planetary Institute, Houston, abstract #1011 (CD-ROM).

Wilhelms, D. E., 1973. Comparison of Martian and lunar multiringed circular basins. Journal of Geophysical Research 78 (20), 4084–4095.

Wilhelms, D. E., 1976. Secondary impact craters of lunar basins. Proceedings of the 7th Lunar Science Conference. Lunar and Planetary Institute, Houston, 2883–2901.

Wilhelms, D. E., 1987. The Geologic History of the Moon. USGS Professional Paper 1348, Washington, United States Printing Office, 302 pp.

Wilhelms, D. E., 1993. To a Rocky Moon – a Geologists History of Lunar Exploration. Tucson, The University of Arizona Press, 477 pp.

Wilhelms, D. E. & Squyres, S. W., 1984. The martian hemispheric dichotomy may be due to a giant impact. Nature 309, 138–140.

Wilhelms, D. E., Hodges, C. A. & Pike, R. J., 1977. Nested-crater model of lunar ringed basins. In: Roddy, D. J., Pepin, R. O. & Merrill, R. B. (Eds.), Impact and Explosion Cratering, pp. 539–562. New York, Pergamon Press.

Wilhelms, D. E., Oberbeck, V. R. & Aggarwal, H. R., 1978. Size-frequency distributions of primary and secondary lunar impact craters. Proceedings of the 9th Lunar and Planetary Science Conference. Lunar and Planetary Institute, Houston, 3735–3762.

Williams, D. A. & Greeley, R., 1994. Assessment of antipodal-impact terrains on Mars. Icarus 110, 196–202.

Williams, K. K. & Greeley, R., 1997. The effect of lunar crustal thickness on the morphologic transition from central peak to peak-ring craters. Lunar and Planetary Science XXVIII. Lunar and Planetary Institute, Houston, abstract #1080 (CD-ROM).

Williams, K. K. & Zuber, M. T., 1998. Measurement and analysis of lunar basin depths from Clementine altimetry. Icarus 131 (1), 107–122.

Wilson, C. W. Jr. & Stearns, R. G., 1968. Geology of the Wells Creek Structure, Tennessee. State of Tennessee, Department of Conservation, Division of Geology, Bulletin 68. Nashville, State of Tennessee, Department of Conservation, 236 pp.

Wood, C. A., 2003. The Modern Moon – a Personal View. Cambridge, Sky Publishing Corporation, 209 pp.

Wood, C. A. & Andersson, L., 1978. New morphometric data for fresh lunar craters. Proceedings of the 9th Lunar and Planetary Science Conference. Lunar and Planetary Institute, Houston, 3669–3689.

Wood, C. A. & Head, J. W., 1976. Comparison of impact basins on Mercury, Mars and the Moon. Proceedings of the 7th Lunar Science Conference. Lunar and Planetary Institute, Houston, 3629–3651.

Wood, C. A., Head, J. W. & Cintala, M. J., 1977. Crater degradation on Mercury and the Moon: clues to surface evolution. Proceedings of the 8th Lunar Science Conference. Lunar and Planetary Institute, Houston, 3503–3520.

Wood, C. A., Head, J. W. & Cintala, M. J., 1978. Interior morphology of fresh Martian craters: the effects of target characteristics. Proceedings of the 9th Lunar and Planetary Science Conference. Lunar and Planetary Institute, Houston, 3691–3709.

Wrobel, K., Schultz, P. & Crawford, D., 2006. An atmospheric blast/thermal model for the formation of high-latitude pedestal craters. Meteoritics & Planetary Science 41 (10), 1539–1550.

Wünnemann, K. & Ivanov, B. A., 2003. Numerical modelling of the impact crater depth–diameter dependence in an acoustically fluidized target. Planetary and Space Science 51, 831–845.

Zimmermann, R. A. & Amstutz, G. C., 1965. The polygonal structure at Decaturville, Missouri: new tectonic observations. Neues Jahrbuch für Mineralogie, Monatshefte, Heft 9-11, 288–307.

Zuber, M. T., Smith, D. E., Lemoine, F. G. & Neumann, G. A., 1994. The shape and internal structure of the Moon from Clementine mission. Science 266 (5192), 1839–1843.

Zuber, M. T., Smith, D. E., Cheng, A. F., Garvin, J. B., Aharonson, O., Cole, T. D., Dunn, P. J., Guo, Y., Lemoine, F. G., Neumann, G. A., Rowlands, D. D. & Torrence, M. H., 2000. The shape of 433 Eros from the NEAR-Shoemaker laser rangefinder. Science 289, 2097–2101, doi:10.1126/science.289.5487.2097.

Appendix 1. Basic data of the successful missions to the Moon. Compiled from data on NASA lunar exploration internet site: http://nssdc.gsfc.nasa.gov/planetary/lunar/ accessed on July 6th, 2009, with additional data from Lodders and Fegley (1998). Asterisk indicates currently (July 2009) active missions.

Launch year	Name	Type	Country	Mission outline
1959	Luna 1	flyby	USSR	First lunar flyby, confirmed solar wind
1959	Pioneer 4	flyby	USA	Partial succes
1959	Luna 2	impact	USSR	First spacecraft to impact the Moon
1959	Luna 3	flyby	USSR	First images from the far side
1962	Ranger 4	impact	USA	Second spacecraft to impact the Moon
1962	Ranger 5	flyby	USA	Partial success, attempted impact
1964	Ranger 7	impact	USA	4308 images, up to 0.5 m resolution
1965	Ranger 8	impact	USA	7137 images, up to 1.5 m resolution
1965	Ranger 9	impact	USA	5814 images, up to 0.3 m resolution
1965	Zond 3	flyby	USSR	Images from the far side
1966	Luna 9	lander	USSR	First lander, four surface panoramas
1966	Luna 10	orbiter	USSR	Magnetic and gravity field, gamma spectrometry
1966	Surveyor 1	lander	USA	11 240 images from the surface
1966	Lunar Orbiter I	orbiter	USA	42 high resolution and 187 medium resolution images
1966	Luna 11	orbiter	USSR	Photography
1966	Luna 12	orbiter	USSR	Photography, up to 14.9–19.8 m resolution
1966	Lunar Orbiter II	orbiter	USA	202 high resolution and 209 medium resolution images
1966	Luna 13	lander	USSR	Surface panoramas
1967	Lunar Orbiter III	orbiter	USA	477 high resolution and 149 medium resolution images
1967	Surveyor 3	lander	USA	6315 images from the surface
1967	Lunar Orbiter IV	orbiter	USA	419 high resolution and 127 medium resolution images covering 99% of the near side up to 58 m resolution
1967	Explorer 35	orbiter	USA	Magnetic field, particle data
1967	Lunar Orbiter V	orbiter	USA	633 high resolution and 211 medium resolution images up to 2 m resolution
1967	Surveyor 5	lander	USA	19 118 images from the surface, soil composition
1967	Surveyor 6	lander	USA	29 952 images from the surface, soil composition
1968	Surveyor 7	lander	USA	20 993 images from the surface, trenches, highland soil composition
1968	Luna 14	orbiter	USSR	Gravity field, particle data
1968	Zond 5	flyby	USSR	Photography, biological samples returned to Earth
1968	Zond 6	flyby	USSR	Panchromatic photography, biological samples returned to Earth
1968	Apollo 8	manned orbiter	USA	First manned lunar orbital flight, photography

▼

Launch year	Name	Type	Country	Mission outline
1969	Apollo 10	manned orbiter	USA	Descent to 14 km from the surface, photography
1969	Apollo 11	manned lander and orbiter	USA	First manned landing, 21.55 kg of samples, seismometry, photography
1969	Zond 7	flyby	USSR	Colour photography
1969	Apollo 12	manned lander and orbiter	USA	Landing next to Surveyor 3, 34.35 kg of samples, seismometry, magnetometry, photography, multispectral orbital photography
1970	Apollo 13	manned flyby	USA	Partial success, photography
1970	Luna 16	lander, sample return	USSR	101 g of samples, temperature and radiation data
1970	Zond 8	flyby	USSR	Photography up to 100 m resolution
1970	Luna 17 / Lunokhod 1	rover	USSR	10.5 km traverse, >20 000 TV images, x-ray spectrometry
1971	Apollo 14	manned lander and orbiter	USA	42.28 kg of samples, active seismometry, magnetometry, photography
1971	Apollo 15	manned lander, rover and orbiter	USA	77.31 kg of samples, 27.9 km traverse on first manned lunar rover, seismometry, magnetometry, heat flow, laser altimetry, orbital gamma spectrometry, photography
1971	Luna 19	orbiter	USSR	Gravity field, photography, radiation environment
1972	Luna 20	lander, sample return	USSR	30 g of samples, surface photography.
1972	Apollo 16	manned lander, rover and orbiter	USA	95.71 kg of samples, 27 km traverse on rover, active seismometry, magnetometry, heat flow, laser altimetry, orbital gamma spectrometry, x-ray fluorescence, photography
1972	Apollo 17	manned lander, rover and orbiter	USA	110.52 kg of samples, 30 km traverse on rover, active seismometry, gravimetry, heat flow, surface electrical properties, laser altimetry, orbital IR radiometry, radar, photography
1973	Luna 21 / Lunokhod 2	rover	USSR	37 km traverse, >80 000 TV images, magnetometry, laser ranging
1973	Luna 22	orbiter	USSR	Magnetic and gravity field, surface composition, photography
1974	Luna 23	lander	USSR	Landed safely but sample return failed
1976	Luna 24	lander, sample return	USSR	170.1 g of samples.
1989	Galileo	flyby	USA	Two flybys, multispectral CCD photography
1990	Hiten (Muses-A)	orbiter	Japan	Mainly a technological experiment
1994	Clementine	orbiter	USA	Nearly global CCD UVVIS and IR photography, laser altimetry, bistatic radar
1997	Lunar Prospector	orbiter	USA	Neutron and gamma spectrometry, magnetometry, electron reflectrometry, alpha particle spectrometry, gravity field

▼

Launch year	Name	Type	Country	Mission outline
2003	SMART-1	orbiter	ESA	Mainly a technological experiment, x-ray spectrometry, VIS/IR spectrometry, photography
2007	Kaguya (SELENE)	orbiter	Japan	Laser altimetry, x-ray fluoresecence spectrometry, gamma spectrometry, magnetometry, radar, HDTV photography
2007	Chang'e 1	orbiter	China	Laser altimetry, x-ray and gamma spectrometry, radiometry, stereo photography
2008	Chandrayaan 1*	orbiter, impact	India	Laser altimetry, x-ray fluorescence and IR spectrometry, spectral imaging, radar, photography
2009	Lunar Reconnaissance Orbiter*	orbiter	USA	Laser altimetry, neutron spectrometry, radiometry, Lyman–Alpha mapping, radiation environment, 1–100 m resolution UV and visual photography
2009	Lunar CRater Observing and Sensing Satellite (LCROSS)*	impact	USA	Launched with LRO. Launch rocket upper stage impact will be monitored by LCROSS VIS and IR spectrometry, photography and radiometry, followed by LCROSS impact.

Appendix 2. Basic data of the successful missions to Mars. Modified after a table in NASA's Mars Exploration Program internet site: http://mars.jpl.nasa.gov/missions/log/ accessed on October 16th, 2008. Asterisk indicates currently (July 2009) active missions.

Launch year	Name	Type	Country	Mission outline
1964	Mariner 4	flyby	USA	Returned 21 images
1969	Mariner 6	flyby	USA	Returned 75 images
1969	Mariner 7	flyby	USA	Returned 126 images
1971	Mars 3	orbiter, lander	USSR	Orbiter obtained approximately 8 months of data and lander landed safely, but returned only 20 s of data
1971	Mariner 9	orbiter	USA	Returned 7329 images
1973	Mars 5	orbiter	USSR	Returned 60 images; only lasted 9 days
1973	Mars 6	orbiter, (lander)	USSR	Occultation experiment produced data, lander failure on descent
1975	Viking 1	orbiter, lander	USA	Located landing site for lander and first fully successful landing on Mars
1975	Viking 2	orbiter, lander	USA	Returned 16 000 images and extensive atmospheric data and soil experiments
1988	Phobos 2	orbiter, (lander)	USSR	Lost near Phobos, only 37 images and limited other data returned
1996	Mars Global Surveyor	orbiter	USA	More images than all earlier Mars missions combined, laser altimetry
1997	Mars Pathfinder	lander	USA	Technology experiment, rover lasting 5 times longer than warranty
2001	Mars Odyssey*	orbiter	USA	High resolution visual and infrared images of Mars
2003	Mars Express* / Beagle 2	orbiter, (lander)	ESA	Stereo colour imaging of Mars in detail, lander lost on arrival
2003	Mars Exploration Rover – Spirit*	lander	USA	Rover lasting >15 times longer than warranty, images, soil spectrometry
2003	Mars Exploration Rover – Opportunity*	lander	USA	Rover lasting >15 times longer than warranty, images, soil spectrometry
2005	Mars Reconnaissance Orbiter*	orbiter	USA	Very high resolution imaging, more data than all other Mars missions combined
2007	Phoenix	lander	USA	Provided surface analyses and over 25 000 images

Appendix 3. Basic data of the successful missions to Venus. Modified after Lodders & Fegley (1998). Asterisk indicates currently (July 2009) active missions.

Launch year	Name	Type	Country	Mission outline
1962	Mariner 2	flyby	USA	First successful planetary mission, magnetic field
1965	Venera 3	lander	USSR	First impact on another planet
1967	Venera 4	lander	USSR	First planetary atmospheric probe, crushed at 25 km
1967	Mariner 5	flyby	USA	Atmospheric studies
1969	Venera 5	lander	USSR	Successful, but crushed at 26 km
1969	Venera 6	lander	USSR	Successful, but crushed at 11 km
1970	Venera 7	lander	USSR	First successful planetary landing
1972	Venera 8	lander	USSR	Measured surface illumination, surface gamma spectrometry
1973	Mariner 10	flyby	USA	First good images of Venus
1975	Venera 9	orbiter, lander	USSR	First images of the surface, surface gamma spectrometry
1975	Venera 10	orbiter, lander	USSR	Images of the surface, surface gamma spectrometry
1978	Pioneer 12 (Pioneer Venus 1)	orbiter	USA	Radar mapping, cloud studies, operated 14 years
1978	Pioneer 13 (Pioneer Venus 2)	impactors	USA	Cluster of 5 atmospheric probes
1978	Venera 11	flyby, lander	USSR	Spectra from clouds and the surface, atmospheric chemistry, cameras and surface analysis failed
1978	Venera 12	flyby, lander	USSR	Spectra from clouds and the surface, atmospheric chemistry, cameras and surface analysis failed
1981	Venera 13	flyby, lander	USSR	Colour images of the surface, surface XRF analysis
1981	Venera 14	flyby, lander	USSR	Colour images of the surface, surface XRF analysis
1983	Venera 15	orbiter	USSR	Radar mapping of the surface
1983	Venera 16	orbiter	USSR	Radar mapping of the surface
1984	Vega 1	flyby, lander	USSR	Balloon probe, surface gamma spectrometry
1984	Vega 2	flyby, lander	USSR	Balloon probe, surface gamma spectrometry and XRF analysis
1989	Magellan	orbiter	USA	High resolution radar mapping of the surface, topography
1989	Galileo	flyby	USA	Atmospheric IR spectroscopy and UV spectrometry, photography
2004	MESSENGER(*)	flyby	USA	Atmospheric spectrometry
2005	Venus Express*	orbiter	ESA	Atmospheric physics and chemistry

Appendix 4a. Data of 269 Martian PICs from the Argyre region. Coordinates and diameters are from Barlow's catalogue (2003), and the geologic units (see chapter 4.2) are from Scott & Tanaka (1986) and Tanaka & Scott (1987). n = number of straight rim segment measurements (in MDIM 2.0).

No.	Block	Lat. [°S]	Long. [°W]	D [km]	Simple / Complex	Degradation	Unit	Strike 1 [°]	Strike 2 [°]	Strike 3 [°]	Strike 4 [°]	Strike 5 [°]	Strike 6 [°]	n
1	A	27.37	69.96	12.6	Complex	Fresh	Hr	10.0	141.8	88.1				3
2	A	27.78	66.52	9.2	Complex	Rimmed	Hpl_3	56.3	105.7	155.0				3
3	A	28.16	71.66	27.2	Complex	Fresh	Nf	24.0	172.4	136.0	88.6	164.1	94.1	6
4	A	28.32	66.59	11.6	Complex	Rimmed	Hpl_3	144.6	82.5	13.5				3
5	A	29.30	71.30	4.2	Simple	Fresh	Hpl_3	17.8	87.4	135.0				3
6	A	30.61	68.45	8.7	Complex	Rimmed	Nplh	62.2	11.1	137.4	144.4			4
7	A	30.86	65.60	15.1	Complex	Rimmed	Nplh	79.0	6.3	49.7	118.2			4
8	A	31.18	64.55	33.3	Complex	Rimmed	Hpl_3	161.3	75.2	145.9				3
9	A	31.15	73.59	8.2	Simple	Rimmed	Hf	138.9	80.7					2
10	A	31.39	73.56	6.2	Simple	Rimmed	Hf	10.3	124.2	74.2				3
11	A	31.73	69.32	9.4	Complex	Rimmed	Npld	135.0	78.1	8.5				3
12	A	32.19	60.90	7.6	Simple	Fresh	Hpl_3	10.0	95.5					2
13	A	32.70	72.10	4.2	Simple	Fresh	Npld	95.9	173.5					2
14	A	32.92	62.96	16.4	Complex	Fresh	Hpl_3	116.0	173.0	129.2				3
15	A	33.75	65.49	8.2	Complex	Fresh	Hpl_3	148.8	95.7	24.8	5.7			4
16	A	33.66	60.60	5	Simple	Fresh	Hpl_3	28.3	123.0					2
17	A	34.47	63.19	10.2	Complex	Fresh	Hpl_3	32.8	152.7	89.0				3
18	A	35.88	64.67	6.7	Simple	Fresh	Hpl_3	43.3	148.7	112.6	38.9			4
19	A	36.43	66.54	6	Complex	Fresh	Hpl_3	30.4	161.6	116.6				3
20	A	37.00	65.78	11	Complex	Rimmed	Hpl_3	104.6	160.6	24.0	109.5			4
21	A	37.25	58.17	21.9	Complex	Degraded	Npld	91.2	180.0					2
22	A	37.19	70.46	39.4	Complex	Rimmed	Npl_2	141.3	178.6	91.9				3
23	A	37.34	67.05	27.3	Complex	Rimmed	Npl_2	27.3	44.7	117.5				3
24	A	38.10	61.60	8.1	Complex	Rimmed	Npl_1	144.6	93.7	30.6				3
25	A	39.29	68.29	18.9	Complex	Fresh	Npl_2	9.4	128.0	92.2	26.6			4
26	A	39.31	73.57	18.3	Complex	Degraded	Npl_2	91.7	139.6	91.0				3
27	A	39.39	67.32	13.8	Complex	Rimmed	Npl_1	9.0	156.5	104.3				3
28	A	39.70	72.80	3.4	Simple	Fresh	Hpl_3	168.5	95.0					2
29	A	39.82	66.55	32.4	Complex	Degraded	Npl_1	40.1	157.0					2
30	A	39.98	63.54	18.3	Complex	Degraded	Hpl_3	42.7	174.6	106.2				3
31	A	40.29	73.76	5.5	Simple	Rimmed	Hpl_3	122.8	2.4	20.7	119.0			4

▼

No.	Block	Lat. [°S]	Long. [°W]	D [km]	Simple / Complex	Degradation	Unit	Strike 1 [°]	Strike 2 [°]	Strike 3 [°]	Strike 4 [°]	Strike 5 [°]	Strike 6 [°]	n
32	A	40.50	62.40	4	Simple	Rimmed	Hpl_3	138.2	86.6	13.1				3
33	A	40.55	67.33	57.4	Complex	Rimmed	Npl_1	19.3	160.1					2
34	A	41.08	65.77	61	Complex	Rimmed	Npl_1	100.4	45.5	167.7				3
35	A	41.82	73.16	31.2	Complex	Rimmed	Npl_1	170.1	97.2					2
36	B	26.52	54.77	16.7	Complex	Fresh	Hr	15.1	91.0	143.7				3
37	B	26.95	45.25	6.5	Complex	Fresh	Npl_1	150.6	85.0					2
38	B	27.41	41.83	20.9	Complex	Fresh	Npl_2	102.1	154.6					2
39	B	29.01	48.50	4.7	Simple	Rimmed	Npl_1	96.7	137.7	52.4	94.6	39.5		5
40	B	30.16	47.26	17.3	Complex	Rimmed	Npl_1	96.9	135.0	2.7	96.5	132.2		5
41	B	30.44	46.52	9.4	Complex	Rimmed	Npl_1	116.6	22.7	110.1				3
42	B	30.98	47.40	9.6	Complex	Rimmed	Npl_1	169.6	86.6					2
43	B	32.04	45.33	10.2	Complex	Fresh	Npl_1	13.6	95.8					2
44	B	32.44	51.85	17.8	Complex	Rimmed	Hr	152.0	28.1	87.5	143.7			4
45	B	33.25	44.40	23.1	Complex	Degraded	Npl_1	152.1	86.5	93.6	154.2			4
46	B	33.15	53.78	26.7	Complex	Degraded	Npl_2	39.3	3.0	130.8				3
47	B	34.02	46.42	22.4	Complex	Rimmed	Npl_1	95.8	150.9	28.2				3
48	B	34.01	53.03	17.1	Complex	Degraded	Npl_2	163.6	101.7	39.5	37.7			4
49	B	34.12	43.51	21.7	Complex	Degraded	Npl_1	114.8	8.0	35.2				3
50	B	34.27	53.78	6.3	Simple	Fresh	Npl_2	145.8	79.9					2
51	B	35.38	50.85	7.9	Complex	Rimmed	Npl_1	141.1	39.0	8.1				3
52	B	35.79	51.82	19.4	Complex	Degraded	Npl_1	133.6	38.9	92.3				3
53	B	36.14	56.88	18.1	Complex	Degraded	Hpl_3	99.5	157.3	142.1				3
54	B	36.56	57.50	20.3	Complex	Rimmed	Hpl_3	98.5	5.5	98.5				3
55	B	36.77	46.48	55.8	Complex	Rimmed	Nplh	10.1	69.5	138.3	7.1			4
56	B	36.89	57.27	9.9	Complex	Degraded	Hpl_3	93.2	21.7	170.3				3
57	B	37.18	43.54	19.7	Complex	Rimmed	Nplh	91.8	138.0					2
58	B	37.16	43.97	49.2	Complex	Rimmed	Nplh	152.1	35.0	93.9				3
59	B	38.88	54.55	8.7	Simple	Fresh	Npl_1	45.9	149.2	88.9				3
60	B	39.02	51.51	23.1	Complex	Rimmed	Nplh	136.1	176.2					2
61	B	39.24	48.74	8.1	Simple	Rimmed	Nplh	145.1	27.1	79.8				3
62	B	39.22	53.18	9.4	Complex	Degraded	Nplh	88.2	32.0	138.9				3
63	B	39.53	43.09	7.4	Simple	Rimmed	Nplh	144.9	88.5	35.3				3
64	B	39.60	47.99	12.9	Complex	Rimmed	Nplh	133.3	94.8	175.2	95.7			4
65	B	39.50	55.30	4.5	Simple	Rimmed	Npl_1	86.5	155.4					2

▼

No.	Block	Lat. [°S]	Long. [°W]	D [km]	Simple / Complex	Degradation	Unit	Strike 1 [°]	Strike 2 [°]	Strike 3 [°]	Strike 4 [°]	Strike 5 [°]	Strike 6 [°]	n
66	B	40.30	42.71	45.5	Complex	Rimmed	Nplh	130.8	77.6	130.2				3
67	B	40.15	49.15	10.3	Complex	Rimmed	Nplh	177.7	84.9					2
68	B	40.43	50.44	29.9	Complex	Rimmed	Nplh	142.3	92.2	6.9	156.8			4
69	C	26.63	41.24	25.4	Complex	Rimmed	Npl_2	180.0	53.5	116.6	174.4	118.0		5
70	C	26.67	29.06	14.4	Complex	Degraded	Npl_1	17.0	6.7	148.1	78.3			4
71	C	27.30	39.67	18.4	Complex	Fresh	Npl_2	135.0	22.5	92.6				3
72	C	27.50	27.30	4.2	Simple	Rimmed	Npl_1	90.0	25.6	145.6				3
73	C	27.49	28.98	9.9	Complex	Rimmed	Npl_1	167.1	74.8	96.1				3
74	C	27.86	32.70	25.8	Complex	Degraded	Npl_1	136.0	144.2	90.6	2.7			4
75	C	28.30	36.07	13.3	Complex	Degraded	Npl_1	90.0	22.5	116.6				3
76	C	28.98	39.90	12.8	Complex	Fresh	Npl_2	151.6	94.6	169.1	36.1	35.8		5
77	C	29.17	38.18	29.1	Complex	Rimmed	Npl_2	24.3	144.2	140.0	91.3			4
78	C	29.71	39.71	26.3	Complex	Rimmed	Npl_1	129.7	89.1					2
79	C	30.11	26.93	13.2	Complex	Degraded	Npl_1	175.1	105.6	45.0				3
80	C	30.11	34.67	18.3	Complex	Rimmed	Npl_1	73.0	12.2	126.7	76.2	18.2	153.9	6
81	C	30.41	36.00	21.1	Complex	Rimmed	Npl_1	96.8	141.0	16.6				3
82	C	30.72	36.36	59.2	Complex	Rimmed	Npl_1	26.7	68.6	148.3	100.8			4
83	C	30.44	28.10	16.9	Complex	Rimmed	Npl_1	180.0	121.8					2
84	C	30.55	26.00	22.3	Complex	Rimmed	Npl_1	152.4	87.1	25.9				3
85	C	30.94	29.46	22.1	Complex	Degraded	Npl_1	119.7	77.7	12.5	147.4	64.7		5
86	C	31.33	39.52	7.4	Simple	Rimmed	Npl_1	19.4	130.4	135.0				3
87	C	31.81	26.77	9.1	Complex	Fresh	Npl_1	10.2	95.5	148.1				3
88	C	32.07	36.55	6.5	Simple	Rimmed	Npl_1	145.8	25.5	92.3				3
89	C	31.88	28.44	8.8	Complex	Rimmed	Npl_1	134.2	175.1	132.6	10.9			4
90	C	32.35	27.38	5.7	Simple	Fresh	Npl_1	11.5	107.9					2
91	C	33.08	36.06	6.5	Simple	Rimmed	Npl_1	10.2	81.3					2
92	C	33.50	29.06	6.6	Complex	Fresh	Npl_1	157.6	74.1					2
93	C	33.72	41.16	24.4	Complex	Rimmed	Npl_1	113.1	174.8	109.2				3
94	C	33.80	28.07	6.8	Simple	Rimmed	Npl_1	158.7	92.0					2
95	C	34.18	30.56	9.2	Complex	Rimmed	Npl_1	133.1	9.5	73.2				3
96	C	34.11	39.01	53	Complex	Rimmed	Npl_1	146.7	14.4	19.3	81.7	153.4		5
97	C	34.94	31.92	44.6	Complex	Degraded	Npl_1	150.2	7.2	149.8				3
98	C	36.23	28.23	4.7	Simple	Rimmed	Npl_2	1.5	107.0					2
99	C	36.50	29.57	13	Complex	Degraded	Npl_2	1.5	63.4	132.2				3

▼

No.	Block	Lat. [°S]	Long. [°W]	D [km]	Simple / Complex	Degradation	Unit	Strike 1 [°]	Strike 2 [°]	Strike 3 [°]	Strike 4 [°]	Strike 5 [°]	Strike 6 [°]	n
100	C	36.93	38.01	15.6	Complex	Degraded	Nplh	168.8	118.3					2
101	C	36.84	29.54	8.9	Simple	Rimmed	Npl_2	11.3	130.4	147.4				3
102	C	37.03	34.78	9.4	Complex	Rimmed	Nplh	162.0	91.5	34.8	91.4			4
103	C	38.09	28.10	19.8	Complex	Degraded	Hpl_3	91.9	130.6					2
104	C	38.37	28.50	74.3	Complex	Rimmed	Nplh	155.3	22.1	85.5				3
105	C	38.99	30.57	14.3	Complex	Degraded	Nplh	145.3	17.1	75.1	130.2			4
106	C	39.48	41.32	5.4	Simple	Rimmed	Hpl_3	175.2	92.9					2
107	C	39.53	27.45	11.2	Complex	Rimmed	Nplh	63.1	131.0	8.0	126.6	69.6	174.5	6
108	C	39.94	34.05	20	Complex	Rimmed	Nplh	129.4	21.3	79.1				3
109	C	41.67	29.37	24.9	Complex	Rimmed	Npl_2	68.1	142.6	13.3				3
110	D	26.51	19.98	18.7	Complex	Degraded	Npl_1	159.2	100.7	136.4				3
111	D	26.93	21.94	14.7	Complex	Degraded	Npl_1	156.4	86.4	28.7				3
112	D	26.93	24.67	16.7	Complex	Degraded	Npl_1	64.9	132.3	3.6				3
113	D	27.17	10.18	26.5	Complex	Degraded	Npl_1	130.7	11.8					2
114	D	27.19	23.04	8.7	Simple	Fresh	Npl_1	96.8	156.9					2
115	D	27.31	20.58	24.9	Complex	Degraded	Npl_1	159.4	102.3					2
116	D	27.54	10.23	25.1	Complex	Degraded	Npl_1	30.6	92.9					2
117	D	27.70	12.13	34.2	Complex	Rimmed	Npld	23.1	154.4	108.2				3
118	D	28.35	11.22	9.1	Complex	Rimmed	Npl_1	160.0	132.4	2.6	87.5			4
119	D	28.59	21.57	15.1	Complex	Degraded	Npl_1	172.6	112.8	90.0	128.5	10.5		5
120	D	28.77	10.40	13.4	Complex	Rimmed	Npl_1	91.8	134.1	23.7	94.2			4
121	D	28.72	19.78	11	Complex	Degraded	Npl_1	133.9	88.3	170.3	136.8	92.9		5
122	D	28.72	24.25	14.6	Complex	Degraded	Npl_1	43.2	102.0					2
123	D	28.98	20.79	6.4	Complex	Fresh	Npl_1	109.6	164.1	50.1				3
124	D	29.34	17.31	17.3	Complex	Fresh	Npl_1	8.3	126.2	89.1				3
125	D	29.28	21.61	25.5	Complex	Degraded	Npl_1	29.6	163.8	113.5	38.3			4
126	D	29.47	23.12	25.9	Complex	Rimmed	Npl_1	144.5	30.2	170.7	29.4	95.2		5
127	D	29.89	12.34	10.3	Complex	Fresh	Npl_1	113.2	156.0	30.5				3
128	D	29.96	11.97	11.1	Complex	Fresh	Npl_1	92.2	133.7					2
129	D	29.95	16.50	19.3	Complex	Degraded	Npl_1	32.7	149.0	135.0	25.3			4
130	D	30.03	24.96	27.6	Complex	Rimmed	Npl_1	26.0	149.1					2
131	D	30.01	22.77	9.5	Simple	Rimmed	Npl_1	146.8	39.2					2
132	D	30.65	16.30	12.7	Complex	Rimmed	Npl_1	23.6	138.6					2
133	D	31.13	20.90	26	Complex	Rimmed	Npl_1	131.8	50.3	9.1				3

▼

No.	Block	Lat. [°S]	Long. [°W]	D [km]	Simple / Complex	Degradation	Unit	Strike 1 [°]	Strike 2 [°]	Strike 3 [°]	Strike 4 [°]	Strike 5 [°]	Strike 6 [°]	n
134	D	31.10	24.10	4.5	Simple	Rimmed	Npl_1	32.6	172.1					2
135	D	31.07	9.92	18.7	Complex	Degraded	Nplr	133.9	12.7	94.3				3
136	D	31.33	12.55	23.2	Complex	Degraded	Npl_1	153.4	109.0	162.0				3
137	D	31.54	24.39	9.6	Complex	Rimmed	Npl_1	96.6	144.1					2
138	D	31.72	16.54	43.4	Complex	Rimmed	Npl_1	2.5	145.0	108.0	88.8			4
139	D	31.65	18.29	21.8	Complex	Degraded	Npl_1	27.0	166.1	109.1				3
140	D	32.36	22.10	23.1	Complex	Degraded	Npl_1	177.8	128.4	35.1				3
141	D	33.28	19.21	13	Complex	Degraded	Npl_1	104.4	161.6	60.6				3
142	D	33.45	15.59	20.1	Complex	Rimmed	Npl_1	86.1	150.0	26.1				3
143	D	33.45	24.42	14.6	Complex	Rimmed	Nplr	177.8	113.7	31.0				3
144	D	33.63	10.79	14.8	Complex	Fresh	Npl_1	119.1	171.0	86.9				3
145	D	33.66	12.48	21.7	Complex	Rimmed	Npl_1	169.8	116.6	61.7				3
146	D	34.14	25.51	18.2	Complex	Degraded	Nplr	176.0	46.8	98.3				3
147	D	34.13	17.03	48.9	Complex	Degraded	Npl_1	116.1	31.0	9.0	159.4	139.1		5
148	D	34.46	13.91	32.1	Complex	Rimmed	Npl_1	97.1	158.7	142.2	28.0			4
149	D	34.65	22.54	58.7	Complex	Degraded	Nplr	59.9	136.1					2
150	D	35.04	23.90	6	Simple	Fresh	Nplr	16.9	90.0					2
151	D	35.58	16.76	13.9	Complex	Degraded	Npl_1	57.7	122.3	91.1				3
152	D	36.60	19.10	4.3	Simple	Fresh	Npl_1	90.0	145.3					2
153	D	37.55	11.67	10.6	Complex	Fresh	Npl_2	150.5	15.8	95.2				3
154	D	37.90	22.39	11	Complex	Fresh	Nplr	88.6	149.0	32.3				3
155	D	38.41	20.35	7.2	Complex	Fresh	Npl_1	33.2	147.5	93.2				3
156	D	38.89	22.19	48.3	Complex	Rimmed	Nplr	83.4	135.0	13.7				3
157	D	39.03	25.79	14.3	Complex	Rimmed	Nplh	67.2	111.6					2
158	D	39.02	17.48	39.7	Complex	Rimmed	Nplr	159.2	20.7	88.4				3
159	D	39.16	21.29	33.6	Complex	Rimmed	Nplr	151.4	126.9	7.6				3
160	D	39.68	16.43	37.5	Complex	Rimmed	Nplr	34.1	93.3	160.6	158.8	35.0		5
161	D	40.03	21.65	32.8	Complex	Degraded	Nplr	91.1	166.4	39.5				3
162	D	40.13	24.23	4.7	Simple	Rimmed	Nplr	94.2	2.5					2
163	D	40.45	13.59	10.1	Complex	Degraded	Nplr	39.0	170.9	117.1				3
164	D	40.73	17.52	8.1	Complex	Rimmed	Nplr	94.8	30.0	138.4				3
165	D	40.94	12.12	11.9	Complex	Degraded	Nplr	138.4	17.4					2
166	E	42.15	69.66	15.8	Complex	Degraded	Npl_1	45.4	91.8					2
167	E	42.19	73.22	12.5	Complex	Degraded	Npl_1	134.3	91.0	6.6				3

▼

No.	Block	Lat. [°S]	Long. [°W]	D [km]	Simple / Complex	Degradation	Unit	Strike 1 [°]	Strike 2 [°]	Strike 3 [°]	Strike 4 [°]	Strike 5 [°]	Strike 6 [°]	n
168	E	42.43	59.87	36.6	Complex	Rimmed	Npl_1	90.5	137.7	15.1	129.1			4
169	E	43.25	64.62	45.6	Complex	Rimmed	Npl_1	75.7	37.0	96.9	45.0			4
170	E	43.61	71.89	9.4	Complex	Rimmed	Npl_1	39.8	93.2	4.5	39.8			4
171	E	43.75	65.99	11.5	Complex	Rimmed	Npl_1	141.3	11.5	87.8	81.5			4
172	E	44.06	66.51	9	Complex	Rimmed	Npld	140.6	91.1	122.1				3
173	E	44.58	58.94	31.5	Complex	Rimmed	Npl_1	139.3	88.7					2
174	E	44.75	70.26	21.6	Complex	Rimmed	Npld	24.9	80.4	47.7	116.6			4
175	E	44.79	69.62	9.8	Complex	Rimmed	Npld	28.3	161.3	91.0				3
176	E	45.28	59.58	13.3	Complex	Rimmed	Npl_1	117.5	25.3					2
177	E	45.84	58.86	9.8	Simple	Rimmed	Npl_1	107.4	44.8	139.3				3
178	E	46.74	64.01	32.6	Complex	Rimmed	Npl_1	152.9	100.1	30.0	139.9			4
179	E	46.97	64.51	32.2	Complex	Degraded	Npl_1	124.5	171.4					2
180	E	47.23	59.68	43.1	Complex	Rimmed	Nplh	85.4	134.6	32.1				3
181	E	47.03	62.83	10.2	Simple	Fresh	Npl_1	18.9	141.8	20.6	81.6			4
182	E	46.99	65.98	15.1	Complex	Degraded	Npl_1	29.6	163.5					2
183	E	47.15	69.73	82.1	Complex	Rimmed	Npl_1	47.5	96.9	5.9				3
184	E	47.25	62.22	14.2	Complex	Rimmed	Npl_1	179.0	131.8	39.2				3
185	E	47.40	65.00	15.7	Complex	Degraded	Npl_1	136.2	20.9	79.0				3
186	E	47.63	64.69	10.8	Complex	Degraded	Npl_1	141.6	84.6					2
187	E	47.76	70.40	11	Complex	Rimmed	Npl_1	138.9	16.9	135.6				3
188	E	47.74	63.23	9.4	Complex	Rimmed	Npl_2	147.9	88.7	7.5				3
189	E	48.46	66.56	7	Simple	Fresh	Npl_1	6.4	80.7	139.1	162.8			4
190	E	49.18	63.20	29.5	Complex	Rimmed	Npl_1	141.3	86.6	93.3				3
191	E	49.47	59.06	14.8	Complex	Rimmed	Nplh	143.3	25.3	91.9	124.2			4
192	E	49.39	67.87	22.7	Complex	Rimmed	Npl_1	174.5	115.5					2
193	E	49.84	72.41	13	Complex	Degraded	Npl_1	112.1	159.4	34.9				3
194	E	50.05	64.26	20.8	Complex	Rimmed	Npl_1	147.5	104.6	96.1	40.7			4
195	E	50.75	58.88	26.5	Complex	Rimmed	Nplh	105.5	136.2	110.6	2.4			4
196	E	50.81	62.39	21.4	Complex	Rimmed	Nplh	32.0	173.0	93.4				3
197	E	51.29	67.33	14.1	Complex	Rimmed	Npl_1	154.1	31.8	92.9				3
198	E	51.73	70.33	90.8	Complex	Rimmed	Npl_1	113.5	153.2	172.0				3
199	E	53.34	73.46	8.7	Complex	Rimmed	Npl_1	117.5	45.7	38.5				3
200	E	53.45	70.47	4.2	Complex	Rimmed	Npl_1	151.5	94.7					2
201	E	54.37	60.52	30.3	Complex	Rimmed	Nplh	98.1	157.0	22.3				3

▼

No.	Block	Lat. [°S]	Long. [°W]	D [km]	Simple / Complex	Degradation	Unit	Strike 1 [°]	Strike 2 [°]	Strike 3 [°]	Strike 4 [°]	Strike 5 [°]	Strike 6 [°]	n
202	E	54.60	63.17	60.5	Complex	Rimmed	Npl1	36.5	146.8	21.1				3
203	E	54.77	66.34	12.4	Complex	Fresh	Npl_1	166.1	32.5	98.7				3
204	E	55.29	69.72	24.4	Complex	Rimmed	Npl_1	99.5	172.8					2
205	E	55.48	60.98	14.6	Complex	Rimmed	Nplh	147.9	44.8					2
206	E	55.92	64.19	36.7	Complex	Rimmed	Npl_1	17.7	69.4	149.5				3
207	E	56.81	66.17	43.6	Complex	Rimmed	Npl_1	30.6	166.4	104.2	84.9			4
208	E	57.29	70.97	21.6	Complex	Degraded	Npl_1	139.7	99.3	28.6	34.2	96.4		5
209	E	57.64	59.99	32.1	Complex	Rimmed	Npl_1	149.6	97.2	120.8	73.6	169.0		5
210	E	57.73	67.52	23.3	Complex	Rimmed	Npl_1	176.7	127.8					2
211	F	42.13	56.68	22.5	Complex	Rimmed	Npl_1	127.4	88.5	3.2	137.5			4
212	F	42.36	55.39	8.4	Complex	Rimmed	Nplh	119.2	165.0					2
213	F	42.87	47.34	5.2	Simple	Degraded	Hpl_3	1.2	117.3	25.3				3
214	F	43.07	56.48	7.6	Complex	Degraded	Npl_1	125.5	65.6					2
215	F	43.11	53.05	10	Complex	Rimmed	Nplh	25.5	140.7	119.6	175.0			4
216	F	43.10	52.16	15.3	Complex	Degraded	Nplh	101.9	166.7	25.8				3
217	F	43.31	43.42	13.7	Complex	Degraded	Nplh	146.3	97.3					2
218	F	43.30	53.72	31.8	Complex	Rimmed	Nplh	153.7	94.1					2
219	F	44.36	52.68	32.6	Complex	Rimmed	Nplh	19.6	151.4					2
220	F	44.38	53.08	12.9	Complex	Rimmed	Nplh	42.4	172.5					2
221	F	44.60	48.70	4.6	Simple	Rimmed	Nplh	88.5	164.7	21.6	125.9			4
222	F	44.60	49.30	4.9	Simple	Rimmed	Nplh	164.9	45.8					2
223	F	44.79	54.00	22.1	Complex	Rimmed	Nplh	20.6	69.4	178.3				3
224	F	46.58	57.41	27.3	Complex	Rimmed	Nplh	159.9	119.9					2
225	F	48.66	55.19	8.1	Complex	Rimmed	Nplh	19.2	145.7	88.1				3
226	F	52.00	42.60	5.8	Simple	Degraded	Nple	59.7	177.7	102.5				3
227	F	52.76	54.49	59.3	Complex	Rimmed	Nplh	145.9	108.9	7.6				3
228	F	53.57	54.64	7.2	Simple	Rimmed	Nplh	135.6	178.9	136.7	89.1			4
229	G	42.81	27.49	7.8	Complex	Rimmed	Npl_2	11.7	71.6					2
230	G	42.99	36.84	18.6	Complex	Rimmed	Nplh	0.5	143.7					2
231	G	43.10	38.40	7.5	Simple	Degraded	Nplh	7.1	132.0	74.5				3
232	G	43.61	25.98	5	Simple	Rimmed	Npl_2	18.0	92.8					2
233	G	44.06	37.15	27.4	Complex	Rimmed	Hpl_3	7.2	140.0					2
234	G	44.52	27.44	21.9	Complex	Degraded	Nplh	15.2	115.4	169.1				3
235	G	45.43	34.96	8.6	Complex	Fresh	Nplh	8.4	127.9					2

▼

No.	Block	Lat. [°S]	Long. [°W]	D [km]	Simple / Complex	Degradation	Unit	Strike 1 [°]	Strike 2 [°]	Strike 3 [°]	Strike 4 [°]	Strike 5 [°]	Strike 6 [°]	n
236	G	45.86	32.02	27.3	Complex	Rimmed	Nplh	95.2	57.1	114.5				3
237	G	47.67	27.17	26.5	Complex	Rimmed	Npl_2	129.4	75.4	19.0	114.6			4
238	G	48.77	37.99	9.5	Complex	Fresh	Nple	24.8	175.5	99.6				3
239	G	49.73	26.12	15.1	Complex	Rimmed	Nplh	135.5	79.2	41.7				3
240	G	53.02	26.60	18.7	Complex	Rimmed	Nplh	107.4	35.6					2
241	G	54.18	26.59	18.6	Complex	Rimmed	Hpl_3	160.5	20.6	94.1				3
242	G	54.58	27.86	16.2	Complex	Rimmed	Nplh	107.4	175.3	45.9				3
243	G	55.28	28.48	27.1	Complex	Rimmed	Nplh	0.6	110.3					2
244	G	55.40	32.80	15.4	Complex	Rimmed	Nplh	2.9	116.0	55.9	82.5			4
245	H	42.13	13.30	21	Complex	Degraded	Nplr	28.1	100.6	138.9	15.5			4
246	H	42.22	16.63	10.6	Complex	Rimmed	Nplr	107.1	173.5	132.5				3
247	H	43.17	20.83	21.4	Complex	Degraded	Nplr	138.9	99.5	106.0				3
248	H	43.64	10.20	23.1	Complex	Degraded	Npl_2	22.1	77.0	135.6				3
249	H	44.34	12.50	13.8	Complex	Degraded	Nplr	37.9	112.5	158.8	174.1			4
250	H	44.68	14.84	22.8	Complex	Rimmed	Nplr	142.0	101.9	179.4				3
251	H	45.63	23.21	28.2	Complex	Degraded	Npl_2	115.9	78.1	77.9				3
252	H	46.90	22.18	40.3	Complex	Degraded	Npl_2	143.5	20.2					2
253	H	47.21	15.47	13.2	Complex	Fresh	Nplr	22.9	142.5	95.7				3
254	H	47.59	17.18	7.9	Complex	Fresh	Nplr	169.7	111.0	56.1				3
255	H	47.72	10.01	19.1	Complex	Rimmed	Nplr	27.4	84.2	128.2				3
256	H	47.80	18.10	4.8	Simple	Rimmed	Nplr	140.3	25.1	88.6	26.6	143.0	84.3	6
257	H	48.10	14.14	45.9	Complex	Rimmed	Nplr	149.2	108.6					2
258	H	48.94	10.59	36.8	Complex	Fresh	Nplr	161.2	31.2	100.6	13.0			4
259	H	49.36	23.33	31.3	Complex	Fresh	Npl_2	80.0	28.8	166.5	41.3	174.3		5
260	H	49.77	13.15	18	Complex	Rimmed	Npl_2	20.0	131.7					2
261	H	50.23	11.46	24.8	Complex	Degraded	Npl_2	167.9	129.0					2
262	H	51.21	16.19	9.9	Complex	Fresh	Npl_2	7.8	64.0					2
263	H	51.83	20.74	24	Complex	Degraded	Npl_2	171.9	107.8	16.3				3
264	H	52.24	13.55	68.9	Complex	Degraded	Npl_2	25.2	107.6	135.6				3
265	H	52.42	23.54	8.9	Complex	Rimmed	Nplh	28.9	74.5					2
266	H	53.19	17.54	10.4	Complex	Fresh	Npl_2	143.1	5.4	94.7	136.2			4
267	H	54.22	23.01	25.8	Complex	Rimmed	Nplh	164.3	97.7	15.3	119.6			4
268	H	55.13	14.63	8.4	Complex	Fresh	Npl_2	11.0	127.9	91.4				3
269	H	55.91	15.94	21.7	Complex	Degraded	Npl_2	108.6	163.6	42.6	102.0			4

Appendix 4b. Straight rim segment strikes of 30 Martian PICs from part of the C- and D-blocks (30°S–42°S, 10°W–42°W) in the Argyre region, as measured from MOC-WA images. Coordinates and diameters are from Barlow's catalogue (2003). Other PIC data, and the rim strike measurements using MDIM 2.0 images are presented in Appendix 4a. n = number of straight rim segment measurements.

No.	Block	Lat. [°S]	Long. [°W]	Strike 1 [°]	Strike 2 [°]	Strike 3 [°]	Strike 4 [°]	Strike 5 [°]	Strike 6 [°]	n
81	C	30.41	36.00	97.0	138.8					2
84	C	30.55	26.00	150.1	95.6	32.8	84.4			4
87	C	31.81	26.77	11.2	75.2	151.1				3
88	C	32.07	36.55	157.6	28.7					2
93	C	33.72	41.16	54.6	104.0	170.3	44.0			4
96	C	34.11	39.01	16.6	50.4	80.9	147.6			4
98	C	36.23	28.23	31.2	101.7	175.9				3
100	C	36.93	38.01	37.6	93.8	45.0				3
102	C	37.03	34.78	166.8	36.9	98.7				3
103	C	38.09	28.10	96.1	53.7	162.1	38.4	79.5		5
104	C	38.37	28.50	14.9	82.6	156.8				3
105	C	38.99	30.57	27.9	150.3	93.6				3
107	C	39.53	27.45	8.3	53.3	109.3				3
108	C	39.94	34.05	9.5	114.4	54.5				3
109	C	41.67	29.37	171.8	65.1	14.5				3
132	D	30.65	16.30	23.3	141.2	88.6	167.2			4
136	D	31.33	12.55	102.7	165.2	157.3				3
139	D	31.65	18.29	32.3	157.0	102.2				3
141	D	33.28	19.21	52.4	104.9	173.9				3
142	D	33.45	15.59	23.9	80.8	157.9	118.2			4
143	D	33.45	24.42	45.0	99.2	163.0	16.9	107.4	172.1	6
146	D	34.14	25.51	172.8	45.0	103.8	98.7			4
148	D	34.46	13.91	41.8	101.5					2
153	D	37.55	11.67	151.4	93.7	48.2				3
154	D	37.90	22.39	160.0	30.8					2
157	D	39.03	25.79	21.6	65.2	110.3				3
158	D	39.02	17.48	18.5	155.1	58.0				3
160	D	39.68	16.43	164.5	87.8	86.7	34.0			4
164	D	40.73	17.52	97.7	40.5					2
165	D	40.94	12.12	142.7	79.2	20.9				3

Appendix 5a. Data of the morphology and rim strikes of 121 Venusian PICs. Morphology data are taken from the database of Herrick et al. (1997).
M – Morphology: 1 – bowl, 2 – knobby base, 3 – central peak, 4 – several peaks, 5 – peak-ring, 6 – multi-ring, 0 – flat floor
T – Rim terraces: t – terraced, u – unterraced
F – Floor brightness: d – dark, i – intermediate, b – bright
P – Parabola: y – yes, n – no, m – maybe
D – Degradation: 1 – pristine with ejecta, 2 – no ejecta, 3 – highly degraded
Str – straight rim segment strike [°]
nL, nR – number of straight rim segment strike measurements in the left- and right-looking data, respectively

No.	ID#	Name	Lat. [°N]	Long. [°E]	Diam. [km]	M	T	F	P	D	Left-looking Str1	Str2	Str3	Str4	Str5	Str6	Right-looking Str1	Str2	Str3	Str4	n L	n R
1	320	Odilia	81.3	200.4	20.4	2	u	i	n	2	48.8	8.7									2	
2	466	Gina	78.1	76.5	14.5	2	u	i	n	2	123.1	177.5	51.7	136.7							4	
3	233	Monika	72.3	122.4	26.1	3	t	b	y	1	174.6	122.2	49.8	50.9							4	
4	331	Wanda	71.2	323.1	19.8	3	u	i	n	2	17.3	131.7	126.7								3	
5	423	Evangeline	69.6	222	15.9	2	u	b	n	1	139.4	179.4	51.5	122.1	168.9						5	
6	545	Zdravka	65.1	299.1	12	2	u	i	n	1	155.3	26.9									2	
7	487	Margit	60	273.1	13.6	2	u	b	n	1	7.2	132.7									2	
8	524	Bineta	57.2	144.1	12.4	2	u	i	n	2	179.5	121.7	51.3								3	
9	258	Johnson	51.8	254.6	24	3	t	d	n	1	47.6	167.6	8.6	34.8	139.8						5	
10	517	Dolores	51.4	201.6	12.5	2	u	i	n	1	160.6	25.3	17.6								3	
11	491	Irene	49.8	134	13.5	2	t	b	n	2	22.9	144.3	117.1	121.8							4	
12	368	Laura	48.9	141.2	18.4	3	t	i	n	1	54.4	116.2	163.5	154.9							4	
13	285	Brooke	48.4	296.6	22.5	3	t	d	n	2	68.2	19.0									2	
14	256	Valentina	46.4	144.1	24.3	3	t	d	n	1	13.9	154.9									2	
15	290	Zvereva	45.3	283.1	22.3	3	t	d	n	1	32.1	147.4									2	
16	154	Mu Guiying	41.2	81.1	32.7	4	t	b	n	1	154.2	28.0	31.8				152.1	44.5			3	2
17	383	Anya	39.5	297.8	17.7	2	t	b	n	1	155.7	35.4									2	
18	402	Datsolalee	38.3	171.8	17	2	u	b	n	1	26.1	164.9									2	
19	289	Bly	37.7	305.6	22.4	3	t	i	n	1	62.0	170.5									2	
20	279	de Stael	37.4	324.2	22.8	2	t	i	n	1	167.4	24.5									2	
21	506	Wilma	36.7	1.7	13	2	u	b	n	1	12.2	149.9	170.0	136.7							4	
22	202	Moses	34.6	119.9	28.1	3	t	d	n	1	173.1	110.2	64.7								3	
23	296	Merian	34.5	76.2	21.9	0	t	i	n	3	12.7	142.5	69.5	34.2	149.6	54.0					6	

▼

No.	ID#	Name	Lat. [°N]	Long. [°E]	Diam. [km]	M	T	F	P	D	Left-looking Str1	Str2	Str3	Str4	Str5	Str6	Right-looking Str1	Str2	Str3	Str4	n L	n R
24	479	Wazata	33.6	298.3	14	2	u	b	n	1	161.0	130.7									2	
25	203	West	26.1	303	28	3	t	i	n	1	161.6	20.8	153.4	100.4							4	
26	250	Horner	23.4	97.8	24.7	3	t	d	n	1	21.4	71.9					30.8	133.1			2	2
27	365	Corinna	22.9	40.6	18.5	3	t	i	n	1	43.1	169.9									2	
28	298	de Lalande	20.4	355	21.6	2	t	i	n	1	168.8	119.2	41.5								3	
29	268	Weil	19.3	283.1	23.4	3	t	b	n	1	173.8	57.1									2	
30	526	Zulfiya	18.4	101.9	12.3	2	u	b	n	1							23.8	61.7	154.9			3
31	348	Hannah	17.9	102.6	19.1	3	t	d	n	1	176.3	120.8	10.0	124.3			140.7	11.6			4	2
32	41	Vigee-Lebrun	17.3	141.4	57.6	4	t	d	n	1	109.5	62.8	144.8	21.5							4	
33	140	Grimke	17.3	215.3	34.6	3	t	d	n	1	38.1	154.5									2	
34	111	Ban Zhao	17.2	146.9	38.3	3	t	b	y	1	3.9	143.0									2	
35	138	Bradstreet	16.5	47.7	35.2	3	t	d	n	1	1.1	111.6	44.6								3	
36	406	Aimee	16.1	127.2	16.8	3	t	i	n	1	163.3	115.7	54.8								3	
37	273	Devorguilla	15.3	4	23.1	3	t	d	n	1	161.6	135.6	10.9								3	
38	529	Anush	14.9	86.5	12.2	3	t	d	n	1	130.5	174.2	115.9				128.8	171.4			3	2
39	1	Mead	12.5	57	269	6	t	i	n	1	18.0	148.9	119.7								3	
40	483	Pamela	11	238.5	13.9	2	u	i	n	1	124.5	175.5									2	
41	447	Lydia	10.7	340.7	15	2	t	b	n	1	107.9	142.6	15.9								3	
42	347	Romola	9.3	54.2	19.1	3	t	i	n	2	169.6	43.8	120.4								3	
43	475	Aita	8.9	270.7	14.1	3	t	d	n	1	47.2	169.0	133.5								3	
44	83	Rhys	8.6	298.8	44	3	t	i	n	1	8.4	128.2	173.9								3	
45	354	Nadine	7.8	359.1	18.8	2	u	b	n	1	161.6	44.5									2	
46	175	Hwangcini	6.3	141.7	30.8	3	t	i	n	1	156.9	21.1									2	
47	497	Susanna	6	93.3	13.2	2	u	i	n	1	1.2	127.9	56.7				162.1	108.6	48.2		3	3
48	515	Ngone	6	331.9	12.6	3	t	b	n	1	31.6	104.9	161.7								3	
49	464	Ketzia	4	300.5	14.5	3	t	i	n	2	20.4	142.2	65.6								3	
50	284	Castro	3.3	233.9	22.6	3	t	i	n	1	59.9	112.8									2	
51	364	Shakira	3	213.6	18.5	2	u	b	n	1	168.7	115.1	33.7	145.1							4	
52	421	Tsiala	2.9	100	16	3	t	i	n	2	126.3	12.3					146.1	112.7	50.5	177.1	2	4
53	114	Uvaysi	2.3	198.2	38	3	t	i	m	2	21.0	148.2					25.2	149.6			2	2
54	48	de Beauvoir	2	96.1	53.3	5	t	i	n	2	162.5	121.8					123.2				2	1
55	249	Piscopia	1.5	190.9	24.8	3	t	d	n	1	136.3	7.9	178.9	138.5	48.7		5.1	135.5			5	2
56	350	Comnena	1.2	343.7	19	3	t	d	y	1	160.9	31.7	123.4								3	

▼

No.	ID#	Name	Lat. [°N]	Long. [°E]	Diam. [km]	M	T	F	P	D	Left-looking Str1	Str2	Str3	Str4	Str5	Str6	Right-looking Str1	Str2	Str3	Str4	n L	n R
57	392	Toklas	0.7	273.1	17.2	2	t	d	n	1	5.3	123.7	146.8								3	
58	28	Andreianova	-3	68.7	69.5	6	t	d	n	1	168.5	123.0	37.5	165.2			125.5	73.9	27.4	166.0	4	4
59	272	Zija	-3.5	265	18.2	3	u	d	n	1	141.8	26.6	144.5								3	
60	198	von Schuurman	-5	191	28.9	3	t	i	y	1	21.0	128.9	148.7				145.7	27.0	63.4	130.4	3	4
61	330	Evika	-5.1	31.4	19.8	3	t	d	n	1	84.7	34.6	131.4								3	
62	275	Quimby	-5.7	76.7	22.9	3	u	b	n	2	130.3	170.0	36.7				136.8	7.9			3	2
63	420	Sabira	-5.8	239.8	16	2	t	d	n	1	3.0	52.2									2	
64	482	Valerie	-6.4	30.9	13.9	2	t	i	n	1	32.5	158.5									2	
65	312	De Witt	-6.5	275.6	20.7	3	t	d	n	1	153.1	28.9									2	
66	413	Vashti	-6.8	43.7	16.5	2	t	i	n	1	9.0	126.0	169.5	62.0							4	
67	236	Thomas	-13	272.5	25.9	3	t	d	n	1	117.9	92.6	41.5								3	
68	283	Frank	-13.1	12.9	22.6	2	t	b	n	1	131.5	120.2	1.9								3	
69	124	Mowatt	-14.6	292.3	36.7	3	t	d	n	1	136.6	15.1	66.2								3	
70	426	Cynthia	-16.7	347.5	15.8	3	t	i	n	1	119.1	48.5									2	
71	458	Fatima	-17.8	31.9	14.7	3	t	d	n	1	151.0	36.7									2	
72	473	Tanya	-19.3	282.8	14.2	0	t	d	n	2	176.6	3.9	138.1								3	
73	303	Halle	-19.8	145.5	21.1	2	t	b	n	1	130.8	12.3					24.4	59.3	26.2	146.9	2	4
74	463	Marie	-21.7	232.4	14.5	3	t	d	n	1							160.6	130.7	26.9			3
75	189	Bugoslavskaya	-23	300.4	29.7	3	t	d	n	1	24.9	143.1									2	
76	214	Scarpellini	-23.3	34.6	27.2	3	t	d	n	1	119.0	180.0	54.3								3	
77	257	Galindo	-23.3	258.9	24	0	u	i	n	2	0.9	119.6					38.3	168.0	103.3	63.4	2	4
78	117	Carson	-24.2	344.1	37.6	3	t	d	y	1	164.6	111.0	144.9								3	
79	84	Austen	-25	168.5	43.9	4	t	b	n	1	122.4	40.9	174.8	133.1			163.5	37.5	127.6		4	3
80	514	Kastusha	-28.6	60	12.7	3	t	i	n	1	124.5	178.7	39.8				18.9				3	1
81	451	Ayana	-29.2	175.5	14.9	2	u	b	n	1	138.9	53.4	154.0	110.6	17.5		42.6	143.0			5	2
82	389	Oakley	-29.3	310.5	17.5	2	t	b	n	1	164.3	35.2									2	
83	206	Sirani	-31.5	230.4	27.7	3	t	d	n	1	136.0	13.5	112.9				7.3	41.0			3	2
84	407	Yoshioka	-32.4	58.9	16.7	0	u	d	n	3	26.4	134.7					25.5	146.2			2	2
85	238	Behn	-32.5	142	25.8	3	t	d	n	1	35.5	97.7	153.4	28.8			130.5				4	1
86	333	Kaikilani	-32.8	163.2	19.6	3	t	d	n	1	174.1	56.3	165.8	106.1			157.5	108.4	157.4		4	3
87	109	Agrippina	-33.3	65.7	38.4	3	t	d	n	1	1.0	123.0					8.6	40.1			2	2
88	489	Jocelyn	-33.3	276.4	13.5	3	t	d	n	1	2.8	121.6	35.3								3	
89	404	Elza	-34.4	275.9	16.9	2	u	i	n	1	148.8	51.7									2	

▼

No.	ID#	Name	Lat. [°N]	Long. [°E]	Diam. [km]	M	T	F	P	D	Left-looking Str1	Str2	Str3	Str4	Str5	Str6	Right-looking Str1	Str2	Str3	Str4	n L	n R
90	252	Woolf	-37.7	27.2	24.6	3	t	d	n	1	167.0	44.0	24.4	122.2			166.3	49.3			4	2
91	380	Veronica	-38.1	124.6	17.9	2	u	d	n	2	40.5	168.7	125.4				162.4	111.8	52.1		3	3
92	94	Agnesi	-39.5	37.7	41.4	4	t	d	n	1	176.0	124.2									2	
93	353	Muriel	-41.7	12.4	18.8	2	u	i	n	1	45.2	112.1	158.5				44.1	121.0			3	2
94	337	Sarah	-42.4	1.8	19.5	2	t	d	n	1	126.6	178.0	29.7	153.1							4	
95	399	Inira	-43.1	239.4	17	2	u	b	n	1	153.4	34.7					151.8	7.8			2	2
96	278	Lehmann	-44.1	39.1	22.8	2	t	d	n	2	155.8	104.6	2.3	120.1							4	
97	343	Leila	-44.2	86.8	19.3	3	t	d	n	1	112.9	156.6	21.6	109.8			156.3	110.0	165.2		4	3
98	107	Howe	-45.7	174.8	38.5	3	t	i	n	1	157.7	111.6	20.8				29.2	178.4			3	2
99	115	Phryne	-46.1	314.7	37.6	3	t	i	n	1	124.2	157.5	122.6	172.0							4	
100	531	Nyogari	-46.5	306.4	12.2	2	u	b	n	1	13.9	139.8	11.1								3	
101	480	Erin	-47	184.8	13.9	2	u	d	n	1	19.7	101.1	20.1				7.1	62.7	120.0		3	3
102	247	Fredegonde	-50.5	93.3	24.9	3	t	d	n	1	166.4	107.9					8.1				2	1
103	29	Henie	-52	146	68.7	4	t	d	n	1	112.5	150.7	23.0	60.5			141.5	156.3	17.7	56.4	4	4
104	362	Abigail	-52.2	111.2	18.5	3	t	d	n	1	135.3	2.1					140.5	177.4	173.8		2	3
105	375	Virginia	-52.9	185.9	18.1	3	t	i	n	1	122.4	176.9	137.3				138.8	16.7	135.0	178.0	3	4
106	215	Huang Daopo	-54.2	165.3	27.2	2	t	i	n	1	40.4	157.0					145.4				2	1
107	442	Yvonne	-56	298.4	15.2	2	u	i	n	1	165.2	115.7									2	
108	229	Guilbert	-58	13.6	26.1	3	t	d	n	1	2.3	36.5					20.0	153.1			2	2
109	277	Nofret	-58.8	252.1	22.9		u			1	146.0	19.9					170.1	15.0			2	2
110	301	Gretchen	-59.7	213.2	21.2	3	t	d	n	1							176.5	15.9	140.9			3
111	307	Blixen	-60.2	145.7	21	3	t	d	n	1	122.3	164.8	38.7				32.3	127.1			3	2
112	478	Colleen	-60.8	162.2	14	2	u	b	n	1	113.2	172.2					142.9				2	1
113	430	Megan	-61.8	130.6	15.6	3	t	i	n	1							20.7	74.6	153.4	131.1		4
114	302	Durant	-62.3	227.6	21.1	2	t	d	n	1							160.6	48.8	2.8			3
115	342	Juanita	-62.8	90	19.4	3	t	d	n	1	141.5	27.9	121.3	169.9			171.6	25.7	51.6	150.5	4	4
116	530	Tuyara	-62.9	15.5	12.2	2	u	i	n	3	155.0	117.6	49.4				156.9	32.2			3	2
117	176	Vacarescu	-63	199.8	30.6	3	t	d	n	1	20.4	131.7	83.1				78.4				3	1
118	69	Marsh	-63.6	46.6	47.4	4	t	d	n	1	119.3	82.3									2	
119	243	Rand	-63.8	59.5	25.2	3	t	d	n	1							162.2	61.5	42.6	5.1		4
120	12	Sayers	-67.5	229.6	93.6	5	t	d	n	1	15.2	64.2	157.5								3	
121	525	Laulani	-68.2	121.2	12.3	2	u	i	n	2	129.2	22.9	179.6				133.8	168.6	164.2	77.5	3	4

Appendix 5b. Data of matches between 121 Venusian PIC rim and surrounding tectonic structure orientations. Plus sign (+) indicates a match (±7.5°) between at least one orientation measured from a specific tectonic structure type and one straight rim segment of the PIC in question. The matches are presented separately for tectonic structures <2 diameters ("1") and 2–10 diameters ("2") from the PIC. Abbreviations of tectonic structures are: YR – young rift zone; OR – old rift zone; WR – wrinkle ridge; MB – mountain belt; L – lineament; TT – tessera terrain; CR – volcano-tectonic feature, radial component; CC – volcano-tectonic feature, concentric component; n – the number of matches

No.	ID#	Name	Lat. [°N]	Long. [°E]	D [km]	YR (1)	YR (2)	OR (1)	OR (2)	WR (1)	WR (2)	MB (1)	MB (2)	L (1)	L (2)	TT (1)	TT (2)	CR (1)	CR (2)	CC (1)	CC (2)	n
1	320	Odilia	81.3	200.4	20.4																	
2	466	Gina	78.1	76.5	14.5						+					+						2
3	233	Monika	72.3	122.4	26.1																	
4	331	Wanda	71.2	323.1	19.8																	
5	423	Evangeline	69.6	222.0	15.9					+			+									2
6	545	Zdravka	65.1	299.1	12.0			+														1
7	487	Margit	60.0	273.1	13.6			+														1
8	524	Bineta	57.2	144.1	12.4											+						1
9	258	Johnson	51.8	254.6	24.0	+		+											+			3
10	517	Dolores	51.4	201.6	12.5					+												1
11	491	Irene	49.8	134.0	13.5											+						1
12	368	Laura	48.9	141.2	18.4							+										1
13	285	Brooke	48.4	296.6	22.5			+						+						+		3
14	256	Valentina	46.4	144.1	24.3																	
15	290	Zvereva	45.3	283.1	22.3																	
16	154	Mu Guiying	41.2	81.1	32.7							+										1
17	383	Anya	39.5	297.8	17.7																	
18	402	Datsolalee	38.3	171.8	17.0					+		+										2
19	289	Bly	37.7	305.6	22.4							+										1
20	279	de Stael	37.4	324.2	22.8															+		1
21	506	Wilma	36.7	1.7	13.0					+							+					2
22	202	Moses	34.6	119.9	28.1			+		+												2
23	296	Merian	34.5	76.2	21.9											+						1
24	479	Wazata	33.6	298.3	14.0											+						1
25	203	West	26.1	303.0	28.0																	
26	250	Horner	23.4	97.8	24.7																	
▼																						

No.	ID#	Name	Lat. [°N]	Long. [°E]	D [km]	YR (1)	YR (2)	OR (1)	OR (2)	WR (1)	WR (2)	MB (1)	MB (2)	L (1)	L (2)	TT (1)	TT (2)	CR (1)	CR (2)	CC (1)	CC (2)	n
27	365	Corinna	22.9	40.6	18.5									+								1
28	298	de Lalande	20.4	355.0	21.6									+						+		2
29	268	Weil	19.3	283.1	23.4																	
30	526	Zulfiya	18.4	101.9	12.3			+			+											2
31	348	Hannah	17.9	102.6	19.1																	
32	41	Vigee-Lebrun	17.3	141.4	57.6				+													1
33	140	Grimke	17.3	215.3	34.6															+		1
34	111	Ban Zhao	17.2	146.9	38.3			+														1
35	138	Bradstreet	16.5	47.7	35.2													+			+	2
36	406	Aimee	16.1	127.2	16.8																	
37	273	Devorguilla	15.3	4.0	23.1	+						+										2
38	529	Anush	14.9	86.5	12.2		+															1
39	1	Mead	12.5	57.0	268.7																	
40	483	Pamela	11.0	238.5	13.9													+				1
41	447	Lydia	10.7	340.7	15.0														+			1
42	347	Romola	9.3	54.2	19.1			+			+								+			3
43	475	Aita	8.9	270.7	14.1					+								+		+		3
44	83	Rhys	8.6	298.8	44.0					+												1
45	354	Nadine	7.8	359.1	18.8				+													1
46	175	Hwangcini	6.3	141.7	30.8									+								1
47	497	Susanna	6.0	93.3	13.2							+					+					2
48	515	Ngone	6.0	331.9	12.6					+												1
49	464	Ketzia	4.0	300.5	14.5	+								+				+		+		4
50	284	Castro	3.3	233.9	22.6	+																1
51	364	Shakira	3.0	213.6	18.5	+																1
52	421	Tsiala	2.9	100.0	16.0					+												1
53	114	Uvaysi	2.3	198.2	38.0	+														+		2
54	48	de Beauvoir	2.0	96.1	53.3																	
55	249	Piscopia	1.5	190.9	24.8																	
56	350	Comnena	1.2	343.7	19.0		+															1
57	392	Toklas	0.7	273.1	17.2			+									+					2
58	28	Andreianova	-3.0	68.7	69.5											+						1
59	272	Zija	-3.5	265.0	18.2											+						1
▼																						

No.	ID#	Name	Lat. [°N]	Long. [°E]	D [km]	YR (1)	YR (2)	OR (1)	OR (2)	WR (1)	WR (2)	MB (1)	MB (2)	L (1)	L (2)	TT (1)	TT (2)	CR (1)	CR (2)	CC (1)	CC (2)	n
60	198	von Schuurman	-5.0	191.0	28.9																	
61	330	Evika	-5.1	31.4	19.8					+											+	2
62	275	Quimby	-5.7	76.7	22.9											+	+					2
63	420	Sabira	-5.8	239.8	16.0						+				+							2
64	482	Valerie	-6.4	30.9	13.9													+				1
65	312	De Witt	-6.5	275.6	20.7									+								1
66	413	Vashti	-6.8	43.7	16.5									+								1
67	236	Thomas	-13.0	272.5	25.9	+																1
68	283	Frank	-13.1	12.9	22.6																	
69	124	Mowatt	-14.6	292.3	36.7	+			+													2
70	426	Cynthia	-16.7	347.5	15.8													+		+		2
71	458	Fatima	-17.8	31.9	14.7																	
72	473	Tanya	-19.3	282.8	14.2																	
73	303	Halle	-19.8	145.5	21.1									+								1
74	463	Marie	-21.7	232.4	14.5	+														+		2
75	189	Bugoslavskaya	-23.0	300.4	29.7					+												1
76	214	Scarpellini	-23.3	34.6	27.2				+	+				+								3
77	257	Galindo	-23.3	258.9	24.0	+														+		2
78	117	Carson	-24.2	344.1	37.6	+																1
79	84	Austen	-25.0	168.5	43.9	+												+		+		3
80	514	Kastusha	-28.6	60.0	12.7																	
81	451	Ayana	-29.2	175.5	14.9					+												1
82	389	Oakley	-29.3	310.5	17.5																	
83	206	Sirani	-31.5	230.4	27.7				+			+										2
84	407	Yoshioka	-32.4	58.9	16.7											+						1
85	238	Behn	-32.5	142.0	25.8	+																1
86	333	Kaikilani	-32.8	163.2	19.6	+								+								2
87	109	Agrippina	-33.3	65.7	38.4																	
88	489	Jocelyn	-33.3	276.4	13.5															+	+	2
89	404	Elza	-34.4	275.9	16.9																+	1
90	252	Woolf	-37.7	27.2	24.6		+							+								2
91	380	Veronica	-38.1	124.6	17.9	+																1
92	94	Agnesi	-39.5	37.7	41.4			+														1
▼																						

No.	ID#	Name	Lat. [°N]	Long. [°E]	D [km]	YR (1)	YR (2)	OR (1)	OR (2)	WR (1)	WR (2)	MB (1)	MB (2)	L (1)	L (2)	TT (1)	TT (2)	CR (1)	CR (2)	CC (1)	CC (2)	n
93	353	Muriel	-41.7	12.4	18.8			+														1
94	337	Sarah	-42.4	1.8	19.5			+						+							+	3
95	399	Inira	-43.1	239.4	17.0			+		+		+										3
96	278	Lehmann	-44.1	39.1	22.8								+									1
97	343	Leila	-44.2	86.8	19.3														+		+	2
98	107	Howe	-45.7	174.8	38.5																	
99	115	Phryne	-46.1	314.7	37.6		+							+								2
100	531	Nyogari	-46.5	306.4	12.2						+											1
101	480	Erin	-47.0	184.8	13.9					+												1
102	247	Fredegonde	-50.5	93.3	24.9					+												1
103	29	Henie	-52.0	146.0	68.7					+				+								2
104	362	Abigail	-52.2	111.2	18.5														+			1
105	375	Virginia	-52.9	185.9	18.1					+												1
106	215	Huang Daopo	-54.2	165.3	27.2					+											+	2
107	442	Yvonne	-56.0	298.4	15.2						+											1
108	229	Guilbert	-58.0	13.6	26.1																+	1
109	277	Nofret	-58.8	252.1	22.9						+				+						+	3
110	301	Gretchen	-59.7	213.2	21.2					+			+									2
111	307	Blixen	-60.2	145.7	21.0										+							1
112	478	Colleen	-60.8	162.2	14.0																	
113	430	Megan	-61.8	130.6	15.6					+					+							2
114	302	Durant	-62.3	227.6	21.1					+											+	2
115	342	Juanita	-62.8	90.0	19.4	+	+											+				3
116	530	Tuyara	-62.9	15.5	12.2											+						1
117	176	Vacarescu	-63.0	199.8	30.6							+										1
118	69	Marsh	-63.6	46.6	47.4													+				1
119	243	Rand	-63.8	59.5	25.2						+											1
120	12	Sayers	-67.5	229.6	93.6					+												1
121	525	Laulani	-68.2	121.2	12.3			+						+								2
Total number of matches						16	5	14	5	23	8	9	3	15	4	10	4	9	5	12	10	152

Appendix 6. 167 lunar PICs identified from the TINN area. Data of the named craters are taken from McDowell (2004). See chapter 7.1.3 for further details.

No.	Name	Lat. [°N]	Long. [°E]	D [km]
1	Boscovich E	9.0	12.7	21
2	Ukert B	8.3	1.3	21
3	Ukert	7.8	1.4	23
4	Bode	6.7	-2.4	18
5	Silberschlag P	6.7	12.0	25
6	Triesnecker	4.2	3.6	26
7	Whewell	4.2	13.7	13
8	Agrippa	4.1	10.5	44
9	Pallas E	4.0	-1.4	26
10	Chladni	4.0	1.1	13
11	Dembowski	2.9	7.2	26
12	Ritter C	2.8	18.9	14
13	d'Arrest	2.3	14.7	30
14	Maskelyne	2.2	30.1	23
15	Ritter	2.0	19.2	29
16	Sabine	1.4	20.1	30
17	Rhaeticus	0.0	4.9	45
18	Mösting	-0.7	-5.9	24
19	Lade	-1.3	10.1	55
20	Delambre	-1.9	17.5	51
21	Torricelli C	-2.7	26.0	11
22	Alfraganus A	-3.0	20.3	13
23	Horrocks	-4.0	5.9	30
24	Saunder	-4.2	8.8	44
25	Taylor A	-4.2	15.4	38
26	Spörer	-4.3	-1.8	27
27	Taylor B	-4.3	14.3	29
28	Lalande	-4.4	-8.6	24
29	Herschel D	-5.3	-4.0	20
30	Gutenberg G	-6.0	40.0	32
31	Zöllner F	-7.5	21.9	25
32	Müller	-7.6	2.1	22
33	Isidorus	-8.0	33.5	42
34	Ptolemaeus	-9.3	-1.9	164
35	Unnamed 1	-9.6	36.7	28
36	Anděl	-10.4	12.4	35
37	Kant	-10.6	20.1	33
38	Gaudibert	-10.9	37.8	34
39	Mädler	-11.0	29.8	27
40	Anděl P	-11.6	12.3	19
41	Albategnius	-11.7	4.3	114
42	Ibn-Rushd	-11.7	21.7	32
43	Davy	-11.8	-8.1	34
44	Klein	-12.0	2.6	44
45	Alphonsus B	-13.2	-0.2	24
46	Parrot V	-13.2	0.8	24
47	Abulfeda D	-13.2	9.5	20
48	Cyrillus	-13.2	24.0	98
49	Burnham	-13.9	7.3	24
►				

No.	Name	Lat. [°N]	Long. [°E]	D [km]
50	Parrot A	-15.3	2.1	21
51	Lassell	-15.5	-7.9	23
52	Alpetragius	-16.0	-4.5	39
53	Parrot F	-16.1	1.4	19
54	Tacitus	-16.2	19.0	39
55	Bohnenberger	-16.2	40.0	33
56	Unnamed 2	-16.3	3.4	11
57	Almanon	-16.8	15.2	49
58	Catharina B	-17.0	24.3	24
59	Catharina P	-17.2	23.3	46
60	Airy B	-17.6	8.5	29
61	Alpetragius G	-18.2	-6.5	12
62	Arzachel	-18.2	-1.9	96
63	Almanon B	-18.3	15.3	25
64	Parrot C	-18.5	1.2	31
65	Almanon P	-18.5	17.0	19
66	Geber B	-19.0	13.0	19
67	Unnamed 4	-20.2	1.7	21
68	Catharina C	-20.3	24.4	28
69	Donati	-20.7	5.2	36
70	Abenezra	-21.0	11.9	42
71	Fermat C	-21.0	18.5	14
72	Sacrobosco F	-21.1	16.7	19
73	Abenezra C	-21.3	11.1	44
74	Faye	-21.4	3.9	36
75	Thebit A	-21.5	-4.9	20
76	Sacrobosco Q	-21.6	17.5	42
77	Sacrobosco D	-21.6	17.7	24
78	Purbach E	-21.7	-0.7	23
79	Fermat A	-21.8	19.6	17
80	Polybius C	-22.0	23.6	29
81	Azophi	-22.1	12.7	47
82	Polybius F	-22.2	23.0	21
83	Polybius	-22.4	25.6	41
84	Fermat	-22.6	19.8	38
85	Unnamed 3	-22.7	-1.6	15
86	Sacrobosco	-23.7	16.7	98
87	Azophi A	-24.4	11.2	29
88	Fracastorius A	-24.4	36.5	18
89	Sacrobosco T	-24.9	16.8	12
90	Pons	-25.3	21.5	41
91	Pons D	-25.5	22.1	15
92	Pontanus D	-25.9	13.2	20
93	Apianus D	-26.1	10.7	35
94	Sacrobosco E	-26.1	17.7	13
95	Werner H	-26.6	1.5	16
96	Werner A	-27.2	1.1	15
97	Pons A	-27.3	20.0	12
98	Weinek	-27.5	37.0	32
▼				

No.	Name	Lat. [°N]	Long. [°E]	D [km]
99	Purbach C	-27.7	-4.6	18
100	Apianus C	-28.1	10.5	20
101	Pontanus Y	-28.7	17.2	23
102	Poisson A	-29.6	9.1	17
103	Aliacensis A	-29.7	7.4	14
104	Hell B	-30.0	-5.8	22
105	Poisson	-30.4	10.6	42
106	Aliacensis	-30.6	5.2	79
107	Pontanus G	-30.6	15.3	21
108	Rothmann	-30.8	27.7	42
109	Zagut E	-31.7	23.1	35
110	Zagut	-32.0	22.1	84
111	Zagut B	-32.1	18.7	32
112	Gemma Frisius H	-32.4	12.2	28
113	Goodacre	-32.7	14.1	46
114	Poisson H	-33.0	7.4	19
115	Gemma Frisius G	-33.2	11.4	37
116	Nonius L	-33.5	3.5	31
117	Nonius K	-33.7	3.9	18
118	Poisson F	-33.7	8.0	14
119	Ball A	-34.7	-9.3	29
120	Rabbi Levi	-34.7	23.6	81
121	Nonius	-34.8	3.8	69
122	Poisson J	-35.0	8.3	27
123	Lexell	-35.8	-4.2	62
124	Lexell D	-36.1	-0.7	20
125	Lexell A	-36.9	-1.4	34
126	Ball C	-37.7	-8.7	31
127	Miller A	-37.7	1.8	39
128	Miller C	-38.2	-0.3	36
129	Wöhler	-38.2	31.4	27
130	Miller	-39.3	0.8	61
131	Sasserides A	-39.9	-7.0	48
132	Riccius D	-40.3	28.9	17
133	Unnamed 5	-40.7	10.8	39
134	Nicolai Z	-40.9	21.5	24
135	Nasireddin	-41.0	0.2	52
136	Huggins	-41.1	-1.4	65
137	Faraday A	-41.5	9.7	21
138	Nicolai Q	-42.3	30.1	26
139	Faraday	-42.4	8.7	69
140	Nicolai M	-42.4	29.0	11
141	Janssen X	-42.9	33.3	24
142	Stöfler P	-43.2	7.3	33
143	Faraday C	-43.3	8.1	30
144	Stöfler G	-43.4	2.0	20
145	Pictet	-43.6	-7.4	62
146	Saussure A	-43.8	-0.5	19
147	Barocius B	-44.0	18.3	39
148	Nicolai C	-44.0	29.0	25
149	Lockyer H	-44.5	32.5	31
150	Pictet A	-45.0	-7.9	34
151	Janssen	-45.4	40.3	199
152	Faraday G	-45.8	10.1	31
153	Unnamed 7	-46.0	7.7	21
154	Spallanzani	-46.3	24.7	32
155	Proctor	-46.4	-5.1	52
156	Dove	-46.7	31.5	30
157	Licetus	-47.1	6.7	74
158	Clairaut S	-47.5	16.3	22
159	Pitiscus B	-47.7	30.5	25
160	Unnamed 6	-47.8	7.9	22
161	Maginus G	-48.0	-7.6	23
162	Breislak	-48.2	18.3	49
163	Maginus F	-48.9	-8.2	18
164	Clairaut A	-48.9	14.8	36
165	Ideler	-49.2	22.3	38
166	Ideler L	-49.2	23.6	36
167	Baco B	-49.5	16.6	43

►

“But today is not going to be a bad day,
I can feel it in my bones.
I can see light on the horizon,
and I might just head on home.”

– TV *SM!TH*